Characterizing methane (CH4) emissions in urban environments (Paris)

Sara Defratyka

▶ **To cite this version:**

Sara Defratyka. Characterizing methane (CH4) emissions in urban environments (Paris). Other. Université Paris-Saclay, 2021. English. NNT : 2021UPASJ002 . tel-03230140

HAL Id: tel-03230140
https://theses.hal.science/tel-03230140

Submitted on 19 May 2021

HAL is a multi-disciplinary open access archive for the deposit and dissemination of scientific research documents, whether they are published or not. The documents may come from teaching and research institutions in France or abroad, or from public or private research centers.

L'archive ouverte pluridisciplinaire **HAL**, est destinée au dépôt et à la diffusion de documents scientifiques de niveau recherche, publiés ou non, émanant des établissements d'enseignement et de recherche français ou étrangers, des laboratoires publics ou privés.

Thèse de doctorat

NNT : 2021UPASJ002

université PARIS-SACLAY

Characterization of CH4 emissions in urban environments (Paris)

Caractérisation des émissions de CH_4 en milieu urbain (Paris)

Thèse de doctorat de l'université Paris-Saclay

École doctorale n° 129 Sciences de l'environnement d'Ile-de-France (SEIF)
Spécialité de doctorat: météorologie, océanographie, physique de l'environnement
Unité de recherche : Université Paris-Saclay, CNRS, CEA, UVSQ, Laboratoire des sciences du climat et de l'environnement
Référent : Université de Versailles-Saint-Quentin-en-Yvelines

Thèse présentée et soutenue à Paris-Saclay, le 19/01/2021, par

Sara DEFRATYKA

Composition du Jury

Valéry CATOIRE Professeur des universités, Université d'Orléans	Président du jury et Rapporteur
Lilian JOLY Directeur de Recherche, UMR CNSR	Rapporteur et Examinateur
Sébastien BIRAUD Directeur de Recherche, CESD	Examinateur
Valérie GROS Directrice de Recherche, LSCE	Examinatrice
Martina SCHMIDT Chercheuse, UHEI	Examinatrice

Direction de la thèse

Philippe BOUSQUET Professeur, LSCE	Directeur de thèse
Camille YVER-KWOK Chercheuse, LSCE	Invitée, Co- Encadrante de thèse
Jean-Daniel PARIS Chercheur, LSCE	Invité, Co-Encadrant de thèse

Acknowledgments

First of all, I wish to express my deepest gratitude to Philippe Bousquet, Camille Yver-Kwok and Jean-Daniel Paris for supervising my Ph.D., continuous trust and support, and being wise and brilliant mentors. Philippe, thank you for your enthusiastic and wise guidance and encouraging me to be professional and to look at my work from a bigger perspective. Jean-Daniel, thank you for the intellectual discussions during our surveys which have allowed me to better understand the scientific questions behind my work. Camille, thank you for answering my never-ending questions, helping me improve my skills, and showing me that it is possible to manage both, a scientific career and a family with passion.

Special regards to Valéry Catoire and Lilian Joly for their acceptance to review this thesis. Many thanks to Sébastien Biraud and Valérie Gros for being part of my PhD jury. I am pleased to thank Dave Lowry, Martina Schmidt and Felix Vogel for being my thesis committee members. I value the constructive and developmental discussions we have shared, which progressed my work.

I wish to show my gratitude to the MEMO^2 European Training Network and Climate Clean Air Coalition Oil and Gas Methane Science Studies for financially supporting this thesis and providing the opportunity to participate in informative schools, workshops, and conferences.

I owe much respect to the Royal Holloway University of London Earth Science Department, especially Rebecca Fisher and Euan Nisbet. Also, respects to the UK's National Physical Laboratory, particularly Rod Robinson and Jon Helmore for serving as my secondment mentors, and for providing a collaborative measurement opportunity with MEMO^2. Additional thanks to James France for organizing the NPL controlled release experiment. Recognition to Jarosław Nęcki and the members of CoMet for allowing me to join an extensive campaign and fulfil my secondment. This experience enriched my knowledge and strengthened skills in the matter of conducting mobile measurements.

I am thank for my LSCE colleagues whose assistance was a milestone in the completion of this project. Thanks to Gregoire and Pramod for assisting me with modelling, explaining different concepts and answering my elementary questions. Thanks to Pierre-Yves and Daniel for numerous hours spent in the car during mobile measurements. Recognition to Abdel and Sebastien who introduced me to secrets of completing a Ph.D. at LSCE and shared useful tips to deal with daily struggles. Also, I am indebted to all of the ICOS team, which always find solutions form any technical problems. Thank you all for time spent during lunch and coffee breaks. Without you, my French articulation would definitely be much lower than today.

From the bottom of my heart, I would like to express immense appreciation for all my substantially supportive friends who were ready to listen my complains whenever I needed it. Barbara and Sophie, thank you for your extensive support during our Social Sundays. Also, a world without unicorns would not be the same. I also want to thank Yunsong for bringing the Ph.D. candidate office large amounts of enthusiasm and energy. Thank you Juli for hosting me during my UK secondments, and numerous hours of interesting discussions. Do not be shy. Malika, thank you for your help with isotopic measurements and data interpretation. Thanks to all MEMO^2 Ph.D. candidates for creating an amazing and support team of young scientists. To my Polish friends, thanks for cheering me up, even from far away, especially Karolcia, Karolina and Piotr who shared their optimism and endless positive energy to get through difficult times. Thanks Ulrich for your endless support and frequent reminders that I am able and ready to finish my Ph.D.

Finally, a very warm thanks to my parents and brother who set me off on the road to my Ph.D. a long time ago. Without their continuous support I would not be able to take on the challenge of doing a Ph.D. Thank you for welcoming me always with open arms and the maximum possible support.

Contents

Figures

Tables

Chapter 1 Introduction

1.1 Global methane budget

Methane (CH_4) is one of the greenhouse gases that occur naturally in the atmosphere. However, its global mean mixing ratio has increased about 2.6 times compared to the pre-industrial times (IPCC 2018; Saunois et al. 2019; Turner et al. 2019) and reached 1880 ppb in July 2020 (Dlugokencky 2020). According to the ice core measurements, over the last millennium before the pre-industrial times, the methane mixing ratio varied around 700 ppb (IPCC 2018; Turner et al. 2019). Moreover, after a short period of stabilization around 1775 ppb, between 2000 and 2007, the atmospheric methane rose again by up to 7.7 ± 0.7 ppb/ year in 2017 (Nisbet et al. 2019). Current CH_4 trend places CH_4 emissions close to the warmest IPCC-AR5 scenario (RCP8.5 scenario) (Saunois et al. 2016; Jackson et al. 2020). Following this trajectory causes a temperature increase above 3 °C by the end of the century (Saunois et al. 2020). It will thus require an extensive reduction of the methane emissions to limit the temperature rise to 1.5-2 °C from the Paris Agreement (Nisbet et al. 2019). The observed global trend of CH_4 concentration is presented in Fig 1.1.

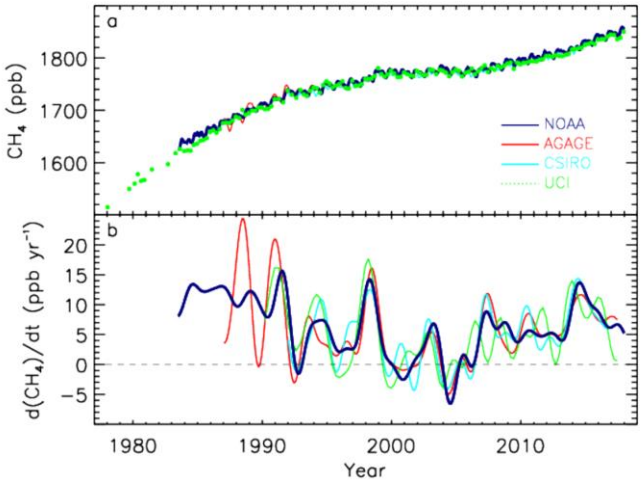

Figure 1.1 From Saunois et al. 2020: Globally averaged atmospheric CH_4 (a) and its annual growth rate GATM (ppb yr^{-1}) (b) from four measurements programs, National Oceanic and Atmospheric Administration (NOAA), Advanced Global Atmospheric Gases Experiment (AGAGE), Commonwealth Scientific and Industrial Research Organization (CSIRO), and University of California, Irvine (U.C.I.).

At current atmospheric concentration, methane global warming potential (GWP) is higher than for carbon dioxide (CO_2) and for a 100-year timeline without considering climate feedback, its GWP is 28 times higher than for CO_2 (IPCC 2018). Additionally, CH_4 has a shorter lifetime than CO_2 and in 2010 was about 9 years (Voulgarakis et al. 2013; Morgenstern et al. 2017). Therefore, CH_4 mitigation actions result in relatively fast stabilization or reduction of atmospheric CH_4 mixing ratio, which can be an efficient way to reduce the global greenhouse gas effect on the decennial time scale (Saunois et al. 2019; Nisbet et al. 2019; Turner et al. 2019).

Implementing efficient mitigation actions requires a good knowledge about the CH_4 emissions, both on the local and global scale. Determination of CH_4 budget can be done using bottom-up or top-down approaches. The bottom-up estimations are based on the calculation of the emissions and

atmospheric chemistry from process-based models, inventories of anthropogenic emissions and data extrapolation. In the case of the inventories, emissions are estimated as multiplication of activity data by emission factors, while activity data are determined based on statistical surveys and default emissions factors are stated by the IPCC guidelines (IPCC 2006). In the case of the bottom-up estimations, obtained values can vary widely depending on the used inventories. This is due to the discrepancy between used activity data and different categorizations in individual inventories. Also, used emission factors may not indicate specific conditions in individual countries in different emission sectors (Saunois et al. 2016).

The top-down studies are based on atmospheric observation within the inverse-modeling network. In the case of top-down studies, the contribution of each particular source to total CH_4 emissions can be difficult to determine (Saunois et al. 2019; Turner et al. 2019).

1.2 CH_4 sources and sinks

According to Saunois et al. (2020), using top-down approach, estimated CH_4 total global emissions was equal to 572 Mt CH_4 yr^{-1} [538-593] (mean, [min - max]) for 2008- 2017, where for bottom-up studies it was ~25% higher and reached 737 Mt CH_4 yr^{-1} [593- 880] for the same period. Using a top-down approach, on a global scale, the uncertainty is about 5%. However, looking at the latitudinal distribution, uncertainty doubles for the tropic and the northern mid-latitudes and it increases to more than 25% in the northern high-latitudes. Based on top-down studies, tropical emissions constitute the biggest contribution to the global CH_4 emissions (~64%), where mid-northern and high-northern latitudes contribute, respectively, ~32% and ~4% (Saunois et al. 2020).

Going from the global scale to individual emitters, methane sources can be divided into categories by emissions processes (biogenic, thermogenic or pyrogenic) or by partitioning methane between natural/anthropogenic sources. Regarding emissions processes, decomposition of organic matter by methanogenic *Archaea* produces biogenic methane by CO_2 reduction or by acetate fermentation (Whiticar 1999). Biogenic processes occur in anaerobic environments, such as rice paddies, landfills, sewage and wastewater treatment facilities, water- saturated soils, marine sediments, swamps or ruminants' digestive system.

Thermogenic methane is created on the geological timescales. It is formed by the breakdown of buried organic matter through pressure and heat deep in the Earth's crust. It is released to atmosphere through land and marine geological gas seeps, including exploitation of fossil fuels. Pyrogenic methane reaches the atmosphere due to the incomplete combustion of biomass and other organic material. Incomplete combustion occurs in wildfires, peat fires, biomass burning in degraded or deforested areas and biofuel burning (e.g., Whiticar 1999; Sherwood et al. 2017; Milkov and Etiope 2018; Saunois et al. 2020).

Studying isotopic signature of methane released to atmosphere extends the knowledge about methane formations. Methane isotopic signature is commonly reported in δ notation, which quantifies relative deviation of isotope ratio and it is expressed in parts per mil (‰). The isotopic signature is calculated as:

$$\delta = \left(\frac{R_A}{R_{std}} - 1\right) \cdot 1000 \qquad (1.1)$$

where R_A is the isotopic ratio of the measured methane sample and R_{std} is the isotopic ratio of the standard gas. Typically, the isotopic ratio represents the ratio of the rare isotope to abundant isotope, like $^{13}C/^{12}C$ or $^{2}H/^{1}H$. To report $\delta(^{13}C, CH_4)$ values, Vienna Pee Dee Belemnite international standard is used (VPDB, $^{13}R_{VPDB}$ = 0.0112372) (Craig 1957), while Vienna Standard Mean Ocean Water (VSMOW, $^{2}R_{VSMOW}$ = 0.0020052) (Baertschi 1976) is an international standard for $\delta(D, CH_4)$. In the manuscript, $\delta(^{13}C, CH_4)$ and $\delta(D, CH_4)$ are abbreviated as $\delta^{13}CH_4$ and δDCH_4.

Isotopic signature varies globally and depends from different factors (e.g., location, formation or management in the case of anthropogenic sources.). Lower $\delta^{13}CH_4$ value (range -80 ‰ to -40 ‰) are connected with biogenic sources like waste disposal and landfill, wastewater treatment or agriculture, as methanogenic bacteria are highly selective for ^{12}C. Biogenic methane from CO_2 reduction is more ^{13}C depleted than from acetate fermentation (Whiticar 1999). Depending from the origin of natural gas, which is dominantly a thermogenic source, its isotopic composition varies between -75 ‰ and -25 ‰. Thermogenic methane become more ^{13}C enriched at high maturity stages (Sherwood et al. 2017). Enriched $\delta^{13}CH_4$ (between -35 ‰ and -7 ‰) come from pyrogenic sources like combustion in energy production or heating. The variety in isotopic signature of pyrogenic sources is related to the type of burned organic material (Chanton et al. 2000).

As $\delta^{13}CH_4$ can overlap between processes, δDCH_4 can be used as additional proxy to determine methane origin. Based on the study of Sherwood et al. (2017), where different isotopic signatures over the world are collected, δDCH_4 for biogenic sources is about -317 ‰ (range -442 ‰ to -281 ‰). Pyrogenic and thermogenic methane is more δDCH_4 enriched. For thermogenic methane, mean δDCH_4 is equal to -197 ‰ (range – 415 ‰to -62 ‰), while for pyrogenic sources it reaches - 211 ‰ (range -232 ‰ to -195 ‰). Again, some δDCH_4 values overlap for different processes. Genetic characterization plot of $\delta^{13}CH_4$ and δDCH_4 can be used to better distinguish methane of different origin (Sherwood et al. 2017; Milkov and Etiope 2018; Whiticar 1999). Figure 1.2 presents an example of application of genetic characterization plot used in study made by Sherwood et al (2017). Methane produced in these three processes has both anthropogenic and natural origin (Nisbet et al. 2019; Turner et al. 2019; Saunois et al. 2020; Jackson et al. 2020).

Methane can also contain ^{14}C, which is a radioactive isotope with 5730 years of half-life. Radiocarbon (^{14}C) is constantly produced in the upper atmosphere by cosmic rays and its concentration remains stable. In the atmosphere, cosmic rays collide with nuclei and liberate neutrons. In the next step, theses neutrons replace one of the 7 protons in the nitrogen nuclei. As a result, the new atom of ^{14}C is created, which contains 6 protons and 8 neutrons. All living organisms contain radiocarbon due to carbon exchange via, for example, photosynthesis process and food chain. After death, their radiocarbon concentration decreases due to radioactive decay. Thus, ^{14}C allows to distinguish fossil fuel emissions as they are almost completely depleted in ^{14}C, cause they were separated from atmosphere over a very long time (e.g., Lowe et al. 1991). Currently measurements of ^{14}C remains scarce as they require a bigger measurement volume and advanced laboratory equipment (e.g., Townsend-Small et al. 2012; Espic et al. 2019; Turner et all. 2019).

Additionally, clumped isotopes (rarer isotopes substitute part of the molecules, such as $^{12}CH_2D_2$ or $^{13}CH_3D$) can be used to separate biogenic/thermogenic emissions or the CH_4 loss trough reaction with OH (Stolper et al. 2014; Haghnegahdar et al. 2017). However, the determination of different clumped isotopes requires expensive and technically advanced measurements technique, and currently, it is not applied for continuous measurements (Turner et al. 2019).

Not only measurements of isotopes can give additional source information. For instance, carbon monoxide (CO) is co-emitted during incomplete combustion. Due to that, it can be a proxy of the methane emissions from biomass burning (Saunois et al. 2020). Ethane (C_2H_6) is a co-component of the fossils fuels, and it is co-emitted during the extraction of coal, oil and natural gas (Simpson et al. 2012; Turner et al. 2019). Additionally, the ethane to methane ratio varies depending on the facility and type of fossil fuel (Lopez et al. 2017; Yacovitch et al. 2014). Also volatile organic compounds (VOC) are co-emitted with natural gas and oil extraction and production. Lighter VOCs are released with natural gas, while heavier VOCs are co-emitted with oil (Warneke et al. 2014). For example, isomeric pentane ratio (*i*-pentane/*n*-pentane) can be used to characterise oil and natural gas activities, vehicle emissions and other urban emissions (Baker et al. 2008; Thompson et al. 2014). As propane is also co-emitted during natural gas and oil activities, it can also be used as additional indicator (e.g., Helmig et al. 2016).

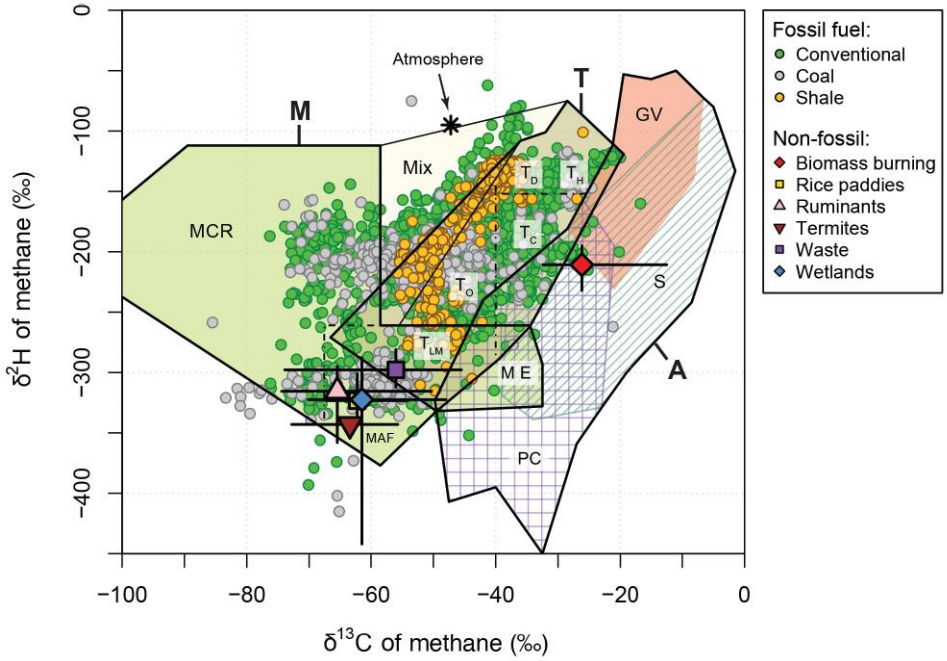

Figure 1.2 From Sherwood et al. 2017: Genetic characterization plot of δDCH_4 (δ^2H) versus $\delta^{13}CH_4$ ($\delta^{13}C$). M: microbial; T: thermogenic; A: abiotic; MCR: microbial CO_2 reduction; MAF: microbial acetate fermentation; ME: microbial in evaporitic environment; T_O: thermogenic with oil; T_C: thermogenic with condensate; T_D: dry thermogenic; T_H: thermogenic with high-temperature CO_2–CH_4 equilibration; T_{LM}: thermogenic low maturity; GV: geothermal–volcanic systems; S: serpentinized ultramafic rocks; PC: Precambrian crystalline shields.

Based on top-down studies, the anthropogenic activities contribute 359 Mt CH_4 yr^{-1} or 60% (range from 55 to 70%) of the total global emissions and natural emissions contribute 40%. Based on the bottom-up approach, the estimated emissions from natural sources are higher than using the top-down approach. Estimated emissions from natural and anthropogenic sources are more balanced, and their contribution is about 50% each. The equal contribution from natural and anthropogenic sources is not consistent with ice cores studies. Ice core and atmospheric methane data confirm the current predominant role of anthropogenic methane (Nicewonger et al. 2016; Turner et al. 2019; Saunois et al. 2020). For natural emissions, the wetlands play a crucial role (178 Mt CH_4 yr^{-1}, top-down study),

where biofuel and biomass burning and other natural emissions (e.g., other inland waters, termites, wild animals) have a smaller contribution to natural CH_4 emissions. Notably, the biggest discrepancy between top-down and bottom-up approaches comes from the "other natural emissions" (37 Mt CH_4 yr^{-1} vs. 222 Mt CH_4 yr^{-1}). Discrepancy between this two approaches can be caused by the lack of some sources of “other natural emissions” like freshwater or permafrost in top-down studies. Moreover, in the case of bottom-up studies, the two biggest contributors, freshwaters (~75%) and geological emissions (~15%) have large uncertainties (Marielle Saunois et al. 2020).

The emissions categories as biomass and biofuel burning have both natural and anthropogenic origin (30 Mt CH_4 yr^{-1}). However, 42% of anthropogenic emissions come from agriculture and waste sector (219 Mt CH_4 yr^{-1}, top-down study) and fossil fuel production and use (109 Mt CH_4 yr^{-1}, top-down study) contribute 31% of anthropogenic emissions. Looking for the uncertainty of the estimated emissions, using the top-down approach, the uncertainty is larger for estimated anthropogenic emissions. In contrast, for wetland emissions, uncertainty is larger using the bottom-up approach (Marielle Saunois et al. 2020).

The global CH_4 budget, including sources and sinks divided by sectors, is presented in figure 1.3. CH_4 emissions come from natural or anthropogenic sources that are partly balanced by four sinks. Total mean global loss of methane is equal to 625 Mt CH_4 yr^{-1} (bottom-up study) or 556 Mt CH_4 yr^{-1} (top-down study). To determine CH_4 sinks, most of the top-down models use the same OH distribution from TRANSCOM experiment. The TRANSCOM experiment was dedicated to intercomparison of chemistry-transport models to investigate the roles of surface emissions, transport and chemical loss in simulating the global methane distribution (Patra et al. 2011). In the case of bottom-up studies, methane sinks and lifetime can be estimated using global model results from the Chemistry Climate Model Initiative (CCMI) (Morgenstern et al. 2017). Oxidation by the hydroxyl radical (OH), mostly in the troposphere, amounts to 90% of the total sinks (Saunois et al. 2020; Turner et al. 2019). Photochemistry loss in the stratosphere is another atmospheric sink of the CH_4. In the stratosphere, methane removal occurs by reactions with OH, O^1D (excited oxygen atoms), atomic Cl and atomic F. The oxidation in soils and chlorine photochemistry in the marine boundary layer are the two remaining CH_4 sinks. Atmospheric chemistry models are used to determine uncertainty of total methane sink. The uncertainties are about 20%-40% and decrease to 10%-20% when atmospheric proxy methods are used (e.g., methyl chloroform) (Saunois et al. 2016).

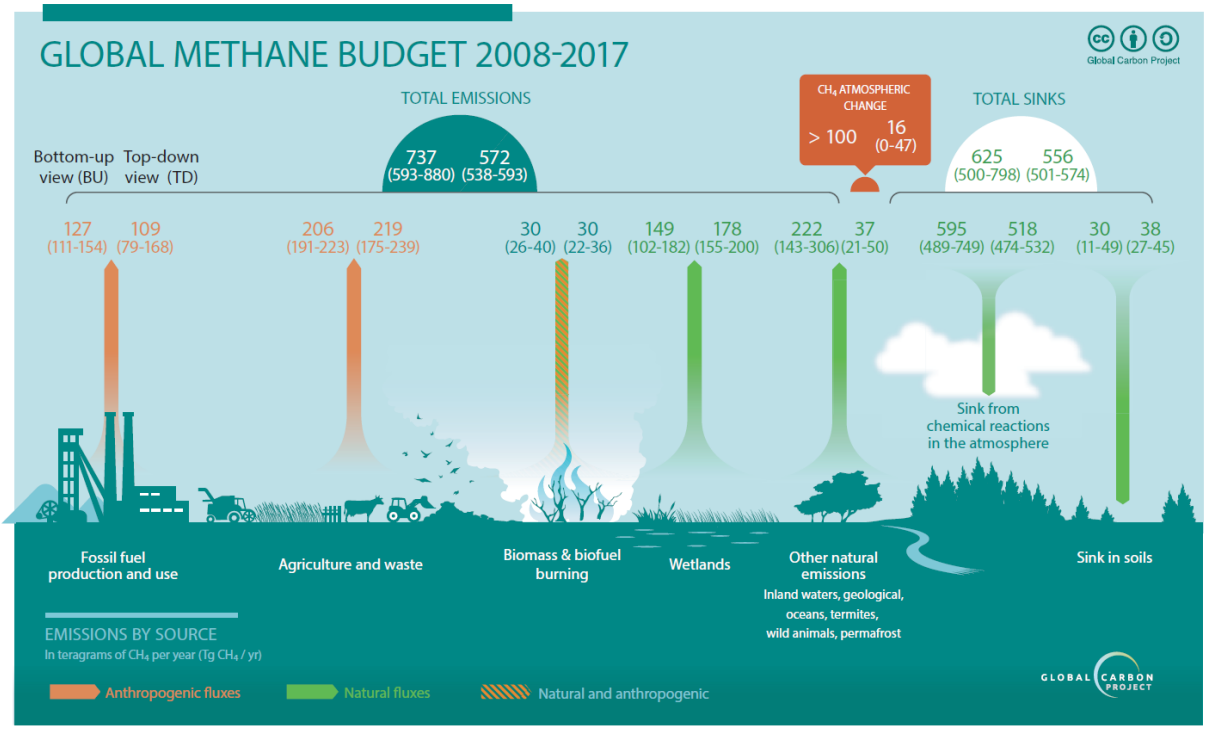

Figure 1.3 From Saunois et al. 2020: Global Methane Budget for the 2008-2017 decade. Both bottom-up (left) and top-down (right) estimates are provided for each emissions and sink category in Mt CH_4 yr^{-1} (Tg CH_4 yr^{-1}), as well as for total emissions and total sinks.

Overall, using top-down approach, estimated CH_4 total global emissions reached 572 Mt CH_4 yr^{-1} [538-593] for 2008- 2017. For bottom-up studies it was ~25% higher and reached 737 Mt CH_4 yr^{-1} [593-880] for the same period. This discrepancy can be caused by using OH distribution from TRANSCOM experiment, which leads to constrained global budget. Likely, the bottom-up budget is overestimated due to up-scaling of local measurements and double-counting of some sources (e.g. wetlands with other natural sources.).

In the following, anthropogenic sources are presented in details, as this Ph.D. study is focused on anthropogenic CH_4 characterization at local scale. Studies on anthropogenic CH_4 emissions allow for taking effective mitigation action to reduce atmospheric CH_4. Reductions of natural CH_4 emissions are more complex cases as they can affect in negative environmental feedback (e.g. drying of wetlands could disturb ecosystems) and it is not described here. It is worth to note that in the northern mid-latitudes, anthropogenic emissions play a dominant role. At the same time, the agriculture and waste sector contributes to 42% of total anthropogenic emissions, followed by the contribution of fossil fuel emissions (31% of total anthropogenic emissions).

1.3 Anthropogenic CH_4 emissions

1.3.1 Agriculture CH_4 emissions

Agricultural emissions reached 141 Mt CH_4 yr^{-1} [131 Mt CH_4 yr^{-1} -154 Mt CH_4 yr^{-1}] over 2008-2017 (bottom-up study) and are mostly connected with livestock production and rice cultivation. For livestock production, the emissions come from enteric fermentation and manure management.

Saunois et al. (2020), using the bottom-up approach, estimated emissions for livestock production (including enteric fermentation and manure management) to 111 Mt CH_4 yr^{-1}, with range 106-116 Mt CH_4 yr^{-1} for a period 2008-2017.

In the case of enteric fermentation, methane is a product of the anaerobic microbial activity in the digestive system of domestic ruminants (e.g., cattle, buffalo). Globally, cattle contribute to the majority of enteric fermentation, due to the large population (~1.4 billion). The methane emissions from the enteric fermentation can vary depending on the country because of different living conditions and the agriculture system (Reay et al. 2010; USEPA 2012; Saunois et al. 2020).

Methane emissions from the manure depends on the manure management system, which affects anaerobic conditions of manure decomposition. For example, handling manure as a solid or depositing it on pasture fosters aerobically decomposition, which results in small or null CH_4 production. Moisture, ambient temperature, residency time, or manure composition also affect the growth of methanogenic bacteria. For example, moisture can foster CH_4 formation when dry storage is provided. The type of diet affects manure composition and typically, higher-energy feed can cause larger methane production (USEPA 2012).

Rice cultivation is the next source of methane in agriculture. As most of the rice grows in flooded paddy, changing the water management system is one of the potent ways to mitigate CH_4 emissions (e.g., seasonally drainage). For the period 2008-2017, rice cultivation contributes to 8% of total anthropogenic emissions of methane (30 [25-38] Mt CH_4 yr^{-1}) (USEPA 2012; Saunois et al. 2020).

1.3.2 Fossil fuels

The second most significant sector of the anthropogenic methane emissions is connected with fossil fuel (natural gas, oil, and coal) production and use. It contributes to 35% of global anthropogenic emissions and reached 128 [113 - 154] Mt CH_4 yr^{-1} over 2008-2017. The coal mining emissions contribute, on average, to 33% of total fossil fuel emissions of methane (42 [29-60] Mt CH_4 yr^{-1}) (Marielle Saunois et al. 2020). Methane is trapped within coal seam and surrounding rock strata over coalification process and can be emitted by natural erosion or by mining operation (USEPA 2012). In underground coal mines, methane emissions come from the shafts' ventilation where air is pumped into the mine to hold the methane mixing ratio < 0.5%. Methane emitted during ventilation can be used as a fuel, however in some countries it is still released to the atmosphere or flared. In the case of surface mining, methane is directly released to the atmosphere (USEPA 2012). Moreover, CH_4 is also emitted during processing and post-processing mining activities and transportation. The abandoned mines and coal waste piles are also sources of methane. They are higher than it was assumed in the past and they count for about 20% of emissions from functioning mines (Saunois et al. 2020).

In the case of oil and natural gas exploitation, methane emissions occur from conventional gas and oil as well as from shale gas exploitation and contribute ~63% of total fossil fuel emissions (76 [66-92] Mt CH_4 yr^{-1}) (Saunois et al. 2020). Methane is a main component of natural gas (~95%) and it is released to the atmosphere through natural gas extraction, processing, distribution and transmission. Natural gas often occurs with petroleum deposits. Thus, methane is also emitted during extraction and upstream production of oil (USEPA 2012). After the Madrid forum (“Potential ways the

gas industry can contribute to the reduction of methane emissions", 5-6 June 2019), the GIE report (Gas Infrastructure Europe) synthesized information and data on European CH_4 emissions of the entire natural gas value chain. The GIE report provides three types of the methane emissions from natural gas industry: fugitives, venting and incomplete combustion (GIE and MARCOGAZ 2019). Fugitive emissions come from the unintended leaks in the infrastructure and can be challenging to determine, depending on their magnitude. During venting, planned releases of methane occur. Methane is emitted for safety reasons, operational procedures or equipment design. Incomplete combustion can occur in the exhaust of natural gas combustion equipment (GIE and MARCOGAZ 2019). Nowadays, in some oil and gas facilities, venting of the natural gas is replaced by flaring with conversion to CO_2. During the oil extraction, natural gas is emitted as well. It can be recovered for utilization as an energy source or re-injection or not recovered. Thus, it is flared or vented. The recovery rate of natural gas from oil extraction varies from country to country. It is the highest in the U.S., Canada, and Europe (Saunois et al. 2020).

Besides the conventional extraction of oil and natural gas, the exploration of shale gas has become more popular over last decades. The extraction of natural shale gas started in the 1980s in the U.S. and since the beginning of this century, the production developed on a large scale and in 2017 reached 62% of total dry natural gas emissions in the U.S. This growing production of shale gas can have a potential effect for the global methane budget. Based on the isotopic signature, Schwietzke et al. (2016) suggested that the underestimated U.S. natural gas emissions can affect a global CH_4 budget and can explain the global increase of concentration observed after 2007. However, other studies (Bruhwiler et al. 2017; Lan et al. 2019; Saunois et al. 2020), did not confirm the increased contribution of North America to the global CH_4 emissions over the last decade. Indeed, in 2017, the total CH_4 emissions in U.S reached 50 Mt CH_4 yr^{-1} and contributed about 8% to global CH_4 emissions, including natural and anthropogenic sources. About 25% of CH_4 emitted in U.S. comes from the fossil fuel sector (Jackson et al. 2020).

Previous studies (Zavala-Araiza et al. 2015; Alvarez et al. 2018) showed that the inventories underestimate CH_4 emissions from the oil and gas value chain. For example, Alvarez et al. (2018) found, based on the ground-based and aircraft observations, that USEPA inventories underestimate the national U.S. emissions by about 60%. Emissions released during abnormal conditions (e.g., malfunctioning equipment and irregular events like uncontrolled flashing and venting) are not included in inventories and it is the most probable reason for the found discrepancy. Operating during the abnormal conditions causes the "fat tail" in the distribution of the emissions distributions. As a result, a small amount of the facilities is responsible for the majority of the emissions (called "super-emitters"). For example, in the Barnett region, the super-emitters represent 2% of the facilities and release 50% of the methane emissions (Zavala-Araiza et al. 2015). Also, in California state, emissions from super-emitters were estimated at about 60% of state CH_4 emissions, while only 10% of the infrastructures were determined as super-emitters (Duren et al. 2019). In the case of the study made in California, the super-emitters occurred not only in the oil and gas sector. They were also observed in solid-waste management and manure management (Duren et al. 2019). Super-emitters lead to the underestimation of the inventories reported values, but they can also be an efficient way to reduce CH_4 emissions. In the case of oil and gas facilities, operating in the most optimal conditions and reducing the number of super-emitters can decrease the emissions from 65% to 87% (Zavala-Araiza et al. 2015).

The role of the distribution of natural gas in CH_4 emissions cannot be neglected. The distribution of the gas contributes to 66% of the European CH_4 emissions from the natural gas value chain (GIE and MARCOGAZ 2019). Emissions from the distribution network strongly depend on the age and material of the pipeline, where steel pipelines represent 40% of the natural gas distribution network and account for the 50% of the methane emission to the atmosphere from the distribution in the European Union (GIE and MARCOGAZ 2019). Methane emissions in the distribution network can come from permeation emissions, where, depending on the pressure conditions, natural gas can migrate through polymers by process of "dissolution diffusion". This process depends on the pipeline material and pressure. Methane emissions from the distribution network can also occur during operations on the network, as the natural gas must be evacuated before an operation, or by incident. In the latest category, the incidents can come from the outside (e.g., operation on the sewage network) or from the distribution system operator (e.g., scratch, corrosion) (GIE and MARCOGAZ 2019). Being mostly distributed in populated areas, natural gas emitted from cities is an important question for the methane cycle. CH_4 emissions from cities are described in section 1.3.6.

1.3.3 Waste management

Using the bottom-up approach, waste management contribute to 12% of the total anthropogenic emissions (65 [60-69] Mt CH_4 yr^{-1}) over 2008-2017. In this sector, the contributions include managed and non-managed landfills and wastewater facilities. Intensive microbial activity occurs on landfills, and most of decomposition of the organic matter occurs through acetate fermentation. Biogas formed on landfills consist of CH_4, CO_2 and numerous trace compounds. Methane primary produced inside deep layers of landfill migrates to the aerobic zone on the top, where is partly oxidized to CO_2. In landfills, methane formation occurs until almost complete decomposition of organic matter. As this process can take some decades, landfills emit methane for long period (Bogner and Spokas 1993).

In the case of landfills, food and organic waste, leaves, and grass ferment quite easily. Thus, the separation of biodegradable waste in compost or bio-digesters is assumed to be an efficient way to reduce methane emissions from landfills. This reduction can also be made by gas collection and capture. However, this method is less efficient than waste separation. If the collected gas is pure enough (>30% of methane), it can be used as a fuel. The cover material, applied to the landfill, reduces the risk to the public health but fosters the anaerobic decomposition of waste (Saunois et al. 2016).

In the wastewater sector, methane is released to the atmosphere by leaks in pretreatment, primary and secondary sludge. Methane production in the wastewater depends on the amount of degradable organic material. If the wastewater is enriched in the organic material, then it is anaerobically decomposed by acetate fermentation, which increases methane production (Daelman et al. 2012; Yver Kwok et al. 2015).

1.3.4 Biomass and biofuel burning

Biomass and biofuel burning is the last category, connected with anthropogenic activities included in global methane budget. Here, the methane is emitted due to incomplete combustion conditions, and its amount varies depending on the amount and type of the biomass and burning conditions. For

the period 2008-2017, the biomass and biofuel sector contributes 30 [26-40] Mt CH_4 yr^{-1}. In the biomass burning category, 90% of fires have an anthropogenic origin, where most of the fires occur in the tropics and subtropics. The biomass burning contributes to about 5% of total anthropogenic methane emissions (17 [14-26] Mt CH_4 yr^{-1}). The biomass used to produce energy is treated as a biofuel and contributes to 30-50% of the biomass and biofuel burning category. According to the study of Saunois et al. (2020), emissions from biofuel burning is equal to 11 [10-14] Mt CH_4 yr^{-1}, which constitutes 3% of the total anthropogenic CH_4 emissions.

1.3.5 Uncertainties in sectoral CH_4 emissions

Anthropogenic CH_4 emissions still remain uncertain, both using bottom-up and top-down approaches. Bottom-up studies can be highly uncertain as used emission factors present large temporal, spatial and site-to-site variations in many CH_4 sectors (e.g. fossil fuel, waste management). Also the activity data can be uncertain, if they are based on an insufficient amount of statistical surveys or on models, which simplified methane production. Also, some emitting sectors can be omitted in inventories and some emissions can be double counted in different sectors, which also increases uncertainty. Thus, top-down studies can be treated as a verification of bottom-up studies, especially in regions with expanded measurement network, like Europe (Bergamaschi et al. 2018). The accuracy of top-down studies depends on the quality of the transport model and the density of measurements network. Top-down studies can be successfully used from global to regional scale, especially to estimate total CH_4 emissions. However, the sectoral estimations are more difficult to determine, especially on smaller scale (Saunois et al. 2020; Turner et al. 2019) like the city scale.

Nowadays, a few networks of continuous measurements of CH_4 mole fraction exist on the global and regional scale. For example, NOAA/ESRL (National Oceanic Atmospheric Administration/ Earth System Research Laboratory) (https://esrl.noaa.gov/gmd/ccgg/flask.php) started working through top-down approaches in the latest 1980. This and other measurements network (e.g., LSCE RAMCES, ICOS) allow to estimate the total CH_4 emissions from regional to global scales and observe the trend of the CH_4 atmospheric mole fraction. As already mentioned (paragraph 1.2), top-down studies allow to determine total CH_4 emissions, while the contribution of individual source categories is more difficult to assess. Thus, using the top-down approach, the source attribution can be significantly imprecise. Measurements of the other species can give additional information, which allows to distinguish the CH_4 sources (Saunois et al. 2020; Turner et al. 2019; Nisbet et al. 2019).

Currently, additional tracers (e.g., isotopes, C_2H_6, CO) are increasingly used to find explanations of the observed increase of the atmospheric CH_4 mole fraction since 2007, after almost ten years of stability (e.g. Turner et al. 2019; Nisbet et al. 2019). However, so far conclusions are different depending on the used tracers. Studies based on the isotopic composition ($\delta^{13}CH_4$) suggested that the decrease and a further increase of the biogenic sources are responsible for the stabilization period and the resumed increase of the methane global mole fraction (Nisbet et al. 2016; Schwietzke et al. 2016). Simultaneously, ethane studies suggest the same changes for fossil fuel emissions (Simpson et al. 2012; Haussmann et al. 2016). Eventually, the decrease of the CO suggests that the observed trend can be caused by an increase in both biogenic and fossil fuel emissions, while biomass burning is reduced (Worden et al. 2017). Recent studies of Jackson et al. (2020) suggest increasing emissions

from agriculture and waste sector and fossil fuel sector. In all cases, it highlights the need of effective mitigation action of anthropogenic methane emissions.

1.3.6 Particular role of cities

Cities can be treated as an additional type of anthropogenic CH_4 emissions, which currently is not separated from other categories, neither in bottom-up nor top-down studies. Urban and suburban areas can be treated like a complex ecosystem, where many different sources co-exist for CH_4: oil and natural gas network, heating system, landfills and waste treatment, wastewater and road transport (Gioli et al. 2012; Townsend-Small et al. 2012; Zazzeri et al. 2017).

Cities' and sites' emissions can be broken down in three categories (called "scopes") to better understand emission sources. Scope 1 includes all direct emissions from organization's activities and under their control. Scope 2 represents indirect emissions from generation and purchased energy. Finally, scope 3 represents all indirect emissions, not included in scope 2. Considering scope 1 emission, urban and sub-urban areas contribute from 30% to 40% of anthropogenic greenhouse gas emission, which is affected by the city population as well as consumption patterns and lifestyle (Satterthwaite 2008). In the 1980s, when methane started being measured, cities were estimated to contribute 8%-15% of the total anthropogenic methane sources (Blake et al. 1984).

Nowadays, urban and suburban areas concentrate more than 50% of the global population (Satterthwaite 2008; Duren and Miller 2012). According to the United Nation predictions (2018), the global urban population will double by 2050, compared to the population from 2010, which will cause the creation of new megacities (Duren and Miller 2012). The significant but not well-determined contribution of urban CH_4 to global emissions requires additional attention. In the case of city emissions, relatively big CH_4 emissions (30%-40% of anthropogenic emissions) occur on a small area. Thus, reducing CH_4 emissions in cities can be one of many effective mitigation actions. A few studies (e.g., Townsend-Small et al. 2012; Jackson et al. 2014; McKain et al. 2015; von Fischer et al. 2017; Zazzeri et al. 2017; Xueref-Remy et al. 2019) have been already conducted to characterize city CH_4, mostly in the U.S. and Europe. In the case of different U.S. cities, like Los Angeles, Boston and Washington, the dominant CH_4 sources are leaks of the natural gas distribution network (Townsend-Small et al. 2012; Jackson et al. 2014; McKain et al. 2015). A similar situation has been observed in Florence, Italy (Gioli et al. 2012). However, in the case of Greater London, landfills, and the waste treatment sector are the major sources of CH_4 (Fisher et al. 2006; Zazzeri et al. 2017).

Refining the global methane budget requires to delve further into more detailed regional and sectoral emissions to better quantify individual processes on local to regional scales. Studies of smaller scale emissions bring a broader knowledge about regional variations in CH_4 emissions between countries and decrease sectoral uncertainties. France and Île-de-France region (Paris agglomeration) can be a good candidate to perform such detailed study, as French national and regional inventories are available and some initial studies (Ars 2017; Assan 2017; Xueref-Remy et al. 2019) were previously made in the region. Additionally, different emitters occur in Île-de-France region (e.g. landfills, gas compressor stations, farms) which represent almost all anthropogenic source categories.

1.4 CH_4 national and regional emissions – example of France and Île-de-France region

Nowadays, different inventories are provided to estimated CH_4 emissions on national scales. For example, Emission Database for Global Atmospheric Research (EDGAR) v5.0 inventories provide the evolution of the emissions over time for all world countries. The EDGAR inventories ensure also 0.1°x01° grid maps representing emission sources. Based on EDGAR v5.0 inventories (Crippa et al. 2019), in 2015, total French CH_4 emissions were equal to 2616 kt CH_4 yr^{-1}. For the same period, the French national inventory Centre Interprofessionel Technique d'Etudes de la Pollution Atmospherique (CITEPA) reported 2263 kt CH_4 yr^{-1} (CITEPA, 2019). Both inventories show a decrease in emissions over time. According to EDGAR inventories, from 1990 to 2015, the emissions are 684 kt smaller, while for CITEPA inventories, it decreases by 509 kt. For both inventories, the agriculture sector plays a dominant role and reaches 65% and 69% for EDGAR and CITEPA, respectively, in 2015. Waste management sector contributes 20.7% for EDGAR inventories and 21.3% in CITEPA inventories. In EDGAR inventories, the oil and natural gas sector represents 6% of the total emissions. For CITEPA inventories, these emissions are included in the energy transformation sector, which, according to these inventories, contribute to 2.2% of total French emissions. A similar contribution of public transportation is determined for both inventories: 0.28% (EDGAR) and 0.26% (CITEPA). The CITEPA inventory uses a category for residential and tertiary where the biggest contribution comes from the heating/cooling system. Emissions from residential and tertiary sectors represents 5.6% of total emissions. EDGAR inventories do not provide this category. Figure 1.4 presents the sector contribution to French emissions from CITEPA inventories.

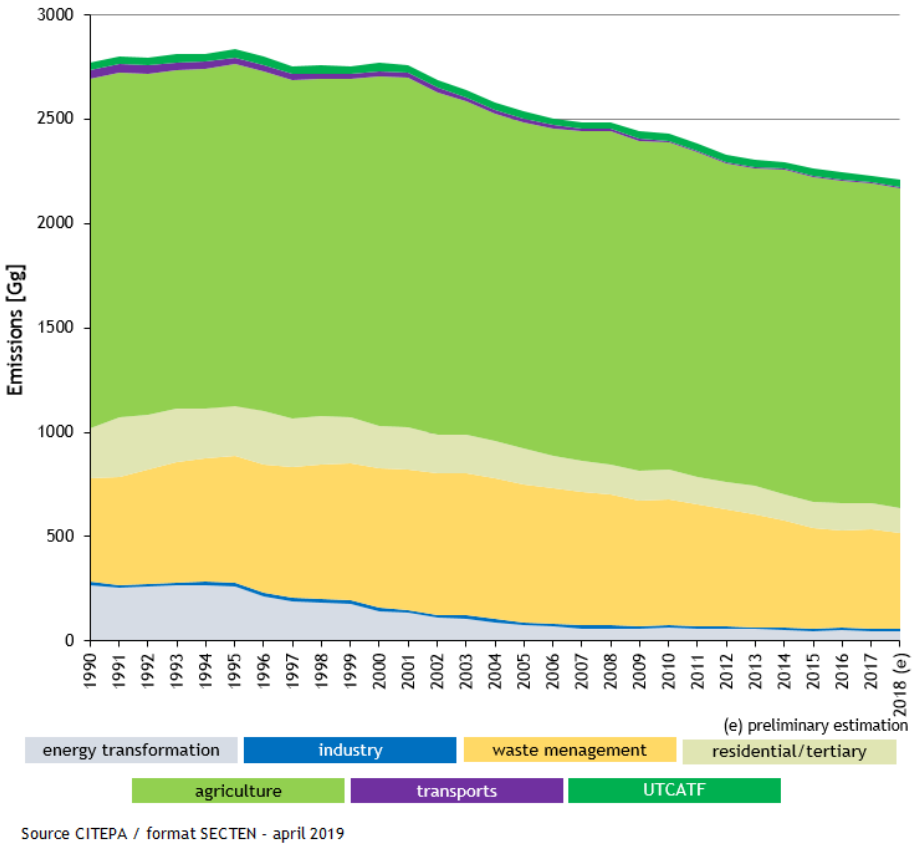

Figure 1.4 From CITEPA, 2019: Evolution of the CH_4 emissions in Metropolitan France since 1990.

Going from national to regional scale, to the most populated French region, Île-de-France (IDF), the Air Quality network of Île-de-France (AIRPARIF) monitors the concentration of pollutants at about 50 stations. It provides emission inventories of the region, using a bottom-up approach. In 2015, the total CH_4 emissions in IDF region was equal to 30 kt CH_4 yr^{-1}, which is 1.3% of total French methane emissions (comparing to the national CITEPA inventory). Île-de-France offers a large ensemble of facilities emitting methane covering different sources (e.g., farms, landfills, wastewater treatment plants, gas storage and compressors) in a relatively small area (12 000 km^2). Compared to the year 2000, regional emissions decreased by about 48%, where the biggest drop comes from the waste management sector (~45%). In 2015, the biggest contribution came from the waste treatment sector (42%) and the sector of extraction, transformation, and distribution of energy (31%) (AIRPARIF 2018).

Additionally, residential and tertiary sectors contributed 13% of total methane emissions in IDF region, which is mostly connected with the heating system (AIRPARIF 2013). It is worth to note that although on the national scale, agriculture contributes to the majority of CH_4 emissions (69%, CITEPA), in IDF region, it reaches only 9%. The sectoral contribution of the CH_4 emissions in IDF region for the year 2015 is presented in figure 1.5.

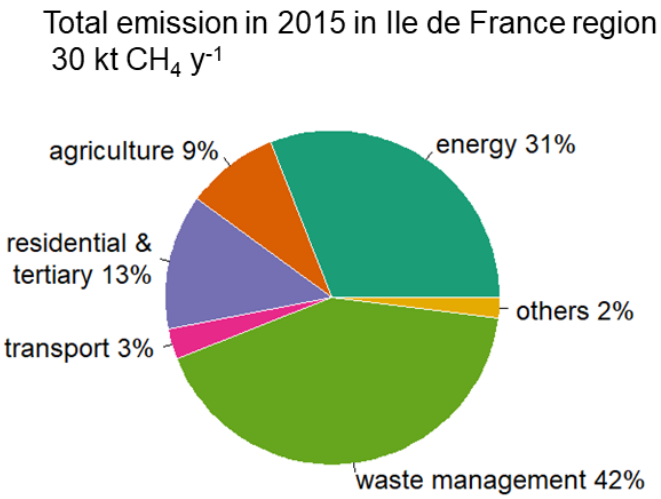

Figure 1.5 Sectoral contribution to IDF region emissions in the year 2015, (AIRPARIF 2018)

Emissions from the waste sector come from household waste through diffusion of the biogas and the incomplete combustion during the flaring of the biogas. According to French legislation, facilities to capture biogas should be installed on landfills and then capture biogas that can be further used to produce energy. However, part of the captured biogas is flared instead of exploited. The flaring process is not strictly controlled by the law. Additionally, leaking emissions of biogas can also occur on landfills (Xueref-Remy et al. 2019). Most of the waste management facilities report their emissions, and they are taken directly into account into inventories. For the others, the emissions are estimated based on their waste tonnage and the activity factor provided by CITEPA. Based on the inventories for the year 2010, 9 landfills contribute to the majority (93%) of the emissions from the waste treatment sector in IDF (Xueref-Remy et al. 2019).

In the AIRPARIF inventories, for the year 2010 and 2015, the wastewater sector was not considered. However, based on personal communication with AIRPARIF, Xueref-Remy et al. (2019) reported that for 2010, the emissions from WWTP in Achères was equal to 66 t CH_4 yr^{-1}. However, as

the WWTP situated in Achères is the biggest WWTP in Europe and second worldwide, the inventory estimation seems indeed to be underestimated. More, previous studies (Ars 2017), estimated the emissions coming from the sludge treatment of this site about 123 kg CH_4 h^{-1} (1000 t CH_4 yr^{-1}) using tracer release method. The same study estimated emissions rate from another smaller WWTP situated in IDF at about 158 t CH_4 yr^{-1}. In total, 5 WWTPs are situated in IDF, and their emissions are not determined in the official AIRPARIF inventory. Additionally, AIRPARIF inventories do not account for the possible emissions from the sewage network in cities (AIRPARIF 2013; Xueref-Remy et al. 2019).

In 2015, the energy sector in IDF contributed 9.3 kt CH_4 yr^{-1}, while in 2010 this sector contributed 10.4 kt CH_4 yr^{-1}. For 2010, where more detailed information is available, emissions from the leaks of natural gas distribution networks account for most of the emissions from this sector (88%) (AIRPARIF 2013). These emissions are calculated based on the length and the material of the natural gas pipelines. As the length of the natural gas network in the IDF region is not available, AIRPARIF provides estimations using the length of the national network and the gas consumption rate on the national and regional scale. In the next step, the national scale activity factor, provided by CITEPA, is used. Afterward, the emissions are spatialized for each municipality as a function of the gas consumption for an individual municipality. The downscaling from the national to regional scale can conduct to overestimation/underestimation. Thus, these estimations are burdened with error and should be verified by additional independent measurements.

The remaining part of the emissions in the energy sector in the IDF region was equal to 1.3 kt CH_4 yr^{-1} in 2010. These emissions come from the thermal power station, refinery, and gas compressors. AIRPARIF inventories do not provide the individual contribution of these three sources to the CH_4 emissions in the region. In these inventories, emissions from the city heat network are placed in the residential and tertiary sectors.

Emissions in the residential and territory sector is mostly connected with the heating/cooling system, cooking, water heating. This sector reached 3.9 kt CH_4 yr^{-1} in 2015. Both in 2010 and 2015, residential and territory sector contributed 13% of total CH_4 emissions. For this sector, in 2010, the combustion of natural gas contributed 24% of residential and territory CH_4 emissions in the IDF region, where the wood combustion approached 60%. Also, the emissions from the city heating network is included. 71% of the heat in this network came from natural gas in 2010.

1.5 Mitigation action in Île-de-France region

Knowing the main CH_4 sources helps to conduct more efficient and reliable mitigation actions. Reductions of methane emissions are necessary to achieve the goal of the Paris Agreement (an increase of the global temperature limited to 2°C) (Nisbet et al. 2019). For the IDF region, the plan *Schema Regional du Climat, de l'Air et de l'Energie de l'Île-de-France* (SRCAE 2012) is planning to reduce greenhouse gases emissions by a factor 4 by 2050 (compared to 1990). This plan implements the European Union's plan "3x20" (20% reduction of greenhouse gases, 20% reusable energy in mixed sources energy and increase of 20% in energy efficiency) in Horizon 2020, compared to the year 2005. This document, as well as the Contrat de Plan Etat-Region 2015-2020 Île-de-France (CPER 2017), assumes an increase of urban heating network users (+40%) and increases from 30% to 50% participation of the renewable energy in the heating network. It also implies the multiplication by 7 of

the biogas production and the progressive decrease of fuel oil, liquefied petroleum gas and coal use (SRCAE 2012; CPER 2017).

The creation of the methanization infrastructure can be one of the examples of mitigation action being in progress. According to SRCAE (2012), in 2030, the biogas should represent 14% of the renewable energy, which is produced in the IDF region. To achieve this goal, about 240 facilities of methanization must be situated in this region and properly managed to avoid gas leaks. In 2018, only 23 facilities already existed. Eleven of them are situated in agriculture sites, and 9 of them are situated in wastewater treatment plants. Produced biogas will be used to provide electricity and heat and also to replace the natural gas, both in the natural gas distribution network and in the vehicles using natural gas (I.A.U 2019).

In the case of the natural gas value chain, in France, GRTgaz company is responsible for the transmission system in almost all territory of Metropolitan France (excluding the South-West part of the country). 40% of the gas imported to France comes from Norway, and 26% comes from Russia. The operator company owns 26 compressor station, with 3 of them situated in IDF region. From the perspective of the year 2020, the company wants to reduce the methane emissions by a factor of 3 (compare to 2016) (GIE and MARCOGAZ 2019; GRTgaz 2019). Additionally, GRTgaz works on the development of installation to inject the biogas to the already existing natural gas facilities.

In the case of the distribution network, the operator company (GRDF) systematically monitors the natural gas distribution network. Studies are made in two ways: pedestrian or vehicular method, depending on the possibility to access the area by car. The frequency of revisiting varies from 4 months to 4 years, depending on the class of the pipeline. The planned annual controlled length is about 90 000 km, while the total operator network is about 200 000 km in France. After leak observation, the leak is classified depending on the repair urgency, then repaired and considered in the GRDF methane emissions evaluation (GIE and MARCOGAZ 2019). The length of the distribution network in the IDF region is not available (AIRPARIF, 2013). However, in Paris city, the length of the distribution network is about 2 000 km, and it serves more than 40 000 buildings and almost all streets. (Le Figaro 2019; La Tribune 2019). Annually, 40 km of the pipelines are repaired in Paris (La Tribune 2019; GRDF on Twitter 2019).

Paris city created a more ambitious plan of reducing greenhouse gases emissions (le Plan Climat Air Energie PCAE 2018) than the IDF region (SRCAE 2012). According to *le Plan Climat Air Energie*, Paris aims to become a "carbon neutral" city in 2050. The first mitigation actions in Paris city allowed decreasing by 10% of the city's carbon emissions over the period 2004-2014 (PCAE 2018). This limitation of greenhouse gas emissions was mostly due to efforts in schools, thermal installations and public lighting renovations and also to the creation of solar panel energy systems and the reduction of diesel car amount inside the city (PCAE 2018). This plan also established a goal of a 25% reduction of emissions and consumption of energy. At the same time perspective, it assumed a 25% contribution to renewable energy.

Both at the regional and city scale, planned mitigation actions consider all greenhouse gases. However, most of the actions are focused on the reduction of CO_2 emissions. The potential possible impact of taken action for mitigating CH_4 emissions is not described. Also, the possible influence of the sewage sector (both wastewater treatment plants and sewage city networks) is omitted in these plans. Aligning region’s and city's ambition for emissions reduction with manageable actions requires the ability to measure the distribution of the emissions and eventually to monitor the actual

implementation of emissions reduction. Such measurements need to be mobile to be able to track plumes emitted by the different anthropogenic sources of methane from site scale to city scale.

1.6 A key role of local mobile measurements

Local mobile measurements can give additional, independent information complementary to other (mostly fixed) observation systems, especially on sites where methane emissions are significant but not very well known. The development of fast sensors based on laser technologies allows delivering mobile and accurate observations of methane concentrations in many experimental conditions (Rella et al. 2015). Combined methane mobile measurements with observations of tracers (e.g., $\delta^{13}CH_4$ or ethane to methane ratio) allow determining the source of observed CH_4 mole fraction enhancement (Lopez et al. 2017; Zazzeri et al. 2015; Hoheisel et al. 2019; Lowry et al. 2020). Moreover, using tracer dispersion method or small scale models (e.g., Gaussian plume models) allows to determine the emission rate of emitted grams per second of CH_4 from the different methane sources like landfills, WWTP or natural gas and oil facilities (Ars et al. 2017; Roscioli et al. 2015; Yver Kwok et al. 2015).

To use the tracer dispersion method, another tracer gas with known release rate is emitted. The tracer gas is assumed to disperse in the same way as methane over the measurement period. Then, concentrations of methane and tracer gas are measured downwind from the source multiple times. Using proportion, methane emission rate can be calculated (e.g., Lamb et al. 1995; Mønster et al. 2014; Yver Kwok et al. 2015; Ars et al. 2017). In some cases, it is not possible to use the tracer dispersion method, for example when access to site is limited. Then small scale models, like Gaussian plume models can be used to estimate emission rate from the site. The emission rate is estimated based on concentration measured downwind from the source, source information (e.g., location and dimensions) and meteorological conditions controlling the atmospheric dispersion. Gaussian models have been already used on industrial sites, for example on natural gas facilities (Roscioli et al. 2015; Yacovitch et al. 2015; Rella et al. 2015).

Also, mobile measurements allowed to observe and estimate emission rates from super-emitters and showed their crucial role in their potential mitigation action (Zavala-Araiza et al. 2015; Alvarez et al. 2018; Duren et al. 2019). In the case of city scale CH_4 observation, mobile measurements conducted in U.S. cities allowed to determinate the leak rate of natural gas distribution systems (Lamb et al. 2016; von Fischer et al. 2017). Moreover, combining mobile measurements with isotopic sampling makes it possible to find the location of methane emissions in an urban environment (Lowry et al. 2001; Zazzeri et al. 2017).

Currently, different projects and initiatives are implemented globally and regionally to measure methane emissions from site to city scale. For example, Climate and Clean Air Coalition (CCAC) (2020) Methane Science Studies aims to improve understanding of the methane emissions from the oil and gas sector. To achieve this goal, a series of peer-reviewed scientific studies are sponsored. These studies help to guide policy and mitigation actions. CCAC Methane Studies provides a project to survey methane emissions from transmission and distribution natural gas infrastructure near urban areas. This project allows to broaden the knowledge about the European CH_4 emissions from this sector. The LSCE laboratory is one of the collaborators of this project, and activities conducted by the LSCE are focused on methane measurements in IDF region. These measurements aim of providing a

cartography of atmospheric methane in Paris and estimations of methane emissions from mid-stream natural gas infrastructure (gas compressor station) in the IDF region.

MEMO^2: MEthane goes MObile- MEasuremnts and MOdeling is another example of scientific collaboration to determine the methane emissions from local to European scale (https://h2020-memo2.eu). The goal of the project is to develop and implement mobile measurements and modeling systems for policy-relevant emissions estimation. It is achieved through European Union research and training collaboration between academic and non-academic partners. The project is focused on the European CH_4 emissions as methane is the biggest contributor to European global warming impact. At the same time, European methane emissions are still not well quantified. The MEMO^2 project is concentrated on the local and regional scale to fill the gap between bottom-up and top-down studies. This collaboration based on the work of 13 Ph.D. candidates in 7 countries. My Ph.D. study is one of them, and it concerns characterizing methane emissions in urban and industrial environments.

1.7 Thesis objectives

Merging the goals of the CCAC Methane studies and MEMO^2 collaboration, the main purpose of my PhD study is to characterize the spatio – temporal variations of mole fraction and isotopic signature of CH_4 in Île-de-France (IDF) region and to infer from that, methane emissions from site to city scale. The main approach to achieve this goal is the design, realization and analysis of field campaigns, taking benefit of laser-based continuous and mobile instruments. The chosen strategy leads to atmospheric methane characterization followed by emission estimations using tracer dispersion method and modeling tools. The study is conducted at city and site scale, as small scale measurements play a key role to explain sectoral uncertainties and can help improve methane regional budget. This objective is a necessary and important step to improve estimates of methane sources in the IDF region. As a consequence, these objectives aim of contributing to the improvement of emission inventories, to gap reduction between top-down and bottom-up studies and to give insights to design more efficient mitigation actions.

At the site scale, some previous studies (Assan 2017; Ars et al. 2017; Xueref-Remy et al. 2019) in this region were already focused on landfill, WWTP or farm. Thus, my study is mostly concentrated on natural gas, although original isotopic data for landfills are also presented as an addition to previous studies. To extend knowledge about emissions from the midstream natural gas infrastructure, mobile measurements were conducted on three gas compressor stations. Measurements were conducted more frequently on the compressor station with the biggest amount of the operating hours. This part of the study allowed estimating the emission rate and to determine the isotopic signature and ethane to methane ratio of gas compressor stations in IDF region. It also leads to a cooperation with the gas compressor station company, giving me useful insight into my results.

At the city scale, the methane spatial distribution in Paris was determined. This part of the studies was mostly focused on the estimation of emissions from the natural gas distribution network (downstream infrastructure). However, as a city is a complex methane source, mobile CH_4 measurements, combined with the determination of isotopic signature, allowed to verify the presence of other methane sources in Paris. So far, CH_4 emissions from European cities remain poorly determined. Therefore, presented studies fill a gap in the cartography of the European city CH_4 emissions.

The manuscript is divided into two parts. The first part describes the instrument specification and the performed tests. Chapter 2 details the laboratory tests of the Cavity Ring-Down Spectroscopy (CRDS) instrument and the mobile set-up deployed the study. Results presented in this chapter concern measurements of CH_4 mole fraction and $\delta^{13}CH_4$ isotopic composition. Chapter 3 presents the possibility and limitation of using the CRDS G2201-i instrument to determine ethane to methane ratio in field conditions during in-situ mobile measurements. Analyses showed in chapter 3 are merged with the article published in discussion in a peer-reviewed journal (doi.org/10.5194/amt-2020-410).

The second part of the thesis describes the results of the mobile surveys performed at site and city scales. Studies made in Paris city are presented in chapter 4. Results obtained in Paris are compared with other cities, and possible mitigation actions in the city are discussed. Paris studies are presented in an article in the revision phase in peer-reviewed journal. Chapter 5 presents the results obtained at the site scale. First, a controlled release experiment is described, which allowed verifying possibility of using modeling tool to estimate emission rate on site scale. Based on multiple transects made downwind from known source, Gaussian model in the Polyphemus platform (Mallet et al. 2007) was used to estimate the emission rates. Then, results of the mobile measurements made on the gas compressor stations are presented, including isotopic signature (both $\delta^{13}CH_4$ and δ_DCH_4), ethane to methane ratio and emissions estimation. Finally, isotopic measurements from landfills and comparison with previous studies in IDF region are concluding chapter 5.

Finally, chapter 6 summarizes my findings and provide an outlook into the possible future of my work.

Chapter 2
Instrument performance in laboratory and field conditions

As highlighted in the previous chapter, local mobile measurements can help fill the gap between top-down and bottom-up studies. They allow to understand better the methane budget and to find the main emitters on a small scale. However, to achieve this goal, precise and sensitive instruments, usable in motion in the field, are required. Currently, numerous instruments for precise continuous CH_4 measurements are available, while part of them can be used during mobile measurements, onboard of car or aircraft. Over last years, successful mobile measurements (e.g., Rella et al. 2015; Lopez et al. 2017; Hoheisel et al. 2019; Xueref-Remy et al. 2019) were made using optical analyzers based on Cavity Ring-Down Spectroscopy (CRDS). In my Ph.D., I used this type of analyzers as well, mostly CRDS Picarro G2201-i (Picarro, Inc. Santa Clara, CA). This instrument model is dedicated to the measurements of CH_4 and CO_2 and their stable carbon isotopes.

The main goal of my study is the determination of source isotopic signature and emission rate. In this chapter, I present the results from the intensive tests I have performed in the laboratory and in the field to characterize and improve my measurement set-up. First, instrument tests were performed in the laboratory. They allowed determining different instrument parameters (e.g., continuous measurements repeatability, Allan deviation). The influence of outside conditions such as pressure and temperature was also verified. During the two-year period of intensive surveys, I calibrated the instrument five times for CH_4 mixing ratio and four times for $\delta^{13}CH_4$ signature. Additionally, over three nights, simultaneous measurements of $\delta^{13}CH_4$ were made by CRDS and CF-GC/IRMS (continuous- flow gas chromatography/isotope-ratio mass spectrometry). Finally, five tanks with different isotopic signature were measured. These tanks were prepared within the MEMO^2 project and were circulating between different collaborators to verify CRDS isotopic signatures.

Then, I present the tools and tests necessary to deploy my set-up in the field. The AirCore tool (Karion et al. 2010) was used as a part of the mobile set-up to determine $\delta^{13}CH_4$ signature from in situ mobile measurements. During some surveys, bag samples were taken inside the plume and measured on CF-GC/IRMS at laboratory afterward. Then the results from the two instruments have been compared.

Finally, my set-up was tested during a controlled release experiment. The experiment allowed to verify the methods used to determine $\delta^{13}CH_4$, C_2H_6:CH_4 ratio and CH_4 emission rate. In this chapter, the verification of $\delta^{13}CH_4$ results from CRDS G2201-i is presented. Measurements of C_2H_6:CH_4 ratio are presented in chapter 3 and estimations of CH_4 emission rate are detailed in chapter 5.

2.1 Principles of cavity ringdown spectroscopy and analyzer description

The CRDS technique uses the laser absorption in a low-loss optical cavity, consisting of at least two high-reflectivity mirrors (typically R > 99.9%). After entering the cavity, the laser beam bounces between the mirrors thousands of times. It steadily loses light intensity in an exponential way during the propagation between the mirrors. The sensitive photodetector measures the time of the laser light decay (also called "ring down"). The presence of absorption gas (e.g., CH_4, H_2O) shortens the decay time (Figure 2.1). Comparison of the decay time of the cavity without and with absorption gas permits to determine the mixing ratio of absorption gas in the measured mixture. Mixing ratio determined in this way does not depend on laser power or intensity fluctuation, which makes the CRDS instruments easier to maintain. Also, it requires easier and rarer calibration procedures than other instruments based on optical techniques. Moreover, this technique allows to conduct highly sensitive measurements down to parts per trillion (Rella et al. 2013). However, the size and shape of spectral lines are function of the pressure and temperature of the sample. Thus the temperature and pressure inside cavity must be controlled and highly stable. Details about this technique can be found in Crosson (2008), Chen et al. (2010; 2013) and Rella and al. (2013; 2015).

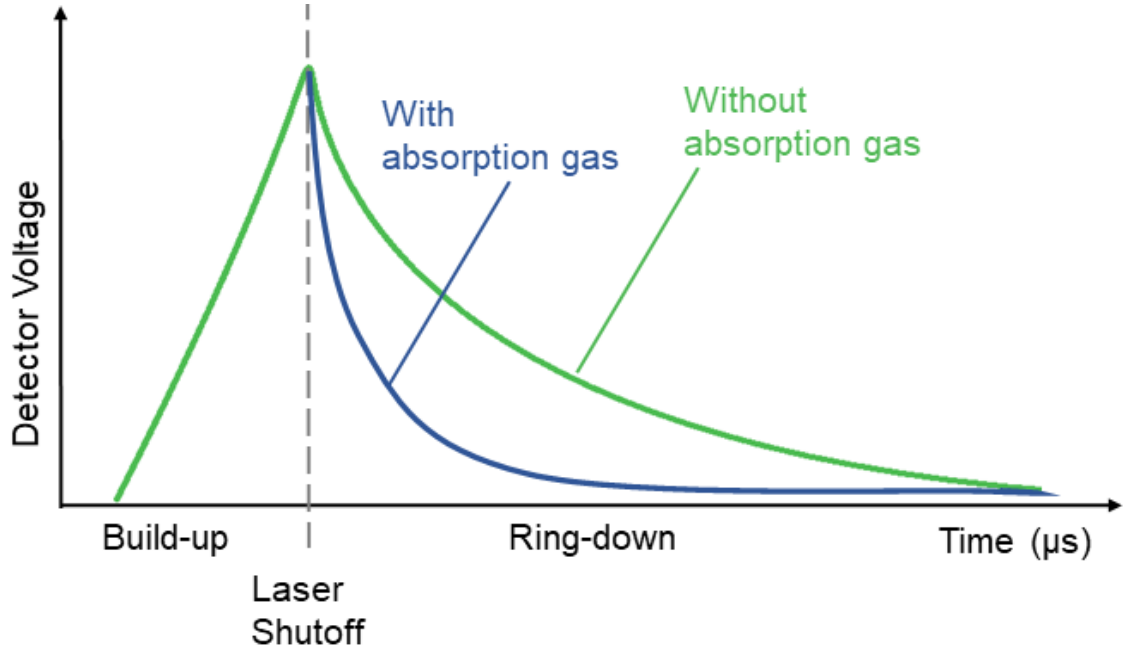

Figure 2.1 Scheme of light intensity decay over time in CRDS analyzer.

CRDS instruments manufactured by Picarro (Picarro, Inc. Santa Clara, CA) are used during this study. They use telecom lasers, which operate in the near-infrared domain. Their optical cavity is built of three high-reflective mirrors, and the cavity volume is less than 10 cm^3. Multiple bounces result in 15 - 20 kilometers of effective path length (Rella et al. 2013; 2015). The temperature and pressure inside the CRDS instrument are permanently stabilized. For example, instrument CRDS G2201-i operates at 45 °C and 148 Torr (Rella et al. 2015). In the CRDS G2201-i, three lasers are used to quantify the mole fraction of the following gases: $^{12}CH_4$ $^{12}CO_2$, $^{13}CH_4$, $^{13}CO_2$, H_2O and C_2H_6. They operate at about 6057 cm^{-1}, 6251 cm^{-1} and 6029 cm^{-1} (Assan et al. 2017). The standard gas flow rate of the instrument

is about 25 sccm (standard cubic centimeters per minute). However, depending on the needs, it can be decreased or increased. Here, the flow rate of the most used instrument (CRDS G2201-i device CFIDS 2072) was increased to 160 sccm for a fast response during mobile measurements and the instrument is used in simultaneous mode, with both CH_4 and CO_2 and their isotopes being measured. In the set-up used in this study, the measurement interval is about 3.7s. Additionally, the instrument can operate in two CH_4 range modes: high precision mode, dedicated to measure in the range 1.8 – 12 ppm and high dynamic range, for measurement between 10 and 500 ppm. Here, data obtained in high precision mode are analyzed. For all measurements, before the instrument inlet, a filter (Swagelok SS-4FW-2, 2 microns) was installed.

2.2 Laboratory tests

2.2.1 Initial test

Following the test protocol of ICOS Atmospheric Thematic Center Metrology laboratory (ATC MLab) (see Yver-Kwok et al. 2015), during Autumn 2017, several laboratory tests were performed on two CRDS G2201-i instruments. They differ in the gas flow rate. It is about 25 sccm for device CFIDS 2067 and about 160 sccm for CFIDS 2072. Provided tests allowed to assess the performance of CRDS CFIDS instrument in laboratory conditions and verify possibility to use them later in mobile, near-source conditions. Tests were made under controlled, repeatability conditions, which stay identical over short period of time.

To conduct experiments, dried or wet ambient air and different tanks filled with ambient dry air were used. For ambient air measurements, an inlet located on the roof of the LSCE building in Gif-sur-Yvette was used. Ambient air was passed through a glass trap placed in an ethanol bath kept at about -70°C to dry the air by using an immersion cooler. A multi-position valve was used to switch automatically from a gas sample to another one. The analyses of the tests use raw data before calibration. Examples of results are presented below.

The following tests were made:

- Continuous measurement repeatability (CMR), often known as precision, to define the closeness of measurements. Here, it is determined as one standard deviation for different averaging times of continuous measurement of the target gas during 24 h,
- Allan deviation to assess instrument stability over integration time and to find the optimal integration time, based on a continuous measurement of the target gas during 24 h,
- Short-term repeatability to verify replication of measured target gas after short break (e.g. to measure ambient air). Test conducted as 10 measurement cycles of 10 minutes target gas alternating with 30 minutes ambient air,
- Long-term repeatability test is similar to short-term repeatability but conducted over extended period of time. Here, test was made for wet air (17 cycles) and for dried air (7 cycles). Both, for wet and dried air, tests were made as 30 minutes measurements of target gas bracketed by 600 minutes ambient air,

- Atmospheric pressure test to verify stability of observed species during changes of outside pressure. Test was based on long-term repeatability, when 15 hPa difference in outside pressure was observed,
- Outside temperature test to verify stability of observed species during changes of room temperature. The room temperature was controlled by air conditioner and reached: 22 °C first day, 18 °C first night and second day, 32 °C second night and third day, 22 °C third night.
- Calibration to report CRDS results in broadly used scales (WMO X2004A for CH_4 and VPDB for $\delta^{13}CH_4$), based on 3 measurement cycles of three calibration gases with different CO_2, CH_4 mole fractions and carbon isotopic compositions.

2.2.1.1 Continuous measurements repeatability

The continuous measurement repeatability (CMR) test, commonly known as precision, has been made by measuring a working gas continuously over 24 hours, and the CMR is calculated as the one standard deviation (SD) over different averaging times (see Yver-Kwok et al., 2015). The CMR improves with increasing averaging times (Figure 2.2, Table 2.1), but even for a short averaging time (10s), the CMR is lower than 1 ppb. Comparing the two instruments, the CMR value for the CH_4 mixing ratio does not change, but in the case of $\delta^{13}CH_4$, it is better for device CFIDS 2072 (higher flow rate), especially for the higher averaging time.

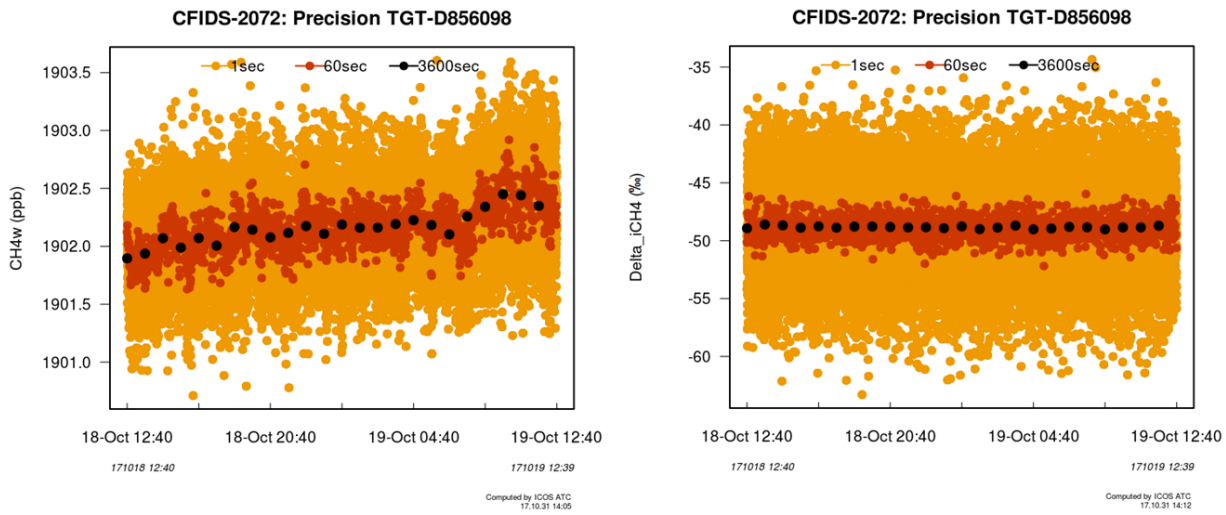

Figure 2.2 CMR test provided for instrument CFIDS 2072. Left: CH_4 mixing ratio [ppb], right: $\delta^{13}CH_4$ isotopic signature [‰].

Table 2.1 CMR test results for CFIDS 2072 and CFIDS 2067

Averaging time	CFIDS 2072		CFIDS 2067	
	CH_4 1σ [ppb]	$\delta^{13}CH_4$ 1σ [‰]	CH_4 1σ [ppb]	$\delta^{13}CH_4$ 1σ [‰]
10 sec	0.27	2.2	0.27	2.7
1 min	0.20	0.9	0.21	1.7
60 min	0.14	0.1	0.14	1.3

2.2.1.2 Allan deviation

Continuous 24 hours measurement of the target gas was also used to determine Allan deviation. This parameter shows the stability as a function of the integration time and informs about the optimal integration time. (Allan 1966). Typically, the Allan deviation decreases with increasing averaging time. However, the time drift of the instrument increases the Allan deviation at longer averaging times.

During the test, the maximum averaging time was equal to 8 hours (Figure 2.3). The Allan deviation achieves smaller values for CFIDS 2072 than for CFIDS 2067 for short averaging time (Table 2.2). Toward longer averaging times, in the case of CH_4 mole fraction, Allan deviation constantly decreases for CFIDS 2067, while for CFIDS 2072, it increases after about 3 hours of averaging and then achieves 0.1 ppb. In the case of $\delta^{13}CH_4$ isotopic signature, both instruments behave in the same way, and the increase of the Allan deviation is not observed, indicating no significant drift of the analyzer over 25 hours of the test.

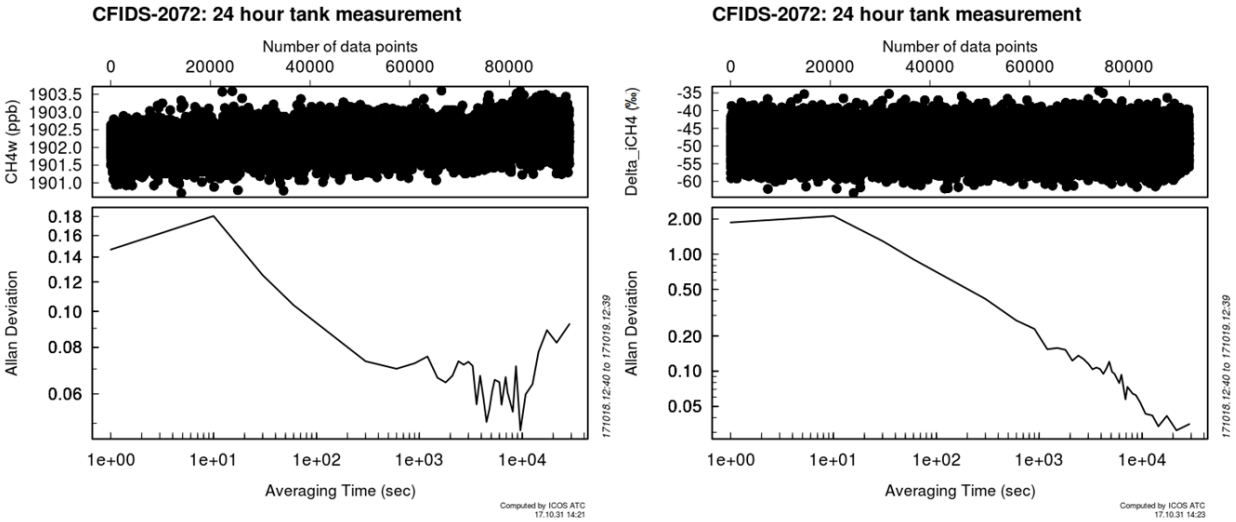

Figure 2.3 Allan deviation for instrument CFIDS 2072. Left: CH_4 mixing ratio [ppb], right: $\delta^{13}CH_4$ isotopic signature [‰].

Table 2.2 Allan deviation results for CFIDS 2072 and CFIDS 2067

Averaging time	CFIDS 2072		CFIDS 2067	
	CH_4 1σ [ppb]	$\delta^{13}CH_4$ 1σ [‰]	CH_4 1σ [ppb]	$\delta^{13}CH_4$ 1σ [‰]
10 sec	0.045	2.1	0.177	2.3
1 min	0.019	0.9	0.010	1.00
60 min	0.003	0.1	0.083	0.3

2.2.1.3 Short-term and long-term repeatability

The short-term test lasts 6 hours with 10 cycles of 10 minutes of target gas bracketed by 30 minutes of wet ambient air measurements. Then, for further analysis, first 20 minute of measurements are discarded to ensure sufficient flushing of the sample cell and the next 9 minutes of each target measurement are analyzed. Short-term repeatability is determined as a mean and standard deviation of these averaged values.

The long-term repeatability test is similar to the short-term repeatability, but it is made on a longer time scale. The target gas was measured 30 minutes bracketed by about 10 hours ambient air. The long-term repeatability test was repeated twice. 17 cycles were made with wet ambient air brackets and 7 cycles with dry ambient air brackets. The last 10 minutes of target measurements were used for further analysis.

Comparing short term repeatability and two long-term repeatability tests (Figure 2.4, Table 2.3), for CFIDS 2072, no significant differences occur for both CH_4 mixing ratio and $\delta^{13}CH_4$ isotopic signature. For CFIDS 2067, the CH_4 mixing ratio is the same for all tests. The $\delta^{13}CH_4$ isotopic signature obtained during long-term repeatability test with dry air brackets differs from values obtained during short-term dry and long-term wet repeatability tests. It is enriched by about 2.2 ‰.

For both instruments, no trends are observed and the short-term and long-term repeatability are below 1 ppb and 1 ‰, which shows the capacity to use these instruments for stable measurements over time.

Table 2.3 Repeatability for CFIDS 2072 and CFIDS 2067

Type of test	CFIDS 2072		CFIDS 2067	
	CH_4 [ppb]	**$\delta^{13}CH_4$ [‰]**	**CH_4 [ppb]**	**$\delta^{13}CH_4$ [‰]**
Short-term dry air	1923.99 ± 0.14	-48.71 ± 0.33	1924.827 ± 0.069	-50.57 ± 0.43
Long-term wet air	1923.73 ± 0.26	-49.07 ± 0.43	1924.74 ± 0.16	-50.64 ± 0.77
Long-term dry air	1924.44 ± 0.26	-48.77 ± 0.15	1925.18 ± 0.15	-48.37 ± 0.76

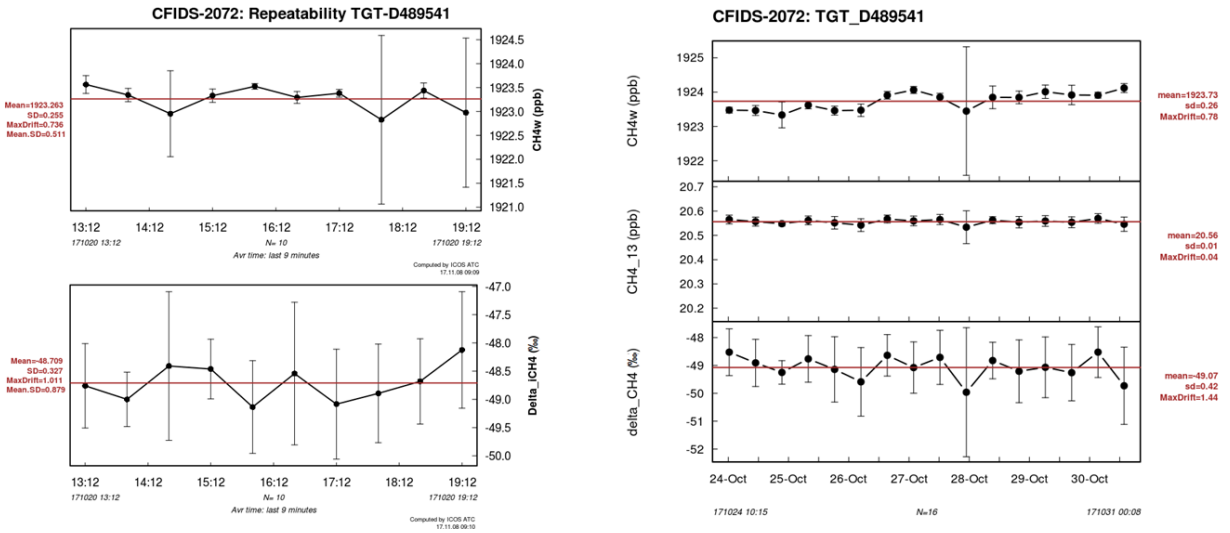

Figure 2.4 Repeatability for instrument CFIDS 2072. Left: short-term repeatability, right: long-term repeatability. Top: CH_4 mixing ratio [ppb], bottom: $\delta^{13}CH_4$ [‰].

2.2.1.4 Ambient pressure and temperature dependence

The pressure and temperature of the sample gas affect the relation between the observed laser light line intensity and the calculated mixing ratio using the CRDS technique. Due to that, the pressure and temperature should be controlled inside the instrument and resistant to outside changing conditions. The target gas measurements from long–term repeatability were plotted against the

ambient pressure, and the correlation was evaluated. Thanks to it, the ambient pressure influence was verified. In the case of the temperature dependence test, the room temperature was changed for a few hours using the air conditioner. During the test, it was equal to 18, 22 or 32 °C. Then, as in the case of pressure dependence, the correlation was evaluated.

Both instruments show no dependence on the pressure and temperature, both for CH_4 mixing ratio and $\delta^{13}CH_4$ isotopic signature. In all cases, the correlation coefficient r^2 is smaller than 0.2, thus pressure and temperature changes are assumed to have no significant impact for observed CH_4 mixing ratio and $\delta^{13}CH_4$ isotopic signature.

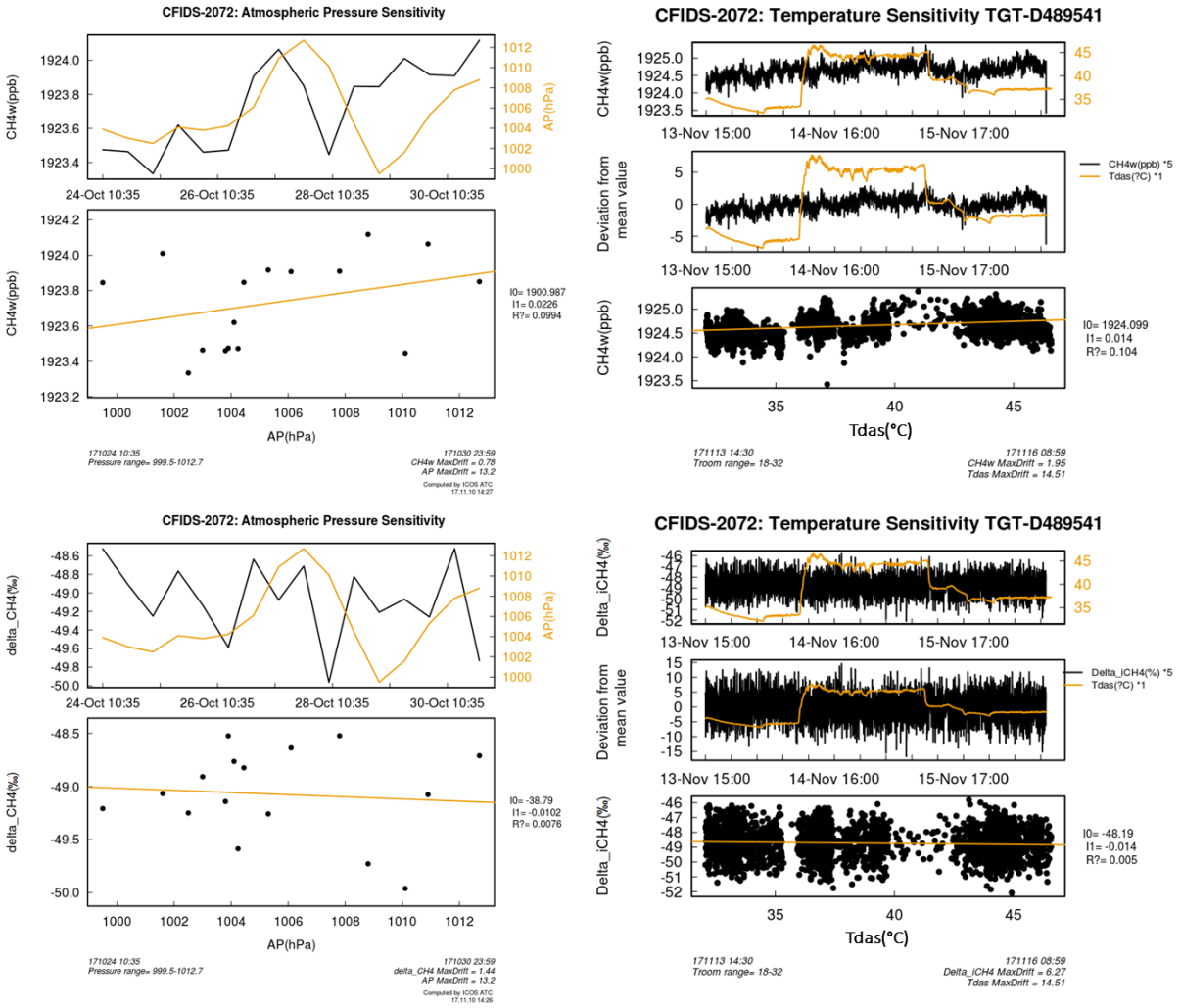

Figure 2.5 Ambient pressure and temperature dependence for instrument CFIDS 2072. Left: pressure dependence, Right: temperature dependence. Top: CH_4 mixing ratio [ppb], bottom: $\delta^{13}CH_4$ [‰].

Table 2.4 Ambient pressure and temperature dependence CH_4 mixing ratio and $\delta^{13}CH_4$ isotopic signature for CFIDS 2072 and CFIDS 2067

Test	CFIDS 2072		CFIDS 2067	
	CH_4 [ppb]	**$\delta^{13}CH_4$ [‰]**	**CH_4 [ppb]**	**$\delta^{13}CH_4$ [‰]**
Pressure test	0.022 ppb/hPa	-0.010 ‰/hPa	0.0007 ppb/hPa	-0.75 ‰/hPa
Temperature test	0.014 ppb/°C	-0.014 ‰/°C	0.002 ppb/°C	0.008 ‰/°C

2.2.1.5 Calibration

The calibration test determines the necessary correction to obtain accurate CH_4 mixing ratio and $\delta^{13}CH_4$ that are traceable to the international scale (WMO X2004A for CH_4 and VPDB for $\delta^{13}CH_4$). A three-point calibration was made, both for CH_4 mixing ratio and $\delta^{13}CH_4$ isotopic signature. Each target was measured 30 minutes, and the last 10 minutes were used for further analysis. Over 2 years, this three-point calibration was repeated four times for CFIDS 2072. Additionally, a two-point calibration was made once with lower and higher mixing ratios, only for the CH_4 mole fraction for the same instrument. The calibration factors are calculated as slope and intercept of the linear fitting, while x-axis represents reference target values, and y-axis represents measured values.

The determined calibration factors did not change significantly over time (Table 2.5). After the application of calibration factors, the residuals from the fit are smaller than 1 ppb for CH_4 and 0.5 ‰ for $\delta^{13}CH_4$ (Figure 2.6). It also shows the negligible role of the long term drift in the instrument.

Here, the calibration was made only until 3000 ppb of CH_4 mixing ratio. Likely, during near-source mobile measurements observed CH_4 mixing ratio can be higher than this value. Based on factory tests, manufacturer guarantee instrument performance between 1800 and 12000 ppb in high precision mode and between 10 000 and 500 000 ppb in high dynamic range mode. The calibration is made in high precision mode and it is assumed to stay stable until 12000 ppb. However, in the future, calibration should be extended with larger CH_4 mixing ratio.

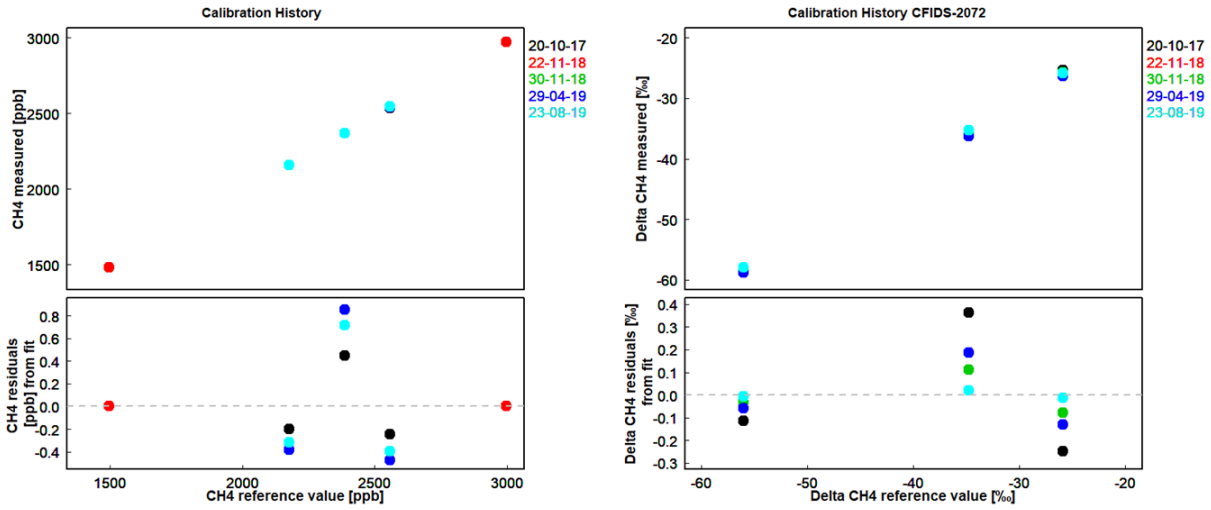

Figure 2.6 The calibration history for CFIDS 2072 over two years. Left: CH_4 mixing ratio [ppb], right: $\delta^{13}CH_4$ [‰].

Table 2.5 Linear regression coefficients of calibration test calculated for CFIDS 2072

	CH_4 [ppb]		$\delta^{13}CH_4$ [‰]		
date	**slope**	**intercept**	**slope**	**intercept**	**comment**
20-10-2017	1.00	14.51	0.91	-2.48	3 points
22-11-2018	1.01	6.33	NaN	Nan	2 points
30-11-2018	0.99	46.41	0.92	-2.26	3 points
29-04-2019	0.99	44.68	0.93	-1.17	3 points
23-08-2019	0.99	41.88	0.94	-1.61	3 points

2.2.1.6 C_2H_6 correction for $\delta^{13}CH_4$

Previous studies (e.g., Rella et al. 2015; Assan et al. 2017) have shown significant cross sensitivities between C_2H_6 and $\delta^{13}CH_4$ in the absorption spectrum around 6029 cm^{-1} wavenumber region (Figure 2.7) . Whereas ethane is one of the most important components of natural gas and can range from 1.5% to 9% (Ortech Report No. 26392, 2017), it can have a significant influence on the measurement of methane isotopic signature. As a result, C_2H_6 correction on $\delta^{13}CH_4$ should be applied. It is worth noting that before applying C_2H_6 correction on $\delta^{13}CH_4$, C_2H_6 mixing ratio must be first corrected due to the interference with other species (CO_2, $^{12}CH_4$ and H_2O) and also calibrated to the commonly used scale (Assan et al. 2017). Also, $\delta^{13}CH_4$ must be calibrated before applying the C_2H_6 correction.

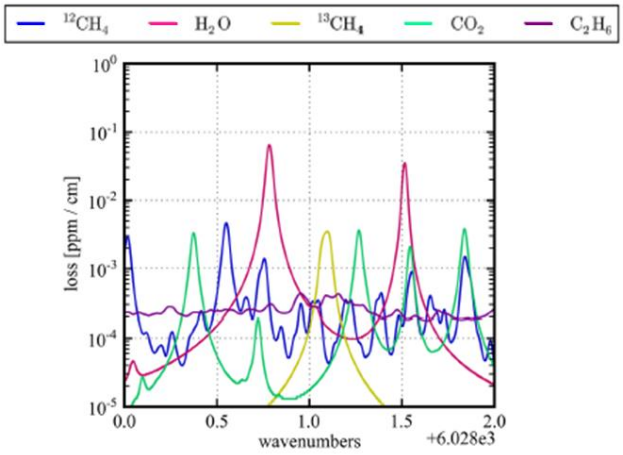

Figure 2.7 From Rella et al. 2015: Spectra of key species in the frequency ranges employed in the spectrometer, displaying loss on a log scale vs. optical frequency in wavenumbers for the low-frequency region (around 6029cm^{-1})

Ethane distorts measured absorption spectrum, which propagates to an error in $\delta^{13}CH_4$ measurements. The effect is proportional to C_2H_6 mixing ratio in measured samples and inversely proportional to CH_4 mixing ratio in the sample. This effect can be quantified using linear regression between $\delta^{13}CH_4$ and C_2H_6:CH_4 ratio. Previously, Rella et al. (2015) evaluated that C_2H_6 presence shifts higher $\delta^{13}CH_4$ by 35 ‰ppm CH_4(ppm C_2H_6)$^{-1}$. The same correction factor was used by Lopez et al. (2017). In the case of the study made by Lopez et al. (2017), due to the high instrument noise for C_2H_6 measurements, this correction was systematically applied only when C_2H_6 mixing ratio exceeded 200 ppb. Assan et al. (2017) also determined this correction factor. In this case, C_2H_6 impact was smaller than in the study of Rella et al. (2015). It enriched $\delta^{13}CH_4$ by 23 ‰ppm CH_4(ppm C_2H_6)$^{-1}$. In the case of the Assan et al. (2017) study, the C_2H_6 mixing ratio was primarily corrected and calibrated before applying its correction on $\delta^{13}CH_4$.

Here, I used the same devices (CFIDS 2072 and CFIDS 2067) as during the study of Assan et al. (2017). Thus, the correction factor was recalculated to check the possible time drift of these previously determined values. To determine C_2H_6 correction for $\delta^{13}CH_4$, I rebuilt the instrumentation set-up used in Assan et al. (2017) (Figure 2.8) and I repeated the linearity test with increasing C_2H_6:CH_4 ratio. During test, $\delta^{13}CH_4$ remained constant. Here, a working gas with an ethane mixing ratio of ~50 ppm is mixed with the dilution gas via two mass flow controllers (MFC). In the set-up, the flow rate of the measured gas is greater than the instrument's inlet allowance. Thus, an open split is installed before the analyzer

to vent the mixture and maintain an ambient pressure at the instrument inlet. The ethane is diluted with the dilution gas in different proportion gradually, going from 1.0 to 0.0 C_2H_6:CH_4 ratio. Then $\delta^{13}CH_4$ is measured. The correction is calculated as a linear fitting, with the x-axis representing C_2H_6:CH_4, and the y-axis representing the reported difference in $\delta^{13}CH_4$ (Figure 2.9). This linearity test was repeated twice: in January 2018 and April 2019. The central 15 minutes of each 20-minute measurement step were kept for further analysis.

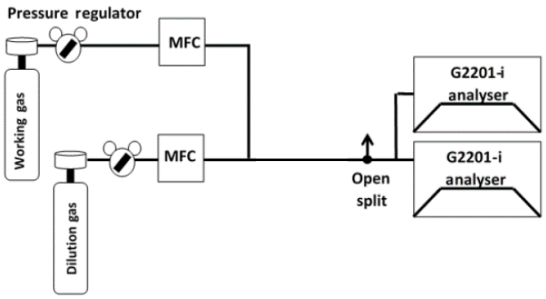

Figure 2.8 From Assan et al. 2017: Set-up used to determine C_2H_6 correction for $\delta^{13}CH_4$

Over 4 years, the correction factors did not change for both instruments (Table 2.6). For both instruments, the correction factor is about 24 ‰ppm CH_4(ppm C_2H_6)$^{-1}$. Both C_2H_6 correction for $\delta^{13}CH_4$ and CH_4 and $\delta^{13}CH_4$ calibration factors are stable over 2 years. As a consequence, calculated once, they can be used for a long time, and there is no need to repeat these tests frequently.

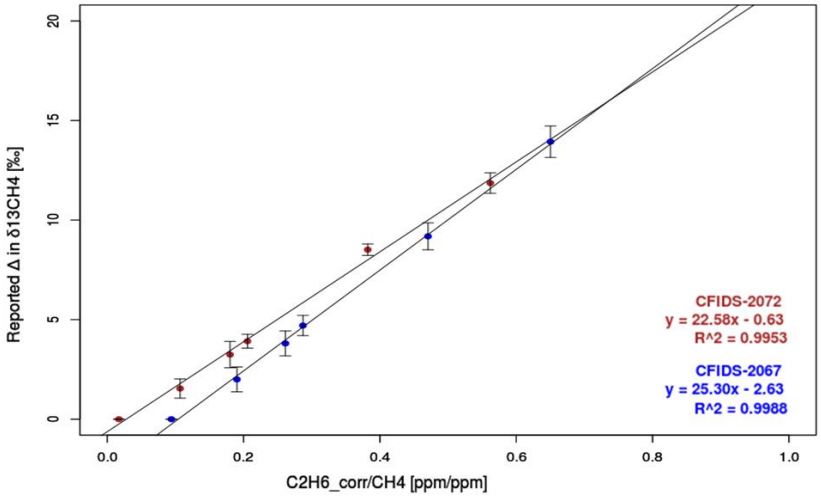

Figure 2.9 The effect of C_2H_6 on reported $\delta^{13}CH_4$.

Table 2.6 Linear regression coefficients calculated for C_2H_6 correction for $\delta^{13}CH_4$

$\delta^{13}CH_4$ Correction	CFIDS 2072		CFIDS 2067		References
	Slope (‰ CH_4/C_2H_6)	Intercept (‰)	Slope (‰ CH_4/C_2H_6)	Intercept (‰)	
July 2015	24 ± 2	0.5 ± 0.6	-	-	Assan et al. 2017
November 2015	23 ± 1	0.2 ± 0.6	23 ± 1	-2.3 ± 0.7	Assan et al. 2017
January 2018	23 ± 1	-0.6 ± 0.2	25 ± 1	-2.6 ± 0.2	This study
April 2019	24 ± 1	-0.3 ±0.2	25 ± 1	-3.1 ± 0.2	This study

2.2.1.7 Initial test - summary

Laboratory tests described above showed that CRDS G2201-i is adaptable for mobile measurements of CH_4 in near-source conditions, as typically, the CH_4 mixing ratio inside the pollution plume is higher than 100 ppb above background. Depending on the strength and distance from the source and meteorological conditions as well, the mixing ratio inside the plume can reach a few ppm or even dozens or hundreds of ppm. Thus, the CMR and Allan deviation of about 1 ppb are significant for mobile measurement purpose. The short– and long–term repeatability tests showed a good repeatability of measured values which indicates a good stability of the instrument over different time scales. These features are crucial during mobile measurements as crossing a plume lasts less than one minute, and one plume is crossed multiple times to determine a CH_4 source.

Moreover, long–term repeatability showed the possibility of comparing measurements during different days. The ambient pressure test and outside temperature showed no influence of pressure and temperature changes for CH_4 mixing ratio and $\delta^{13}CH_4$. Moreover, the instrument is situated in the car during mobile measurements made in this study. In these conditions, the temperature does not change rapidly and stays rather stable. Thus the temperature dependency in real field conditions is even smaller than during laboratory test.

The performances determined in this part of study are better for CFIDS 2072 than for CFIDS 2067, both for CH_4 mixing ratio and $\delta^{13}CH_4$ isotopic signature. Additionally, CFIDS 2072 has a bigger flow rate (160 vs. 25 sccm), which leads to a shorter response time of the instrument. As a consequence, CRDS G2201-i CFIDS 2072 was used during mobile measurements. Additional laboratory tests were made to evaluate $\delta^{13}CH_4$ results from CRDS G2201-i device CFIDS 2072 and compare them with results from the IRMS instrument.

2.2.2 $\delta^{13}CH_4$ results from CRDS G2201-i versus IRMS

To evaluate the accuracy of the isotopic measurements, the CRDS G2201-i results are compared with results from continuous-flow gas chromatography/isotope-ratio mass spectrometry (CF-GC/IRMS), further called IRMS. This high-precision instrument allows for the analysis of methane isotopes at ambient air mixing ratio with a CMR of ~0.05‰ (Fisher et al. 2006). This precision is much better than for the CRDS instrument (~2 ‰ in 10 s). Two tests were made to compare CRDS and IRMS results. These two tests were made thanks to collaboration within the MEMO^2 project, as two institutions inside the project own IRMS instruments: Royal Holloway University of London (RHUL) and Utrecht University (UU). The first test was made at RHUL during three nights of continuous, simultaneous measurements, where the inlet of ambient air was shared by CRDS and IRMS instruments. Secondly, five tanks were measured over a short time (~20 minutes). They differed in $\delta^{13}CH_4$ isotopic signature and CH_4 mixing ratio. The second test was part of the MEMO^2 isotopic tanks experiment, and these tanks were measured in different institutions within the project, which own the instrument capable of measuring $\delta^{13}CH_4$ isotopic signature. During the second test, the CRDS values were compared with values from both IRMS instruments.

2.2.2.1 Continuous simultaneous measurements

In summer 2018, the CRDS G2201-i was used during a secondment at RHUL. During three nights, ambient air was measured by CRDS and IRMS simultaneously, from the shared inlet. The instruments inlet was situated at the roof of the university, about 40 km away from London. The IRMS gave one value every 20 minutes. To compare the results, 20 minutes' averages of calibrated CRDS data were calculated. The air was not dried before the CRDS inlet, which can have an impact for C_2H_6 mixing ratio measured by CRDS. However, C_2H_6 mixing ratio was inside instrument noise (details in chapter 3). Thus, the presented $\delta^{13}CH_4$ isotopic signature is only calibrated, without applying C_2H_6 correction.

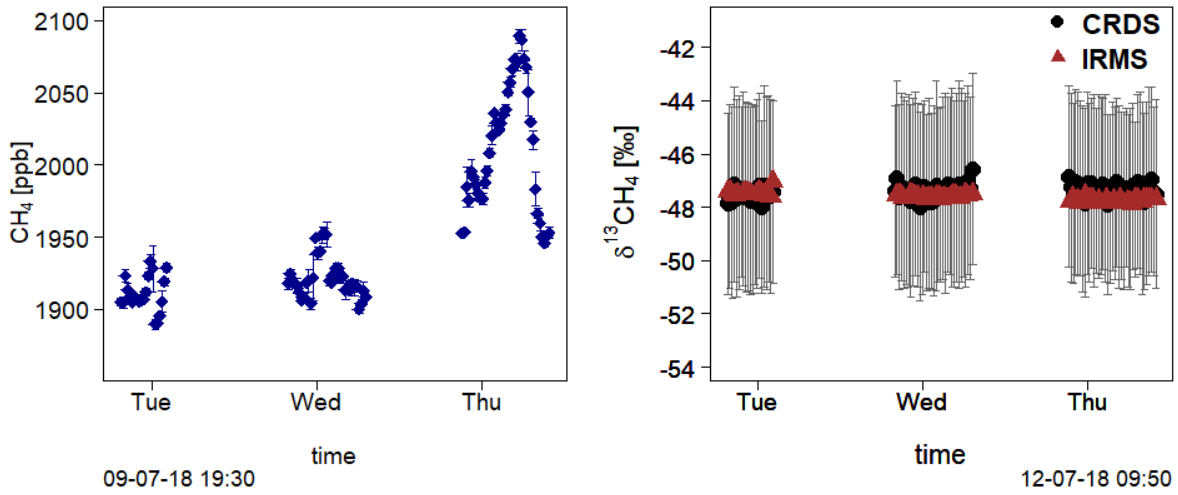

Figure 2.10 CRDS 2072 and RHUL IRMS comparison. 20 minutes' averages CRDS value with calibration, without C_2H_6 correction, error bars represent 1 standard deviation of CRDS measurements

As expected from the previous laboratory tests, the standard deviation of CRDS measurements is higher than for IRMS and achieved about 3.5 ‰ per night (Figure 2.10). During the first night, the difference between averaged CRDS and IRMS value was negligible and reached 0.06 ‰. During the next nights, the discrepancy was a little bigger. Over the second night, it was equal to 0.21‰ and over the third night, it equaled to 0.37‰. However, these offset are much smaller than the CMR of the tested CRDS instrument. Thus, results obtained by CRDS and IRMS are comparable in laboratory conditions.

2.2.2.2 MEMO^2 isotopic tanks

As part of MEMO^2 project, inter-comparison of $\delta^{13}CH_4$ results from participating laboratories was made. Within project, IRMS is used in two laboratories and CRDS G2201-i in three laboratories, including LSCE to determine $\delta^{13}CH_4$. Isotopic signature comparable and reported in common scale can be provided to the project database and used to characterize source categories and individual sources. To provide instrument inter-comparison, five 22-liters cylinders were filled with air to 2 bars. Four tanks were filled with gas sampled directly from methane sources and diluted with zero air (nitrogen and oxygen mix). Two tanks contained air from a natural gas source, diluted to CH_4 mixing ratio ~2 ppm (Tank 1) and ~10 ppm (Tank 2). Tanks 1 and 2 were filled with natural gas from gas supply from RHUL geochemistry laboratory. The gas contains more than 90% of methane and 4-6% of ethane.

Two tanks contained air from a landfill. For these two tanks, gas was collected from the gas engines at the Heathfield landfill site, Devon (Virdor, UK). Before dilution, the landfill gas contained about 20% of CH_4 and CO_2 was most of the remaining gas. In tanks filled with the landfill gas, CH_4 mixing ratio was similar to tanks from the natural gas source (Tank 4 ~2 ppm, Tank 5 ~10 ppm). The air in these four tanks was dried. Tank 5 contained wet ambient air, which was sampled from 2m above the roof of the RHUL Earth Science building.

At LSCE, the measurement of the MEMO^2 tanks was conducted on 23.08.2019. In total, measurements lasted 6 hours and were conducted according to the ICOS ATC calibration procedure. The five tanks where measured alternatively during 20 minutes. This cycle was repeated three times. Between cycles, LSCE target tank was also measured for 20 minutes. 10 minutes within the 20-minutes measurement period was used for further analysis (9 minutes from the beginning of measurements and 1 minute from the end of measurement were removed). For every 10 minutes' measurement period, the mean value and the standard deviation were calculated for every species. Directly after measurements of MEMO^2 tanks, a calibration was run (according to the ATC Mlab calibration procedure) (Table 2.6). Then, CH_4 and $\delta^{13}CH_4$ were calibrated to commonly used scales based on the calibration procedure.

The interference correction from calibrated CO_2, CH_4 and H_2O on C_2H_6 was applied. As correction factors depend on the water vapor level (see Assan et al. 2017 and chapter 3), different factors were applied for Tank 5 with wet ambient air and for others, dry tanks 1, 2, 3 and 4. Corrected in this way, C_2H_6 mixing ratio was calibrated, and correction from interference C_2H_6 on calibrated $\delta^{13}CH_4$ was applied. The final tank values are reported as a mean value of 3 measured cycles, and the uncertainty is treated as a mean of the standard deviation of the three cycles (Figure 2.11).

The results of the experiment are presented in Figure 2.11 and Table 2.7. The IRMS values were validated at RHUL and UU. In the case of the natural gas source, the CRDS values are more enriched, about 3 ‰, than IRMS. This difference is halved after applying C_2H_6 correction. For the landfill tanks, the observed discrepancy between instruments is smaller and in this case, the CRDS value is depleted about 0.5 ‰. As biogenic sources do not contain C_2H_6, the ethane correction should not be applied. However, even the application of this correction does not change the CRDS value significantly.

In the case of wet ambient air measurements, another situation was observed. For wet ambient air, applying C_2H_6 correction increases the discrepancy between instruments, from 0.4 ‰ to 2 ‰. This situation is caused by applying the interference correction from CO_2, CH_4 and H_2O in the presence of water vapor (details in chapter 3).

In all cases, the discrepancies are smaller than the instrument precision, showing again a good agreement between the two methods.

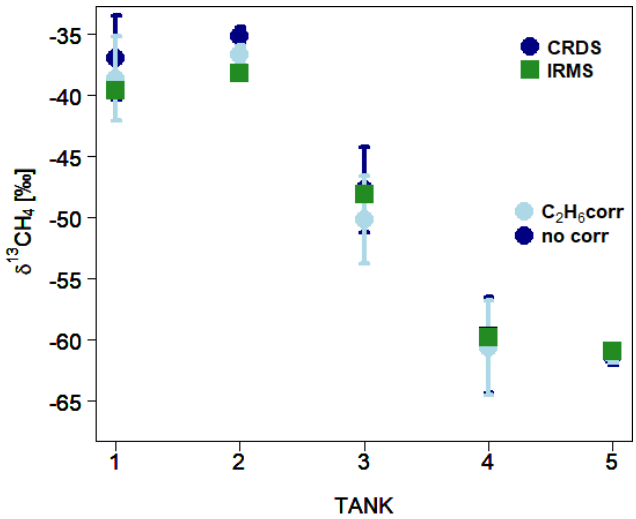

Figure 2.11 Comparison $\delta^{13}CH_4$ value IRMS and CRDS, with CRDS 2072 calibration and C_2H_6 correction, error bars represent 1 standard deviation

Table 2.7 Comparison $\delta^{13}CH_4$ value IRMS and CRDS, with CRDS 2072 calibration

source	TANK	CH_4 [ppm]	IRMS [‰]	CRDS [‰]	IRMS-CRDS [‰]	$CRDS_{C2H6corr}$ [‰]	IRMS-$CRDS_{C2H6corr}$ [‰]
Ambient wet air	3	1.96	-48.1	-47.7 ± 3.5	-0.4	-50.1 ± 3.6	2
natural gas	1	1.97	-39.6	-37.0 ± 3.4	-2.6	-38.6 ± 3.4	-1
natural gas	2	10.09	-38.2	-35.2 ± 0.7	-3	-36.7 ± 0.7	-1.5
landfill	4	1.77	-59.8	-60.4 ± 3.9	0.6	-60.6 ±3.9	0.8
landfill	5	9.99	-60.9	-61.4 ± 0.7	0.5	-61.2 ±0.7	0.3

Thanks to this test, the influence of CH_4 mixing ratio on the $\delta^{13}CH_4$ precision was observed. In both cases, for natural gas tanks and landfill tanks, the CRDS precision increases significantly when the CH_4 mixing ratio reached 10 ppm. For both sources, the standard deviation decreases fivefold and achieves 0.7 ‰. Indeed, three factors have an impact on determined $\delta^{13}CH_4$ isotopic signature: instrument precision, plume enhancement above background and number of measurement points (Hoheisel et al. 2019). This test clearly shows that better source type determination can be achieved when a higher CH_4 plume is crossed.

2.3 Mobile measurements set-up

After the laboratory tests, the instrument was tested during mobile near-source measurements. Here, the mobile measurements are based on crossing the plume of CH_4 enhancement. During measurements, one or two CRDS instruments were installed in the car. They were connected to two 12 V batteries using an inverter. The AirCore tool was a part of the set-up to increase the number of measurements point for measurements of $\delta^{13}CH_4$ isotopic composition (Figure 2.12). (Karion et al. 2010; Rella et al. 2015; Lopez et al. 2017; Hoheisel et al. 2019). The AirCore allows storing and remeasuring the air from plume crossing. Using AirCore, the measurements can be made in two modes: monitoring and replay mode. In the monitoring mode (blue arrows in Figure 2.12), the air is going simultaneously to the instrument and to the AirCore storage tube. In replay mode (green arrows in Figure 2.12), the car is stopped outside of the plume and the air from the storage tube is measured. In the set-up used in this study, the AirCore is built from 50 meters long Decabon tube. The sampling frequency in replay mode increases three times. In the replay mode, after the AirCore, magnesium perchlorate ($MG(ClO_4)_2$) was installed as a drier to avoid water vapor interference and dilution effects on absorption lines (Chen et al. 2010; Rella et al. 2013). In the monitoring mode, CH_4 and CO_2 mixing ratio corrected by the manufacturer are used. This correction is already applied during converting ring–down time to the measured mixing ratio, and the wet and dry CH_4 values are shown directly on the instrument screen.

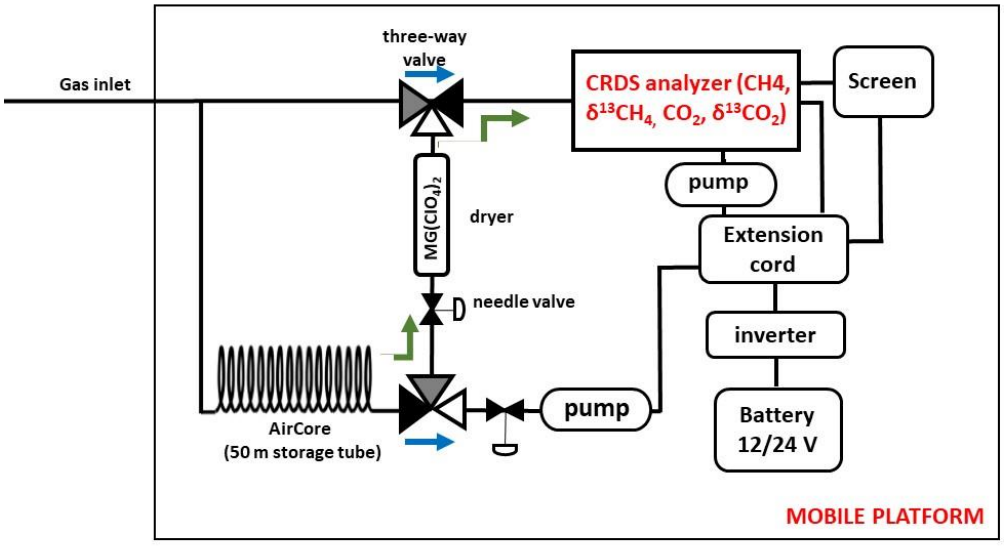

Figure 2.12 Scheme of mobile measurement set-up. The blue arrows show the airflow in monitoring mode. The green arrows show the airflow in the replay mode.

The exact position of the detected plume is also crucial to identify a CH_4 source in small scale measurements. Here, the GPS receiver Navilock NL-602U was used. This receiver has 1 Hz frequency and 2.5 m of horizontal precision. Before merging GPS and CRDS data, the inlet delay is applied to CRDS data. Depending on the instrument model and the length of the tubing, the applied delay varies between 10 and 40 seconds. The inlet delay is determined for each measurement day. During this test, one person blows for one second into the inlet to create a spike in mixing ratio. Then another person records the time after which H_2O and CO_2 enhancements appear on the instrument screen. This test is repeated about five times, and the averaged delay time is applied to the CRDS data.

Knowing the exact position of the CH_4 plume is also crucial to calculate the emission rate of CH_4 source. Here, for the point sources such as gas compressors station, the CH_4 emission rate is calculated using the Gaussian model, as this simple method permits for quick and effortless estimations of emissions rate. Using 20 Hz meteorological data from 3D sonic Gill Windmaster anemometer and approximate source information, the CH_4 plume is modeled in the same distance as the measured plume. Afterward, the area under the curve of these two plumes is compared, and the emission rate is estimated. Depending on the meteorological conditions and number of transects, these calculations are repeated for individual plumes and then averaged model results are calculated or one averaged plume is estimated from the measured plumes, and then the model is used (details in chapter 5). Thus, the application of proper time delay and frequent meteorological data decrease the uncertainty of the calculated CH_4 emission rate.

Additionally, different proxies can be co-measured with CH_4 mixing ratio to determine the origin of the observed CH_4 plume. Commonly, $\delta^{13}CH_4$ and ethane to methane ratio are already measured in in-situ near source conditions. Here, AirCore tool is included in the mobile set-up to increase the sampling frequency and measure $\delta^{13}CH_4$. Additional tests were also made to verify the possibility of using CRDS G2201-i to determine the ethane to methane ratio (chapter 3). Figure 2.13 presents the schematic summary of the methods used during mobile measurements.

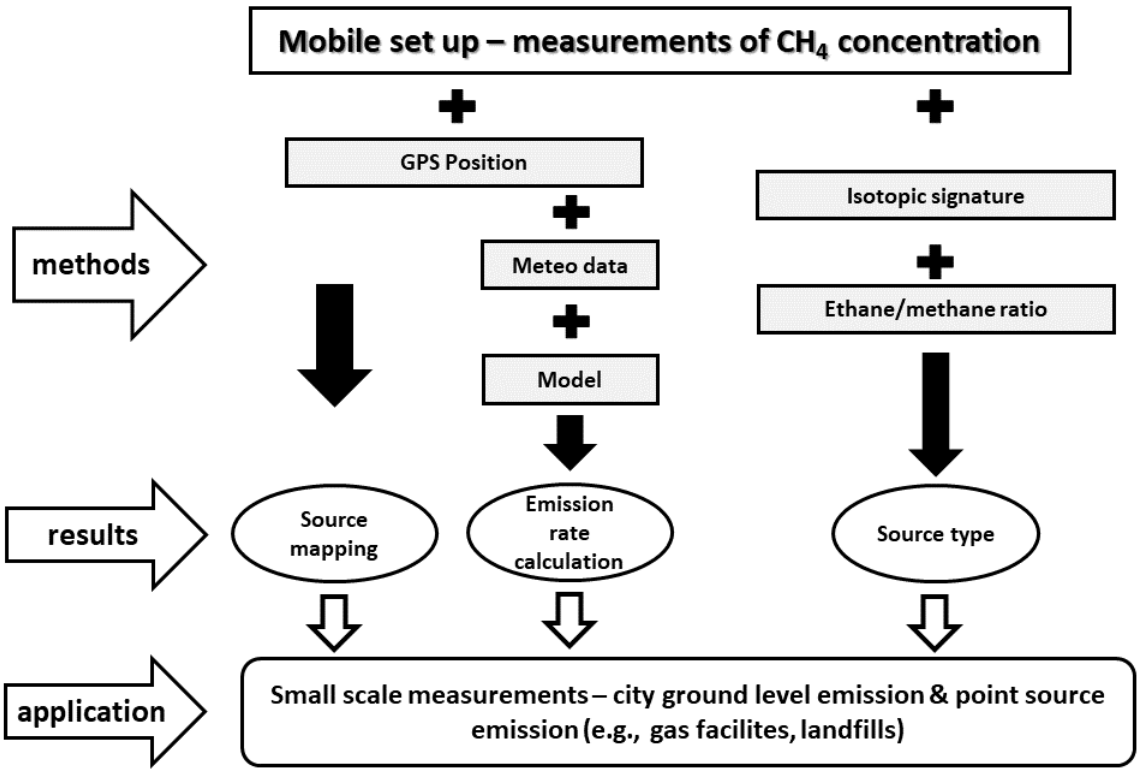

Figure 2.13 The scheme of methods used during mobile measurements

2.3.1 $\delta^{13}CH_4$ measured during in-situ mobile measurements

$\delta^{13}CH_4$ can be also measured in near-source conditions and be used to determine the source of observed CH_4 plume. It can be measured by taking bag/canister samples and measured afterward in the laboratory (e.g., Townsend-Small et al. 2012; Zazzeri et al. 2015; Lowry et al. 2020) or by in-situ measurements, for example with CRDS G2201-i with AirCore tool (e.g., Rella et al. 2015; Lopez et al. 2017; Hoheisel et al. 2019). In the case of $\delta^{13}CH_4$ measurement by CRDS G2201-i, the CH_4 mixing ratio of measured sample has an impact on $\delta^{13}CH_4$ uncertainty. A previous study (Hoheisel et al. 2019) showed that the maximum of CH_4 plume should be at least 500 ppb above background. Smaller CH_4 mixing ratio causes lower precision of $\delta^{13}CH_4$, which leads to higher uncertainty of source isotopic signature. Due to that, AirCore samples were kept when the maximum plume enhancement was above this threshold. If it was possible, from one emitter, more than one AirCore sample was taken during one survey. Ideally, from one site 4-6 AirCore samples were taken and the average values from these samples are used as an isotopic signature of the source.

$\delta^{13}CH_4$ source signature can be calculated in two ways: Keeling plot (Pataki et al. 2003) or Miller-Tans plot (Miller and Tans 2003). The Keeling plot method is built on the principle of mass conservation. Due to that, observed enhancement of CH_4 mixing ratio is a combination of CH_4 atmospheric background and methane source mixing ratio. This principle is also applied to methane signature, both $\delta^{13}CH_4$ and δDCH_4. Using this approach, isotopic signature must be plotted against the inverse of methane mixing ratio and y-intercept is interpreted as the isotopic signature of observed CH_4 source. Two basic assumption should be fulfilled in Keeling plot method. First, observed enhancement is a simple combination of only two components: CH_4 background and one source of CH_4. Second, the isotopic ratio of these two components is stable over the time of the observation. In this method background values of CH_4 mixing ratio and isotopic signature stay unknown (Keeling 1958; Pataki et al. 2003). Compare to Keeling plot approach, Miller-Tans method is more flexible approach, as it includes explicit specification of the background values, both for CH_4 mixing ratio and isotopic signature. After background subtraction, isotopic signature can be determined even when background is changing, for example when surveys are made during different days or in different regions. After removing background, the x-axis represents CH_4 mole fraction, and y-axis represents $\delta^{13}CH_4$ multiplied by CH_4. The $\delta^{13}CH_4$ isotopic signature is determined as a slope of the linear fitting (Miller and Tans 2003).

In this study, the Miller-Tans approach is used, where background is removed both for CH_4 and $\delta^{13}CH_4$ (Figure 2.14). Here, the background is calculated as an averaged value from data in the replay mode directly before and after CH_4 plume. In the study, the fitting is calculated as a linear regression type II, where both x and y are assumed to be dependent on some other unknown parameters. Thus, both x and y are measured and affect fitting (Sokal and Rohlf 1995). Here, the linear regression was fitted using ordinary least squares (OLS) method. In previous studies, averaged data were used to determine isotopic signature of the CH_4 source (Hoheisel et al. 2019 – 15 s averaging time; Lopez et al. 2017 – 10 s averaging time). Here, instead of averaging, data are grouped in 50 ppb bins and the $\delta^{13}CH_4$ is reported when the results from Miller-Tans plot yield a correlation coefficient $r^2 > 0.85$, in order to balance precise results and quantity of kept values. Ideally, only AirCore samples where 1-sigma uncertainty of fitted $\delta^{13}CH_4$ is lower than 5 ‰ should be kept for further analysis. However,

during my Ph.D., enhancement above background was smaller than 1000 ppb which increases $\delta^{13}CH_4$ uncertainty. Thus samples whose $\delta^{13}CH_4$ uncertainty ranged between 5 ‰ and 10 ‰ are also included in analysis.

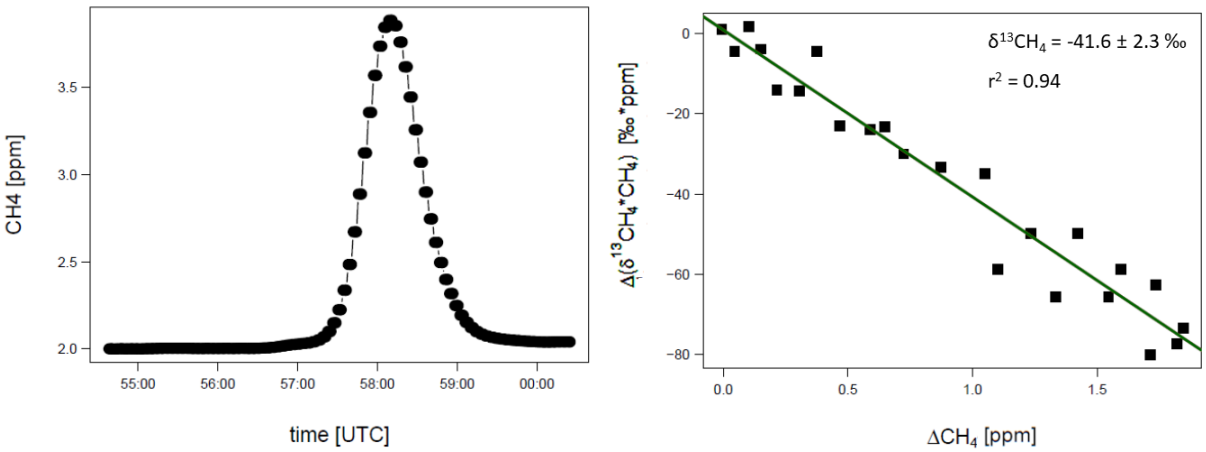

Figure 2.14 Example of AirCore sample. Left: CH_4 plume measured in replay mode, right: Miller-Tans plot

For part of measurements made on industrial sites, AirCore results are compared with IRMS results. As the IRMS instrument cannot be moved out of the laboratory, during mobile measurements, the air is collected into bag samples and measured afterward in the laboratory. Typically, three bag samples are taken inside the CH_4 plume and one outside the plume as a background sample. Then, Keeling plot or Miller-Tans plot is used to determine $\delta^{13}CH_4$ isotopic signature (e.g., Zazzeri et al. 2015; Xueref-Remy et al. 2019; Lowry et al. 2020). IRMS measurements achieve better $\delta^{13}CH_4$ precision. However, taking bag samples from the middle of the plume can be challenging and not possible to perform in every condition. For example, it can affect the flow of urban traffic and potentially cause car accident. My study allows to compare the application and precision of CRDS with AirCore tool and IRMS measurements.

2.4 Testing of the mobile set-up for $\delta^{13}CH_4$

In addition to laboratory tests, described in chapter 2.2, some tests were made while the instrument was installed in the car. First, during three days, two instruments were used simultaneously to verify the possible influence of the inlet position on the measured CH_4 mixing ratio. Then a target with dried ambient air was measured before and/or after randomly chosen surveys. Finally, the mobile measurements of $\delta^{13}CH_4$ isotopic signature were verified. This validation was made during a gas release experiment organized by National Physical Laboratory (NPL) and RHUL in Bedford, UK. This gas release experiment was also used as one of the experiments to determine the possibility of C_2H_6:CH_4 measurements by CRDS G2201-i (chapter 3) and to verify results from the Gaussian model on Polyphemus platform (chapter 5).

2.4.1 Inlet position

During measurements in Paris city, the influence of the inlet position on the observed CH_4 mixing ratio was investigated. During three days (one in January 2019, another in February 2019 and the last in March 2019), two instruments with different inlet locations were used. One inlet was installed on the top of the car (~170 cm above ground), and the other was on the lower skirt of the car (~50 cm above ground). During the first two days, CRDS analyzers G2201-i and G2203 (measuring CH_4 and C_2H_2) were used for the upper and lower inlet, respectively. They have different measurement frequency, one measurement per ~3.7 s for CRDS G2201-i and one per 2 s for G2203. During the third day (March 2019), two CRDS of the same type (G2401, measuring CO_2, CH_4 and CO) were used. The sampling frequency is equal to 0.5 Hz for G2401. Thus, for March survey, possible differences in CH_4 plumes are caused only by inlet position. In case of the two previous surveys, observed difference could be also caused by different sampling frequencies and omitting measurements by lower frequency instrument. Thus, here only results from March survey are described. That day, the car was parked about 2 hours in a place where almost no CH_4 enhancement above background was observed. Over this period, with the same type of instruments, all three plumes, which were observed from the lower inlet, were not observed from the upper inlet. These CH_4 plumes can come from the exhaust of passing buses (some buses in Paris are using biogas and natural gas). Looking for measurements when the car was moving, six other plumes are detected in synchronicity by both of the inlets. Overall the regression slope between upper and lower inlet, when the car was moving, is 0.871 ± 0.026 ppb/ppb, which points to an underestimation by the lower inlet of 13% compared to the upper inlet (Figure 2.15). As a consequence, the inlet situated on the car roof was chosen for the mobile measurements. Additionally, this location gives better protection of the instrument against water and pollution.

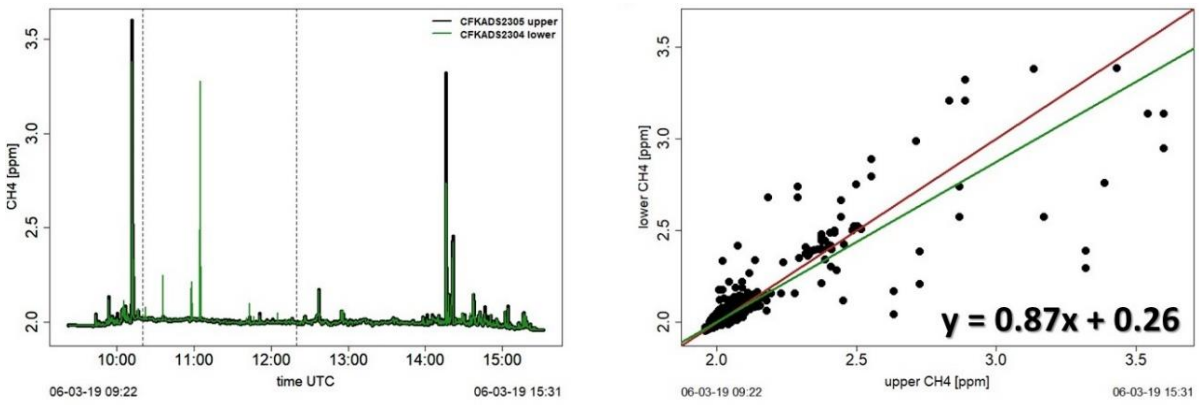

Figure 2.15 Observed mixing ratio at the lower and upper inlets; left panel: CH_4 mixing ratio over time, dotted lines indicate a time when car was parked. Right panel: correlation lower - upper inlet during comparison inlet position with subtracted time when the car was parked. The red line corresponds to y=x. The green line shows the linear fitting.

2.4.2 Target gas measurements

During 21 randomly chosen surveys, made on city or site scale, an additional tank with dried ambient air was measured before or/and after the survey for about 20 minutes. This test aimed to check the analyzer stability and lack of influence of switching on/off analyzer for CH_4 and $\delta^{13}CH_4$ values. Due to its small volume, the tank was refilled twice between September 2018 and August 2019: in December 2018 and June 2019. For all tanks, the measured values are stable and do not change over time. This stability is observed both for CH_4 mixing ratio and $\delta^{13}CH_4$. Figure 2.16 and Table 2.8 present measurements made between December 2018 and July 2019 as it was the longest period of measuring one target.

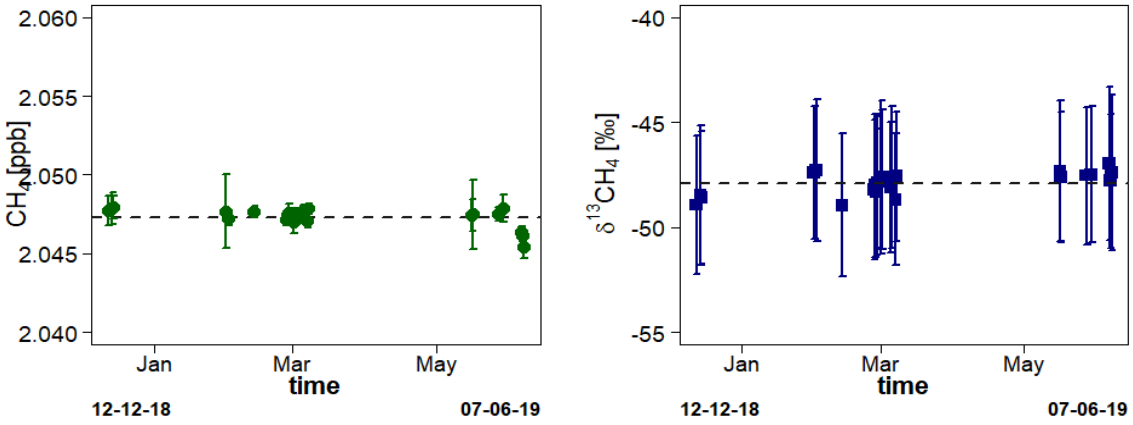

Figure 2.16 Tank measurement before/after mobile measurements between December 2018 and June 2019. The dotted line marks mean value over measurement period. Error bars represent 1 standard deviation, left: CH_4 over the time; right: $\delta^{13}CH_4$ over the time.

Table 2.8 CH_4 and $\delta^{13}CH_4$ from tank measurement before/after mobile measurements between December 2018 and June 2019.

compound	**Target II**
CH_4 [ppb]	2047.3 ±0. 2
$\delta^{13}CH_4$ [‰]	-47.9 ± 0.7

2.4.3 Gas release experiment $\delta^{13}CH_4$ measure

A gas release experiment allowed verifying methods used in my study to determine $\delta^{13}CH_4$, C_2H_6:CH_4 ratio and CH_4 emission rate. The experiment was performed by NPL and RHUL and took place at the airport in Bedford, UK, between 09.09.2019 and 13.09.2019. Each release lasted about 45 minutes. Over 5 days, $\delta^{13}CH_4$ was supposed to be the same all the time, while C_2H_6:CH_4 ratio varied between 0.00 and 0.07. CH_4 emission rate varied up to 70 L/min. In total, 24 releases were made. Part of releases was used to determine $\delta^{13}CH_4$ isotopic signature and C_2H_6:CH_4 ratio and part to determine CH_4 emission rates. In the first case, during one release, all measurements were made in the same distance from the source. The plume was crossed, and simultaneously, the air was measured by instrument and collected in AirCore. After crossing a peak, the car was stopped, and the air stored in AirCore was remeasured in the replay mode. From each release, few AirCores were taken (between 2

and 3 AirCores per release). Magnesium perchlorate was installed all the time before the instrument inlet. In total, 12 releases were used to determine $\delta^{13}CH_4$ by AirCore sampling. During the first three releases, a problem with the batteries occurred, and in situ measurements were not conducted during that time. However, bag samples were taken and remeasured without a dryer in the laboratory to determine $\delta^{13}CH_4$.

For bag samples, the isotopic signatures were calculated twice: using Miller Tans and Keeling approach (Miller and Tans 2003; Pataki et al. 2003). As for bag samples, ethane results are not deemed valid (details in chapter 3), the ethane correction on $\delta^{13}CH_4$ was not applied. The results are the same using two methods: -40.6 ± 1.7 ‰ for the Miller-Tans approach and -40.6 ± 1.9 ‰ using the Keeling approach (Figure 2.17). Obtained values are slightly enriched in comparison to results from direct measurements of released gas. The isotopic signature of released gas was measured on IRMS at RHUL and reached -41.27 ± 0.06 ‰. Notable, CRDS results from released 1.1 and 1.2 are in better agreement with isotopic signature of released gas than from release 2.1. During releases 1.1 and 1.2 only methane was emitted, while during release 2.1 ethane was also co-emitted. Potentially, C_2H_6 presence could affect determined $\delta^{13}CH_4$ at CRDS. In this case, applying ethane correction could improve determined $\delta^{13}CH_4$. However, here, C_2H_6 correction was not used because of not valid bag samples for C_2H_6 collection and presence of water in measured air, which caused bigger discrepancy between $\delta^{13}CH_4$ measured on CRDS and IRMS during laboratory test (Table 2.7). Notable $\delta^{13}CH_4$ obtained at IRMS at RHUL varied between -41.95 ‰ and -39.37 ‰ for plume sampling of individual releases over five days.

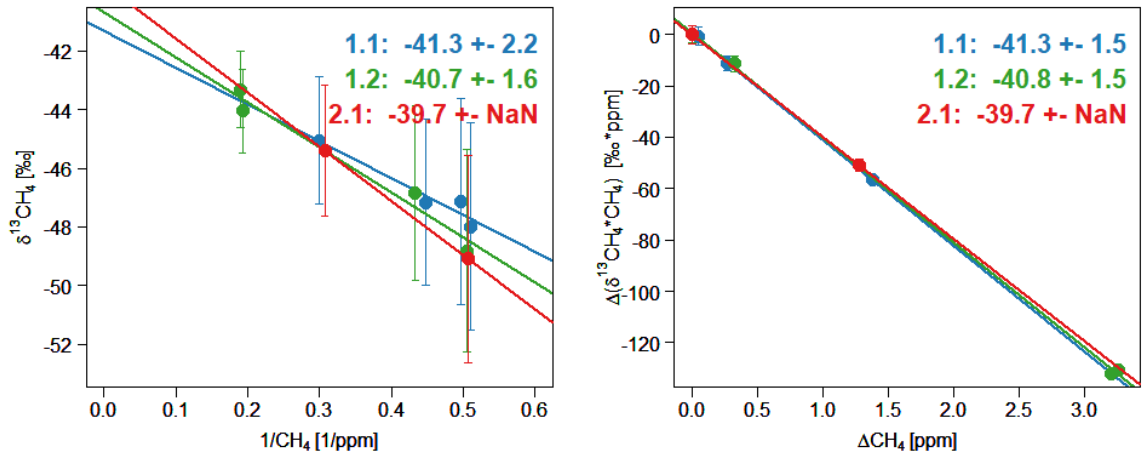

Figure 2.17 Determined $\delta^{13}CH_4$ from bag samples. Left Keeling plot, right: Miller-Tans plot. Error bars represent 1 standard deviation.

During in situ mobile measurements, 30 AirCores were taken. Then looking at results using the Miller-Tans approach with model II regression, two criteria were used to select data: the r^2 correlation coefficient > 0.85 and fitting uncertainty < 5 ‰. Using these criteria, 11 AirCore samples are rejected. For 19 remaining AirCores, the analysis was repeated four times: using Keeling or Miller-Tans method and with or without ethane correction. The results are presented in Table 2.9 and Figure 2.18. Observed in situ values are more depleted than results from bag samples, measured both by IRMS and CRDS. Also, the results are more depleted than $\delta^{13}CH_4$ measured directly from the release tank (-41.27 ± 0.06 ‰.). The possible difference can be explained by the fact that the instrument was turned off for several days during its transport to the United Kingdom. Usually CRDS can take up to several hours to be stable after being turned off for a few hours (in the laboratory, between campaigns the

instrument is always on and then is only switched off for a few minutes). Indeed, after switching on the instrument, the $\delta^{13}CH_4$ reached about -90 ‰ during ambient air measurements and slowly increased to atmospheric background value (~-47‰) in a few hours. Every day, after the experiment, the instrument was switched off, as batteries had to be charged overnight. Thus, it could happen that the approximately two hours between switching on instrument and starting the experiment was not enough to stabilize it. Regrettably, the target gas was not present on the measurement site to confirm this hypothesis. However, this explanation is highly possible, as during field work in the Île-de-France region, the results from bag sampling with IRMS and AirCore sampling with CRDS were in better agreement in most of the cases (chapter 5). It is worth noting that this observed 2.2 ‰ shift to depleted values is still smaller than the uncertainty of each individual AirCore sample and also smaller than the CMR of ambient air sample.

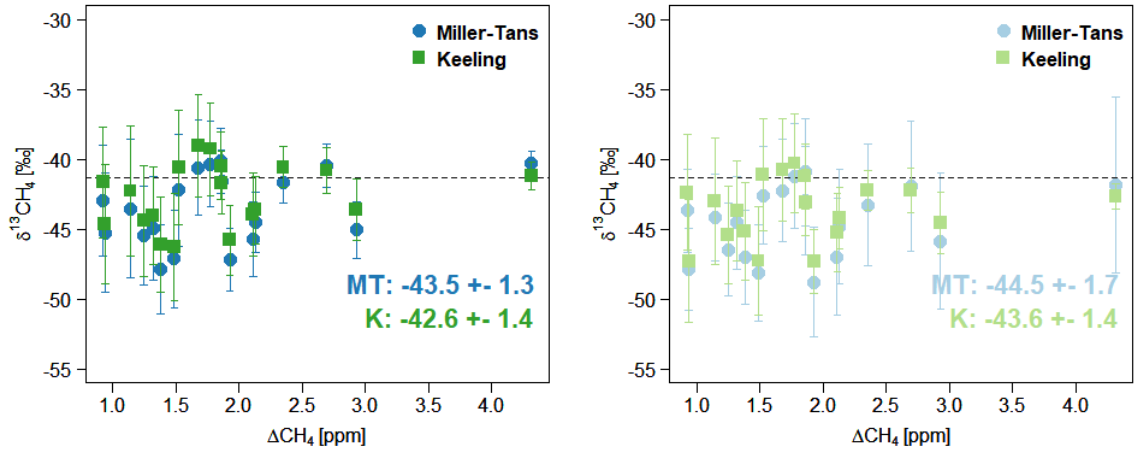

Figure 2.18 Determined $\delta^{13}CH_4$ from in situ mobile measurements. Left without C_2H_6 correction, right: with C_2H_6 correction

Overall both laboratory and field experiments showed the capability of CRDS G2201-i instrument to perform mobile measurements. The CMR and Allan deviation are below 1 ppb which is much smaller than the CH_4 mixing ratio inside a typical CH_4 plume. Additionally, short – and long- term repeatability tests and target measurements before and after surveys showed the stability of the instrument during the period where the surveys were made. Additional tests focused on $\delta^{13}CH_4$ show a good comparison between CRDS and IRMS results, especially in the laboratory conditions. In the case of the mobile in situ experiment, CRDS values were more depleted than IRMS results (~2.2 ‰), which is explained by the needed stabilization time after cold start with the CRDS instrument during the experiment. Nonetheless, this discrepancy is smaller than the CMR of ambient air sample and the uncertainty of individual AirCore sample.

Table 2.9 Isotopic signature determined during in situ mobile measurements

id	ΔCH_4 max [ppm]	Miller-Tans	Keeling	Miller-Tans C_2H_6 correction	Keeling C_2H_6 correction
5	2.1	-45.7 ± 2.7	-44.0 ± 3.0	-47.0 ±4.2	-45.2 ± 2.8
	0.9	-42.9 ± 4.0	-41.7 ± 4.0	-43.7 ±3.0	-42.4 ± 4.2
6	1.9	-41.6 ± 2.3	-41.7 ± 2.2	-43.0 ±3.9	-43.1 ± 2.4
7	2.4	-41.7 ± 1.4	-40.6 ± 1.4	-43.3 ± 4.4	-42.2 ± 1.4
	1.8	-40.3 ± 3.1	-39.3 ± 3.3	-41.2 ± 3.8	-40.3 ± 3.5
	4.3	-40.3 ± 0.9	-41.2 ± 1.0	-41.8 ± 6.3	-42.7 ± 0.9
8	2.7	-40.5 ± 1.6	-40.8 ± 1.6	-41.9 ± 4.7	-42.2 ± 1.6
	1.7	-40.6 ± 3.4	-39.0 ± 3.7	-42.2 ± 3.7	-40.8 ± 3.7
9	0.9	-45.3 ± 4.3	-44.6 ± 4.2	-47.9 ± 2.9	-47.3 ± 4.4
12	2.1	-44.5 ± 2.2	-43.6 ± 2.4	-44.8 ± 4.1	-44.2 ± 2.2
	1.9	-40.1 ± 2.3	-40.5 ± 2.4	-40.9 ± 3.8	-41.2 ± 2.3
	1.5	-42.2 ± 4.0	-40.6 ± 4.1	-42.6 ± 3.5	-41.1 ± 4.0
13	1.1	-43.5 ± 4.9	-42.3 ± 4.7	-44.2 ± 3.1	-43.0 ± 4.5
	1.5	-47.1 ± 3.5	-46.2 ± 3.8	-48.1 ± 3.4	-47.3 ± 3.8
17	1.9	-47.2 ± 2.2	-45.8 ± 2.5	-48.8 ± 3.9	-47.3 ± 2.3
23	2.9	-45.0 ± 2.0	-43.6 ± 2.2	-45.8 ± 4.9	-44.5 ± 2.2
	1.2	-45.4 ± 3.5	-44.4 ± 3.9	-46.5 ± 3.3	-45.4 ± 3.5
33	1.3	-44.9 ± 3.7	-44.0 ± 3.5	-44.5 ± 3.3	-43.7 ± 3.6
	1.4	-47.8 ± 3.2	-46.1 ± 3.4	-47.0 ± 3.3	-45.1 ± 3.5
	1.9	-43.5 ± 1.3	-42.6 ±1.4	-44.5 ± 1.7	-43.6 ± 1.4

Measurement of CH_4 mixing ratio and $\delta^{13}CH_4$ already characterize the CH_4 emitters on a small scale. However, some other proxies can be used to separate CH_4 sources. Beside stable carbon isotopes, the hydrogen isotopes can be measured and then δD is determined. In the case of some surveys, where bag samples were collected to measure on IRMS at Utrecht University, δD was also determined for industrial sites like gas compressors and landfills. Also, C_2H_6:CH_4 ratio can be used to partial biogenic and thermogenic sources (e.g., Lopez et al. 2017; Yacovitch et al. 2015). During this study, an instrument dedicated to determining this ratio was not available. However, in CRDS G2201-i, the C_2H_6 is measured to apply the interference correction on $\delta^{13}CH_4$. Thus, I tested this instrument to verify the possibility of using it in field conditions to measure C_2H_6:CH_4 ratio. Finding the possibilities and limitations of this instrument allows using one instrument to measure CH_4 mixing ratio, $\delta^{13}CH_4$ and C_2H_6:CH_4 ratio. This possibility broadens the use of instrument and simplifies the measurement set-up. Details of the test conducted to describe the possibility of measure C_2H_6:CH_4 ratio by CRDS G2201-i are presented in the next chapter.

Chapter 3
Ethane measurement by Picarro CRDS G2201-i in laboratory and field conditions: potential and limitations

3.1 Introduction

The contemporary methane trends are still under broad discussion (e.g., Saunois et al. 2016; Turner et al. 2019; Nisbet et al. 2019). So far, different hypotheses are proposed to explain the temporary CH_4 atmospheric mixing ratio stabilization from 2000 to 2007 and its growth from 1982 to 2000 and from 2007 until now. To support these hypotheses, the different tracers, co-emitted with methane, can be used to partition CH_4 emissions (e.g., Simpson et al. 2012; Schwietzke et al. 2016; Hausmann et al. 2016; Helmig et al. 2016; Sherwood et al. 2017; Worden et al. 2017; Nisbet et al. 2019). In particular, C_2H_6 is co-emitted with CH_4 from fossil fuels, and it is used to determine their contribution to the CH_4 budget (Aydin et al. 2011; Simpson et al. 2012; Hausmann et al. 2016; Helmig et al. 2016). Based on it, some studies found that the decrease in fossil fuel emissions caused the stabilization of atmospheric CH_4 in 2000 (e.g., Aydin et al. 2011; Simpson et al. 2012). Furthermore, other studies connected the increase of atmospheric methane since 2007 with an increase of fossil fuel emission, as an increase of C_2H_6 was observed (Hausmann et al. 2016; Helmig et al. 2016). As after 2007, the C_2H_6 concentration grew on the Northern Hemisphere and stayed stable on the Southern Hemisphere, the growth of ethane was interpreted as coming from the increasing shale oil and gas production in the U.S. (Hausmann et al. 2016; Helmig et al. 2016). However, this method relies on the calculation of the CH_4 emissions using constant C_2H_6:CH_4 ratio. This assumption can lead to bias in calculated CH_4 emissions as C_2H_6:CH_4 ratio can varies spatially and over time (Kort et al. 2016; Lan et al. 2019; Turner et al. 2019; Yacovitch et al. 2020).

A recent study (Lan et al. 2019), based on the measurements from 20 North American sites, showed that the increase of the U.S. emissions of CH_4 is moderate, and it is smaller than the growth predicted by the studies using ethane concentration and constant C_2H_6:CH_4 ratios. In the same study of Lan et al. (2019), the increase of C_2H_6:CH_4 ratio was observed over the measurement period. This indicated that the assumption of time constant C_2H_6:CH_4 may cause an overestimation of oil and gas CH_4 emission trade in previous studies. Moreover, the C_2H_6:CH_4 ratio can also vary spatially, even on the local scale (e.g., Turner et al. 2019; Yacovitch et al. 2020). This variation can depend on the amount of extracted ethane from the natural gas, which is affected by the petrochemical feedstock and economic value (Smith et al. 2015; Turner et al. 2019; Lan et al. 2019). Kort et al. (2016) showed that the growth of the atmospheric C_2H_6 is connected with increasing production of gas in wet oil fields, which contains more C_2H_6 than conventionally extracted gas. In that study, conducted on the Bakken shale basis, the C_2H_6:CH_4 ratio reached 0.42. Moreover, these basins were estimated to contribute 1-3% of the global C_2H_6 budget (Kort et al. 2016).

The C_2H_6:CH_4 ratio of 0.42 on the Bakken shale basis is much higher than ratios observed in other, focused on conventional sources, studies. Based on the available database, mostly from samples collected in U.S., Canada, Russia and Australia, the averaged C_2H_6:CH_4 ratio for conventional natural gas is about 0.074 ± 0.121 (Sherwood et al. 2017). In detail, this ratio ranges between 0.01 and 0.06 for gas leaks and gas compressors (Lopez et al. 2017; Lowry et al. 2020; Yacovitch et al. 2014). It can be higher than 0.3 for processed natural gas liquids (Yacovitch et al. 2014). Also, different ratios are observed in the case of dry gas (0.01-0.06) and wet gas (> 0.06). In the case of offshore oil and gas platforms, C_2H_6:CH_4 ratios typically are around 0.05, but ratios equal to 0.002 and 0.17 were observed as well (Yacovitch et al. 2020).

A better understanding of C_2H_6 and CH_4 co-emissions from different sources in numerous locations can help to decrease the uncertainty of CH_4 emission partitioning. To achieve it, the local measurements of C_2H_6:CH_4 ratios are crucial. For example, mobile near-source measurements allow determining the ratios of individual sources. Systematical repetitions of these measurements can be used to observe possible changes of ratios over time. On a wider scale, it allows comparing C_2H_6:CH_4 ratios for sources in different locations over the world. As a consequence, they can help to validate the hypothesis of the increasing C_2H_6 emission due to the growth of CH_4 emissions from fossil fuels.

Mobile near-source measurements of C_2H_6:CH_4 ratio also allows for partitioning sources between biogenic (e.g., landfill, farms) and thermogenic (e.g., oil and natural gas facilities) on a small scale, as biogenic sources do not co-emit ethane (Yacovitch et al. 2014; Assan et al. 2017). So far, to achieve it, $\delta^{13}CH_4$ is commonly used, as typically, biogenic sources are more depleted than thermogenic sources (Nisbet et al. 2019; Turner et al. 2019; Saunois et al. 2020). However, recent studies showed that some fossil fuel sources can also emit more depleted CH_4 (e.g., Schwietzke et al. 2016; Sherwood et al. 2017; Yacovitch et al. 2020). These more depleted ^{13}C values are caused by the biogenic origin of the extracted gas. Based on the current database, 14% of conventional natural gas samples have a biogenic origin ($\delta^{13}CH_4$ < -55‰) (Sherwood et al. 2017). In this case, it is crucial to use an additional tracer to portion CH_4 sources during mobile near-source measurements. For this purpose, C_2H_6:CH_4 measurements can be adapted during mobile near-source surveys.

Nowadays, different laser-based cavity instruments can be used to measure C_2H_6:CH_4 ratio directly from the source or during mobile near-source measurements (C. W. Rella et al. 2015; Assan et al. 2017; Lopez et al. 2017; Kim-Hak et al. 2017; Lowry et al. 2020). As a part of my PhD, I investigated the possibility of using CRDS G2201-i to determine C_2H_6:CH_4 ratio during mobile, near-source measurements. This instrument is not dedicated for C_2H_6 measurements. However, as the interferences of C_2H_6 with stable carbon isotopes are observed in the absorption spectrum, C_2H_6 is measured as an additional value to apply an interference correction for $\delta^{13}CH_4$ (C. W. Rella et al. 2015; Assan et al. 2017). The adaptation of CRDS G2201-i allows using one instrument to determine two emitters tracers: $\delta^{13}CH_4$ and C_2H_6:CH_4 ratio. Thus, it can be possible to use one instrument during mobile measurements to partitioning CH_4 sources, which simplifies the measurement set-up.

Overall, my studies allowed determining the limitations and capabilities of the CRDS G2201-i application to measure C_2H_6:CH_4 ratio. This hypothesis is tested in laboratory and field conditions, and the results are combined in the hereafter submitted article. Currently, article is in open discussion (doi.org/10.5194/amt-2020-410). The main motivation of this work was to evaluate limitation and possibilities to use this instrument to measure ethane to methane ratio in a car setting (one conclusion was that, indeed, it needs to be stationary during measurements but is mobile over a site). This study

can be useful for other scientific teams, which do not have an instrument dedicated for ethane measurements, but already have the CRDS G2201-i and would like to use it in field conditions for measuring both $\delta^{13}CH_4$ and ethane to methane ratio. Thus, the article can be viewed as a protocol where all necessary steps are described and verified before field work. There, the work is divided into three parts: first, the laboratory tests to determine instrument noise and precision are described. Then the results from the controlled gas release experiment are shown. Finally, the results from in-situ mobile near-source measurements are presented. Also, the CRDS G2201-i is compared to other instruments dedicated to ethane measurement. The results from this study are also compared with previous works dedicated to near-source C_2H_6:CH_4 measurements.

Conducted tests showed bias of observed C_2H_6 mixing ratio about 30 ppb. As C_2H_6 mixing ratio in ambient air reaches about 2 ppb, Picarro CRDS G2201-i should not be used to measure an absolute value of the C_2H_6 in ambient air. However, field tests showed the possibility of using this instrument to determine the C_2H_6:CH_4 ratio in the mobile near-source conditions. To achieve it, the car should be stopped inside the CH_4 plume and observed CH_4 enhancement above background should be higher than 1 ppm. In the case of C_2H_6, observed enhancement inside the plume should be higher than 100 ppb. During conducted tests, the released C_2H_6:CH_4 ratio varied between 0.0355 and 0.0758. In all cases, the uncertainty of observed by CRDS G2201-i values was smaller than 0.01. In the case of the controlled gas release, the observed ratio was underestimated in comparison to the released value. This difference varied between -0.018 and -0.002. The differences between measured and released values were smaller for the measurement made at gas compressors stations and more symmetrically distributed over released value. In this case, the residuals between released and observed value were in the range from -0.006 to 0.009. To conclude, CRDS G2201-i can be used during mobile near-source measurements to distinguish thermogenic and biogenic sources. Also, it can be helpful to distinguish thermogenic sources if their ratios differ more than 0.01.

3.2 Publication: Ethane measurement by Picarro CRDS G2201-i in laboratory and field conditions: potential and limitations

https://doi.org/10.5194/amt-2020-410
Preprint. Discussion started: 17 October 2020
© Author(s) 2020. CC BY 4.0 License.

Atmospheric Measurement Techniques Discussions

Ethane measurement by Picarro CRDS G2201-i in laboratory and field conditions: potential and limitations

Sara M. Defratyka[1], Jean-Daniel Paris[1], Camille Yver-Kwok[1], Daniel Loeb[1, *], James France[2, 3], Jon Helmore[4], Nigel Yarrow[4], Valérie Gros[1], Philippe Bousquet[1]

1 Laboratoire des sciences du climat et de l'environnement (LSCE-IPSL) CEA-CNRS-UVSQ Université Paris Saclay, Gif-sur-Yvette, 91191, France
2 Royal Holloway University of London, Egham, TW20 0EX, United Kingdom
3 British Antarctic Survey, Natural Environment Research Council, Cambridge CB3 0ET, UK
4 National Physical Laboratory (NPL), Hampton Road, Teddington, TW11 0LW Middlesex, UK
*Now at Université Paris-Saclay, Orsay 91400

Correspondence to: Sara M. Defratyka (sara.defratyka@lsce.ipsl.fr)

Abstract Ethane can be used as a tracer gas to distinguish methane sources, both at the local and global scale. Currently, ethane can be successfully measured using flasks or dedicated in-situ analyzers. In our study, we consider the possibility of using the CRDS Picarro G2201-i instrument, dedicated to isotopic CH_4 and CO_2, for suitable measurements of ethane:methane ratio in mobile field, near-source conditions. Our work was divided into three steps. First, laboratory tests were run to characterize the instrument in stationary conditions. Then the instrument performance was tested in the field, as part of a controlled release experiment and finally during mobile measurements focused on gas compressor stations. The results from the field are compared with the results from other instruments, dedicated to ethane measurements. Our study clearly shows the potential of using the CRDS G2201-i instrument to determine the ethane:methane ratio in methane plumes in mobile condition with an ethane uncertainty of 50 ppb. Assuming typical ethane to methane ratio ranging between 0 and 0.1 ppb ppb^{-1} we conclude that the instrument can correctly estimate the "true" ethane to methane ratio within 1-sigma uncertainty in CH_4 enhancements of 1 ppm or more as can be found in the vicinity of strongly emitting sites (such as natural gas compressor station).

1. Introduction

Methane (CH_4) is the second most potent anthropogenic greenhouse gas, and its global average mixing ratio reached 1.876 ppm in the atmosphere in March 2020 (Dlugokencky, 2020), approximately three times more than during the pre-industrial era. Anthropogenic methane emissions amount to half of the total input of methane to the atmosphere and include a range of sources such as landfill, wastewater treatment plants, agriculture, coal, oil, and natural gas industries (IPCC, 2018; Turner et al., 2019; Saunois et al., 2020). Large uncertainties remain in the quantification of these sources magnitudes and locations (Saunois et al., 2016). The variety of methane sources and their geographical overlap increase the difficulty of closing the present methane budget from global to local scales.

https://doi.org/10.5194/amt-2020-410
Preprint. Discussion started: 17 October 2020
© Author(s) 2020. CC BY 4.0 License.

Atmospheric Measurement Techniques Discussions

Some methane sources also co-emit other gases that can be used as tracers to identify them. For instance, ethane (C_2H_6) is associated with thermogenic methane and it is therefore co-emitted during extraction of coal, oil and natural gas as well as transportation of the latter (e.g., Aydin et al., 2011; Hausmann et al., 2016; Helmig et al., 2016; Schwietzke et al., 2014; Sherwood et al., 2017; Simpson et al., 2012). In the case of the natural gas industry, a range of values for ethane:methane (C_2H_6:CH_4) ratio are observed according to the geological reservoir from which the gas has been extracted and by its eventual processing. The reported ratios depend on the type of facilities and type of the reservoirs: between 0.01 and 0.06 for gas leaks and gas compressors (Lopez et al., 2017; Lowry et al., 2020; Yacovitch et al., 2014), or higher than 0.3 for processed natural gas liquids (Kort et al., 2016; Yacovitch et al., 2014). Also, different ratios are observed in the case of dry gas (0.01-0.06) and wet gas (>0.06). In the case of offshore oil and gas platforms, C_2H_6:CH_4 ratios typically were around 0.05, but ratios equal to 0.002 and 0.17 were observed as well (Yacovitch et al., 2020). On the contrary, biogenic sources such as landfills and cattle farms show null to very small C_2H_6:CH_4 ratio (< 0.002) (Assan et al., 2017; Yacovitch et al., 2014).

At the local scale, observing changes in C_2H_6:CH_4 ratio provides additional information about specific methane enhancement source, especially in areas with multiple CH_4 enhancements from unknown origins (Assan et al., 2017; Lopez et al., 2017; Lowry et al., 2020; Yacovitch et al., 2014, 2020). The currently available techniques, such as Gas Chromatography with Flame Ionization Detector (GC-FID) and Fourier-Transform Infrared Spectroscopy (FTIR) provide access to long-term or short-term measurements of ethane and other components in stationary conditions (Bourtsoukidis et al., 2019; Gros et al., 2011; Hausmann et al., 2016; McKain et al., 2015; Yang et al., 2005). Additionally, laser-based instruments, such as the Los Gatos Research (LGR) Ultraportable Methane:Ethane Analyzer (UMEA), based on a cavity-enhanced absorption technique, the Picarro Cavity Ring Down Spectroscopy (CRDS) analyzers (Rella et al. 2015) and the tunable infrared laser direct absorption spectroscopy (TILDAS) analyzer (Smith et al., 2015; Yacovitch et al., 2014) make it possible to perform measurements of ethane using a mobile platform.

Previous studies already showed the possibility of using a laser based cavity instrument to determine the C_2H_6:CH_4 ratio (Rella et al. 2015; Assan et al. 2017; Lopez et al. 2017, Lowry et al. 2020). In the study of Assan et al. (2017), a CRDS G2201-i dedicated to the measure of $^{12}CO_2$, $^{13}CO_2$, $^{12}CH_4$, $^{13}CH_4$ and H_2O was located stationary nearby natural gas facilities. Over two weeks, dried ambient air was measured simultaneously by CRDS G2201-i and GC-FID, using the 10-minute averages for 16 “events” of high methane mixing ratios lasting more than 1 hour. The C_2H_6:CH_4 ratio separated events of biogenic or thermogenic origin. Moreover, during that study, flask samples were collected and further analyzed in the laboratory. The laboratory values showed good agreement between field CRDS G2201-i and GC-FID results (Assan et al. 2017).

Rella et al. (2015) and Lopez et al. (2017) used the CRDS instrument as part of a mobile setup enhanced with a storage tube, called AirCore (Karion et al. 2010). This storage tube allows to improve time resolution and hence precision. The mobile measurements can be made in two modes using this setup. During the “monitoring mode” the air is split and injected at the same time directly to the instrument and to the AirCore. In the “replay mode”, air from the AirCore is measured. Using the AirCore with a lower flow rate increases the sampling frequency. The replay mode is only used after observation of a methane plume (Rella et al. 2015; Lopez et al. 2017; Hoheisel et al. 2019). In the study by Lopez et al. (2017), C_2H_6:CH_4 ratios were

https://doi.org/10.5194/amt-2020-410
Preprint. Discussion started: 17 October 2020
© Author(s) 2020. CC BY 4.0 License.

Atmospheric Measurement Techniques Discussions

estimated for natural gas facilities. For gas pipelines, the CRDS G2201-i results were compared with results obtained from flask measurements analyzed by gas chromatography. The results showed good agreement between the two methods (Lopez et al. 2017).

Here, the main purpose of this study is to evaluate the performance of the CRDS G2201-i and the applicability of making short-term, direct, continuous, mobile measurements of ethane in methane-enriched air, with sufficient precision during near source ("pollution plume conditions") surveys. To achieve this goal, following Assan et al. (2017), the first step consists of laboratory tests to calculate the calibration factors and also to check the instrument performance in stationary, laboratory conditions. The second step is to investigate the performance of the instrument during field measurements. A tracer release experiment was performed where a methane and ethane mixture with known C_2:C_1 ratio and emission flux was emitted and compared to measured ratios from CRDS G2201-i and LGR UMEA. Thirdly, the instrument has also been evaluated in real field conditions, during surveys conducted at gas compressor stations and one landfill. In this step, measured values are compared to values from gas chromatography and those provided by the owner of the gas compressor stations. These extensive and complex tests allow for a full characterization of the CRDS G2201-i instrument to ethane measurements and provide broader knowledge about the limitations of this instrument when measuring C_2H_6:CH_4 ratios.

Subsequently, after presenting material and methods for these three steps (section 2), their results are presented (section 3) and discussed (section 4).

2. Material and Methods:

The CRDS G2201-i (Picarro Inc., Santa Clara USA), used during this study, is dedicated to the measurements of the mixing ratio of $^{12}C^{16}O_2$, $^{13}C^{16}O_2$, $^{12}C^{1}H_4$, $^{13}C^{1}H_4$ and $^{1}H_2{}^{16}O$ (further H_2O). It operates in three spectral lines: 6057, 6251 and 6029 cm^{-1}. As there is an interference of $^{12}C_2{}^{1}H_6$ (further C_2H_6) on $^{13}CH_4$ in the absorption spectra, this instrument also measures C_2H_6 to correct this interference. Due to observed interferences with $^{12}C^{16}O_2$ (further CO_2), H_2O and $^{12}CH_4$, measured C_2H_6 values must be first corrected. The study performed by Assan et al. (2017) provided the strategy to determine the factors to correct the measured C_2H_6 mixing ratio due to the interference with other species:

$$C_2H_{6\,corrected} = C_2H_{6\,raw} + A \cdot H_2O + B \cdot CH_4 + C \cdot CO_2 \quad (1).$$

Based on their tests, the interference of other species on C_2H_6 changes in relation to the water vapor level in the measured sample. The correction factors were determined for two different CRDS G2201-i devices (CFIDS 2067 and CFIDS 2072) (see Assan et al. 2017). According to that study, if the water vapor level in the measured gas is less than 0.16% ("low humidity case"), then interference correction factors are the same for both devices. In the presence of water vapor (=>0.16%, "high humidity case"), the correction factors were different for each device. The threshold of 0.16% corresponds to 26.14% of relative humidity in standard conditions of temperature and pressure. Due to these differences, drying air is strongly recommended before making measurements (Assan et al. 2017). In the study presented in this article, the correction factors, determined by Assan et al. (2017) are used.

https://doi.org/10.5194/amt-2020-410
Preprint. Discussion started: 17 October 2020
© Author(s) 2020. CC BY 4.0 License.

Atmospheric Measurement Techniques Discussions

Ethane measured by the G2201-i must eventually be linked to a widely used scale, to ensure comparability and traceability. Finally, corrected and calibrated C_2H_6 values can be used to determine the C_2H_6 correction on $\delta^{13}CH_4$ mixing ratio or, as in this study, to determine the ethane to methane ratio. Here, the same device (CRDS G2201-i CFIDS 2072) was used as by Assan et al. (2017); which allows checking possible long-time drift in previously-calculated calibration factors. As outlined in the introduction, three different setups were used to test the instrument capability: laboratory, controlled-release experiment, and field experiment.

2.1. Laboratory setup

We conducted four different tests: the first one to determine the calibration factors, then the others to evaluate the instrument continuous measurement repeatability (CMR, commonly known as precision), Allan variance, time drift and water vapor sensitivity (Allan, 1966; Yver Kwok et al., 2015).

Here, the calibration factors are calculated using the approach presented by Hoheisel (2018), where a synthetic gas mixture of known C_2H_6 ("target"), is diluted with a dilution gas with known CO_2 and CH_4 mixing ratios and applying the following equation:

$$C_2H_{6\,\mathrm{true}} = \left(1 - \frac{1}{2}\left(\frac{CH_{4\,\mathrm{meas}}}{CH_{4\,\mathrm{dilution}}} + \frac{CO_{2\,\mathrm{meas}}}{CO_{2\,\mathrm{dilution}}}\right)\right) \cdot C_2H_{6\,\mathrm{target}} \quad (2).$$

where $C_2H_{6\,\mathrm{true}}$ is the ethane mole fraction obtained by mixing air from two cylinders, one containing ethane at a known value ($C_2H_{6\,\mathrm{target}}$) (without presence of methane or carbon dioxide) and one without ethane but with typical ambient mole fraction methane and carbon dioxide mixing ratio (dilution gas) using a mass flow controller (MFC). $CH_{4\,\mathrm{dilution}}$ and $CO_{2\,\mathrm{dilution}}$ are the mixing ratio of the dilution gas. $CH_{4\,\mathrm{meas}}$ $CO_{2\,\mathrm{meas}}$ are average measured mixing ratios after dilution. This calculation is repeated for different C_2H_6:CH_4 ratios, determined using the MFCs. The calibration factors are calculated as the slope and intercept of the linear regression of measured C_2H_6 versus true C_2H_6.

The calculation of the calibration factors is implemented through a linearity test, where the C_2H_6:CH_4 ratio is gradually increased from 0.00 to 0.15 and measured for 20 minutes for each step. This measurement cycle is repeated three times. To do so, based on the setup presented by Assan et al. (2017), a working gas with ethane mixing ratio ~50 ppm is mixed with the dilution gas via two mass flow controllers. As the flow rate of the measured gas is greater than the instrument's inlet allowance, an open split is installed before the analyzer to vent the generated mixture and maintain an ambient pressure at the instrument inlet. This test was repeated twice: in January 2018 and April 2019. The central 15 minutes of each 20-minute measurements are kept for further analysis. Then, the calibration factors are calculated as a regression slope and an intercept of the linear fitting, of theoretical (Eq. 2) against measured C_2H_6 with already applied correction factors from Equations 1.

The CMR test has been made by measuring a working gas continuously over 24 hours and CMR is calculated as the one standard deviation (SD) over different averaging times (see Yver Kwok et al., 2015). This test was made twice: first using a working gas with negligible amount of ethane and the second time with a gas mixture where C_2H_6:CH_4 ratio was equal to 0.05. This test helps to determine the CMR and instrument noise in the absence or presence of ethane. Moreover, the Allan deviation

https://doi.org/10.5194/amt-2020-410
Preprint. Discussion started: 17 October 2020
© Author(s) 2020. CC BY 4.0 License.

Atmospheric Measurement Techniques Discussions

is also calculated to determine the noise response of the instrument over different averaging times. Typically, the Allan deviation decreases for increasing averaging time. However, depending on the instrument, with increasing of averaging time, the instrument drift can contribute to the increase of the Allan deviation. Thus, the optimal averaging time can be identified (Allan, 1966).

Also, another target gas, traceable to the WMO X2004A CH_4 scale, has been measured during 20 minutes, with a CH_4 mixing ratio about 10 000 ppb and a C_2H_6 mixing ratio about 1 000 ppb. The CH_4 mixing ratio was measured with a CMR of about 1 ppb, while for C_2H_6 the CMR of the measurement was about 50 ppb (Section 3.1). This test allows us to determine the linearity and short-time precision of the instrument for a gas with a higher mixing ratio than that of ambient air, both of C_2H_6 and CH_4.

The drift of the C_2H_6 baseline between December 2018 and May 2019 has also been investigated. The known working gas (dry atmospheric mixing ratio of CH_4 with negligible C_2H_6) was measured during 11 randomly chosen days, 20 times over that period, about 20 minutes each time. That measurement was made systematically as part of the mobile-measurement protocol (described below). The gas was measured before and after surveys to check instrument stability and influence of switching it on and off.

We finally ran a water vapor sensitivity test to revise the parameters of the correction (Eq. 1) in wet air. The target gas had a negligible C_2H_6 mixing ratio. During the test, the target gas was progressively humidified (0 to 3 %) by steps of 0.25%, using a liquid flow controller (Liquiflow, Bronkhorst, Ruurlu, the Netherlands) and MFC coupled to a controlled evaporator mixer (CME). Each step lasted 20 minutes. The cycle was repeated three times. During data analysis, the interference correction factors determined by Assan et al. (2017) were applied. Three cases were tested: no interference correction ("Protocol 1"), high humidity case ("Protocol 2") and low humidity case ("Protocol 3") (excepted for the first step with dry air, where only the low humidity correction was applied).

2.2. Controlled-release experiment setup

This section describes the car-based instrument set-up in a controlled gas release experiment. The measurement set-up used here is the same as in the field (Section 2.4). The general principle of the setup is comparable to the previous works (e.g., Hoheisel et al., 2019; Lopez et al., 2017; Rella et al., 2015). As the instrument is not dedicated to C_2H_6 measurements, the vibrations induced by the motion of the car cause noise in the instrument readouts. Such a constraint can be overcome using two approaches. First, by stopping the car and standing some time inside the plume. Second, by accumulating air in the AirCore (Karion et al. 2010; Rella et al. 2015; Lopez et al. 2017) while moving through the plume and eventually reinjecting the AirCore's air into the analyzer while stopped. Previously, the AirCore tool was successfully used as part of a mobile measurement setup to determine the isotopic composition of the methane source (Rella et al. 2015; Hoheisel et al. 2019; Lopez et al. 2017) and to determine C_2H_6:CH_4 ratio (Lopez et al. 2017).

https://doi.org/10.5194/amt-2020-410
Preprint. Discussion started: 17 October 2020
© Author(s) 2020. CC BY 4.0 License.

Atmospheric Measurement Techniques Discussions

For all mobile measurements, the background mixing ratios are calculated as the 1st percentile of the data sampled just before and just after the plumes, both for CH_4 and C_2H_6. Then the data with CH_4 enhancements above background are further analyzed. The C_2H_6:CH_4 ratio is calculated for each release as the slope of the linear regression of C_2H_6 against CH_4.

In September 2019, during five days, a gas release experiment was conducted by the National Physical Laboratory (NPL, UK) and the Royal Holloway University of London (RHUL, UK). The experiment took place in Bedford Aerodrome, UK. The description of experimental setup configuration can be find in Gardiner et al. (2017) The goal was to evaluate the methods for calculating C_2H_6:CH_4 ratios, emission flux and isotopic composition during local mobile measurements. Each release lasted about 45 minutes. During the experiment, the parameters of each release: C_2H_6:CH_4 ratio (0.00 to 0.07), emission flux (until 70 L/min) and the source height (ground or ~4 m source) could vary. Here, results from 10 releases with known parameters and varying ethane:methane ratios are presented.

Seven releases were measured using the mobile setup (AirCore and standing in the plume). Air was dried before entering the analyzer using a magnesium perchlorate cartridge. Due to the limited time of the releases, the time of standing inside the peaks field was in the range of 15 to 20 minutes. After correcting raw data according to Eq. (1), following Protocol 3 (low humidity case), the calibration factors (section 2.1) are applied for the trace release and field work datasets.

Three other releases were measured using sampling bags (5 liters' skc flexfoil sample bags) only. Between 1 and 3 bags sampled inside the plume and one sampled outside as a background sample. Afterward, bags samples were measured in the laboratory using the CRDS G2201-i. The samples were measured without drying and the correction was applied for water vapor higher than 0.16% (Protocol 2). Then the C_2H_6:CH_4 enhancement ratio was calculated for every bag separately and also as a regression slope of C_2H_6 against CH_4 values.

2.3. Field experiment setup

As a final step to evaluate G2201-i performance in mobile, real field conditions, the mobile-measurement set-up, described in Sect. 2.2 has been used during surveys made in the Paris area (see Defratyka et al., 2020, submitted). During spring and summer 2019, 6 surveys focused on three gas compressor stations (one survey for one of them and two surveys for the other two) and one landfill (one survey). All measurements were made outside of the sites, from the closest public road. To measure C_2H_6:CH_4 ratio, the car was stopped inside the plumes for about 35 minutes, and the central 30 minutes were analyzed. Part of the measurements was made with magnesium perchlorate as a dryer before the instrument inlet and part of measurements without dryer. For each measurement site, three previously evacuated 800 mL flask samples were also taken to be measured within three weeks after sampling at LSCE (Assan et al., 2017). Measurements were performed with a GC-FID (HP6890) equipped with a CP-Al_2O_3 Na_2SO_4 column and coupled to a preconcentrator (Entech 2007) to allow automatic injections. A standard cylinder (Messer) containing 5 non-methane hydrocarbons including ethane was used to check the stability of the instrument, while calibration was done against a reference standard from NPL (National Physics Laboratory, Teddington, UK). A previous characterization of the system had shown that the detection limit is a few ppt, the reproducibility of measurements is about 2% and the precision is better than 5% (Bonsang and Kanakidou, 2001).

https://doi.org/10.5194/amt-2020-410
Preprint. Discussion started: 17 October 2020
© Author(s) 2020. CC BY 4.0 License.

Atmospheric Measurement Techniques Discussions

3. Results and discussion

3.1. Laboratory work

3.1.1. Ethane calibration

During the first part of the laboratory work, the calibration slope and intercept were calculated using linear fitting of C_2H_6 true (Eq. 2) versus C_2H_6 observed and compared with the factors previously obtained. The calibration factors were determined after applying the interference correction (Eq. 1). Table 1 compares new calibration slopes and intercepts for the specific CRDS G2201-i device CFIDS 2072 obtained in 2018 and 2019 with previous results by Assan et al. (2017). The calibration factors have not changed significantly between 2015 and 2019.

Figure 1 shows the time series of working gas measurements with a low amount of C_2H_6 during the period of December 2018 - May 2019. The C_2H_6 mixing ratio does not change here significantly and is equal to 23 ± 12 ppb (Figure 1). It is in contrast to Assan et al. (2017), where a time drift of the baseline was observed. This difference can be caused by fact that during previous studies, the drift was determined for corrected but not calibrated data. Here, we applied both correction and calibration before determination of time drift. Moreover, during previous studies bigger changes in determined calibration factors were observed over time. Therefore, in the following analyses, no baseline drift correction is applied.

Table 1. Summary of the calibration factors for CRDS G2201-i device CFIDS 2072

C_2H_6 calibration	Slope	Intercept [ppm]	Reference
February 2015	0.49 ± 0.03	0.00 ± 0.01	(Assan et al. 2017)
October 2015	0.51 ± 0.01	-0.06 ± 0.04	(Assan et al. 2017)
January 2018	0.51 ± 0.01	-0.03 ± 0.01	This study
April 2019	0.54 ± 0.01	-0.03 ± 0.01	This study

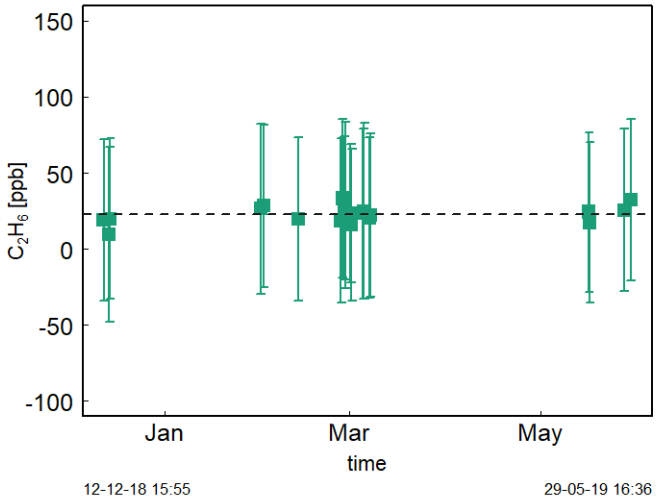

Figure 1. Working gas 20 minutes measurements over half a year, for each measurement point: squares represent averaged value, error bars – 1 standard deviation

https://doi.org/10.5194/amt-2020-410
Preprint. Discussion started: 17 October 2020
© Author(s) 2020. CC BY 4.0 License.

Atmospheric Measurement Techniques Discussions

3.1.2. CMR and Allan variance

We determined the instrument CMR and Allan variance by measuring a working gas for 24 hours. It was also measured by GC-FID coupled to a preconcentrator, and its C_2H_6 mixing ratio equals 2.2 ppb. Using the CRDS G2201-i, the corrected and calibrated value is different and steadily equals 33.2 ± 1.7 ppb over the 24 hour duration. This value suggests a bias of the CRDS instrument of 31 ppb at low concentrations.

As the result of the 24 hour test, CMR and Allan deviation (Figure 2) are calculated for target gases with different C_2H_6 mixing ratios: low mixing ratio, 100 ppb and 1 000 ppb. In all cases, increasing the ethane mixing ratio does not affect the determined CMR and Allan deviation. Looking at raw data (one data point every 3.7 s) for different mixing ratios, CMR and Allan deviation are about 50 ppb and 25 ppb, respectively. Increasing averaging time improves these parameters and for 1 minute average, all achieve about 13 ppb. For CRDS model G2132-i, also not dedicated to the measure of ethane (Rella et al. 2015), the CMR in 1 min is about 20 ppb and Allan deviation in 1 minute is about 25 ppb. Currently, new CRDS instruments dedicated to ethane measurements are available, for example, the CRDS 2210-i, which also measures $\delta^{13}CH_4$. Recently (in February 2020), at the ICOS Atmosphere Thematic Centre (ATC) Metrology Laboratory (MLab), the CRDS G2210-i was tested and for C_2H_6 its CMR and Allan deviation are equal to 0.9 ppb and 0.8 ppb in 1 minute (ATC Mlab, personal communication). The comparison between instruments are presented in Table 2

Table 2. CMR and Allan deviation for G2201-i G2132-1 and G2210-i.

Averaging time	Id	G2201-i Low C_2H_6	G2201-i ~100 ppb C_2H_6	G2201-i ~1000ppb C_2H_6	G2132-i (Rella et al., 2015)	G2210-i (ATC MLab) (personal communication)
Raw data	CMR [ppb]	51	50	50	NA	4.6
	Allan deviation [ppb]	25	25	26	NA	NA
10 second	CMR [ppb]	30	29	30	NA	NA
	Allan deviation [ppb]	29	29		NA	NA
1 minute	CMR [ppb]	13	12	12	20	0.9
	Allan deviation [ppb]	13	12	12	25	0.8

https://doi.org/10.5194/amt-2020-410
Preprint. Discussion started: 17 October 2020
© Author(s) 2020. CC BY 4.0 License.

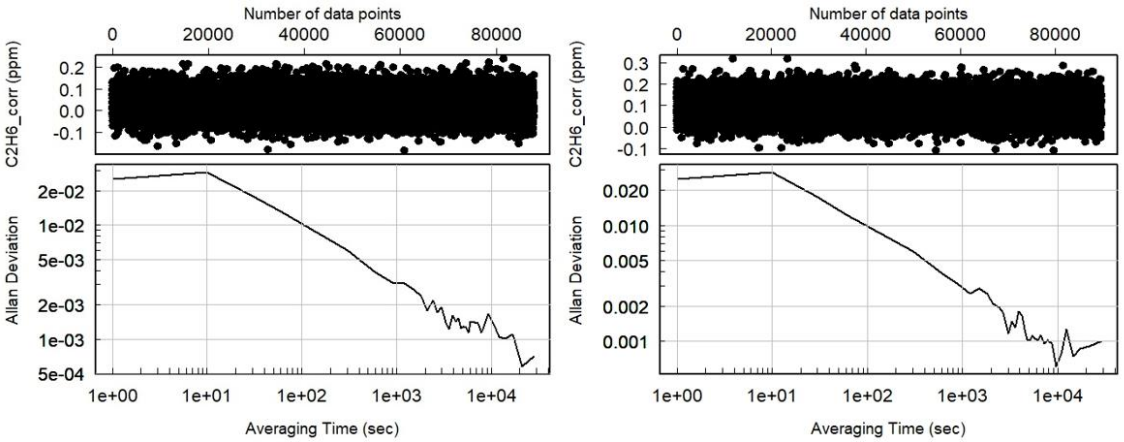

Figure 2. Allan deviation for corrected and calibrated C_2H_6. Left: Measurement of working gas with negligible C_2H_6 mixing ratio, right: measurement of the mixture of working gas with ~100 ppb of C_2H_6.

With a 30 ppb bias and a CMR of 50 ppb, the CRDS G2201-i cannot be used to measure ethane absolute value. However, this instrument can be used to observe ethane enhancement near the source and to estimate ethane to methane ratios. From these numbers, we can deduct that the smallest enhancement that the analyzer can measure with significant precision at the highest possible data acquisition frequency is 50 ppb. This value was obtained both for gas with a low and high C_2H_6 mixing ratio (~100 ppb and ~1 ppm). We can assume that a C_2H_6 enhancement is significant when the maximum C_2H_6 mixing ratio in the peak is higher than 2xSD, i.e., 100 ppb above background.

3.1.3. Sensitivity to water vapor

We also verified the cross-sensitivity correction proposed by Assan et al. (2017) in the presence of water vapor. Equation 1 corrects the interference of H_2O, CO_2 and CH_4 in the absorption spectrum and dilution to report C_2H_6 mixing ratio in dry air. Figure 3 shows that without interference correction (Protocol 1), the C_2H_6 mixing ratio is underestimated and the instrument displays a negative correlation with water vapor (r = -0.96). In Protocol 2 (high humidity interference correction), C_2H_6 is overestimated and increases with increasing water vapor (r = 0.86). Regarding Protocol 3 (low humidity interference correction), C_2H_6 shows the smallest dependency on water vapor (r = -0.19). Applying Protocol 3, the C_2H_6 average value is 28 ± 61 ppb, which is similar to the C_2H_6 average value obtained during the previously described CMR test (33 ± 51 ppb for raw data), in dry air. Overall, according to this study, after applying Protocol 3, the water vapor has the smallest impact for observed C_2H_6 mixing ratio and its averaged value is similar to the one obtained in the absence of water vapor. Therefore, the correction factors determined for the low humidity case (Protocol 3) should also be used in water vapor presence. Our results differ from the findings of Assan et al. (2017), where they observed changing values of the interference correction depending on the humidity. In the absence of further tests to conclude, we recommend drying air for the C_2H_6 measurements with the CRDS G2201-i instrument. Details of the water vapor tests are presented in appendix A.

https://doi.org/10.5194/amt-2020-410
Preprint. Discussion started: 17 October 2020
© Author(s) 2020. CC BY 4.0 License.

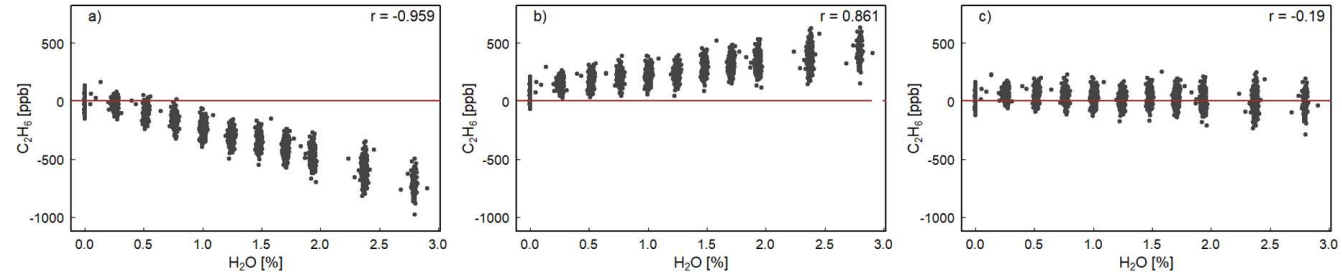

Figure 3. H_2O influence on corrected C_2H_6. Water vapor is increased in small steps for 4 hours while measuring a target gas. The three panels show the result of applying different water correction protocols for next steps: a) no correction (Protocol 1) b) high humidity interference correction (Protocol 2) c) low humidity interference correction (Protocol 3). In all cases, for H_2O= 0.00%, C_2H_6 is corrected using low humidity interference correction. The red line represents 0 ppb.

3.2. Controlled release experiment

Figure 4 shows ethane to methane ratios measured in situ during the controlled release experiment (see Section 2.2). During these 7 releases, the C_2H_6:CH_4 ratio was set to ~0.032 for one release, ~0.00 for two releases and ~0.07 for four releases. For measurements with the car stopped inside the plume, most of the data from the CRDS G2201-i are found lower than known emitted C_2H_6:CH_4 ratio, (mean absolute deviation = 0.011, standard deviation = 0.004) with residuals in the range -0.018 to -0.002 for raw data (Table 3). The observed underestimation can be caused by an insufficient number of measurement points (15-20 minutes of measurement). For AirCore measurements, there is more discrepancy than for the plume standing situation, with residuals in the range -0.025 to 0.027 (mean absolute deviation = 0.017, standard deviation=0.009). For 10 s averaged data, the range of residuals is only marginally modified, ranging from -0.019 to -0.002 and from -0.022 to 0.027 for plume standing and AirCore, respectively. Additionally, the mean absolute deviation and standard deviation are also marginally modified for both measurement situations. For example, for stationary plume standing, the absolute deviation improves marginally from 0.0111 to 0.0107. The plume standing set-up shows less noisy data and a smaller range of residuals than AirCore results. Moreover, the plume standing approach has a (small) regular bias (mean bias = -0.011), higher than in the AirCore approach (mean bias = -0.004). These results show that in the case of C_2H_6:CH_4 ratio measurements, standing inside the plume gives results closer to the reality than AirCore sampling. The example of observed CH_4 and C_2H_6 mixing ratio while standing inside the peak during one of the gas releases is presented in appendix B.

https://doi.org/10.5194/amt-2020-410
Preprint. Discussion started: 17 October 2020
© Author(s) 2020. CC BY 4.0 License.

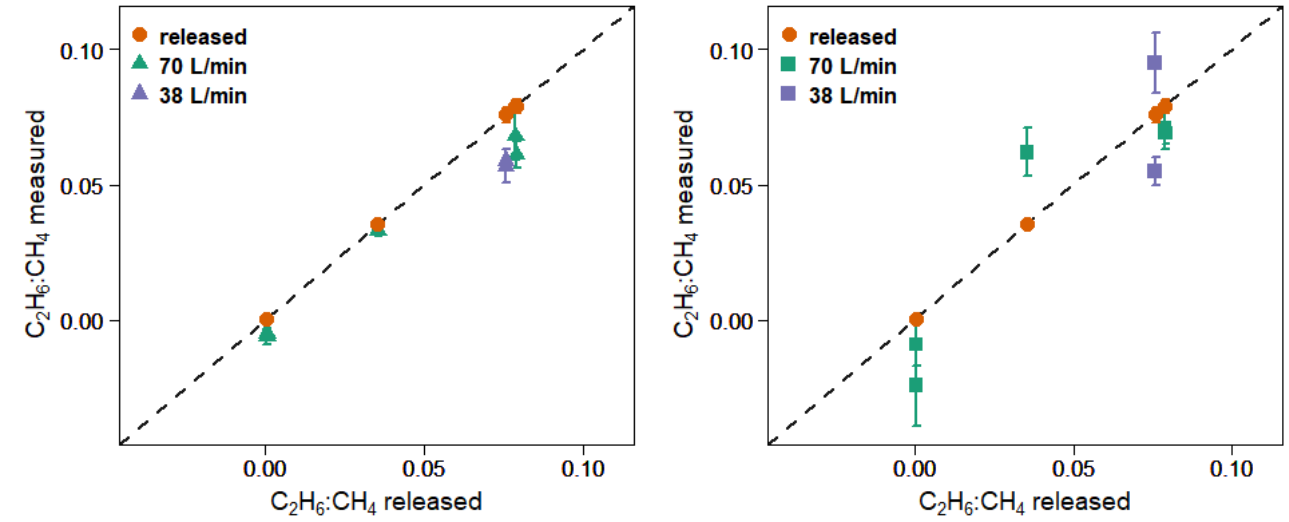

Figure 4. C_2H_6:CH_4 ratio observed using G2201-i as a part of a mobile setup. Left: measured standing inside the plumes. Right: measured using AirCore. Red points: known released C_2H_6:CH_4 ratio. Error bars represent 1 standard deviation. The uncertainties of released values are invisible on the graph.

We also investigated the sensitivity of the C_2H_6:CH_4 ratio to emission rates. During releases there were two different emission rates: 38 L/min and about 70 L/min. In the latest category, the releases while the emission rate was equal to 72 L/min and 73 L/min are grouped. The ethane to methane ratio is better estimated by the measurements for higher emission rates (bias is divided by more than 2 when increasing flow rate from ~38 to ~70 L/min). This is true both with stationary measurements and using AirCore sampler. However, only 2 different emission rates were implemented and most of the released occurred at the rate of 70 L/min, limiting the representativity of this sensitivity.

Table 3. Residuals between measured and released C_2H_6:CH_4 ratio, comparison of results made using CRDS G2201-i and LGR UMEA, AC- AirCore measurements. * Small amount of ethane impurity in the methane

Emitted C_2H_6:CH_4	emitted emission flux [L/min]	Source height [m]	LSCE CRDS G2201-i					RHUL LGR UMEA
			n	Residuals C_2H_6:CH_4 1s	Residuals C_2H_6:CH_4 AC 1s	Residuals C_2H_6:CH_4 10s	Residuals C_2H_6:CH_4 AC 10s	Residuals C_2H_6:CH_4
0.0355 ± 0.0011	70	4	382	-0.002	0.027	-0.002	0.027	-0.004
0.0788 ± 0.0025	72	4	149	-0.011	-0.008	-0.009	-0.009	-0.006
0.0790 ± 0.0025	73	0	220	-0.018	-0.010	-0.016	-0.010	-0.001
0.0758 ± 0.0028	38	0	142	-0.017	-0.020	-0.018	-0.022	-0.007
0.0758 ± 0.0028	38	4	191	-0.018	0.019	-0.019	0.020	-0.015
0.0005 ± 0.0006*	70	0	350	-0.005	-0.025	-0.005	-0.022	-0.004
0.0005 ± 0.0006*	70	4	202	-0.007	-0.010	-0.006	-0.009	-0.001
Mean residuals				**-0.011**	**0.004**	**-0.011**	**-0.004**	**-0.0051**

In Table 3 we also report the residuals of C_2H_6:CH_4 ratio independently measured by RHUL using an LGR UMEA in another car. The residuals in C_2H_6:CH_4 ratios of LGR UMEA are in the range [-0.015 to -0.001], and their mean is -0.0051 (mean absolute deviation = 0.0051). Therefore, the LGR UMEA is predictably more accurate than the CRDS G2201-i standing inside

https://doi.org/10.5194/amt-2020-410
Preprint. Discussion started: 17 October 2020
© Author(s) 2020. CC BY 4.0 License.

Atmospheric Measurement Techniques Discussions

the plumes (CRDS residuals in range -0.018 to -0.002 with mean -0.011). Despite the observed differences, results obtained by these two methods are comparable and both instruments are capable of resolving the variation of C_2H_6:CH_4 in the release experiment.

Additionally, three releases were measured offline using 5 liters' bag samples filled with air from the plumes. The bag samples were measured afterward in the laboratory without drying. During release one and two, emitted C_2H_6:CH_4 ratio was equal 0.00, the third release having a C_2H_6:CH_4 ratio about 0.032. In all cases, for background samples, the C_2H_6 mixing ratio was found higher than for the bag samples collected inside the plumes. Due to that, results from the bag samples are rejected from further analysis. There are two possible reasons for the incorrect values obtained with bag samples. First, these bags could not be adapted for storing ethane. Secondly, as the samples were wet, the H_2O, CO_2 and other species interferences on C_2H_6 could be higher and not linear. Thus, the applied interference correction did not improve the measured C_2H_6 mixing ratio. In appendix C, the table of results from bag sampling is presented.

3.3. Field work

As a final step, the CRDS G2201-i was evaluated in real field conditions. Measurements were collected in the Paris area downwind of three gas compressor stations (referred to as A, B, C) and one landfill (D). All measurements in this section were done stationary inside the plume.

Table 4 presents only values based on raw data (~3.7 s). We postulate that mobile applications usually aim at the highest possible acquisition frequencies. However, as the 10 s averaging increases r^2 fitting by about a factor two, comparison of raw data and 10 s averaged data is presented in appendix D.

Table 4. Ratio measured at three different gas compressor stations (A, B, C) and a landfill (D); Numbers after identification letters refer to different surveys. *: A1, B1 and B2 (wet air) and ** C1 (low enhancement) are rejected from further analysis (see text). ΔCH_4 and ΔC_2H_6 are defined as the difference between background value (1st percentage) and the observed value inside the peak

id	max ΔCH_4 [ppm]	max ΔC_2H_6 [ppm]	C_2H_6:CH_4 ratio 1 s	r^2 fitting	n (data point)	Data
A2	1.737	0.269	0.060 ± 0.005	0.195	533	16.05.2019
A3	5.85	0.414	0.045 ± 0.002	0.489	495	15.07.2019
B3	1.454	0.260	0.052 ± 0.007	0.082	613	12.07.2019
B4	1.677	0.236	0.046 ± 0.008	0.086	336	12.07.2019
D1	1.516	0.266	0 ± 0.006	0	712	16.05.2019
A1*	1.486	0.309	0.070 ± 0.013	0.162	138	16.05.2019
B1*	7.314	0.878	0.090 ± 0.001	0.852	811	27.05.2019
B2*	0.513	0.323	0.085 ± 0.022	0.024	594	12.07.2019
C1**	0.495	0.284	0.091 ± 0.037	0.037	711	28.05.2019

Campaigns A1, B1 and B2 (Table 4) were made without using a dryer before the instrument inlet. Due to previous results that have cast doubts about the water vapor correction, the high humidity measurements have been rejected from further analysis.

https://doi.org/10.5194/amt-2020-410
Preprint. Discussion started: 17 October 2020
© Author(s) 2020. CC BY 4.0 License.

Atmospheric Measurement Techniques Discussions

Surveys B2 and C1 exhibited the highest uncertainties in the estimated ratio and the lowest correlation between the two species. These two surveys had the lowest CH_4 enhancements above background, about 0.5 ppm. Based on error propagation (Taylor, 1997) and using 2x CMR (100 ppb) as C_2H_6 detection threshold, for a typical C_2H_6:CH_4 ratio of interest about 0.1, the minimal CH_4 enhancement above background would also be equal to 1 ppm. It suggests that a minimum CH_4 enhancement of 1 ppm could be required to calculate ethane to methane ratio in field conditions. As our observations are in line with the error propagation, we use 1 ppm CH_4 enhancement above background as a detection limit to use the CRDS G2201-i to determine ethane to methane ratio in the field conditions close to the methane source, and exclude B2 and C1 from subsequent analysis.

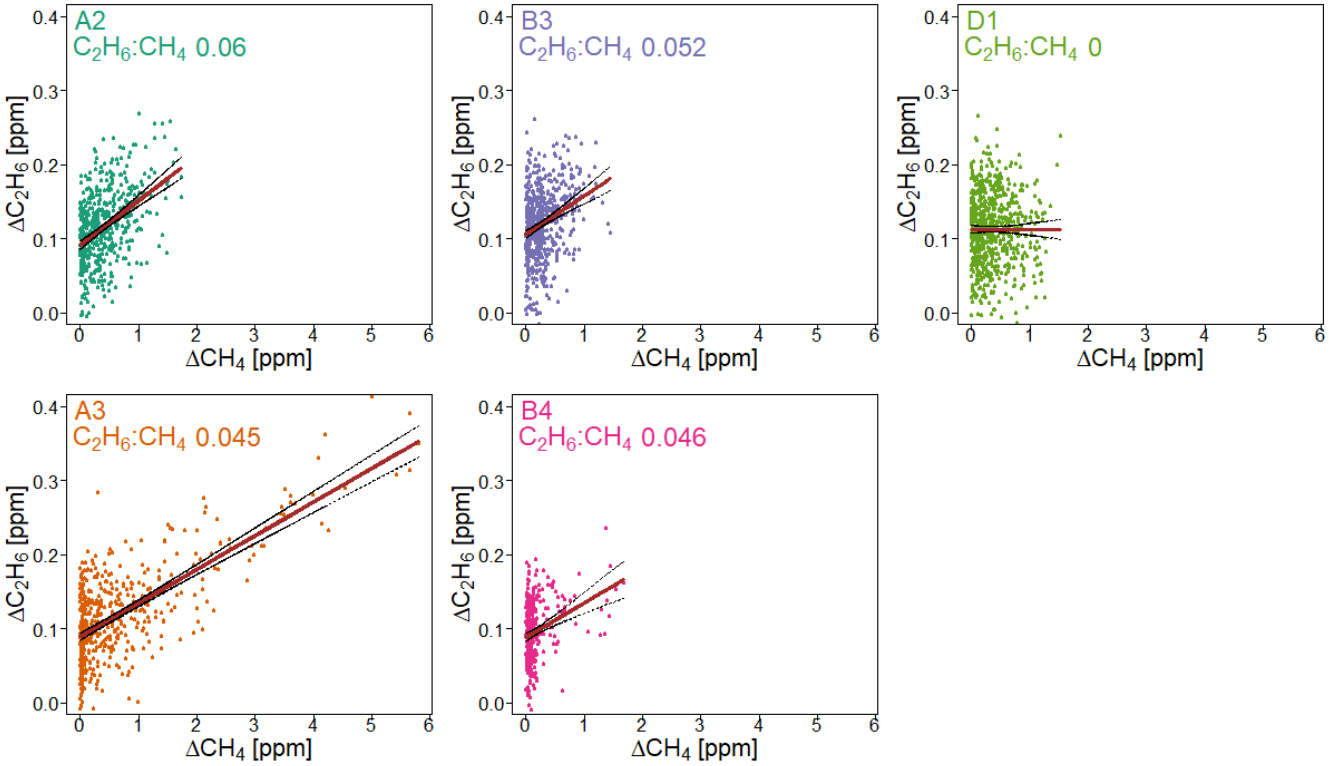

Figure 5. C_2H_6:CH_4 ratio for gas compressor stations (A and B) and the landfill (D), calculated for non-averaged data. Linear fitting (red line) with confidence intervals (black lines)

Figure 5 presents observations from the valid cases. We compared the observed ratios with the values provided by the owner of the gas compressor stations. The comparison is presented in Table 5. The residuals between values measured by CRDS and values provided by the owner (considered as the "true" values) are in the range -0.006 to 0.009. This range is more symmetrically distributed around the released value than for the controlled release experiment (-0.018 to 0.002, Section 3.2). The uncertainty of C_2H_6:CH_4 ratio measured using the CRDS G2201-i in the field conditions is smaller than the differences between the ratios of CH_4 sources (e.g., biogenic sources C_2H_6:CH_4 ~0.00, natural gas leaks and compressors stations ~0.06, processed natural gas liquids ~ 0.30). These results clearly show that C_2H_6:CH_4 ratio measured by the CRDS G2201-i can be used to portion the origin of the CH_4 during mobile measurements.

https://doi.org/10.5194/amt-2020-410
Preprint. Discussion started: 17 October 2020
© Author(s) 2020. CC BY 4.0 License.

Atmospheric Measurement Techniques Discussions

Table 5. Comparison of results obtained by CRDS G2201-i with the values from the operator company.

id	CRDS 1s C_2H_6:CH_4 ratio	Operator data C_2H_6:CH_4 ratio	Residuals C_2H_6:CH_4 ratio	Date
A2	0.060 ± 0.005	0.051	0.009	16.05.2019
A3	0.045 ± 0.002	0.049	-0.004	15.07.2019
B3	0.052 ± 0.007	0.052	0.000	12.07.2019
B4	0.046 ± 0.008	0.052	-0.006	12.07.2019
D1	0 ± 0.006	NA	NA	16.05.2019

Finally, C_2H_6 mixing ratios measured by the CRDS G2201-i are compared with results from GC-FID. Three flask samples were taken from every surveyed site and measured afterward in the laboratory using GIC-FID. Then, the average of these three measures was calculated and for all sites their standard deviation is smaller than 1 ppb. On Figure 6, flask results are compared to results obtained by the CRDS G2201-i during the time of flask sampling. One should keep in mind that due the very short time sampling (<3s), the comparison of concentrations is only indicative. For landfill D, the C_2H_6 mixing ratio measured by GC-FID is 4.9 ppb. For A and C gas compressor stations, the C_2H_6 mixing ratio is 20.5 ppb and 13.7 ppb, respectively. Due to the instrument noise, for the landfill and two compressor stations (A and C), C_2H_6 mixing ratio measured by CRDS is higher than measured by GC- FID (Figure 6) and averaged observed overestimation for these three sites is about 40 ppb. This discrepancy is similar to the one observed in laboratory conditions, where CRDS result has been higher by about 30 ppb (section 3.1). A different situation is observed in the case of the gas compressor station B where higher C_2H_6 mixing ratio is observed. The results from flask samples are higher by about 7 ppb than from CRDS analyzer, what suggest a better agreement between instruments in the higher C_2H_6 mixing ratio. For all sites, in the case of CRDS measurements the standard deviation is almost equal to the averaged value over the sampling time. It is caused by high instrument noise (~50 ppb CMR and 25 ppb Allan deviation for raw data) and short sampling time (less than one minute).

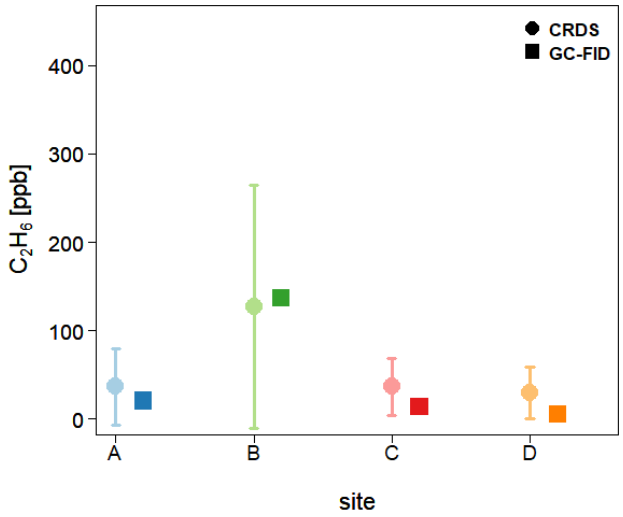

https://doi.org/10.5194/amt-2020-410
Preprint. Discussion started: 17 October 2020
© Author(s) 2020. CC BY 4.0 License.

Atmospheric Measurement Techniques Discussions

Figure 6. Comparison of the C_2H_6 mixing ratio measured in-situ by CRDS G2201-i and in the laboratory by GC-FID from flasks measurements. CRDS G2201-i measurements during the time of flask sampling. Uncertainties (1 SD) are indicated both for CRDS and GC-FID.

4. Discussion: Overall comparison with other instruments and methods

Based on the series of tests conducted in our study, using the CRDS G2201-i in a mobile set-up to measure C_2H_6:CH_4 ratio in methane plumes appears possible and can provide useful scientific results under specific conditions. In laboratory conditions, during measurements of gas containing C_2H_6, the CRDS G2201-i has a better CMR (12 ppb in 1 min) and a smaller noise calculated from Allan deviation (¬10 ppb in 1 min) than the CRDS G2132-i, which are equal 20 ppb and 25 ppb, respectively, in 1 min timeframe (Rella et al. 2015), where both instruments are not dedicated for C_2H_6 measurements. However, both instruments have lower performance than the CRDS G2210-i, dedicated to C_2H_6 measurement. For the latter instrument, both CMR and Allan deviation are smaller than 1 ppb (ATC Mlab test, personal communication). Additionally, based on a literature comparison, for both CRDS instruments, CMR and noise are higher than those obtained for the instrument based on the TLDAS method, dedicated for mobile measurements of C_2H_6 (as described by Yacovitch et al. 2014). For that instrument, the CMR is as low as 19 ppt in stationary conditions, and 210 ppt in motion.

Based on Assan et al. (2017), the correction of the sensitivity to other species is necessary (Eq. (1)) to account for the different instrument responses to water level lower or higher than 0.16% (low and high humidity). In this study, during laboratory work, the water vapor sensitivity was evaluated and results showed that applying interference correction factors determined for low humidity gave better results, including for more humidified air measurements. It is in opposition to results obtained by Assan et al. (2017). Therefore, we consider that water presence should be avoided and we recommend drying air before C_2H_6 measurement using CRDS G2201-i.

Previously, the CRDS G2201-i device CFIDS 2072 has only been used in stationary field work over two weeks (Assan et al. 2017) to make continuous measurements of CH_4, $\delta^{13}CH_4$ and C_2H_6 from gas facilities. The CRDS G2201-i and GC-FID measured air simultaneously from the shared inlet and were located 200 – 400 m from the gas facilities (pipelines and compressors). The GC-FID used in Assan et al. (2017) was a field instrument described in Gros et al. (2011) and Panopoulou et al. (2018) which has an overall uncertainty estimated to be better than 15%. For GC-FID 10 minutes of ambient air collection was measured during 20 minutes. Thus, for that instrument, the sampling time is 10 minutes sampling average over 30 minutes. To have identical timestamps as GC-FID, corrected and calibrated CRDS data were averaged for 10 min every 30 min. Flask samples were taken as well during that field work. That study was the first attempt to propose a protocol to use CRDS G2201-i to measure C_2H_6:CH_4 ratio, both from flask sampling and from continuous measurements, and found a good agreement between CRDS and GC-FID measurements (Assan et al. 2017). In our study, we went one step further and considered the constraints associated with a mobile setup within a car. As the instrument noise increases during the motion of the car, we decided to stop the car for about 35 minutes inside the plume to acquire the observations. As it is not possible to stop the car in every place where measurements are made, it is a limitation for this application of the instrument, compared to other

https://doi.org/10.5194/amt-2020-410
Preprint. Discussion started: 17 October 2020
© Author(s) 2020. CC BY 4.0 License.

Atmospheric Measurement Techniques Discussions

instruments able to measure C_2H_6 while moving across the plume, like the LGR UMEA (Lowry et al. 2020) or the instrument based on TILDAS method (Smith et al., 2015; Yacovitch et al., 2014, 2020).

During our trace release experiment, C_2H_6:CH_4 ratio was calculated from measurements made when the car was standing inside the plume. With this approach, measured ratios were underestimated. However, using the LGR UMEA instrument, dedicated to mobile C_2H_6:CH_4 ratio measurements, some discrepancy between the measured and released value was also observed, albeit smaller. Indeed, in the case of the LGR UMEA measurements, the residuals between measurements and released value were in the range -0.015 to -0.001, where using the CRDS G2201-i the residuals are in the range -0.018 to -0.002. It is also worth noting that the more precise instrument, presented by Yacovitch et al. (2014), also inferred a systematical underestimation of the C_2H_6 mixing ratio by ~6% of the measured value. In their study, this systematic error was added as a reported statistical error (Yacovitch et al. 2014).

In our study, during the trace release experiment, we also compared results obtained by stationary standing inside the plume and by sampling air with an AirCore system. The absolute deviation is equal to 0.011 and 0.017 for stationary mode and AirCore mode, respectively. The residuals between released and measured values are from -0.018 to -0.002 for stationary mode and from -0.025 to 0.027 for AirCore mode. Thus, the agreement with released C_2H_6:CH_4 ratio is better for measurements made by standing inside the plumes than with AirCore sampler. However, during previous studies where CRDS instruments were used (Rella et al. 2015; Lopez et al. 2017), C_2H_6:CH_4 ratio was also measured using AirCore sampler. In the study made by Lopez et al. (2017) for pipelines measurements, gas flasks were also collected and measured at INSTAAR (Boulder, CO, USA) using gas chromatography. Overall, AirCore sampler results were in good agreement with the results for flasks measurements. During these measurements, the CRDS was flushed continuously with a flow rate of 1000 mL/min and a mass flow controller was part of the setup. During AirCore analysis, the airflow rate was equal to 40 mL/min. This change allowed to increase the number of measurements point by 25, when the replay mode was used. In our study, in the monitoring mode, we flushed the CRDS instrument with a flow rate of 160 mL/min and in the replay mode, we increased the number of points only by 3. These differences could contribute to explaining the discrepancies between measured and released C_2H_6:CH_4 ratio. Further decreasing the flow rate will increase the number of sampling points and could improve the agreement between AirCore-based estimations and actual ratios. This should be tested to conclude the optimal use of AirCore setup to improve the characterization of methane sources.

Finally, the C_2H_6:CH_4 ratios obtained by standing inside the plumes are accurate and allow to separate the different releases at the resolution of the conducted experiment. They are also comparable with results obtained using LGR UMEA. This agreement between measurements and reality has also been confirmed during real field conditions mobile measurements. During these measurements, residuals for dry air sampling were between -0.006 and 0.009. Additionally, during field work, flasks samples have been taken and measured by GC-FID in the laboratory. During the time of flask sampling at the two gas compressors stations, the C_2H_6 mixing ratios were below the value of the instrument CMR (~50 ppb). For the third gas compressor station, the C_2H_6 mixing ratio was above the detection threshold and C_2H_6 mixing ratio measured by GC-FID was higher than measured by CRDS. Nevertheless, due to the short sampling time of the flasks, these first comparisons are only indicative and more

https://doi.org/10.5194/amt-2020-410
Preprint. Discussion started: 17 October 2020
© Author(s) 2020. CC BY 4.0 License.

Atmospheric Measurement Techniques Discussions

comparison campaigns should help to understand the discrepancies between these instruments. In all cases, the standard deviation of C_2H_6 measured by CRDS was close to the averaged value. It shows the CRDS G2201-i should not be used for the measurements of the absolute value of the C_2H_6 mixing ratio.

Overall, using C_2H_6:CH_4 ratio measured by the CRDS G2201-i, it is possible to separate methane sources between a biogenic origin (C_2H_6:CH_4 ~ 0.00), natural gas leaks and compressors (C_2H_6:CH_4 ~ 0.06, can vary between 0.02-0.17) and processed natural gas liquids (C_2H_6:CH_4 ~ 0.3). C_2H_6:CH_4 ratio of natural gas can vary on origin and processing. Thus, determining the exact source of methane inside the industrial site, with a lot of potential methane emitters, can be more challenging to achieve. However, looking at the results of our study, if the differences between C_2H_6:CH_4 ratios are higher than 0.01, it is still possible to determine the source of the observed CH_4 plume using C_2H_6:CH_4 ratio measured by the CRDS G2201-i.

5. Conclusions

The instrument CRDS G2201-i measures $^{12}CO_2$, $^{13}CO_2$, $^{12}CH_4$, $^{13}CH_4$, H_2O and C_2H_6, the latter being initially present to correct $^{13}CH_4$ measurements. This study investigates the possibility to make ethane measurements, made by a CRDS G2201-i instrument, useful for methane source apportionment. The interest is to be able to better constrain methane sources at the laboratory and in the field with only one instrument. Before any analysis, C_2H_6 raw data must be corrected and calibrated. The linearity test showed good stability over time, with only a small change of calibration factors over 4 years. Contrary to the previous studies (Rella et al. 2015; Assan et al. 2017), we do not observe any time drift of the C_2H_6 baseline. Nevertheless, regular calibrations and target measurements are advised.

The controlled release experiment revealed a small systematical underestimation of measured ratios inside the plumes compared to released ones. The larger discrepancy from released C_2H_6:CH_4 occurs in the case of AirCore samplings. Due to that, we recommend standing inside the plumes instead of taking AirCore samples to measure C_2H_6:CH_4 ratios. However, decreasing the flushing flow rate of the CRDS can improve the performance of the instrument during AirCore sampling and should be further investigated in the next campaigns.

In this study, we find some limitations of using CRDS G2201-i to measure C_2H_6:CH_4. First of all, we found that we need at least a peak maximum of 100 ppb in ethane to get useful results to help portioning methane sources. Additionally, the required maximum CH_4 enhancement above background should be higher than 1 ppm. This threshold is determined using error propagation for a typical C_2H_6:CH_4 ratio equal to 0.1. In the field conditions, this threshold was successfully used for C_2H_6:CH_4 ratio close to 0.05. For weak sources with enhancements below 1 ppm, this limitation prevents providing C_2H_6:CH_4 ratio measurements using our approach. Secondly, we have observed significant changes in observed C_2H_6 mixing ratios in the presence of water vapor and we strongly recommend drying air before making measurements.

Third, due to an increase of the instrument noise during the motion of the car, it is not possible to measure C_2H_6:CH_4 ratio when moving across plumes as currently made to estimate methane emissions (e.g., Ars et al. 2017). Other dedicated

https://doi.org/10.5194/amt-2020-410
Preprint. Discussion started: 17 October 2020
© Author(s) 2020. CC BY 4.0 License.

Atmospheric Measurement Techniques Discussions

instruments have to be used in this case for ethane (Yacovitch et al. 2014; Lowry et al. 2020). To fix this problem, C_2H_6:CH_4 ratio can be measured by standing inside the plumes or by AirCore sampling after solving the flushing issue.

Despite these limitations, this study shows the possibility of using the CRDS G2201-i to measure C_2H_6:CH_4 ratio in the field conditions in strong methane enhancements, using mobile platforms. Even though the instrument is not dedicated for C_2H_6:CH_4 ratio measurements, after applying correction and calibration factors, when the air is dried and methane maximum in a peak is 1 ppm above background, the CRDS G2201-i gives results comparable with released values in controlled experiments. Therefore, under these conditions, the CRDS G2201-i instrument can contribute to better constrain methane sources deploying only one instrument.

Appendix A

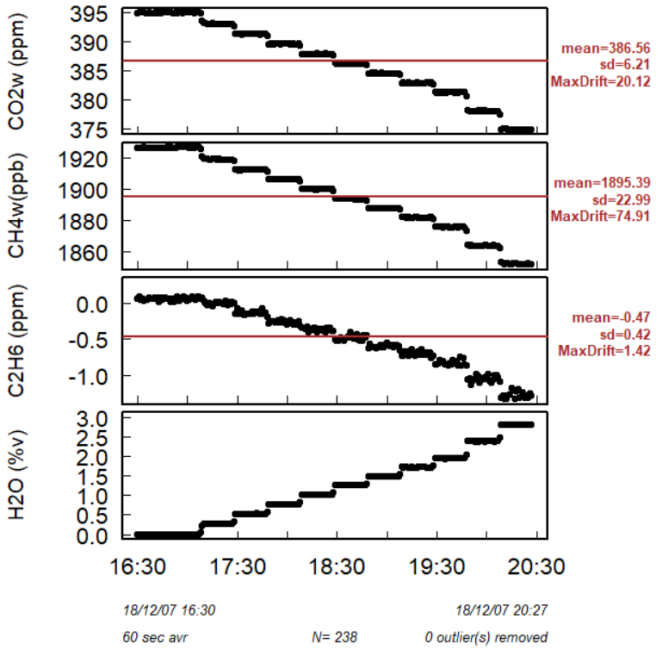

Figure A1. H_2O influence on CO_2, CH_4 and C_2H_6.

The results, presented in Figure 3 in the paper, were obtained using wet CH_4 and CO_2 values. In the next step, the analysis of the water vapor sensitivity test was repeated using dry CH_4 and CO_2 values. These dry values are corrected by default already in the instrument. For all three cases, using dry or wet CH_4 and CO_2 values did not change the C_2H_6 values, which suggests a bigger influence of H_2O than CH_4 and CO_2 on C_2H_6. When the interference correction for low humidity was applied for all steps, the average C_2H_6 mixing ratio is equal 28 ± 62 ppb and 28 ± 61 ppb for wet and dry CH_4 and CO_2, respectively. Figure A2 presents a comparison of wet and dry CO_2 and CH_4 values.

https://doi.org/10.5194/amt-2020-410
Preprint. Discussion started: 17 October 2020
© Author(s) 2020. CC BY 4.0 License.

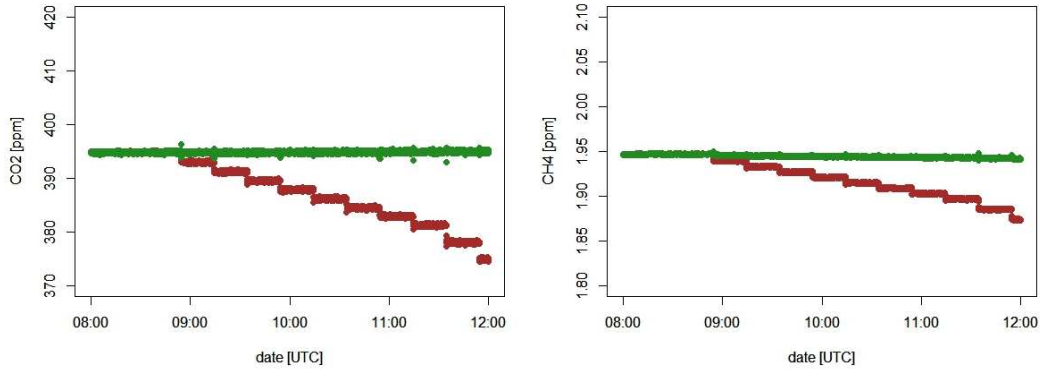

Figure A2. Dry (manufactured correction) and wet values of CO_2 and CH_4. Green – dry values, red – wet values. Left: CO_2 mixing ratio, right CH_4 mixing ratio.

Appendix B

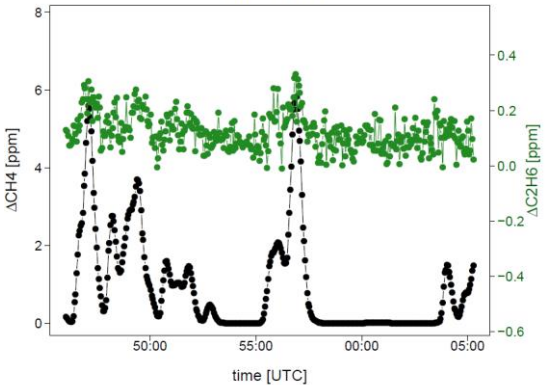

Figure B1. CH_4 and C_2H_6 mixing ratio observed during standing inside the plume

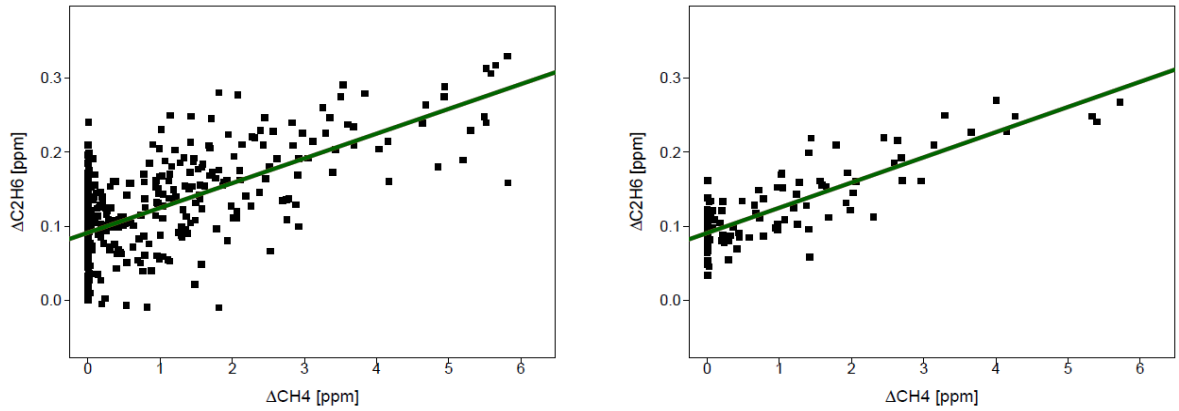

Figure B2. C_2H_6 mixing ratio vs. CH_4 mixing ratio observed while standing inside the plume. Left: non-averaged data. Right: 10 s averaged data. Green line: linear fitting

https://doi.org/10.5194/amt-2020-410
Preprint. Discussion started: 17 October 2020
© Author(s) 2020. CC BY 4.0 License.

Atmospheric Measurement Techniques Discussions

Appendix C

Table C1 C_2H_6:CH_4 ratio with interference correction for high humidity. * background samples

name.id	CO_2 [ppm]	CH_4 [ppm]	$\delta^{13}CH_4$ [‰]	H_2O [%]	C_2H_6 [ppm]	C_2H_6:CH_4 ratio
1.1b	402	2.23	-47	1.25	0.27 ± 0.06	0.12 ± 0.03
1.2b	397	2.01	-47	1.22	0.27 ± 0.06	0.13 ± 0.03
1.3b	399	3.34	-45	1.22	0.39 ± 0.06	0.12 ± 0.02
1.4b*	395	1.96	-48	1.23	0.44 ± 0.06	0.22 ± 0.03
1.5b	399	2.31	-46	1.29	0.43 ± 0.06	0.19 ± 0.03
1.6b	399	5.25	-43	1.29	0.45 ± 0.07	0.09 ± 0.01
1.7b	402	5.19	-44	1.29	0.62 ± 0.09	0.12 ± 0.02
1.8b*	396	1.98	-48	1.25	0.55 ± 0.08	0.28 ± 0.04
2.1b	420	3.25	-45	1.27	0.55 ± 0.07	0.17 ± 0.02
2.2b*	397	1.97	-49	1.17	0.72 ± 0.15	0.36 ± 0.08

Appendix D

Comparison of raw data and 10 s averaged data from measurements in the Ile-de-France region

Table D1. Field work analysis A, B and C- gas compressor, BB – landfill; *: A1, B1 and B2 rejected from further analysis (wet air) and ** C1 rejected from further analysis (low enhancement), raw and 10 s averaged data

id	max ΔCH_4	max ΔC_2H_6	1 s	r^2	10 s	r_2	n	data
A1*	1.486	0.309	0.070 ± 0.013	0.162	0.066 ± 0.018	0.235	138	16.05.2019
A2	1.737	0.269	0.060 ± 0.005	0.195	0.059 ± 0.007	0.303	533	16.05.2019
A3	5.85	0.414	0.045 ± 0.002	0.489	0.044 ± 0.003	0.645	495	15.07.2019
B1*	7.314	0.878	0.090 ± 0.001	0.852	0.091 ± 0.002	0.927	811	27.05.2019
B2*	0.513	0.323	0.085 ± 0.022	0.024	0.083 ± 0.029	0.044	594	12.07.2019
B3	1.454	0.26	0.052 ± 0.007	0.082	0.05 ± 0.009	0.15	613	12.07.2019
B4	1.677	0.236	0.046 ± 0.008	0.086	0.05 ± 0.011	0.174	336	12.07.2019
C1**	0.495	0.284	0.091 ± 0.037	0.037	0.09 ± 0.021	0.082	711	28.05.2019
D1	1.516	0.266	0 ± 0.006	0	0 ± 0.007	0	712	16.05.2019

Data availability

Data from the field work and most of the laboratory tests are available on the Carbon Portal and waiting to obtain a DOI number. Data from time drift test are available on demand.

https://doi.org/10.5194/amt-2020-410
Preprint. Discussion started: 17 October 2020
© Author(s) 2020. CC BY 4.0 License.

Author contribution

Conceptualization, S.D., JD.P.; Methodology, S.D., JD.P. C.Y.K., D.L., J.F., J.H., N.Y, V.G.; Software, S.D., C.Y.K., D.L.; Formal Analysis, S.D., D.L., N.Y.; Investigation, S.D., JD.P. C.Y.K., D.L.; Resources, JD.P. C.Y.K., P.B., J.H.; Data Curation S.D., D.L.; Writing – Original, S.D.; Draft Writing – Review & Editing, S.D., JD.P. C.Y.K., D.L., J.F., J.H., N.Y. V.G., P.B.; Visualization, S.D., D.L.; Supervision, JD.P. C.Y.K., P.B.

Competing interests

The authors declare that they have no conflict of interest.

Acknowledgments

We acknowledge our laboratory colleagues C. Philippon and L. Lienhardt, for sharing results of tests made in ATC Mlab. We thank also gratefully D. Baisnee for the measurements of flask samples on the GC-FID. We gratefully acknowledge GRTgaz company for sharing data with us and helping to improve the manuscript, especially: P. Guillo-Lohan, P. Alas, F. Bainier and JL. Fabre.

References

Allan, D. W.: Statistics of atomic frequency standards, Proc. IEEE, 54(2), 221–230, doi:10.1109/PROC.1966.4634, 1966.

Assan, S., Baudic, A., Guemri, A., Ciais, P., Gros, V. and Vogel, F. R.: Characterization of interferences to in situ observations of delta13CH4 and C2H6 when using a cavity ring-down spectrometer at industrial sites, Atmospheric Measurement Techniques, 10(6), 2077–2091, doi:10.5194/amt-10-2077-2017, 2017.

Aydin, M., Verhulst, K. R., Saltzman, E. S., Battle, M. O., Montzka, S. A., Blake, D. R., Tang, Q. and Prather, M. J.: Recent decreases in fossil-fuel emissions of ethane and methane derived from firn air, Nature, 476(7359), 198–201, doi:10.1038/nature10352, 2011.

Bonsang, B. and Kanakidou, M.: Non-methane hydrocarbon variability during the FIELDVOC'94 campaign in Portugal, Chemosphere - Global Change Science, 3(3), 259–273, doi:10.1016/S1465-9972(01)00009-5, 2001.

Bourtsoukidis, E., Ernle, L., Crowley, J. N., Lelieveld, J., Paris, J.-D., Pozzer, A., Walter, D. and Williams, J.: Non Methane Hydrocarbon sources and sinks around the Arabian Peninsula, Atmospheric Chemistry and Physics Discussions, 1–45, doi:https://doi.org/10.5194/acp-2019-92, 2019.

Defratyka, S., Paris, J. D., Yver-Kwok, C., Fernandez, J. M., Korben, P. and Bousquet, P.: Mapping urban methane sources in Paris, France, Manuscript submitted for publication, 2020.

Dlugokencky, E.: NOAA/ESRL, 2020.

https://doi.org/10.5194/amt-2020-410
Preprint. Discussion started: 17 October 2020
© Author(s) 2020. CC BY 4.0 License.

Gardiner, T., Helmore, J., Innocenti, F. and Robinson, R.: Field Validation of Remote Sensing Methane Emission Measurements, Remote Sensing, 9(9), 956, doi:10.3390/rs9090956, 2017.

Gros, V., Gaimoz, C., Herrmann, F., Custer, T., Williams, J., Bonsang, B., Sauvage, S., Locoge, N., d'Argouges, O., Sarda-Estève, R. and Sciare, J.: Volatile organic compounds sources in Paris in spring 2007. Part I: qualitative analysis, Environ. Chem., 8(1), 74, doi:10.1071/EN10068, 2011.

Hausmann, P., Sussmann, R. and Smale, D.: Contribution of oil and natural gas production to renewed increase in atmospheric methane (2007–2014): top–down estimate from ethane and methane column observations, Atmos. Chem. Phys., 16(5), 3227–3244, doi:10.5194/acp-16-3227-2016, 2016.

Helmig, D., Rossabi, S., Hueber, J., Tans, P., Montzka, S. A., Masarie, K., Thoning, K., Plass-Duelmer, C., Claude, A., Carpenter, L. J., Lewis, A. C., Punjabi, S., Reimann, S., Vollmer, M. K., Steinbrecher, R., Hannigan, J. W., Emmons, L. K., Mahieu, E., Franco, B., Smale, D. and Pozzer, A.: Reversal of global atmospheric ethane and propane trends largely due to US oil and natural gas production, Nature Geosci, 9(7), 490–495, doi:10.1038/ngeo2721, 2016.

Hoheisel, A.: Characterisation of delta13CH4 source signatures from methane sources in Germany using mobile measurements, University of Heidelberg, Institute of Environmental Physics, 1 October., 2018.

Hoheisel, A., Yeman, C., Dinger, F., Eckhardt, H. and Schmidt, M.: An improved method for mobile characterisation of δ13CH4 source signatures and its application in Germany, Atmospheric Measurement Techniques, 12(2), 1123–1139, doi:https://doi.org/10.5194/amt-12-1123-2019, 2019.

IPCC: Climate Change 2013: The Physical Science Basis. Contribution of Working Group I to the Fifth Assessment Report of the Intergovernmental Panel on Climate Change, Cambridge University Press, Cambridge, United Kingdom and New York, NY, USA., 2018.

Kort, E. A., Smith, M. L., Murray, L. T., Gvakharia, A., Brandt, A. R., Peischl, J., Ryerson, T. B., Sweeney, C. and Travis, K.: Fugitive emissions from the Bakken shale illustrate role of shale production in global ethane shift: Ethane Emissions From the Bakken Shale, Geophys. Res. Lett., 43(9), 4617–4623, doi:10.1002/2016GL068703, 2016.

Lopez, M., Sherwood, O. A., Dlugokencky, E. J., Kessler, R., Giroux, L. and Worthy, D. E. J.: Isotopic signatures of anthropogenic CH4 sources in Alberta, Canada, Atmospheric Environment, 164, 280–288, doi:10.1016/j.atmosenv.2017.06.021, 2017.

Lowry, D., Fisher, R. E., France, J. L., Coleman, M., Lanoisellé, M., Zazzeri, G., Nisbet, E. G., Shaw, J. T., Allen, G., Pitt, J. and Ward, R. S.: Environmental baseline monitoring for shale gas development in the UK: Identification and geochemical characterisation of local source emissions of methane to atmosphere, Science of The Total Environment, 708, 134600, doi:10.1016/j.scitotenv.2019.134600, 2020.

McKain, K., Down, A., Raciti, S. M., Budney, J., Hutyra, L. R., Floerchinger, C., Herndon, S. C., Nehrkorn, T., Zahniser, M. S., Jackson, R. B., Phillips, N. and Wofsy, S. C.: Methane emissions from natural gas infrastructure and use in the urban region of Boston, Massachusetts, Proceedings of the National Academy of Sciences, 112(7), 1941–1946, doi:10.1073/pnas.1416261112, 2015.

Panopoulou, A., Liakakou, E., Gros, V., Sauvage, S., Locoge, N., Bonsang, B., Psiloglou, B. E., Gerasopoulos, E. and Mihalopoulos, N.: Non-methane hydrocarbon variability in Athens during wintertime: the role of traffic and heating, Atmos. Chem. Phys., 18(21), 16139–16154, doi:10.5194/acp-18-16139-2018, 2018.

https://doi.org/10.5194/amt-2020-410
Preprint. Discussion started: 17 October 2020
© Author(s) 2020. CC BY 4.0 License.

Atmospheric Measurement Techniques Discussions

Rella, C. W., Hoffnagle, J., He, Y. and Tajima, S.: Local- and regional-scale measurements of CH4, δ13CH4, and C2H6 in the Uintah Basin using a mobile stable isotope analyzer, Atmospheric Measurement Techniques, 8(10), 4539–4559, doi:10.5194/amt-8-4539-2015, 2015.

Saunois, M., Bousquet, P., Poulter, B., Peregon, A., Ciais, P., Canadell, J. G., Dlugokencky, E. J., Etiope, G., Bastviken, D., Houweling, S., Janssens-Maenhout, G., Tubiello, F. N., Castaldi, S., Jackson, R. B., Alexe, M., Arora, V. K., Beerling, D. J., Bergamaschi, P., Blake, D. R., Brailsford, G., Brovkin, V., Bruhwiler, L., Crevoisier, C., Crill, P., Covey, K., Curry, C., Frankenberg, C., Gedney, N., Höglund-Isaksson, L., Ishizawa, M., Ito, A., Joos, F., Kim, H.-S., Kleinen, T., Krummel, P., Lamarque, J.-F., Langenfelds, R., Locatelli, R., Machida, T., Maksyutov, S., McDonald, K. C., Marshall, J., Melton, J. R., Morino, I., Naik, V., O'Doherty, S., Parmentier, F.-J. W., Patra, P. K., Peng, C., Peng, S., Peters, G. P., Pison, I., Prigent, C., Prinn, R., Ramonet, M., Riley, W. J., Saito, M., Santini, M., Schroeder, R., Simpson, I. J., Spahni, R., Steele, P., Takizawa, A., Thornton, B. F., Tian, H., Tohjima, Y., Viovy, N., Voulgarakis, A., van Weele, M., van der Werf, G. R., Weiss, R., Wiedinmyer, C., Wilton, D. J., Wiltshire, A., Worthy, D., Wunch, D., Xu, X., Yoshida, Y., Zhang, B., Zhang, Z. and Zhu, Q.: The global methane budget 2000–2012, Earth System Science Data, 8(2), 697–751, doi:10.5194/essd-8-697-2016, 2016.

Saunois, M., Stavert, A. R., Poulter, B., Bousquet, P., Canadell, J. G., Jackson, R. B., Raymond, P. A., Dlugokencky, E. J., Houweling, S., Patra, P. K., Ciais, P., Arora, V. K., Bastviken, D., Bergamaschi, P., Blake, D. R., Brailsford, G., Bruhwiler, L., Carlson, K. M., Carrol, M., Castaldi, S., Chandra, N., Crevoisier, C., Crill, P. M., Covey, K., Curry, C. L., Etiope, G., Frankenberg, C., Gedney, N., Hegglin, M. I., Höglund-Isaksson, L., Hugelius, G., Ishizawa, M., Ito, A., Janssens-Maenhout, G., Jensen, K. M., Joos, F., Kleinen, T., Krummel, P. B., Langenfelds, R. L., Laruelle, G. G., Liu, L., Machida, T., Maksyutov, S., McDonald, K. C., McNorton, J., Miller, P. A., Melton, J. R., Morino, I., Müller, J., Murgia-Flores, F., Naik, V., Niwa, Y., Noce, S., O'Doherty, S., Parker, R. J., Peng, C., Peng, S., Peters, G. P., Prigent, C., Prinn, R., Ramonet, M., Regnier, P., Riley, W. J., Rosentreter, J. A., Segers, A., Simpson, I. J., Shi, H., Smith, S. J., Steele, L. P., Thornton, B. F., Tian, H., Tohjima, Y., Tubiello, F. N., Tsuruta, A., Viovy, N., Voulgarakis, A., Weber, T. S., van Weele, M., van der Werf, G. R., Weiss, R. F., Worthy, D., Wunch, D., Yin, Y., Yoshida, Y., Zhang, W., Zhang, Z., Zhao, Y., Zheng, B., Zhu, Q., Zhu, Q. and Zhuang, Q.: The Global Methane Budget 2000–2017, preprint, Atmosphere – Atmospheric Chemistry and Physics., 2020.

Schwietzke, S., Griffin, W. M., Matthews, H. S. and Bruhwiler, L. M. P.: Natural Gas Fugitive Emissions Rates Constrained by Global Atmospheric Methane and Ethane, Environ. Sci. Technol., 48(14), 7714–7722, doi:10.1021/es501204c, 2014.

Sherwood, O. A., Schwietzke, S., Arling, V. A. and Etiope, G.: Global Inventory of Gas Geochemistry Data from Fossil Fuel, Microbial and Burning Sources, version 2017, Earth Syst. Sci. Data, 9(2), 639–656, doi:10.5194/essd-9-639-2017, 2017.

Simpson, I. J., Sulbaek Andersen, M. P., Meinardi, S., Bruhwiler, L., Blake, N. J., Helmig, D., Rowland, F. S. and Blake, D. R.: Long-term decline of global atmospheric ethane concentrations and implications for methane, Nature, 488(7412), 490–494, doi:10.1038/nature11342, 2012.

Smith, M. L., Kort, E. A., Karion, A., Sweeney, C., Herndon, S. C. and Yacovitch, T. I.: Airborne Ethane Observations in the Barnett Shale: Quantification of Ethane Flux and Attribution of Methane Emissions, Environ. Sci. Technol., 49(13), 8158–8166, doi:10.1021/acs.est.5b00219, 2015.

Taylor, J. R.: An introduction to error analysis. The study of uncertainties in physical measurements, second., University Science Books., 1997.

Turner, A. J., Frankenberg, C. and Kort, E. A.: Interpreting contemporary trends in atmospheric methane, Proc Natl Acad Sci USA, 116(8), 2805–2813, doi:10.1073/pnas.1814297116, 2019.

Yacovitch, T. I., Herndon, S. C., Roscioli, J. R., Floerchinger, C., McGovern, R. M., Agnese, M., Pétron, G., Kofler, J., Sweeney, C., Karion, A., Conley, S. A., Kort, E. A., Nähle, L., Fischer, M., Hildebrandt, L., Koeth, J., McManus, J. B., Nelson,

https://doi.org/10.5194/amt-2020-410
Preprint. Discussion started: 17 October 2020
© Author(s) 2020. CC BY 4.0 License.


D. D., Zahniser, M. S. and Kolb, C. E.: Demonstration of an Ethane Spectrometer for Methane Source Identification, Environ. Sci. Technol., 48(14), 8028–8034, doi:10.1021/es501475q, 2014.

565 Yacovitch, T. I., Daube, C. and Herndon, S. C.: Methane Emissions from Offshore Oil and Gas Platforms in the Gulf of Mexico, Environ. Sci. Technol., 54(6), 3530–3538, doi:10.1021/acs.est.9b07148, 2020.

Yang, K., Ting, C., Wang, J., Wingenter, O. and Chan, C.: Diurnal and seasonal cycles of ozone precursors observed from continuous measurement at an urban site in Taiwan, Atmospheric Environment, 39(18), 3221–3230, doi:10.1016/j.atmosenv.2005.02.003, 2005.

570 Yver Kwok, C., Laurent, O., Guemri, A., Philippon, C., Wastine, B., Rella, C. W., Vuillemin, C., Truong, F., Delmotte, M., Kazan, V., Darding, M., Lebègue, B., Kaiser, C., Xueref-Rémy, I. and Ramonet, M.: Comprehensive laboratory and field testing of cavity ring-down spectroscopy analyzers measuring H2O, CO2, CH4 and CO, Atmos. Meas. Tech., 8(9), 3867–3892, doi:10.5194/amt-8-3867-2015, 2015.

Chapter 4 Mapping urban methane sources in Paris, France

4.1 Introduction: motivation and summary of the publication

Urbanized areas concentrate more than 50% of the global population and emit more than 70% of fossil fuel CO_2. They are also responsible for CH_4 emissions within their area and elsewhere, like emissions from landfills, wastewater treatment plants and natural-gas delivery infrastructure. For example, urban areas contributed 42% to the global CH_4 emission of the energy sector and 40% to the global waste sector in 2000 (Hopkins et al. 2016; Marcotullio et al. 2013) considering scope 1 and 2. An urban area's contribution can gain importance in the future, as the global urban population is predicted to double by 2050, compared to 2010 (Duren and Miller 2012). Currently, different definitions of urban and city area are used over the world, what cause discrepancies between observations (Satterthwaite 2008; Marcotullio et al. 2013; Hopkins et al. 2016). As a consequence, representative studies of CH_4 emissions in urban areas are necessary. They can provide crucial information to develop efficient mitigation actions, with the observations made on a relatively small scale (Duren and Miller 2012; "CCAC" 2020). As previous studies already showed, local mobile measurements can be used to broaden knowledge about city CH_4 emissions (e.g., Lowry et al. 2020; Jackson et al. 2014; Townsend-Small et al. 2012; von Fischer et al. 2017; Zazzeri et al. 2017).

Tests presented in chapter 2 and 3 clearly showed that CRDS G2201-i can be efficiently used during mobile measurements. In my study, this instrument was used for measurements on industrial site and city scales in IDF region. Here, I am focus on Paris city, which is the densest area in Metropolitan France and reached 20,000 people km^{-2}. Its population is about two mln people (INSEE 2019). Mobile measurements in Paris city allow defining city CH_4 emissions in scope 1.

Between September 2018 and March 2019, 17 surveys were made in the Paris city and its south-west suburbs using a CRDS analyzer with the AirCore tool. During surveys, the CH_4 mixing ratio was observed in situ. The background was calculated as 2 minute moving average. Leak indications are defined as a CH_4 enhancement larger than the threshold (10% above background CH_4). In locations where CH_4 enhancement reached more than 500 ppb above background, the isotopic signature was sampled using the AirCore tool (chapter 2.3). In total, 28 AirCores were taken in 17 locations. However, only samples with fitting standard deviations < 10 ‰ and coefficient correlation $r^2 > 0.85$, were used for further analysis in order to balance precise results and quantity of kept values. According to these criteria, 12 AirCores from 11 locations are used. Additionally, during four days, walking measurements using LGR MGGA were made, which allowed determining the exact position of some CH_4 leak indications observed from the car. In total, 500 km out of the 1800 km roads in Paris and suburbs were driven. Part of the streets was passed multiple times (2-5).

Overall, 90 leak indications were observed and the origin of 27 of them was determined based on the isotopic signature or walking measurements. Three main methane sources were observed: natural gas distribution network leaks, sewage network leaks and building's venting grids. The emission from venting grids was observed during walking measurements and was not reported in previous studies.

As the emission observed from venting grids probably come from leaking heating installation, this category is further called "furnaces". The biggest contribution comes from natural gas leaks. Fifteen leaks were observed from this source. Two clusters with a denser spatial distribution of CH_4 leak indications were observed. Cluster A is situated in west Paris, and six defined leak indications were observed there. Cluster B is located in the south-west suburbs of Paris, and 15 defined leak indications occurred there. In Cluster A majority of defined leaks come from furnaces (3 leaks). In contrast, in cluster B, emissions were attributed to gas leaks (9 leak indications) or sewage (6 leaks).

It was not possible to determine the origin of 63 remaining leak indications. Their enhancement was too small to take isotopic samples, and the instrument to make walking measurements was not available. Part of these leak indications was observed once and part of them multiple times. Seven unknown leak indications are localized in Cluster A and 17 in Cluster B. The simple assumption was made based on the detected leaks with the known origin to attribute unknown leak indication to Paris' methane sources. As furnaces were detected only during walking measurements, they are not possible to see from the road. Thus, 66% of leak indications determined from the road in Paris come from gas leaks and 34% from the sewage network. This percentage of source categories is expanded for 63 unknown leak indications, and 41 leaks are attributed to gas leaks and 22 as sewage network leaks. Using this assumption, the gas leak indications rate (gas leak indications/ unique kilometers) is equal to 0.11 km^{-1}.

Based on von Fisher et al. (2017) and Weller et al. (2019), the emission rate of individual leaks was calculated. For the natural gas distribution leak indications, indicated using $\delta^{13}CH_4$ or walking measurement, the mean estimated emission rate for an individual leak location is equal to 1.4 L/min (range 0.5 – 3.87 L/min). They are categorized as small leaks (< 6 L/min), according to the categorization proposed by von Fischer et al. (2017). The mean estimated emission rate for an individual location is equal to 2.2 L/min (0.7 to 6.5 L/min) for the sewage sector. In this case, seven leak indications are in the small leak category, and one leak indication is in the medium category. The mean emission rate for an individual location is equal to 3.5 L/min (0.7 to 5.9 L/min) for the furnace sector. For the remaining 63 leak indications, the mean estimated emission rate is equal to 1.4 L/min (0.5 – 10.5 L/min). Only one is categorized as a medium, and it reached 10.5 L/min. Thus, the emission rate for individual leaks is skewed for lower emission rates with a median value equals to 0.8 L/min. Overall, on a unique 500 km, the accumulated emission rate is equal to 140 L/min. The gas sector contributes 56% under the attribution assumption. The sewage sector and furnaces contribute 34% and 10%, respectively. After upscaling to the Paris road length, the city emission rate is equal to 500 L/min (190 t/yr).

Based on these surveys, Paris is in the middle to low range compared to U.S cities, according to von Fischer et al. (2017) leak size categories. Overall, the results for the leak rate in Paris are two to four times smaller than the rates calculated for the cities with an old pipeline system in the U.S. and two to forty times higher than cities with a modern pipeline system in the U.S.(von Fischer et al. 2017).

During this study, the possibility of using AirCore sampling inside the city was tested, while the previous studies (Lopez et al. 2017; Rella et al. 2015; Hoheisel et al. 2019) were focused on point sources like gas facilities or landfills. The proposed measurement protocol allows distinguishing CH_4 sources inside the city. It also provides the possibility to conduct surveys focused on individual streets or districts, which gives information about real small scale sources in the city. The study can potentially be important and meaningful for several operators and public authorities. An attempt to establish

contact with the gas distribution operator, to exchange data and share results, was made. No relevant interlocutor was successfully identified, possibly because gas distribution company data are not public. Likely, the publication of the results will be useful for the operators and public authorities.

The detailed explanation of surveys conducted in Paris is presented in the article draft already submitted to the scientific journal. It is presented in chapter 4.3 of this manuscript. After the method section, the results broken down into clusters are presented. The results of this study are compared to previous knowledge about the CH_4 observed in Paris, based on inventories (AIRPARIF) and mobile measurements (Xueref-Remy et al. 2019). Furthermore, the observation made in Paris city is compared with observations made in other cities (e.g., Zazzeri et al. 2017; Townsend-Small et al. 2012; McKain et al. 2015; von Fischer et al. 2017). Finally, the possible methods of improvements and implementations for policymakers are discussed. Supplementary Information to article is presented in Appendix 1 of the manuscript.

Additionally, five surveys were made during the summer of 2019. They were focused on revisiting the location, where previously leak indications were observed. The results of these surveys are presented below. It allows verifying possible temporal variations of observed CH_4 plumes inside Paris city.

4.2 Observation of temporal variation within mapping urban methane sources in Paris

During Summer 2019, five surveys were made in Paris, and 200 km of roads were driven. The verification of previously observed leak indication was the main purpose of these surveys. The measurement protocol was similar to the measurement made previously. All surveys were made using CRDS G2201-i with the AirCore tool, and the inlet was situated on the car roof. The calibration factors were applied both for the CH_4 mixing ratio and $\delta^{13}CH_4$ isotopic signature. The background was determined as a 2-minute moving average, and leak indications are defined as CH_4 enhancement 10% above the background.

9 AirCore samples were taken and 6 of them fulfilled the criteria and were used for further analysis. Three of them were determined as coming from the sewage as $\delta^{13}CH_4$ was more depleted and reached less than -50 ‰. All of them were observed in cluster B. Two leak indications were attributed to gas leaks as they were more enriched and reached -48.0 ± 6.9 ‰ and -46.2 ± 4.34 ‰. The first leak indication was observed out of clusters, and the second one was observed inside cluster B. The one remaining leak reached -34.3 ± 5.5 ‰, and despite passing this street three times in a row, this leak was observed only once. Thus, it is attributed to traffic.

In total, 38 leak indications were observed. Two of them are determined as coming from traffic and rejected from further analysis. In cluster A, observed enhancement was small, and no leak indication was observed there. Twelve leak indications were localized in Cluster B. The remaining 24 leak indications are situated out of Clusters A and B. In Cluster B, in addition to two leak indications, which isotopic signature were determined, two leaks were observed in the same position as sewage leaks previously. Thus, probably these two leak indications come from the sewage.

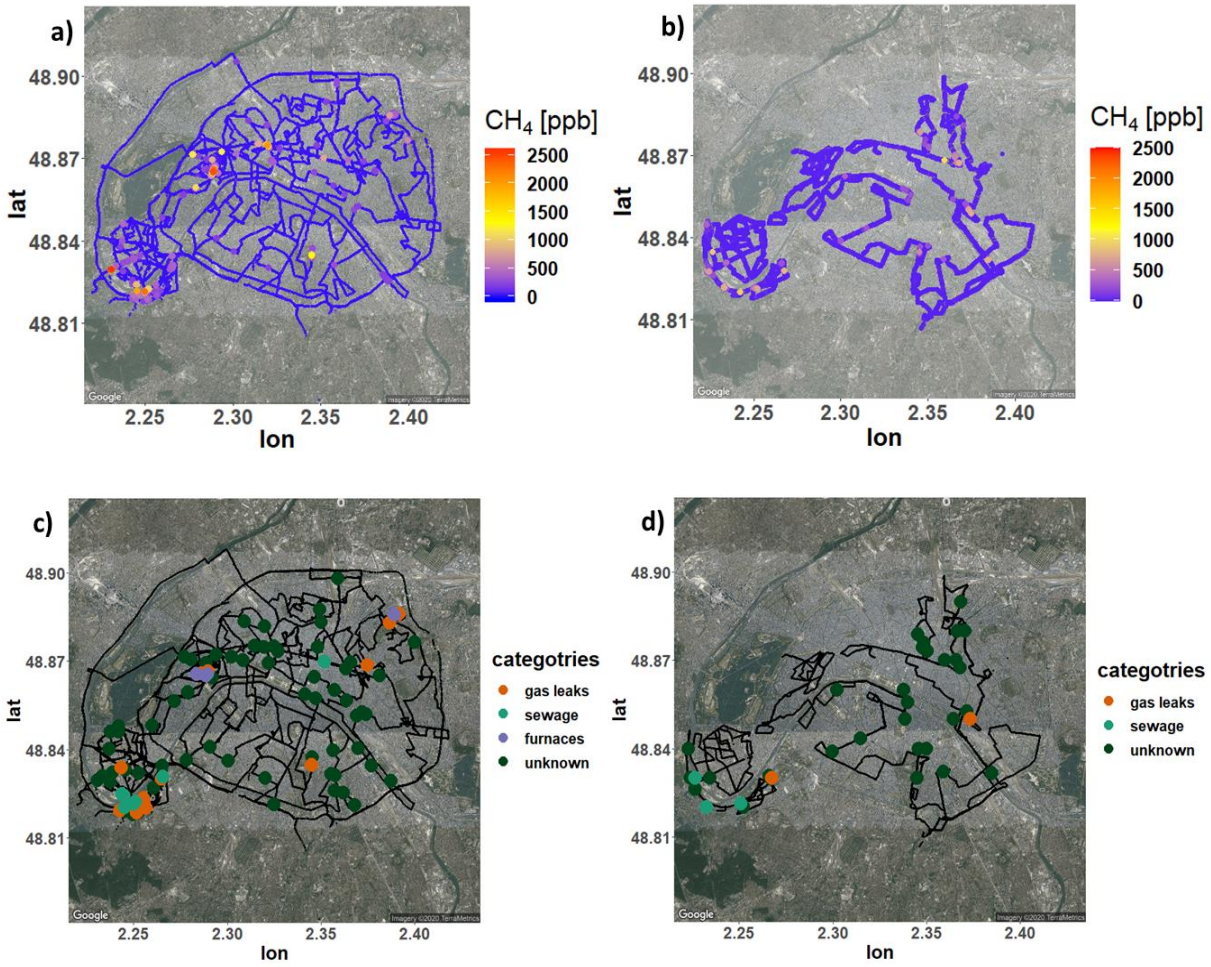

Figure 4.1 Comparison of observed CH_4 mole fraction between September 2018 and March 2019 (plots a) and c)) and summer 2019 (plots b) d)). Top: observed CH_4 mixing ratio above background. Bottom: determined leak indications

Over five days of summer measurements, CH_4 enhancement above background was in a smaller range than for the measurement made during autumn 2018 and winter 2019. The maximum 5% of all measurements ranged from 44 ppb to 1270 ppb (Figure 4.1). The observed emission rate is equal to 41 L/min over 200 km. After upscaling to the whole road length, it is equal to 370 L/min (140 kt/yr). It is about 50 t less than the total emission rate obtained from previous measurements. There exist a few possible explanations of it. First of all, furnaces emission contribution during winter can be larger than determined 10% (19 t). Thus, as during summer, the buildings do not use heating, the emission from this category should be decreased to 0. During summer measurements, no leak indications were observed in cluster A, while during wintertime, about 13 leaks indication were observed (~40 L/min). They contributed to about 30% of the total emission rate from driven streets. This discrepancy can be caused by a lack of the emission from furnaces during summer or by the natural gas distribution network's possible reparation. Table 4.1 shows the difference between these two measurement periods. In summer measurements, all observed leak indications are categorized as small (< 6 L/min). The mean value is equal to 1.17 L/min (range of 0.46 L/min - 4.49 L/min.), which is smaller than during previous measurements.

Based on winter measurements, 65% of unknown leak indications can be contributed to natural gas leaks. Using this assumption, 22 leaks over driven 200 km come from leaks in natural gas distribution network. Thus, in Summer 2019 gas leak indication rate reached 0.11 km^{-1}, what is equal to gas leak indication rate observed between September 2018 and March 2019. However, in Summer 2019, 40% of leaks indications were determined as coming from natural gas distribution network. Then, assuming that in Summer 2019, 40% of unknown leak indication come from natural gas distribution network, 14 leak indications would be ascribed to leaks in natural gas distribution network. In this case, gas leak indication rate would reach 0.07 km^{-1}, what is smaller than gas leak indication rate (0.11 km^{-1}) observed between September 2018 and March 2019.

Table 4.1 Comparison of CH_4 observed in Paris between September 2018 and March 2019 with Summer 2019

Feature	**September 2018- March 2019**	**Summer 2019**
Number of surveys	17	5
Crossed km of streets	500	200
Detected peaks (cluster A, cluster B)	90 (13, 32)	36 (0, 12)
Emission rate upscale to total road length	190 t/yr	140 t/yr
Mean emission rate of individual leak [L/min]	1.56 (0.47 – 10.50)	1.17 (0.46 – 4.49)
Median emission rate [L/min]	0.86	0.81
Source categories: small, medium (< 6 L/min, 6-40 L/min)	88,2	36,0

4.3 Publication: Mapping urban methane sources in Paris, France

Mapping urban methane sources in Paris, France

Sara M. Defratyka[1], Jean-Daniel Paris[1], Camille Yver-Kwok[1], Julianne M. Fernandez[2], Piotr Korben[3], Philippe Bousquet[1]

[1] Laboratoire des Sciences du Climat et de l'Environnement (LSCE-IPSL) CEA-CNRS-UVSQ Université Paris Saclay, Gif-sur-Yvette, France

[2] Royal Holloway University of London, Egham, United Kingdom

[3] Heidelberg University, Institute of Environmental Physics, Germany

ABSTRACT Megacities, with their large and complex infrastructures, are significant sources of methane emissions. To develop a simple low-cost methodology to quantify these globally important methane sources, this study focuses on mobile measurements of methane (CH_4) and its isotopic composition in Paris. Data collected between September 2018 to March 2019 resulted in 17 days of measurements, which provided spatial distribution of street-level methane mixing ratios, source type identification, and emission quantification. Consequently, 90 potential leaks were detected in Paris sorted into three leak categories: natural gas distribution network emissions (63%), sewage network emissions (33%), and emissions from heating furnaces of buildings (4%). The latter category has not previously been reported in urban methane studies. Accounting for the detectable emissions from the ground, the total estimated CH_4 emission rate of Paris was 5000 L/min (190 t/yr), with the largest contribution from gas leaks (56%). This ranks Paris as a city with medium CH_4 emissions. Two areas of clusters were found, where 22% and 56% of the total potential emissions of Paris were observed. Our findings suggest that the natural gas distribution network, the sewage system, and furnaces of buildings are ideal targets for street-level CH_4 emission reduction efforts for Paris.

INTRODUCTION

Atmospheric methane (CH_4) is a potent greenhouse gas that is emitted by a large number of sources, both anthropogenic (e.g. fossil fuels, agriculture, and waste) and natural (e.g. wetlands, freshwaters, termites, and wildfires). Globally and regionally, CH_4 emissions are still poorly quantified per sector, leading to emissions uncertainties for anthropogenic and natural sources (20% to 50% and50% to 100% respectively)[1]. Such uncertainties reflect emission factors and activity data discrepancies, which are used not only for emission quantification, but also for hypothesizing the distribution and magnitude of sectoral emissions[1,2]. These discrepancies point toward a need to better constrain emissions at a local-scale. Moreover, a better understanding of CH_4 emissions spatially and temporally is a mandatory path to achieve effective mitigation strategies.

Urban and suburban areas compose a complex environment, where different sources of CH_4 coexist: heating systems (including oil and natural gas networks, domestic networks and individual combustion systems), landfills, wastewater and road transport[3–5]. Therefore, an important matter to address is the need for a better understanding of the contribution of urban CH_4 to global emissions.

The complexity and imbrication of city methane sources requires specific observations tools and strategy. Mobile observation approaches provide powerful independent information to constrain emissions and improve inventories at the local scale, and to contribute to reduce uncertainties on emissions at larger scales. Mobile measurements have been successfully used to detect leaks in different cities, helping to prioritize mitigation strategies and verifying existing inventories[5–8]. Combining mobile concentration measurements with chemical fingerprinting, such as determining stable isotopic signatures of CH_4, enables the partitioning of methane emissions by source type[4,5,9–13]. This allows for the identification and attribution of the source emitters in urban environments.

Globally, in the case of isotopes, more depleted $\delta^{13}CH_4$ values (-80‰ to -40‰) (median ~-62‰) are signatures of microbial sources, which are highly selective for ^{12}C[5,9,11,12]. In contrast, methane from fossil fuels typically varies between -75‰ and –25‰ (median ~-44‰) and methane from pyrogenic sources varies between -35‰ and -7‰[5,9,11,12] (median ~-22‰). In the case of the region Ile-de-France (IDF), based on data from surveys conducted between 2012 and 2015, when CH_4 enhancements were measured downwind from sources, narrower signature ranges were found: from -55.3 ± 0.1‰ to -51.9 ± 0.1‰ for wastewater treatment plants (WWTP) and from -43.4 ± 01‰ to -33.8 ± 01‰[14] for natural gas storage facilities.

In 2015, according to the Air quality agency of Ile-de-France (AIRPARIF), the total estimated CH_4 emissions from IDF were 30 kt/year[15]. The AIRPARIF emission inventory for the region (including Paris city) uses a bottom-up technique based on sectoral approaches, emission factors, and activity data. The largest CH_4 contributions in IDF were from waste management (42%), and the energy sector (31%)[15]. Additionally, the residential and tertiary sector contributed to 13% of the total CH_4 emission in IDF.

In 2012, a regional plan for climate, air and energy[16] was approved for IDF. This plan envisages a 20% reduction of greenhouse gases for 2020, compared to the year 2005. Plans for reducing greenhouse gas emissions in Paris are more ambitious and expect to reach carbon neutrality by 2050[17]. Understanding the CH_4 emission trajectory in Paris, toward the completion of these ambitious plans, requires mapping and quantification of atmospheric CH_4 and the attribution of the observed leaks to identified sources.

To achieve quantification and source attribution of methane emissions in the Paris area, we conducted repeated field measurement campaigns and monitoring activities, such as walking measurements and determining isotopic signatures of methane for the distinction of emission sources. The present work offers an approach to draw a baseline to assess the efficiency of future mitigation policies and actions. Based on these independent atmospheric measurements, we provide a sectoral perspective of CH_4 emissions in Paris.

MATERIALS AND METHODS

The results presented in this paper were obtained from 17 surveys conducted between 07 September 2018 and 07 March 2019. The surveyed area includes Paris with its west and south

suburbs (mostly Boulogne-Billancourt and Issy-les-Moulineaux). Cavity ring-down spectrometers (CRDS) and an AirCore sampler[12,18–20] (Figure 1 and isotopic section) were installed into a vehicle equipped with a GPS device (NAVILOCK NL-602U). Vehicle-mounted instruments had air-inlets situated on the roof of the car. Walking measurements using a portable instrument were conducted to obtain detailed information about the source(s) of the observed enhancements. The AirCore sampler[12,18,20] was used to determine the isotopic composition of observed enhancements and is described in the isotopic measurement section.

Instruments (detailed specifications are in the supplementary material). Measurements during this study were made using CRDS analyzers manufactured by Picarro (Santa Clara, California) and a Los Gatos Research (LGR) analyzer (San Jose, California) model MGGA for more walking surveys. The LGR MGGA measures CH_4, CO_2 and H_2O. All the analyzers have an uncertainty below 1 ppb for CH_4.

The base of our mobile set-up is the CRDS G2201-i which was used for sixteen of the surveys. This instrument measures CO_2, $\delta^{13}CO_2$, CH_4, $\delta^{13}CH_4$, and H_2O, with a gas flow of ~160 sccm and a frequency of ~0.27 Hz. $\delta^{13}CH_4$ is reported using the international standard Vienna Pee Dee Belemnite (VPDB, $^{13}C/^{12}C_{VPDB}=0.0112372$)[21] and CH_4 using the WMO X2004A scale. Our CRDS G2201-i has a $\delta^{13}CH_4$ precision of ~ 3.5‰ for ambient air CH_4 mixing ratios, but as CH_4 mixing ratios increase to ~10 ppm, $\delta^{13}CH_4$ precision improves to 0.7‰.

During 12 of the surveys, two other CRDS instruments, measuring CH_4 and H_2O, were also used (G2401 or G2203). Details on which analyzer was used on any given day are shown in S1. To determine the influence of inlet height for measuring CH_4 mixing ratios, two identical CRDS G2401 instruments were used during one of the surveys. One inlet was installed on the roof of the car (~170 cm above the ground) and the second on the upper skirt of the car (~50 cm above the ground). No significant difference was observed. Details of this test are presented in section S2. All measurements are time-corrected to account for the delay (20 to 30 s) induced by the travel time from the inlet (synflex 1/4") to the analyzers.

Between September 2018 and March 2019, a 3-point concentration and isotopic composition calibration was completed for CRDS G2201-i. The three calibration gases were made by different dilutions of pure CH_4 and CO_2 with ambient air and calibrated against primary standards. Calibration factors are hereafter applied. CRDS G2201-i calibration details are presented in section S3. In addition, to check the CH_4 and $\delta^{13}CH_4$ measurement stability and the influence of powering on/off the analyzer, a known gas was measured for 20 minutes before and after 11 randomly-selected surveys. In all cases, the analyzer was stable and there was no detectable influence observed from powering on/off the instrument. The LGR MGGA analyzer was also tested and calibration factors were applied.

Vehicle-mounted mobile surveys and leak indications analysis

Atmospheric background mixing ratios are calculated as 2-min running averages, and the enhancement threshold, to determine a leak indication of CH_4, is defined as >10% above background as in von Fisher et al[7]. We assume leak indications are from the same source when their maximum enhancements are located no more than 150 m apart. Additionally, during a controlled release experiment, the spatial scale of CH_4 enhancements were smaller than 160 m

for leaks ≤ 40 L/min[7]. Thus, CH_4 enhancement with lengths >160 m are not considered as leaks. In total 90 enhancements above background were retained.

High-resolution $\delta^{13}CH_4$ signature measurements

To obtain high precision in-situ measurements of $\delta^{13}CH_4$ for individual leak indications, our mobile set-up was equipped with an AirCore sampler, which consists of a 50 m storage tube, a dryer (magnesium perchlorate), and valves (Figure 1)[12,18–20]. During surveys, air is continuously measured by the analyzer and simultaneously stored in the tube ("monitoring mode"). When a leak indication is detected and once the readings return to the background CH_4 levels, the air within the storage tube is remeasured ("replay mode")[12,19,20]. The uncertainty of isotopic signatures determined with the AirCore sampler depends on the instrument precision, the observed CH_4 enhancement above background (higher enhancements lead to lower $\delta^{13}CH_4$ uncertainties), and on the number of data points used for analysis[12]. In the set-up used in this study, replay mode is equivalent to increasing the sampling frequency by a factor of 3. Therefore, we used the AirCore to measure isotopic signatures only for significant CH_4 enhancements above background. Based on all our observations, we chose to define a CH_4 enhancement as 'significant' if its maximum mixing ratio is greater than 500 ppb above local background. In previous work, where the AirCore was a part of a mobile set-up, the same threshold was also used[12,20]. Local background values were calculated as the mean CH_4 mixing ratio measured immediately before and after each leak indication in the replay mode.

In total, 28 leak indications from 17 different locations were found significant. Isotopic signatures were calculated using the Miller-Tans approach[19,23], offering comparison possibilities with previous studies. Fitting of the observations were calculated as a linear regression type II using the ordinary least squares method, while data was grouped in 50 ppb bins. As previous works[19,24] showed $^{13}CH_4$ and C_2H_6 cross-sensitivities in CRDS instruments, it is recommended to apply the C_2H_6 correction in the case of leak indications of thermogenic origin. However, in this study, the observed CH_4 mixing ratios remained relatively low (max of 2.7 ppm above background), and the C_2H_6 mixing ratio was within instrumental noise. Here, we only report the isotopic $\delta^{13}CH_4$ signature of leak indications where the Miller-Tans approach yields a 1-sigma uncertainty less than 10‰ and with a correlation coefficient R^2>0.85. Twelve of the 28 AirCores samples fulfilled the criteria, with two AirCores measuring the same leak indication. Details of using the AirCore sampler and isotopic data processing are presented in Section S4.

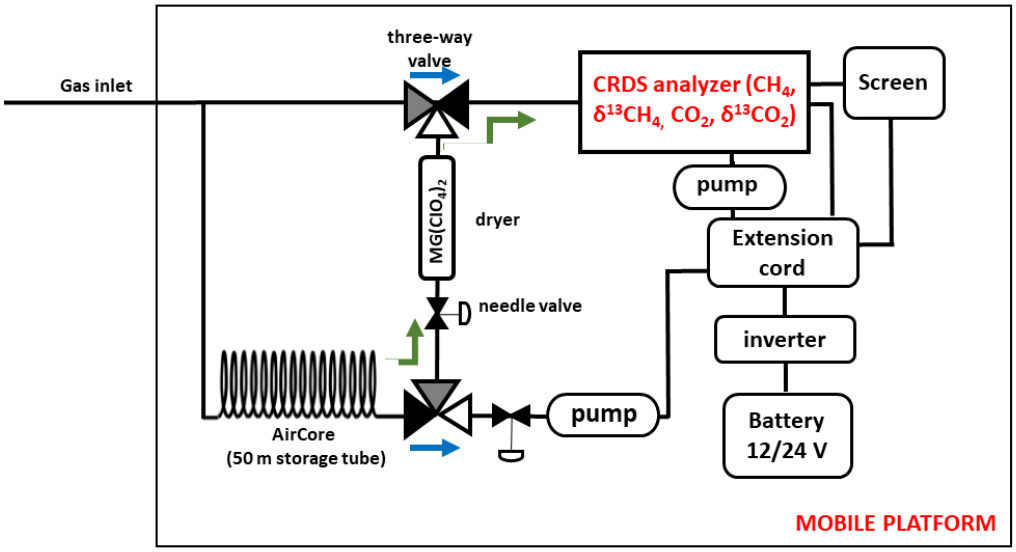

152 **Figure 1**. Scheme of mobile measurement set-up. The blue arrows show the airflow in
153 monitoring mode. The green arrows show the airflow in the replay mode.

154 **Estimation of the leak indications' emission rate**

155 While the source strength of each individual leak indication remains challenging to estimate,
156 especially in urban areas, Weller et al.[8], building on von Fischer et al.[7], proposed an improved
157 equation, using a statistical calibration model:

158 $\ln(M\ CH_4) = -0.988 + 0.817 \cdot \ln(CH_4 \text{ emission rate})$ (1).

159 M is the maximum CH_4 enhancement above the background of the leak indication [ppm], and
160 emission rates are estimated in L/min. The method is developed and tested for point sources of
161 methane situated at ground level in an urban environment. In previous studies[7,8], this approach
162 was used only for leak indications from the natural gas distribution network, but it can also be
163 extended to other sources. In our study, we have applied this equation to all leak indications in
164 order to estimate the contribution of these different sources to city-scales CH_4 emissions. The
165 uncertainties of this equation are discussed in Weller et al.[25] showing a slight overestimation
166 for the small leak indications.

167 **Mobile surveys protocol**

168 Overall, among 720 km driven in the area of interest, 500 "unique" kilometers (driven
169 without counting the revisits) were covered representing 30% of the entire Paris road network.
170 Surveys were conducted in different neighborhoods of the city during daytime hours, which
171 included the coverage of major roads as well as part of the smaller roads. Locations where CH_4
172 enhancements above background were observed to be lower than 500 ppb were of low priority
173 for a second survey. Initial surveys were used to identify areas with the largest number of CH_4
174 enhancements above background, designated as 'clusters'. Two cluster areas were identified: 1)
175 cluster area A, located in downtown Paris and 2) cluster area B, in the south-west suburbs. Five
176 days of repeated surveys were focused on both clusters A and B (respectively three and two
177 days). In total, clusters A and B represent respectively 10% (50 km) and 20% (100 km) of the
178 unique kilometers (Figure 2). Primarily, during revisits of cluster areas A and B, the
179 measurements were concentrated at the locations where CH_4 enhancements above background
180 were previously observed. They were also extended to additional streets which were not

previously investigated. In total, during the days that focused on cluster areas A and B, we covered every street at least twice.

Walking measurements using LGR MGGA

We collected additional measurements by foot using a LGR MGGA to find the exact position of the sources causing a significant CH_4 enhancement above background when driving measurements were ambiguous. This protocol was implemented twice in cluster area A, once in cluster area B, and once in the central and north-east part of Paris (details in section S5).

RESULTS AND DISCUSSION

Mapping of methane leak indications in Paris.

Figure 2 is a map of CH_4 mixing ratio enhancements above background, along with the $\delta^{13}CH_4$ signatures measured in Paris. Data represented in Figure 2 is from the CRDS G2201-i and the AirCore sampler, and includes streets that were only passed once. Zooms of cluster area A and B are included. Overall, methane enhancements above background are within a relatively low range (maximum 5% of all measurements in the range 43 to 2700 ppb). Typically, crossing a leak indication took 12 to 20 seconds. Overall 90 enhancements above threshold were observed, with 14% from area A, and 36% from area B. In cluster area A and B, 7 and 17 single passed leak indications respectively were observed from streets passed twice. In the case of streets passed only once, single passed leak indications were observed 39 times outside of clusters. Some leak indications that were observed once may be due to vehicles using natural gas or to changing wind direction. Only considering the leak indications observed at least twice in the same location, 27 leak indications were detected in the Paris city. 22% of these leak indications are from cluster area A, and 56% from cluster area B, though these areas represent only 10% (area A) and 20% (area B) of the unique km of the surveyed area.

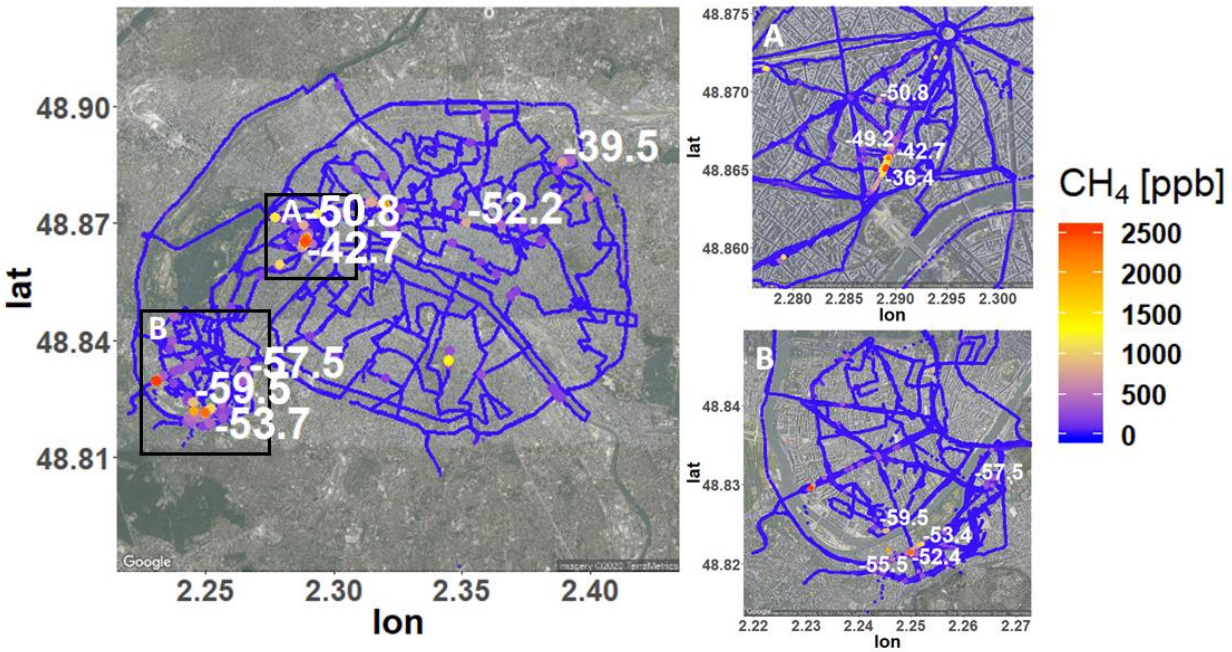

Figure 2. Paris CH_4 enhancements above background with $\delta^{13}CH_4$ signature (white numbers) determined for 11 leak indications selected by criteria: 1-sigma uncertainty less than 10‰ and a correlation coefficient R^2>0.85 from a Miller-Tans plot. Leak indications observed only once are also included. Left panel – whole measured area. To make the map more legible, part of

leak indications in cluster areas A and B are treated as one leak indication with an averaged value. Right panel – zoom of cluster area A (top right) and B (bottom right). Base map provided by Google Maps.

Identification of leak indications' origins.

In this section, based on measured isotopic values using the CRDS G2201-i with an AirCore sampler, and from additional walking observations using the LGR MGGA, we identify the origin of the leak indications shown in Figure 2.

Cluster area A. The $\delta^{13}CH_4$ isotopic signatures for the cluster area A range between -50.8 ± 6.0‰ and -36.4 ± 2.6‰. The isotopic range for these leak indications are compatible with thermogenic sources, which are frequently connected to fugitive natural gas sources. During two days of walking measurements in cluster area A, one CH_4 enhancement was observed directly from a sewage ground cover, and another enhancement was from the ground cover of the natural gas network (Figures S9 - S11). Additionally, CH_4 enhancements were observed three times from ventilation grids connected to boiler rooms of buildings. To ensure the origin of an observed leak indication, using the portable LGR MGGA, measurements were taken directly above the venting grids and ground covers. With this approach, we could clearly distinguish that these leak indications were venting from the natural gas distribution network or from boiler rooms of certain buildings. Based on the location of detected peaks from venting grids and the location where isotopic samples were collected, we determined two isotopic source signatures: one equal to -36.4 ± 2.6‰ and another equal to -39.5 ± 5.0‰. To our knowledge, the latter source category (natural gas from boiler room venting) is not reported in previous studies that focus on urban environment[4–7].

The highest enhancement measured directly from a ventilation grid of a boiler room was around 40 ppm (Section S7). In buildings, boiler room ventilation systems are typically independent and separated from the buildings' ventilation of general air. Boilers are generally situated in the basement of a building[26]. The discovery of high methane emissions suggests leaky installations of some furnaces, posing the presence of a safety hazard (although measured values are far from methane exploding zone) as well as a greenhouse gas emitter. As leaky furnace installations are a probable source of the methane from ventilation grids of boiler rooms, we will further call this category "furnaces". Walking measurements indicated a contribution of methane emissions from the city sewage network sector (i.e. pipes, covers), which in some previous studies was only briefly mentioned[4,5] or not investigated at all[6,7,10,22].

Leak indications identified by combining the determined isotopic signatures with the observed CH_4 enhancements from walking measurements are presented in Figure 3. In cluster area A, in total, 6 leak indications were detected. Three leak indications are from furnaces, two are from natural gas distribution network, and one is from the sewage network system. Using equation (1), the total estimated emission, combining all leak indications observed twice is 21 L/min. However, if one considers all leak indications, including leak indications observed only once, the total emission in cluster area A reaches 39 L/min.

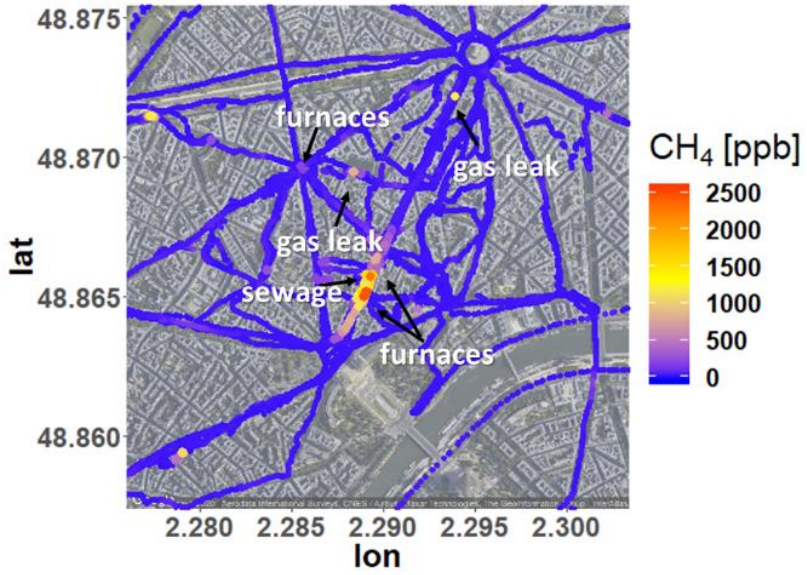

Figure 3. Type of CH_4 sources detected in cluster area A. Source types are defined using isotopic compositions and detected CH_4 emissions measured directly from ground covers (both sewage and the natural gas network) and boiler rooms of buildings venting through street-level grids (furnace category). Base map provided by Google Maps.

Cluster area B. In cluster area B, 15 leak indications have been found. Here, 5 AirCore samples were collected. All isotopic signatures associated with these leak indications fall within the range of -59.5 ± 8.1‰ to -52.4 ± 3.1‰. This range of values suggest more a microbial origin of the emissions than a thermogenic one. As cluster area B has no landfills and because the IDF region uses natural gas of thermogenic origin (personal communication,[14]), these leak indications are assigned to sewage emissions. Walking measurements were done during one measurement day (27.02.2019) in cluster area B, and indicated that CH_4 enhancements were discharging from sewage ground covers and natural gas ground covers. However, leak indication from natural gas ground covers were too small to determine their isotopic signature using AirCore sampler. In cluster area B, 9 leak indications are from the natural gas distribution network and 6 leak indications are from the sewage network. The total emission rate for the identified leak indications is 23 L/min. In cluster area B, emissions from furnaces were not observed. The total emission rate in cluster area B, adding leak indications observed only once, reaches 50 L/min.

A small isolated CH_4 leak indication (238 ppb above local background), that was observed twice in the central part of the city of Paris, had a $\delta^{13}CH_4$ isotopic signature of -52.2 ± 8.1‰. This signature is compatible to isotopic signatures observed in cluster area B, where sewage covers were directly measured and to the WWTP in the IDF region (-51.9 ± 0.2‰ and -55.3 ± 0.1‰)[14]. Accordingly, the leak indication's origin is attributed to sewage. Another isolated leak indication, observed in the north-east part of Paris, had an isotopic signature of -39.5 ± 5.0‰ which is comparable to thermogenic sources. Outside of cluster areas A and B, 6 leak indications were observed twice. Of these six, one leak indication was determined by walking measurements, two others using isotopic signatures, and for the remaining three leak indications, neither isotopic signature nor walking measurements were possible to conduct.

Outside of the cluster areas A and B, including single observations, the total CH_4 emission rate is equal to 51 L/min.

Synthesis. Overall, 90 leaks were detected and an origin of 27 leak indications was identified. Out of the latter 27, 15 are attributed to the natural gas network, 8 to sewage, and 4 to furnaces. The 63 remaining leak indications could not be attributed using isotopes or walking measurements (Figure 4a). From the road, furnaces and natural gas network are not distinguishable from each other. Thus, 66% of leak indications in Paris come from natural gas leaks and 34% from sewage network. This distribution of source categories is propagated to the 63 leaks of unknown origin and 41 additional leaks are considered as coming from gas leaks and 22 as sewage network leaks (Figure 4b). Isotopic signatures and their source locations are presented in Table S4, and pictures of examples from CH_4 sources in cluster areas A and B are presented in section S7.

Using the method from Weller et al.[8] (equation (1)), we calculated the emission rate for the 90 leak indications determined in Paris. For the fifteen determined natural gas distribution leak indications, the mean estimated emission rate is equal to 1.4 L/min (range 0.5 – 3.87 L/min) for individual leak indication. These natural gas leaks are categorized as small leaks (< 6 L/min), according to the categorization proposed by von Fischer et al.[7] For the sewage sector, the mean estimated emission rate for an individual leak indication is equal to 2.2 L/min (0.7 to 6.5 L/min). In this case, 7 leak indications are within the small category and one leak indication is within the medium category. For the furnace sector, the mean emission rate for an individual leak indication is equal to 3.5 L/min (0.7 to 5.9 L/min). The remaining 63 leak indications have a mean estimated emission rate equal to 1.4 L/min (0.5 – 10.5 L/min), where only one is categorized as a medium, which reached 10.5 L/min. Thus, in this group, the emission rates for individual leaks are skewed for lower emissions, with median values equal to 0.8 L/min.

Overall, for 500 unique km, the accumulated emission rate is equal to 140 L/min, where the gas sector contributes 56% under our attribution assumption (Figure 4b). The sewage sector and furnace category respectively contribute to 34% and 10% of the accumulated rate. After upscaling this value to all kilometers of road in Paris and suburbs, the accumulated CH_4 emission rate of sources detectable from the ground is estimated to be equal to 500 L/min (190 t/yr). Such a simple extrapolation assumes a reasonable homogeneity of the leak distribution regarding the fraction of the total kilometers sampled during our surveys. Thus, in Paris at the street-level, 54% of total CH_4 emissions come from leaks in natural gas distribution network, 34% from leaks in sewage network and 10% from furnaces leaking emissions. Looking only for the leaks in the natural gas distribution network, the natural gas leak indication rate (gas leak indications/ unique kilometers) is equal to 0.11 km^{-1}.

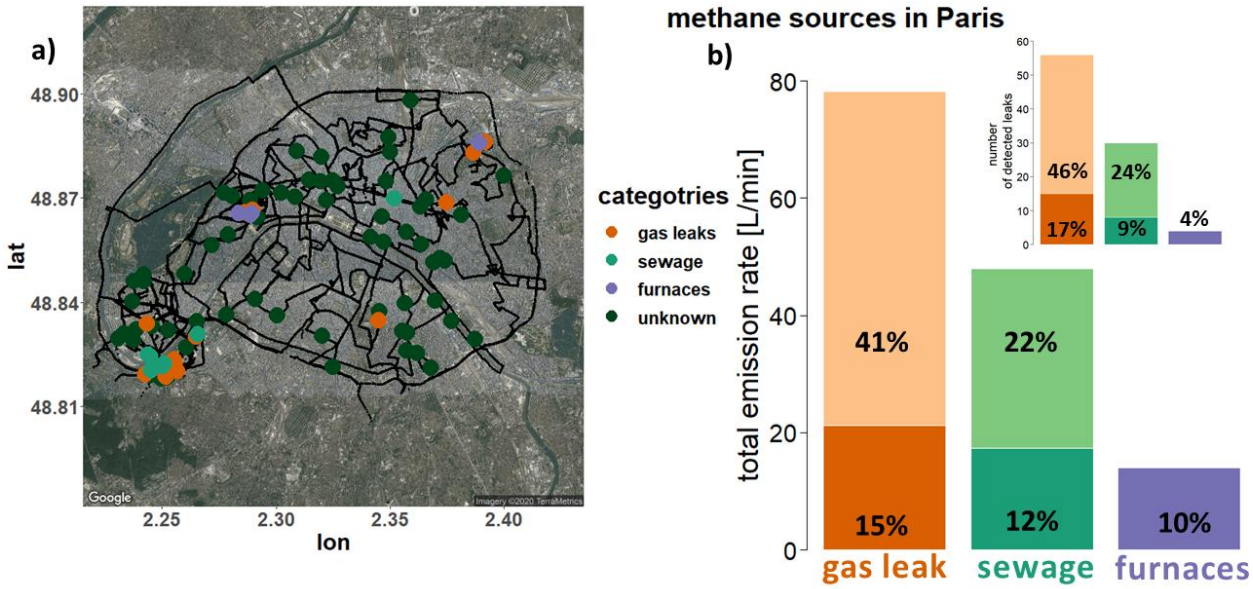

Figure 4. CH_4 leak indication categories detected in the Paris area. a) Map of the surveyed area with positions of the detected sources. b) Distribution of the emission of the leak indication categories in the Paris area, inner figure: number of detected leaks. Paler colors represented unknown leaks attributed to gas leaks (orange) or sewage (green), based on the percent of defined leak indication. Base map provided by Google Maps.

However, it may be considered a lower bound estimate as additional sources may not be detectable from the ground or with our set up. Indeed, we do not report mobile CH_4 sources from road transport. A fraction of the bus fleet in Paris uses natural gas and biogas as fuel, which can cause additional emission of CH_4[27–29]. According to the AIRPARIF inventory, road transport contributed to 3% of CH_4 emissions in Paris for the year 2015[15]. In our study, we attribute CH_4 emission to road transport if the detected leak indication does not occur during the second passing of the same street in a short time. One leak indication is associated with emissions from road transport and has been excluded from the analysis (Section S9). Addressing a road transport category would necessitate specifically-designed campaigns.

More diffused CH_4 sources, like emissions from the Seine river could be missing. However, during our study we did not observe any CH_4 enhancement along the Seine, what is in the line with previous, focused on Seine greenhouse gases emissions study[30,31]. Finally, the roof-top venting of buildings could also be a source of methane that we can hardly track with our setup.

Outlook on improvements to the measurement method. We see three main ways to improve our method: better instrumentation, additional tracer and multiples revisits.

Indeed, we were able to obtain $\delta^{13}CH_4$ signatures through mobile measurements of the combined G2201-i analyzer and AirCore sampler only if a CH_4 enhancement above background was at least 500 ppb. It constitutes a bias toward large sources, possibly ignoring potentially numerous small or more diffused sources. Using another instrument with higher precision would decrease the threshold for the observed CH_4 enhancements above background. This would allow for the isotopic composition measurement of smaller leak indications and thus, allow the detection of more leaks.

Additionally, measurements of δD and radiocarbon (^{14}C) could provide supplementary information about emission sources. Continuous δD observations, based on CRDS technology, have only started to be used[32]. For radiocarbon however, with current techniques, leak indications should be measured through canister collections instead of through continuous measurements, which can cause some difficulties in the flow of urban traffic[4,33–35].

Measurements of ethane to methane ratios can also help to distinguish thermogenic from microbial sources since ethane is not observed in microbial sources[6,10,20]. These measurements can be included during mobile surveys[20] or they can be stationary[36,37]. The measurements of ethane to methane ratios can be useful to determine the possibility of migrating methane from the natural gas distribution network to the sewage network, as seen in McKain et al[23]. Lastly, CO observations can identify events of incomplete combustion, which can differentiate emissions from bus exhaust or, what is observed in Paris, from furnaces. Taking into account the efficiency of identifying CH_4 combustion sources with CO measurements, it is recommended to systematically measure CO during future urban quantification investigations.

Finally, the systematic repetition of measurements would allow for an observation of seasonal variations of CH_4 emissions in an urban structure. Also, measuring both in winter and summer can separate gas leak emissions from the heating system emissions and leaks in natural gas distribution network, as gas leaks have little seasonal variation[3,5,34]. However, in this case, maintenance, repairs, and replacement plans of gas pipeline infrastructure should be documented to inform emission measurement investigations. In our work, we analyze leak indications, which were systematically observed between September 2018 and March 2019. Systematic repetitions could help distinguishing stationary methane sources (e.g. natural gas network or sewage system) from moving sources (e.g. car exhaust).

Comparison to previous studies about Paris methane emissions.

Inventories. In IDF region, the total CH_4 emission in 2015 from the AIRPARIF inventory[15] was equal to 30 kt, with the largest emission coming from the solid waste management sector (47%)[15]. However, AIRPARIF inventory does not take sewage emissions into consideration. Emissions from furnaces are part of the tertiary and residential sector, but considering that these leak indications were only found for a limited number of walking passes, their emission rates are not representative of the total emission from furnaces, and even less for the whole tertiary and residential sector. For our study, the sector of interest is thus "energy sector", which emitted 9.3 kt/yr in IDF region in 2015[15], according to AIRPARIF. Within the energy sector, gas leaks represent 87% (8.1 kt/yr) of annual emissions[38]. This estimate relates to the downscaled national length of distribution network and real natural gas consumption in IDF.

In Paris, the natural gas distribution network has a length of about 2000 km and serves almost all streets and more than 40 000 buildings[39,40]. Annually, 40 km of the pipelines are repaired in Paris[40,41]. More detailed information, such as age and type of the pipelines or the location of the repair works are not freely available for Paris. This lack of information makes it difficult to assess the leak rate based on actual conditions of the natural gas network.

From the 2010 AIRPARIF inventory map[14,38], the largest emission from oil and gas distribution is shown in the northern part of Paris, especially along the right bank of the Seine River, which is not in agreement with our study. The discrepancy between the inventory and our study may be influenced by the time gap (10 years ago) between the two investigations and

possibly from repairs or pipeline replacements of less leak prone pipe material made in this area over this time. However, based on the AIRPARIF inventory[38], (i) gas emissions are broadly distributed spatially and larger CH_4 emission was determined in cluster A, which is consistent with our work, and (ii) CH_4 emissions exist in cluster B, though less than in cluster A, which may imply the lack of accounting for sewage emissions in the inventory.

In 2015, the AIRPARIF regional inventory emissions from the energy sector, downscaled by the population of Paris, reached 1.6 kt/y for Paris city. Another inventory, using national emissions reported to the UNFCCC from fossil fuel exploitation[42], reports an annual 2016 emission for the grid cell that contains most of Paris of 1.25 kt/yr, which is in agreement with AIRPARIF.

In our study, we upscaled our emission rates for the energy sector to the road total length of the city, resulting in an emission of 106 t/yr, which is fifteen times less than in the downscaled AIRPARIF estimate. It does not seem possible to directly compare the gas distribution network CH_4 emission estimates of our study with AIRPARIF inventory, given (i) the source aggregation in the inventory (i.e., gas distribution network, end use, and road transport using natural gas as a fuel), (ii) the downscaling by population in the inventory instead of using absolute information regarding pipe length and material, and (iii) the possibly underestimation of our estimate as noted previously.

Mobile measurements. A previous study, also using mobile measurements, surveyed about 1000 km of Paris and the south/southeast suburbs between December 2013 and December 2015[14]. This study focused on different methane sources like gas storage facilities, but the methodology of the city surveys was not fully described. Also, information about repeated street measurements is not provided[14]. That study detected 40 local enhancements above background, where the maximum leak indication was 3500 ppb.

Additionally, this former study observed two enhancements > 3500 ppb located in a northern part of Paris. Isotopic measurements using a CRDS analyzer yielded values of -39.1 ± 2‰ and -41.8 ±2‰[14]. Our study detected a leak indication close to the area of their second value, which we measured with an isotopic composition equal to -39.5 ± 5.0‰. In this residential area, both results consistently indicate, for two different periods, a thermogenic origin of the CH_4 emission.

Comparison to other cities. Several U.S. cities received attention regarding their methane emissions. For Indianapolis, Lamb et al.[6] identified leaks from the natural gas pipeline network as the main source of CH_4 emissions (43%, leaks rate 0.08 leak/km)[6]. According to McKain et al.[10], depending on the season, the natural gas sector of Boston, contributes 60-100% of the total emission[10], and had a mean leak rate of 0.74 leak/km[6]. In Indianapolis, 41% of the pipeline system consists of cathodically protected steel and 51% of the main pipelines are plastic[6], while Boston's pipelines are mostly composed of unprotected steel and cast iron[10]. Also, von Fischer et al.[7] confirmed that the number of gas leaks in U.S. cities, with older corrosion-prone pipeline network (Boston, New York, Staten Island and Syracuse), is higher than for cities with a higher proportion of plastic or protected steel low-pressure distribution systems (Burlington and Indianapolis). In the case of the study made by von Fischer et al.[7], leak rates vary from 0.004 leaks/km (Indianapolis) to 0.63 leaks/km (Staten Island)[7]. Depending on the U.S. city, the small gas leak indications contribute to 83%-100% of total detected gas leak indications. However,

gas leak indications categorized as medium (0-17%) and large (0-2%) are responsible for the majority of the emissions. In our study, Paris leak indications from the natural gas network resulted in a leak rate of 0.11 leak indications per unique driven km and are categorized as small leaks. Therefore, Paris is in the middle to low range compared to U.S cities, according to von Fischer et al.[7] leak size categories[7].

In our study, only two leak indications exceeded 2.5 ppm above background over 500 unique km driven in Paris, where one is from sewage and the second is from an unknown source.

Mobile measurements conducted in 2014 in London (UK) found 11 gas leaks with enhancement larger than 2.5 ppm above background over 260 km[5], which suggests that London is a city with larger CH_4 emissions than Paris. The London results[5] allowed for the verification of the National Atmospheric Emission Inventory (NAEI) of CH_4 reflecting a significant discrepancy of natural gas leak locations between the inventory and the mobile measurements. There, the CH_4 emissions from sewage works determined by inventory and mobile measurements were in good agreement, while for natural gas leaks, observed leak indications were incorrectly spatially disaggregated, and likely underestimated in the NAEI inventory[5]. In contrast to the London study, the discrepancy found between inventory and the present work appears to be likely caused by an absence of sewage sector estimations in the AIRPARIF inventory, and also by possible repairs works of the natural gas distribution network in the measured area[38,43].

Studies in London[5] and Los Angeles[4] found contributions from the sewage sector to urban CH_4 emission. In both studies[4,5], CH_4 contributions from the sewage sector were observed from WWTP, which can be linked to the type of the collecting system (open versus closed system). Moreover, Zazzeri et al.[5] reported the possibility of CH_4 emission from toilet/sewage vent. No WWTP is located in the city of Paris, but CH_4 leak indications were observed from ground covers of the sewage network. Their isotopic signatures are linked to biogenic sources.

Implications for policymakers.

Actions to reduce greenhouse gas emissions in IDF region and Paris already exist or are planned both on the regional and city scales[16,17]. These plans consider all greenhouse gases, but mostly focus on decreasing CO_2 emissions. Mitigation of CH_4 emissions is not discussed in detail.

Our findings provide evidences of existing methane leaks that can be reduced, offering possibilities to mitigate greenhouse gas emissions in the Paris area. However, additional measurements are required to improve the data coverage of the city more extensively and to precisely identify the origin of each source. Also, the nature and magnitude of furnace emission should be identified and quantified to be mitigated. Buses which use natural gas and biogas as fuel instead of petrol and diesel are already used in Paris and will be more frequent in the future, being a possible increasing source of methane to watch closely.

Additionally, Paris plans to replace natural gas in the distribution network with biogas partially produced locally[17,39]. This should be monitored as well, being another potential source of CH_4 in Paris. The method presented in this paper can be reproduced at multi-year intervals to assess the changes in the structure of CH_4 emissions in Paris, and to determine the impact of the mitigation actions for CH_4 emissions.

ASSOCIATED CONTENT

Supporting Information.
The Supporting Information is available free of charge (PDF file).

AUTHOR INFORMATION

Corresponding Author

* E-mail: sara.defratyka@lsce.ipsl.fr

Author Contributions

The manuscript was written through contributions of all authors. All authors have given approval to the final version of the manuscript.

Funding Sources

This work was partly funded under European Union's Horizon 2020 research and innovation programme under the Marie Sklodowska-Curie grant agreement No 722479. This work was partly funded under the Climate and Clean Air Coalition (CCAC) Oil and Gas Methane Science Studies (MSS), hosted by the United Nations Environment Programme. Funding was provided by the Environmental Defense Fund, Oil and Gas Climate Initiative, European Commission, and CCAC.

ACKNOWLEDGMENT

This project has received funding from the European Union's Horizon 2020 research and innovation programme under the Marie Sklodowska-Curie grant agreement No 722479. This work was funded under the Climate and Clean Air Coalition (CCAC) Oil and Gas Methane Science Studies (MSS), hosted by the United Nations Environment Programme. Funding was provided by the Environmental Defense Fund, Oil and Gas Climate Initiative, European Commission, and CCAC. The authors are grateful to PY. Quehe for his help with driving and collecting measurements in the field. We thank AIRPARIF and in particular O. Perrussel for access to the AIRPARIF 2018 methane emissions inventory.

ABBREVIATIONS

^{14}C radiocarbon; AIRPARIF Air Quality network of Ile-de-France; CH_4 methane; CRDS cavity ring-down spectrometer analyzer; IDF region Ile-de-France region; LGR MGGA Los Gatos Research MGGA portable analyzer; NAEI National Atmospheric Emission Inventory; VPDB Vienna Pee Dee Belemnite; WWTP wastewater treatment plant

REFERENCES

(1) Global Carbon Project (GCP) https://www.globalcarbonproject.org/methanebudget/index.htm (accessed Dec 5, 2019).

(2) Saunois, M.; Bousquet, P.; Poulter, B.; Peregon, A.; Ciais, P.; Canadell, J. G.; Dlugokencky, E. J.; Etiope, G.; Bastviken, D.; Houweling, S.; Janssens-Maenhout, G.; Tubiello, F. N.; Castaldi, S.; Jackson, R. B.; Alexe, M.; Arora, V. K.; Beerling, D. J.; Bergamaschi, P.; Blake, D. R.; Brailsford, G.; Brovkin, V.; Bruhwiler, L.; Crevoisier, C.; Crill,

P.; Covey, K.; Curry, C.; Frankenberg, C.; Gedney, N.; Höglund-Isaksson, L.; Ishizawa, M.; Ito, A.; Joos, F.; Kim, H.-S.; Kleinen, T.; Krummel, P.; Lamarque, J.-F.; Langenfelds, R.; Locatelli, R.; Machida, T.; Maksyutov, S.; McDonald, K. C.; Marshall, J.; Melton, J. R.; Morino, I.; Naik, V.; O'Doherty, S.; Parmentier, F.-J. W.; Patra, P. K.; Peng, C.; Peng, S.; Peters, G. P.; Pison, I.; Prigent, C.; Prinn, R.; Ramonet, M.; Riley, W. J.; Saito, M.; Santini, M.; Schroeder, R.; Simpson, I. J.; Spahni, R.; Steele, P.; Takizawa, A.; Thornton, B. F.; Tian, H.; Tohjima, Y.; Viovy, N.; Voulgarakis, A.; van Weele, M.; van der Werf, G. R.; Weiss, R.; Wiedinmyer, C.; Wilton, D. J.; Wiltshire, A.; Worthy, D.; Wunch, D.; Xu, X.; Yoshida, Y.; Zhang, B.; Zhang, Z.; Zhu, Q. The Global Methane Budget 2000–2012. Earth System Science Data 2016, 8 (2), 697–751. https://doi.org/10.5194/essd-8-697-2016.

(3) Gioli, B.; Toscano, P.; Lugato, E.; Matese, A.; Miglietta, F.; Zaldei, A.; Vaccari, F. P. Methane and Carbon Dioxide Fluxes and Source Partitioning in Urban Areas: The Case Study of Florence, Italy. Environmental Pollution 2012, 164, 125–131. https://doi.org/10.1016/j.envpol.2012.01.019.

(4) Townsend-Small, A.; Tyler, S. C.; Pataki, D. E.; Xu, X.; Christensen, L. E. Isotopic Measurements of Atmospheric Methane in Los Angeles, California, USA: Influence of "Fugitive" Fossil Fuel Emissions: LOS ANGELES METHANE EMISSIONS. Journal of Geophysical Research: Atmospheres 2012, 117 (D7), n/a-n/a. https://doi.org/10.1029/2011JD016826.

(5) Zazzeri, G.; Lowry, D.; Fisher, R. E.; France, J. L.; Lanoisellé, M.; Grimmond, C. S. B.; Nisbet, E. G. Evaluating Methane Inventories by Isotopic Analysis in the London Region. Scientific Reports 2017, 7 (1). https://doi.org/10.1038/s41598-017-04802-6.

(6) Lamb, B. K.; Cambaliza, M. O. L.; Davis, K. J.; Edburg, S. L.; Ferrara, T. W.; Floerchinger, C.; Heimburger, A. M. F.; Herndon, S.; Lauvaux, T.; Lavoie, T.; Lyon, D. R.; Miles, N.; Prasad, K. R.; Richardson, S.; Roscioli, J. R.; Salmon, O. E.; Shepson, P. B.; Stirm, B. H.; Whetstone, J. Direct and Indirect Measurements and Modeling of Methane Emissions in Indianapolis, Indiana. Environmental Science & Technology 2016, 50 (16), 8910–8917. https://doi.org/10.1021/acs.est.6b01198.

(7) von Fischer, J. C.; Cooley, D.; Chamberlain, S.; Gaylord, A.; Griebenow, C. J.; Hamburg, S. P.; Salo, J.; Schumacher, R.; Theobald, D.; Ham, J. Rapid, Vehicle-Based Identification of Location and Magnitude of Urban Natural Gas Pipeline Leaks. Environmental Science & Technology 2017, 51 (7), 4091–4099. https://doi.org/10.1021/acs.est.6b06095.

(8) Weller, Z. D.; Yang, D. K.; von Fischer, J. C. An Open Source Algorithm to Detect Natural Gas Leaks from Mobile Methane Survey Data. PLoS ONE 2019, 14 (2), e0212287. https://doi.org/10.1371/journal.pone.0212287.

(9) Schwietzke, S.; Sherwood, O. A.; Bruhwiler, L. M. P.; Miller, J. B.; Etiope, G.; Dlugokencky, E. J.; Michel, S. E.; Arling, V. A.; Vaughn, B. H.; White, J. W. C.; Tans, P. P. Upward Revision of Global Fossil Fuel Methane Emissions Based on Isotope Database. Nature 2016, 538 (7623), 88–91. https://doi.org/10.1038/nature19797.

(10) McKain, K.; Down, A.; Raciti, S. M.; Budney, J.; Hutyra, L. R.; Floerchinger, C.; Herndon, S. C.; Nehrkorn, T.; Zahniser, M. S.; Jackson, R. B.; Phillips, N.; Wofsy, S. C. Methane Emissions from Natural Gas Infrastructure and Use in the Urban Region of Boston, Massachusetts. Proceedings of the National Academy of Sciences 2015, 112 (7), 1941–1946. https://doi.org/10.1073/pnas.1416261112.

(11) Sherwood, O. A.; Schwietzke, S.; Arling, V. A.; Etiope, G. Global Inventory of Gas Geochemistry Data from Fossil Fuel, Microbial and Burning Sources, Version 2017. Earth Syst. Sci. Data 2017, 9 (2), 639–656. https://doi.org/10.5194/essd-9-639-2017.

(12) Hoheisel, A.; Yeman, C.; Dinger, F.; Eckhardt, H.; Schmidt, M. An Improved Method for Mobile Characterisation of Δ13CH4 Source Signatures and Its Application in Germany. Atmospheric Measurement Techniques 2019, 12 (2), 1123–1139. https://doi.org/10.5194/amt-12-1123-2019.

(13) Lowry, D.; Holmes, C. W.; Rata, N. D.; O'Brien, P.; Nisbet, E. G. London Methane Emissions: Use of Diurnal Changes in Concentration and δ13C to Identify Urban Sources and Verify Inventories. Journal of Geophysical Research: Atmospheres 2001, 106 (D7), 7427–7448. https://doi.org/10.1029/2000JD900601.

(14) Xueref-Remy, I.; Zazzeri, G.; Bréon, F. M.; Vogel, F.; Ciais, P.; Lowry, D.; Nisbet, E. G. Anthropogenic Methane Plume Detection from Point Sources in the Paris Megacity Area and Characterization of Their δ13C Signature. Atmospheric Environment 2019, 117055. https://doi.org/10.1016/j.atmosenv.2019.117055.

(15) AIRPARIF. Ile-de-France Inventoires for a Year 2015. 2018.

(16) SRCAE. Schéma Régional Du Climat, de l'Air et de l'Energie de l'Île-de-France. November 23, 2012.

(17) PCAE. Le Plan Climat Air Energie. March 2018.

(18) Karion, A.; Sweeney, C.; Tans, P.; Newberger, T. AirCore: An Innovative Atmospheric Sampling System. J. Atmos. Oceanic Technol. 2010, 27 (11), 1839–1853. https://doi.org/10.1175/2010JTECHA1448.1.

(19) Rella, C. W.; Hoffnagle, J.; He, Y.; Tajima, S. Local- and Regional-Scale Measurements of CH4, δ13CH4, and C2H6 in the Uintah Basin Using a Mobile Stable Isotope Analyzer. Atmospheric Measurement Techniques 2015, 8 (10), 4539–4559. https://doi.org/10.5194/amt-8-4539-2015.

(20) Lopez, M.; Sherwood, O. A.; Dlugokencky, E. J.; Kessler, R.; Giroux, L.; Worthy, D. E. J. Isotopic Signatures of Anthropogenic CH4 Sources in Alberta, Canada. Atmospheric Environment 2017, 164, 280–288. https://doi.org/10.1016/j.atmosenv.2017.06.021.

(21) Craig, H. Isotopic Standards for Carbon and Oxygen and Correction Factors for Mass-Spectrometric Analysis of Carbon Dioxide. Geochemica et Cosmochemica Acta 1957, 12, 133–149.

(22) Jackson, R. B.; Down, A.; Phillips, N. G.; Ackley, R. C.; Cook, C. W.; Plata, D. L.; Zhao, K. Natural Gas Pipeline Leaks Across Washington, DC. Environmental Science & Technology 2014, 48 (3), 2051–2058. https://doi.org/10.1021/es404474x.

(23) Miller, J. B.; Tans, P. P. Calculating Isotopic Fractionation from Atmospheric Measurements at Various Scales. Tellus B: Chemical and Physical Meteorology 2003, 55 (2), 207–214. https://doi.org/10.3402/tellusb.v55i2.16697.

(24) Assan, S.; Baudic, A.; Guemri, A.; Ciais, P.; Gros, V.; Vogel, F. R. Characterization of Interferences to in Situ Observations of Delta13CH4 and C2H6 When Using a Cavity Ring-down Spectrometer at Industrial Sites. Atmospheric Measurement Techniques 2017, 10 (6), 2077–2091. https://doi.org/10.5194/amt-10-2077-2017.

(25) Weller, Z. D.; Roscioli, J. R.; Daube, W. C.; Lamb, B. K.; Ferrara, T. W.; Brewer, P. E.; von Fischer, J. C. Vehicle-Based Methane Surveys for Finding Natural Gas Leaks and Estimating Their Size: Validation and Uncertainty. Environ. Sci. Technol. 2018, 11922-11930. https://doi.org/10.1021/acs.est.8b03135.

(26) Cegibat, G. Aménagement d'une chaufferie en sous-sol https://cegibat.grdf.fr/reglementation-gaz/amenagement-chaufferie-sous-sol (accessed Oct 29, 2019).

(27) Hesterberg, T. W.; Lapin, C. A.; Bunn, W. B. A Comparison of Emissions from Vehicles Fueled with Diesel or Compressed Natural Gas. Environ. Sci. Technol. 2008, 42 (17), 6437–6445. https://doi.org/10.1021/es071718i.

(28) Clark, N. N.; Johnson, D. R.; McKain, D. L.; Wayne, W. S.; Li, H.; Rudek, J.; Mongold, R. A.; Sandoval, C.; Covington, A. N.; Hailer, J. T. Future Methane Emissions from the Heavy-Duty Natural Gas Transportation Sector for Stasis, High, Medium, and Low Scenarios in 2035. Journal of the Air & Waste Management Association 2017, 67 (12), 1328–1341. https://doi.org/10.1080/10962247.2017.1368737.

(29) Kollamthodi, S. The Role of Natural Gas and Biomethane in the Transport Sector; 2016; p 85.

(30) Garnier, J.; Vilain, G.; Silvestre, M.; Billen, G.; Jehanno, S.; Poirier, D.; Martinez, A.; Decuq, C.; Cellier, P.; Abril, G. Budget of Methane Emissions from Soils, Livestock and the River Network at the Regional Scale of the Seine Basin (France). Biogeochemistry 2013, 116 (1–3), 199–214. https://doi.org/10.1007/s10533-013-9845-1.

(31) Marescaux, A.; Thieu, V.; Garnier, J. Carbon Dioxide, Methane and Nitrous Oxide Emissions from the Human-Impacted Seine Watershed in France. Science of The Total Environment 2018, 643, 247–259. https://doi.org/10.1016/j.scitotenv.2018.06.151.

(32) Isotopic Measurements | Aerodyne Research, Inc. http://www.aerodyne.com/application/isotopic-measurements (accessed Dec 6, 2019).

(33) Nakagawa, F.; Tsunogai, U.; Komatsu, D. D.; Yamada, K.; Yoshida, N.; Moriizumi, J.; Nagamine, K.; Iida, T.; Ikebe, Y. Automobile Exhaust as a Source of 13C- and D-Enriched Atmospheric Methane in Urban Areas. Organic Geochemistry 2005, 36 (5), 727–738. https://doi.org/10.1016/j.orggeochem.2005.01.003.

(34) Moriizumi, J.; Nagamine, K.; Iida, T.; Ikebe, Y. CARBON ISOTOPIC ANALYSIS OF ATMOSPHERIC METHANE IN URBAN AND SUBURBAN AREAS: FOSSIL AND NON-FOSSIL METHANE FROM LOCAL SOURCES. 1998, 9.

(35) Espic, C.; Liechti, M.; Battaglia, M.; Paul, D.; Röckmann, T.; Szidat, S. Compound-Specific Radiocarbon Analysis of Atmospheric Methane: A New Preconcentration and Purification Setup. Radiocarbon 2019, 61 (5), 1461–1476. https://doi.org/10.1017/RDC.2019.76.

(36) Simpson, I. J.; Sulbaek Andersen, M. P.; Meinardi, S.; Bruhwiler, L.; Blake, N. J.; Helmig, D.; Rowland, F. S.; Blake, D. R. Long-Term Decline of Global Atmospheric Ethane Concentrations and Implications for Methane. Nature 2012, 488 (7412), 490–494. https://doi.org/10.1038/nature11342.

(37) Wunch, D.; Toon, G. C.; Hedelius, J. K.; Vizenor, N.; Roehl, C. M.; Saad, K. M.; Blavier, J.-F. L.; Blake, D. R.; Wennberg, P. O. Quantifying the Loss of Processed Natural Gas within California's South Coast Air Basin Using Long-Term Measurements of Ethane and Methane. Atmos. Chem. Phys. 2016, 16 (22), 14091–14105. https://doi.org/10.5194/acp-16-14091-2016.

(38) AIRPARIF. Emission Bilans of Pollutants Ang Greenhouse Gases in Ile-de-France Region in 2010 and History 2000/2005; 2013; p 109.

(39) Le Figaro, A. Paris resigne avec GRDF pour distribuer du gaz, mais plus propre https://www.lefigaro.fr/flash-eco/paris-resigne-avec-grdf-pour-distribuer-du-gaz-mais-plus-propre-20191115 (accessed Apr 23, 2020).

(40) La Tribune. Polémique sur l'état du réseau de gaz parisien https://www.latribune.fr/entreprises-finance/industrie/energie-environnement/polemique-sur-l-etat-du-reseau-de-gaz-parisien-803664.html (accessed Apr 23, 2020).

(41) GRDF on Twitter. GRDF sur Twitter : "[Communiqué de Presse] « Réaction de #GRDF suite aux propos de Monsieur @A_Vesperini sur la sécurité du réseau #gaz à #Paris » #Trévise #Explosion #Paris9 https://twitter.com/grdf/status/1084437895841280000/photo/1 (accessed Apr 23, 2020).

(42) Scarpelli, Tia R.; Daniel J. Jacob; Joannes D. Maasakkers; Melissa P. Sulprizio; Jian-Xiong Sheng; Kelly Rose; Lucy Romeo; John R. Worden; Greet Janssens-Maenhout. A Global Gridded (0.1∘× 0.1∘) Inventory of Methane Emissions from Oil, Gas, and Coal Exploitation

649 Based on National Reports to the United Nations Framework Convention on Climate Change.
650 Earth System Science Data 2020, 12.1.

651 (43) AIRPARIF. Analyss of Inventory and Emissions' Cadastres of Principal Greenhouse
652 Gasses in Ile-de-France Region; 2005.

653 For Table of Contents Only

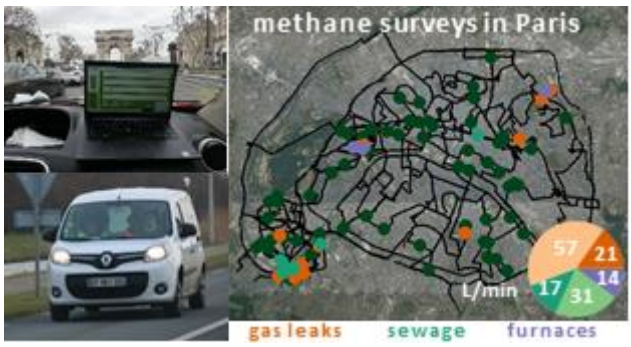

Chapter 5 Direct estimation of methane emissions from gas compressor stations and landfills in Île-de-France

5.1. Introduction

Based on the study presented in the previous chapter, CH_4 emissions in Paris city are equal to 0.19 kt CH_4 y^{-1} and 0.15 kt CH_4 y^{-1} for winter and summer surveys, respectively. Compared to the AIRPARIF inventories for the year 2015, these values are smaller than 1% of total CH_4 emissions in IDF region dominated by waste management (42%) and energy (31%) sectors. Thus, I have extended my measurements to CH_4 emitters localized outside of Paris city, but still included in IDF region. As a consequence, my studies dedicated to IDF CH_4 sources at the site scale were focused on facilities from the energy and waste management sectors. Here, the results from the mobile measurements made on three gas compressor stations (A, B and C) and two landfills (D and E) are presented. The sites are anonymized to answer the need for confidentiality for some of the sites according to agreements with owners, as well as for simplicity for the readers. They are identified by letters (A-E) throughout the rest of the chapter. For the landfills, previous studies had been conducted and their results are presented hereafter.

Solid waste management. According to AIRPARIF inventory for 2015, the solid waste management sector emits 12.6 kt CH_4 y^{-1}, and it is the major source of methane in IDF region (AIRPARIF 2018). Emissions from this sector decreased from 16.9 kt CH_4 y^{-1} in 2010, when 98% of the waste management emissions came from 10 landfills (Xueref-Remy et al. 2019). For these ten landfills, based on inventories, emissions varied from 0.32 to 5.58 kt CH_4 y^{-1}. In 2015, mobile measurements were conducted on these landfills and bag samples were taken to determine their isotopic signature using the IRMS instrument. During that study, CH_4 plumes were not observed on four out of ten landfills. On three of them, CH_4 enhancement was not observed due to unfavorable meteorological conditions, while one landfill was closed in 2008 and currently seems not to emit methane anymore. Overall, from six landfills, $\delta^{13}CH_4$ signatures were in the range of -63.7 ‰ ± 0.3 ‰ to -58.2 ± 0.3 ‰ (Xueref-Remy et al. 2019).

The isotopic signature of landfill D was also determined. This landfill is situated about 35 km south-west of the Paris city and in the article of Xueref-Remy et al. 2019 is called Soignolles-en-Brie. During the study conducted by Xueref-Remy et al. (2019), $\delta^{13}CH_4$ was equal to -63.2 ± 0.1 ‰ in December 2015, while in December 2016, it was equal to -60.0 ± 1.3 ‰ (Assan 2017). The isotopic composition of this landfill is more depleted than the landfill E (in Xueref-Remy et al. 2019 called Le Plessis-Gassot). For the landfill E, in December 2015, the determined isotopic signature was equal to -58.2 ± 0.3 ‰. According to AIRPARIF, in 2010, landfill E emitted 5 kt CH_4/y (570 kg CH_4 h^{-1}) and was second largest landfill in IDF region (Xueref-Remy et al. 2019).

According to AIRPARIF inventories, landfill D is also a smaller CH_4 emitter than landfill E and it emitted 0.93 kt CH_4 y^{-1} (106 kg CH_4 h^{-1}) in 2010 (Xueref-Remy et al. 2019). In 2015, based on the statistic from ADEME (Agence de l'environnement et de la maîtrise de l'energie), emissions from this site were

about 79 kg CH_4 h^{-1}. These statistics are based on the total amount of collected and burnt biogas, compared to the collection capacity, linked to the coverage of wastes. For the emission calculation for 2016, the model SIMECT was used, and the estimated emission was between 160 and 320 kg CH_4 h^{-1}. This model estimates the theoretical production of biogas using the quantity of available waste and their composition (Ars 2017). These variations can be due to the different methodologies but also to the filling of the landfill over time.

During a previous study (Ars 2017), landfill D was visited three times. During mobile measurements, the tracer dispersion method (see Chapter 5.2.3.3) was used to determine methane emission from the site. Between visits, some improvements were implemented on the site, which should have decreased the CH_4 emission. The first measurement was conducted in September 2016, and the determined emission rate was equal to 240 ± 16 kg CH_4 h^{-1}, inside the range estimated by the SIMECT model. Then the biogas collection network was extended, and in November 2016, the observed CH_4 emission was equal to 152 ± 22 kg CH_4 h^{-1}. In the next step, the previously closed part of the landfill was covered by geomembrane. Then, in December 2016, the observed emission rate was equal to 84.0 ± 8.6 kg CH_4 h^{-1} (Ars 2017). The emission rate decreased by 65% from September to December 2016. Most likely, this reduction was achieved thanks to the implemented improvements. However, seasonality and meteorological conditions could also affect observed emission rate, as they influence microbial processes in soil (Chanton and Liptay 2000; Reay et al. 2010).

Energy sector. After the solid waste management sector, the energy sector is determined as the second major CH_4 source in IDF region, and it emitted 9.2 kt CH_4 y^{-1} in 2015 decreasing from 10.4 kt CH_4 y^{-1} in 2010. In the energy sector, different facilities can be source of CH_4 emissions (e.g., natural gas storage and distribution). Based on AIRPARIF inventories, in 2010, the emissions from 4 natural gas storage sites were equal to 1.2 kt CH_4 y^{-1}. They are filled during summer, and in winter, the gas is supplied to the IDF region and West of France. During previous studies, $\delta^{13}CH_4$ of two of them was determined and was equal to -43.4 ± 0.5 ‰ and -41.6 ± 2.4 ‰. In the case of the remaining two storage sites, CH_4 plumes were not observed. Isotopic signatures indicate thermogenic source of natural gas used in IDF. Natural gas used in France is imported from different regions, but it is mostly extracted in the North Sea and Russia. Norway is the first provider of natural gas (40%), and is followed by Russia (26%), the Netherlands (11%), Algeria (9%) and few other sources (14%), including Nigeria (GRTgaz 2019). Different geological origins of used gas can explain a potential variation of detected $\delta^{13}CH_4$. According to previous studies, the Russian gas is more depleted and can reach -50 ‰ (Dlugokencky et al. 2011), while gas from Norway and the North Sea are more enriched even until -24 ‰ (Zazzeri et al. 2015).

Work done during Ph.D. To extend the current knowledge about CH_4 emissions in IDF region, and confirm, reinforce or contradict previous studies, mobile measurements were focused on the two major CH_4 sources, reported by AIRPARIF inventories: solid waste management and energy sector. In the case of the waste management sector, observations are focused on two landfills (D, E). In the case of previous studies focused on the energy sector, the storage sites were the main area of interest. In a complementary approach, here, we focused on three gas compressors stations (A, B, C) situated in IDF region. All sites are operated by GRTgaz company, which is the major gas transmission operator in France. In practice, in gas compressor station B, the gas compressor and the gas storage are situated in the same area.

As some studies were already performed in landfills, here, most of the work is focused on gas compressor stations. The emission rate, isotopic signature and ethane to methane ratio were determined to characterize landfills and gas compressor stations. Sources characterization was made based on in-situ mobile surveys merged with Gaussian model and tracer dispersion method which are described below.

5.2. Methods used on site scale

As methods to determine isotopic signature and ethane to methane ratio were already explained in previous chapters, they are only briefly reminded below. The two methods to determine emission rates are described in detail, and examples of the application outside IDF are presented. In my study, the Gaussian model on the Polyphemus platform was used to model CH_4 plumes and estimate emissions. This method was tested during a controlled gas release experiment, already described in previous chapters (Chapter 2 and 3). Also, the tracer dispersion method was used. Before applying it to facilities in IDF region, it was used during the first MEMO^2 school to estimate emission from one of the compressor stations in the Netherlands.

5.2.1. Isotopic signature

During mobile measurements, isotopic signatures were determined using CRDS G2201-i with the AirCore tool. First, the plume was crossed, and then the car was stopped outside the plume and the air stored in the AirCore was dried and measured. The plume from one site was typically crossed several (between 3 and 7) times during one survey. Then, data were treated using the Miller-Tans approach (Miller and Tans 2003) and linear regression type II, which accounts for uncertainty in x and y (Sokal and Rohlf 1995). If the coefficient correlation r^2 remains below 0.85 and uncertainty determined as one standard deviation of linear regression is above 10 ‰, the data are rejected for further analysis. Then, the isotopic signature of the site for the individual day is calculated as the mean of the remaining samples.

Additionally, during part of the measurements, bag samples were taken to measure isotopic signature afterward in the laboratory on IRMS instruments. In this study, Supelco 2L or SKC 3L Flexfoil sample bags were used. They were filled with a KNF pump during surveys. Typically, three bag samples were taken inside the CH_4 plume, and one bag sample was taken outside as a background sample. One background sample was taken per survey. Most often, bags were sent to UU (Utrecht University). There, the IRMS instrument can measure $\delta^{13}CH_4$ and δDCH_4 (Röckmann et al. 2016). Moreover, during two surveys, additional bag samples were taken and then they were sent to RHUL (Royal Holloway University of London) also to measure using IRMS. This instrument is capable of measuring only $\delta^{13}CH_4$ (Fisher et al. 2006). This protocol allowed comparing the results from CRDS with the AirCore tool and two IRMS instruments for measurements of $\delta^{13}CH_4$.

5.2.2. Ethane to methane ratio

The ethane to methane ratio was determined for three gas compressor stations and one landfill. The measurements were made standing about 35 minutes inside the plume. Then the C_2H_6:CH_4 ratio was calculated as a slope of a linear regression between C_2H_6 and CH_4. The ratio was determined for

cases where CH_4 mixing ratio was more than 1 ppm above the background, and the sampled air was dried. Methods, Results and Discussion are detailed in Chapter 3.

5.2.3. Emission rate

In this chapter, two methods were used to calculate emission rates. Both are based on crossing the CH_4 plume multiple times. The first method is based on a Gaussian model, and it also requires the meteorological data as an input to the model (e.g., Hilst 1957; Gifford 1968; Weil and Brower 1984). The second requires an additional tracer and access to the site. The cylinder with the tracer gas should be situated as close as possible to the sources, and then the tracer gas should be released with a known rate (e.g., Allen et al. 2013; Roscioli et al. 2015; Yver Kwok et al. 2015; Ars et al. 2017).

5.2.3.1 Gaussian model in the Polyphemus platform

Polyphemus is a modeling platform dedicated to the study of air quality (Mallet et al. 2007). This platform gives the possibility to model emissions from the local to the continental scale. It includes two Gaussian and two Eulerian models. Models include representation of passive tracers' dispersion, radioactive decay, aerosol dynamics and photochemistry. Two Gaussian models are dedicated to dispersion at a local scale. The Gaussian plume model is applicable for continuous emission, while the Gaussian puff model is used for instantaneous emission (Mallet et al. 2007).

Here, I used the Gaussian plume model in the Polyphemus platform. The Gaussian model is a common air pollution model, which is based on a simple formula that describes the three-dimension concentration field given by a point source (Mallet et al. 2007; Roscioli et al. 2015; Yacovitch et al. 2015; Rella et al. 2015; Caulton et al. 2017). It considers a Gaussian distribution of mean concentration in the horizontal and vertical directions during homogeneous and steady-state meteorological conditions. The concentration C in the location x, y, z is given by:

$$C(x,y,z) = \frac{Q}{2\pi\sigma_y\sigma_z\bar{u}} exp\left[\frac{-(y-y_s)^2}{2\sigma_y^2}\right] \cdot \left\{exp\left[\frac{-(z-z_p)^2}{2\sigma_z^2}\right] + exp\left[\frac{-(z+z_p)^2}{2\sigma_z^2}\right]\right\} \quad (5.1),$$

where:

- Q is the emission rate of the source (mass per second),
- $\bar{u}$ is the mean wind speed,
- σ_y and σ_z are the Gaussian plume standard deviations in the horizontal and vertical directions,
- x is the downwind distance from the source,
- y is the horizontal crosswind coordinate,
- y_s is the source coordinate in the horizontal direction,
- z is the vertical coordinate,
- z_p is the plume height above ground.

The Gaussian plume standard deviations, σ_y and σ_z, are the sum of the spread due to turbulence, plume rise and the diameter of the source. They are also known as crosswind (σ_y) and vertical (σ_z) turbulence components. Different empirical schemes are used to estimate these standard deviations. In the Polyphemus platform, the standard deviations σ_y and σ_z are determined using Briggs parametrization, Doury formulations or a parametrization on similarity theory.

In the Polyphemus platform, the Briggs parametrization is based on the Pasquill – Turner stability classes, with six stability classes establishing σ_y and σ_z. These classes are determined by wind speed and solar irradiance (Table 5.1). They vary from extremely unstable class A to extremely stable class F, while class D is a neutral one. Classes E and F are dedicated for the nighttime observation (Pasquill 1961).

Table 5.1 Meteorological conditions defining Pasquill – Turner stability classes (Pasquill 1961).

Surface wind speed (m/s)	Daytime isolation			Nighttime isolation	
	Strong	Moderate	Slight	Thin overcast or > 4/8 low cloud	<= 4/8 cloudiness
<2	A	A – B	B	E	F
2-3	A – B	B	C	E	F
3-5	B	B – C	C	D	E
5-6	C	C – D	D	D	D
>6	C	D	D	D	D

A validation study (Korsakissok and Mallet 2009), performed to verify different parametrizations in different distances from sources, showed a good representation of the observation using the Briggs parametrization. In Polyphemus platform, this parameterization can be used to represent land category, defined on platform as urban or rural territory. Using Briggs formula requires only basic meteorological conditions (temperature, wind direction and speed, stability class) to use a Gaussian model. Within Briggs parametrization, the standard deviations σ_y and σ_z are calculated as:

$$\sigma_y = \frac{\alpha x}{\sqrt{1+\beta x}}, \qquad \sigma_z = \alpha x (1+\beta x)^{\gamma} \qquad (5.2),$$

where α, β, γ – coefficients depending on the Pasquill – Turner stability class (Table 5.2 and 5.3).

Table 5.2 Diffusion equations for Briggs formula for the rural area as a function of Pasquill – Turner stability class and downwind distance from the source (Briggs 1973)

Conditions	Stability class	Horizontal (σ_y) [m]	Vertical (σ_z) [m]
Extremely unstable	A	$0.22\ x\ (1 + 0.0001\ x)^{-0.5}$	0.20 x
Moderately unstable	B	$0.16\ x\ (1 + 0.0001\ x)^{-0.5}$	0.12 x
Slightly unstable	C	$0.11\ x\ (1 + 0.0001\ x)^{-0.5}$	$0.08\ x\ (1 + 0.0002\ x)^{-0.5}$
Neutral	D	$0.08\ x\ (1 + 0.0001\ x)^{-0.5}$	$0.06\ x\ (1 + 0.0015\ x)^{-0.5}$
Slightly stable	E	$0.06\ x\ (1 + 0.0001\ x)^{-0.5}$	$0.03\ x\ (1 + 0.0003\ x)^{-0.5}$
Moderately stable	F	$0.04\ x\ (1 + 0.0001\ x)^{-0.5}$	$0.016\ x\ (1 + 0.0003\ x)^{-0.5}$

Table 5.3 Diffusion equations for Briggs formula for the urban area as a function of Pasquill – Turner stability class and x downwind distance from the source (Briggs 1973)

Stability class	Horizontal (σ_y) [m]	Vertical (σ_z) [m]
A – B	$0.32\ x\ (1 + 0.0004\ x)^{-0.5}$	$0.24\ x\ (1 + 0.001\ x)^{-0.5}$
C	$0.22\ x\ (1 + 0.0004\ x)^{-0.5}$	0.20 x
D	$0.16\ x\ (1 + 0.0004\ x)^{-0.5}$	$0.14\ x\ (1 + 0.0003\ x)^{-0.5}$
E – F	$0.11\ x\ (1 + 0.0004\ x)^{-0.5}$	$0.08\ x\ (1 + 0.00015\ x)^{-0.5}$

Besides meteorological data, a source characterization is required as a model input: source position and length, and source input strength (Q_{input}). Then, the modeled and observed concentrations are summed along y crosswind horizontal coordinate. As the concentration is linearly proportional to the emission rate (Eq. 5.1), the emission rate can be calculated as:

$$Q = \frac{\sum C_{observation} - C_{background}}{\sum C_{model}} \cdot Q_{input} \quad (5.3)$$

Based on study of Caulton et al. (2018), different factors can cause under- or over- estimations of the calculated emission rate. Based on comparison of Gaussian models and large eddy simulations merged with Monte Carlo method, Caulton et al. (2018) observed that the largest uncertainty comes from the atmospheric variability. This uncertainty is caused by the insufficient averaging of turbulent variations in the atmosphere and the associated uncertainty is about 77% of the value. Multiple transects can decrease this uncertainty. Inaccurate wind speed data can cause uncertainty about 50% of the value. In-situ wind measurements should be provided during mobile measurements, to decrease this source of uncertainty. During a short time of survey (1-3 h), the atmosphere can still change rapidly, for example, from class B to D and cause the miscategorization of the applied stability class. Modeled concentration will increase and will cause a decrease of the emission retrieval, if a more stable stability class is used than the one corresponding to the actual meteorological conditions. Using less stable class have the opposite effect. Potentially, one stability class discrepancy can cause up to 40% change of the modeled emission rate. The turbulent plume diffusion was determined as the next source of uncertainty and expected to reach 25% of emission rate. This uncertainty was determined by comparison of the Gaussian modeling and large eddy simulation results. Also, the uncertainty on the source location and height contribute to the uncertainty of the calculated emission rate. In the distance from the source bigger than 150 m, uncertainties reach 20% of the value for source location and 15% for source height. The way of background calculation also impacted the uncertainty and reaches 5%. Its impact can increase for plumes with smaller enhancements (Caulton et al. 2018).

A Monte Carlo simulation was performed to determine the combined uncertainty of calculated emission as a 95% confidence interval. The simulation was performed 1000 times, while $C_{observation}$, $C_{background}$ and C_{model} were randomly obtained. For mobile measurements, when the plume was crossed only once, flux estimates range from 0.05q to 6.5q, where q is the nominal flux rate. This combined uncertainty decreases when multiple transects (10 transects) are made, and in situ wind measurements are provided. In this case, the uncertainty range is 0.10q to 3.0q (Caulton et al. 2018). This combined uncertainty is similar to results obtained during other controlled releases: 0.28q-3.6q (Rella et al. 2015) and 0.334q-3.34q (Yacovitch et al. 2015).

Here, the Gaussian plume model in the Polyphemus platform was used to estimate emission rates, based on the mobile measurements and it was tested during a controlled release experiment. Methane mixing ratio was measured downwind from the known source. It was also applied in real field conditions to determine the emission rate of the gas compressor stations in IDF. During the controlled release experiment, the distance between source and measurement varied between 150 m and 250 m. In the case of IDF measurements, the downwind distance between the source and measurement path depended on the available infrastructure and was about 100 m. This distance can be too small to apply the Gaussian plume model, potentially causing a bias in the determined emission rate. However, the validation test (Korsakissok and Mallet 2009) showed that using the Gaussian model with the Briggs parametrization is a good representation of the observation in the distance

between 50 m and 800 m from the source, and can estimate the emission rate in this relatively small distance.

Here, multiple transects were made (at least 10), and in situ wind measurements were provided. The Gaussian plume model in the Polyphemus platform was tested during the gas release experiment in Bedford, UK. This model was also used on the gas compressor stations in IDF region. Below, the results from the controlled release experiment are presented. The emission calculations for gas compressor stations are presented in section 5.3, as an illustration of the method. All calculations are made for a rural area.

5.2.3.2 Gaussian model in Polyphemus platform- controlled release experiment

The details of the set-up of the controlled release experiment are described in chapter 2. Briefly, the CRDS G2201-i with AirCore tool was used during mobile measurements (Karion et al. 2010; Rella et al. 2015; Lopez et al. 2017; Hoheisel et al. 2019) conducted in the Bedford Aerodrome, UK. GPS receiver (NAVILOCK NL-602U) was also a part of the set-up. Part of measurements was made with magnesium perchlorate as a dryer and part without it. For all measurements, inlet delay was accounted for during data analysis. For measurements made with magnesium perchlorate, the applied delay was equal to 46 s, without it - 24 or 27 s. Each release lasted about 45 minutes. Part of the releases was used to determine the isotopic signature (chapter 2) and C_2H_6:CH_4 ratio (chapter 3) and part to estimate the emission rate.

Emission rates were estimated for 8 releases. The plume was crossed in three downwind transects paths. Transect path A was in the closest distance to the source (~ 150 m), followed by transect path B (~200 m) and transect path C (~250 m). In each distance, the CH_4 plume was crossed ten times (Figure 5.1). Afterward, data were analyzed using the Gaussian model in the Polyphemus platform (Mallet et al. 2007; Korsakissok and Mallet 2009). During four releases, magnesium perchlorate as a dryer was installed before instrument inlet, and during four releases, wet air was measured. During four releases, the source was on the ground and during four others, it was situated 4.37 m above ground. The two-dimension meteorological station was situated in the distance ~50 m away from the release tower. The meteorological station supplies 1-minute averaged wind speed and direction, pressure, relative humidity and temperature. For all cases, boundary level height was set-up to 1000 m in the Gaussian model in the Polyphemus platform. Used stability class were chosen based on the meteorological conditions, both wind speed and insolation. Emission rate of the first six releases was calculated using stability class D, for the other two, stability class C was used.

In this experiment, the CH_4 background was calculated as the 1st percentile of the survey data and subtracted before calculating the emission rate. For every transect, the emission rate was calculated separately for every distance. The model was used for individual plumes. The initial input emission rate was set on 1 g/s, and the emission rate was calculated for individual transects using Eq. 5.3 and then averaged for each transect path. The distance is calculated from the beginning of the model window, both for modeled and observed CH_4 plumes. Figure 5.2 shows the example of a single plume crossing. Figure 5.3 compares the observed and modeled plumes for one release for different transect paths. The overall results are presented in Table 5.5 and Figure 5.4.

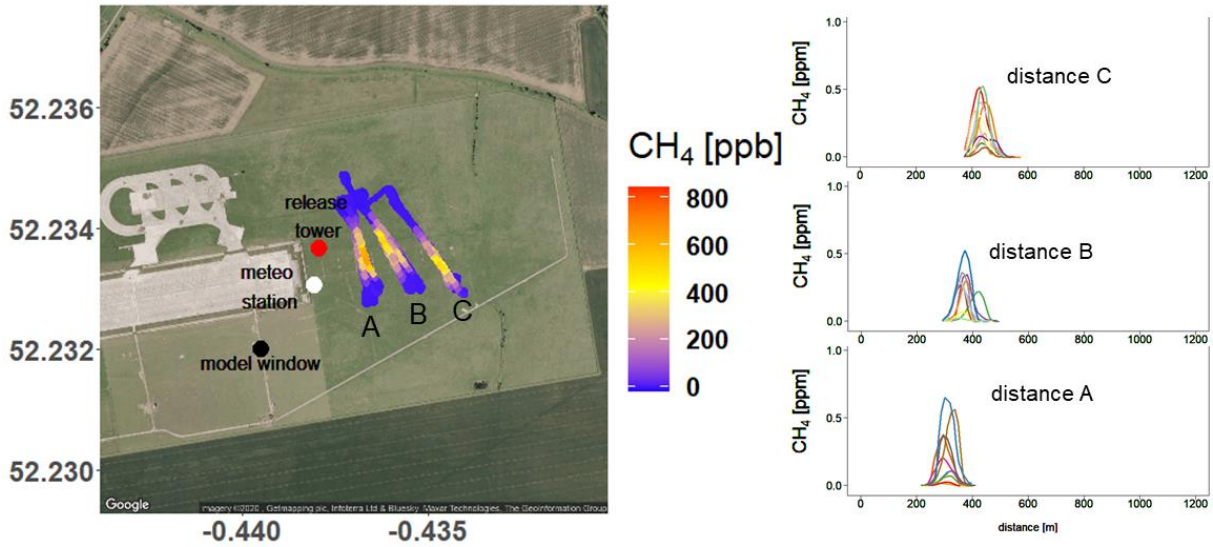

Figure 5.1 Example of transects made downwind from the source during the controlled release experiment. CH_4 enhancement above background is presented. Left: map with made downwind transects; red point – release tower, white point – meteorological station, black point – the beginning of the model window set in Polyphemus. Transects are made in three different distances (A, B, C). Right: Observed CH_4 enhancement in three different distances from source

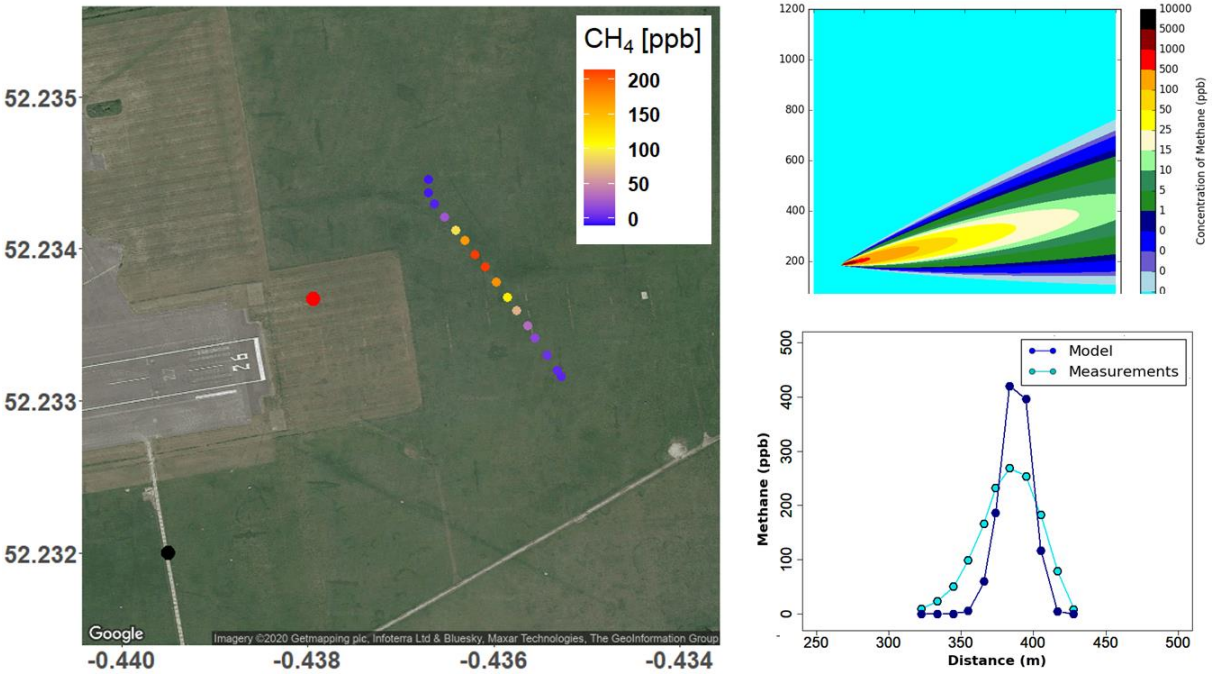

Figure 5.2 Example of individual transect, release 15 transect 8. Red point – release tower, black point – the beginning of model window set in Polyphemus. CH_4 enhancement above background is shown. Left: measurement while crossing a peak. Right: Gaussian model; top: modeled dispersion, bottom: comparison of modeled and measured CH_4 mixing ratio.

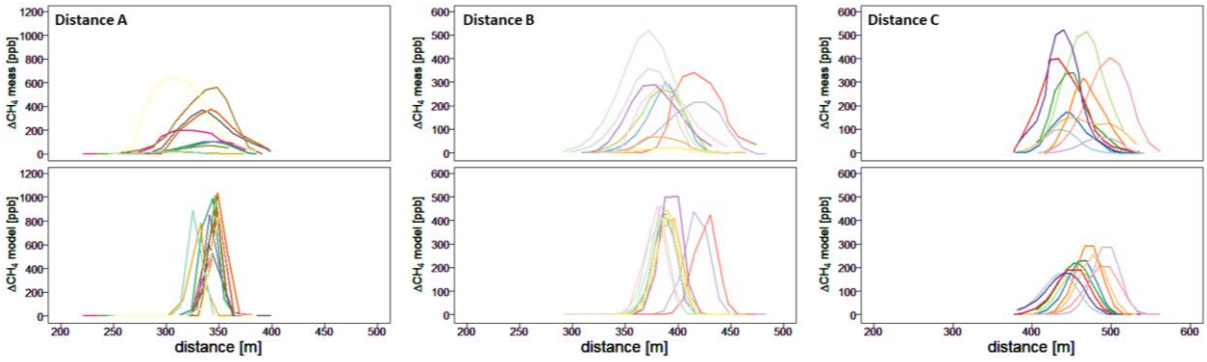

Figure 5.3 Release 15. Example of measured (top) vs. modeled (bottom) plumes for three different distances. CH_4 enhancement above background is presented. X axis represents distance from the beginning of the model window set in Polyphemus. Note that scale used for distance A differs from scales for distance B and C.

Table 5.4 CH_4 emission rate calculated using the Gaussian model on the Polyphemus platform. Emission rates are calculated in L CH_4 min^{-1}

id	height	dryer	Stability Class	Distance A [L CH_4 min^{-1}]	Distance B [L CH_4 min^{-1}]	Distance C [L CH_4 min^{-1}]
10	4	1	D	34 ± 8	60 ± 8	45 ± 9
11	0	1	D	73 ± 13	64 ±10	52 ± 9
15	4	1	D	69 ± 21	101 ± 20	135 ± 26
16	0	1	D	222 ± 56	249 ± 26	173 ± 22
19	4	0	D	110 ± 22	91 ± 15	121 ± 20
20	0	0	D	156 ± 26	87 ± 19	124 ± 18
21	0	0	C	99 ± 10	142 ± 22	86 ± 16
22	4	0	C	26 ± 5	44 ± 9	59 ± 11

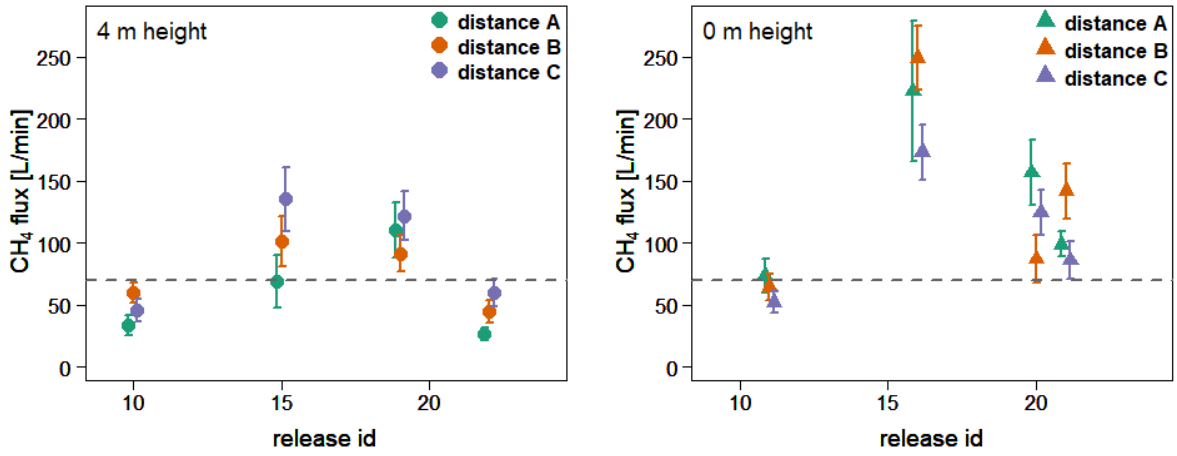

Figure 5.4 Emission rate calculated for individual transects. Left: source height 4.37 m, right source height 0.1 m. In both plots, two first measurements were made with a dryer before the instrument inlet, while the next two – without a dryer.

During all eight releases, actual emissions rate was unknown for measurement teams. The actual emission rate will be revealed by the organizer NPL after all calculations will be provided by measurement teams. However, it was indicated prior to the experiment, that the release rates would not be higher than 70 L CH_4 min^{-1}. The same emission rate was released for a pair of releases (e.g., the same emission rate for releases 10 and 11). Moreover, for one transect, estimated emission rate should be similar for calculations made for distance A, B and C. Using the Gaussian model on the Polyphemus platform, for releases pairs 15 - 16 and 19 - 20, the values are higher than the maximum released values, and a large difference between emission rates obtained for different transect paths are observed. The differences between calculated emissions rate for different transects path are higher for the releases from the ground level (Figure 5.4, right panel). These discrepancies can be caused by computation of σ_y and σ_z in the Gaussian model on the Polyphemus platform. Standard deviations σ_y and σ_z are calculated with the Briggs parametrization, not from 3-dimension wind direction, and it can have a crucial impact on the calculated emission rate. Moreover, during all eight releases, the wind direction and speed were not stable and could cause discrepancies. Additionally, Gaussian models do not include obstacle treatment or complex processes in the first meter above ground. Consequently, emissions at ground level can be harder to represent for a simple Gaussian model than emissions released higher.

Currently, data collected during the controlled release experiment are still being analyzed. Due to that, blind values are still unknown. After finishing all computations, the released emission rates will be revealed. Then, more detailed conclusions can be made and published in an article. A comparison of calculated and released emissions rates will determine the influence of the downwind distance of the transect path, the source height and of using a dryer for obtained values.

5.2.3.3 Tracer dispersion method

The tracer dispersion method (also called “dynamic plume tracer dispersion method”) is another method to determine emission rates. Similar to the Gaussian model, it is based on measurements of the CH_4 mixing ratio in atmosphere around the site. It was already applied to determine the emission rate from local CH_4 sources, like landfills, gas facilities or wastewater treatment plants (e.g., Allen et al. 2013; Mønster et al. 2014; Roscioli et al. 2015; Yver Kwok et al. 2015). In the tracer dispersion method, the additional tracer gas is used and emitted with a known rate. Methane and tracer gas are assumed to disperse in the same way (Lamb et al. 1986; 1995). CH_4 and tracer gas plumes are crossed a few times during mobile measurements, while the instrument capable of measuring CH_4 and tracer gas is mounted inside the car (Figure 5.5). Then, the ratio between observed downwind methane and tracer gas concentration is determined and used to calculate CH_4 emission rate:

$$Q = \frac{C_{methane} - C_{methanebackground}}{C_{tracer} - C_{tracerbackground}} \cdot Q_{tracer} \quad (5.4)$$

where:

- Q is the methane emission [g/s],
- Q_{tracer} is the tracer gas emission [g/s],
- $C_{methane}$ is the CH_4 concentration measured downwind from the source [g/m^3],
- C_{tracer} is the tracer gas concentration measured downwind from the source [g/m^3].

Different approaches exist to determine the ratio between methane and tracer gas. Commonly, the integrated (summed as measurements consist of discrete points) plume concentrations are compared ("plume integration approach"). Also, the emission rate can be calculated using plume heights ratios. In this case, the ratio between methane and tracer gas is obtained using the maximum concentration of methane and tracer gas plumes. Finally, the ratio can be determined as a slope of the linear regression of methane versus tracer gas. As the peak integration approach is less sensitive for the incompletely mixed methane and tracer plumes, it is implemented in this study. Also, previous studies confirmed the best accuracy of the tracer release method using the plume integration approach (Borjesson et al. 2009; Mønster et al. 2014). Then, to calculate CH_4 emission rate:

$$Q = \frac{\sum(C_{methane} - C_{methanebackground})}{\sum(C_{tracer} - C_{tracerbackground})} \cdot \frac{MW_{methane}}{MW_{tracer}} \cdot Q_{tracer} \quad (5.5)$$

where $C_{methane}$ and C_{tracer} are measured concentrations downwind in ppb, and $MW_{methane}$ and MW_{tracer} are the molar weight of methane and tracer gas.

Different gases can be used as a tracer gas in the tracer dispersion method. Previously, nitrous oxide (N_2O) and sulfur hexafluoride (SF_6) were broadly used. However, as they are greenhouse gases, they are less used nowadays. Currently, acetylene (C_2H_2) is used as a tracer gas. It can be observed during mobile measurements with CRDS G2203 (Picarro Inc., Santa Clara, CA, US). This instrument is dedicated to the field work application, and its frequency is equal to 0.5 Hz. The precision is 3 ppb for CH_4 and < 600 ppt for C_2H_2. In this study, CRDS G2203 was used during mobile measurements to observe CH_4 and C_2H_2 mixing ratios.

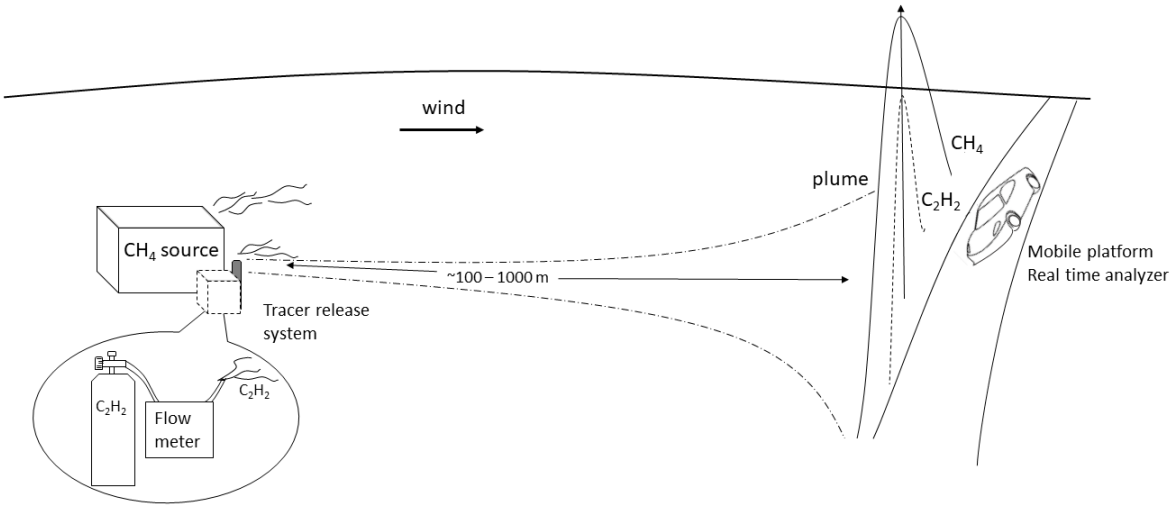

Figure 5.5 Based on Lamb (1995): Scheme of the tracer dispersion method during mobile measurements with analyzer situated inside the car

The placement of the tracer gas is crucial to obtain the correct quantification of CH_4 emission rate. The best accuracy is achieved when the tracer gas is situated at the same location as the targeted methane source. Different configurations of the placement of the tracer gas cause different biases. For example, when the measurements are made about 370 m from the source, 20 m sideways shift from the methane source caused an underestimation of about 12%. The impact of moving upwind 50 m the tracer gas from the source caused a 36% overestimation of emission rate (Mønster et al. 2014). Ars et al. (2017) observed a similar contribution of the upwind and sideway misallocation of the tracer gas. The influence of the tracer gas misallocation decreased with an increase in the distance

of the transect path from the methane source. It is explained by the decrease of the relative dispersion differences with distance.

Therefore, the distance of the transect path from the source should fulfill some compromised criteria. First of all, it should be large enough to ensure the smallest possible relative dispersion difference between misallocated methane and tracer gas. If the tracer gas is misallocated, the ratio of the distance between methane source and tracer gas to the distance of the transect path should be less than 0.2 - 0.5. For example, if the distance between CH_4 source and tracer release gas is 50 m, the required distance of the transect path is >100 m for low winds and > 250 m for high winds (Roscioli et al. 2015). Secondly, distance has to be short enough to limit dilution and to ensure high enough amplitude of the measured concentration compared to the instrument precision and background fluctuation. In practice, the choice of the distance is conditioned by the access to the road downwind from the source and by the possibility of tracer release gas collocation with targeted methane source. Regarding described criteria, measurements may be conducted too close or too far from the source, increasing the uncertainty of the calculated emission rate.

The impact tracer gas misplacement can be reduced when the local-scale transport modeling and the statistical atmospheric inversion approach are used during data treatment. For example, it can reduce the bias from 32% to 16% for the tracer situated 60 m upwind of the methane source (Ars et al. 2017). Moreover, applying local-scale transport model allows partitioning CH_4 emissions from multiple sources localized at one site (e.g., farms or gas facilities). Indeed, applying this more advanced data analysis could reduce the uncertainty of calculated emission rates. However, as this study is focused more on the measurements than data assimilation, emission rates were calculated either using the Gaussian model or the tracer dispersion method.

During my Ph.D., the tracer dispersion method was applied less often than the Gaussian model to calculate the emission rate from the site, as it requires access to the measured site which was not always possible. The tracer dispersion method was used in the landfill D just after starting my Ph.D. study. Afterward, it was used during the first $MEMO^2$ winter school to determine the emission rate from one of the gas compressor stations in the Netherlands. Studies made in IDF are presented in section 5.3, while study made in the Netherlands is presented below. In this illustrative case, besides the tracer release method, GRAL version 18.1 (Graz Lagrangian Model) and Polyphemus version 1.8.1 (Gaussian Model) were used to calculate the emission rate.

Based on study of Mønster et al. (2014), the comparison of the tracer dispersion method and Gaussian model showed that the model overestimated CH_4 emission rate. In that study, transects were made in three distances: 370 m, 770 m and 1200 m from the source. Using tracer dispersion method with perfect colocation of methane and tracer gas cylinders, estimated emission rate fluctuated around real emitted value. In this case, estimated emission rate reached 103 ± 2%, 106 ± 6% and 98 ± 6% of released value in three distances respectively (370 m, 770 m and 1200 m). In the case of estimation from the Gaussian model, the closest estimated value was obtained 370 m from the source and reached 97 ± 6% of released value. Bigger distance from the source resulted in an increase of estimated value and uncertainty. For transects made 770 m from source estimated emission rate reached 123 ± 15%, while in the case of 1200 m distance emission rate was estimated for 131 ± 20% of released value (Mønster et al. 2014)

5.2.3.4 Tracer dispersion method – example of application

Three mobile surveys were organized during MEMO^2 school in February 2018 in the Netherlands. Measurement campaigns were conducted 08.02, 09.02 and 12.02. During these surveys, the CRDS G2203 instrument was used. The best meteorological conditions (i.e. stable wind speed and wind direction) to successfully execute the tracer dispersion method was 12.02.2018, and the measurements were conducted near Koedijk gas compressor station (Figure 5.6 a-b). As from the road, two CH_4 plumes were observed, we assumed that two CH_4 sources are situated on this gas compressor station. However, their exact position is hard to find. On the map, their probable localization is marked (Figure 5.6 c-d). These localizations were used as the source coordinates in modelling. The station is hidden behind trees and situated in an urban area. The tracer gas (C_2H_2) was misallocated and situated outside the site, about 150 m from the first source and 210 m from the second source. The transect path was about 120 m from the methane source, and the canal was situated between sources and transect path. This configuration would likely cause bias in the calculated emission rate as explained before.

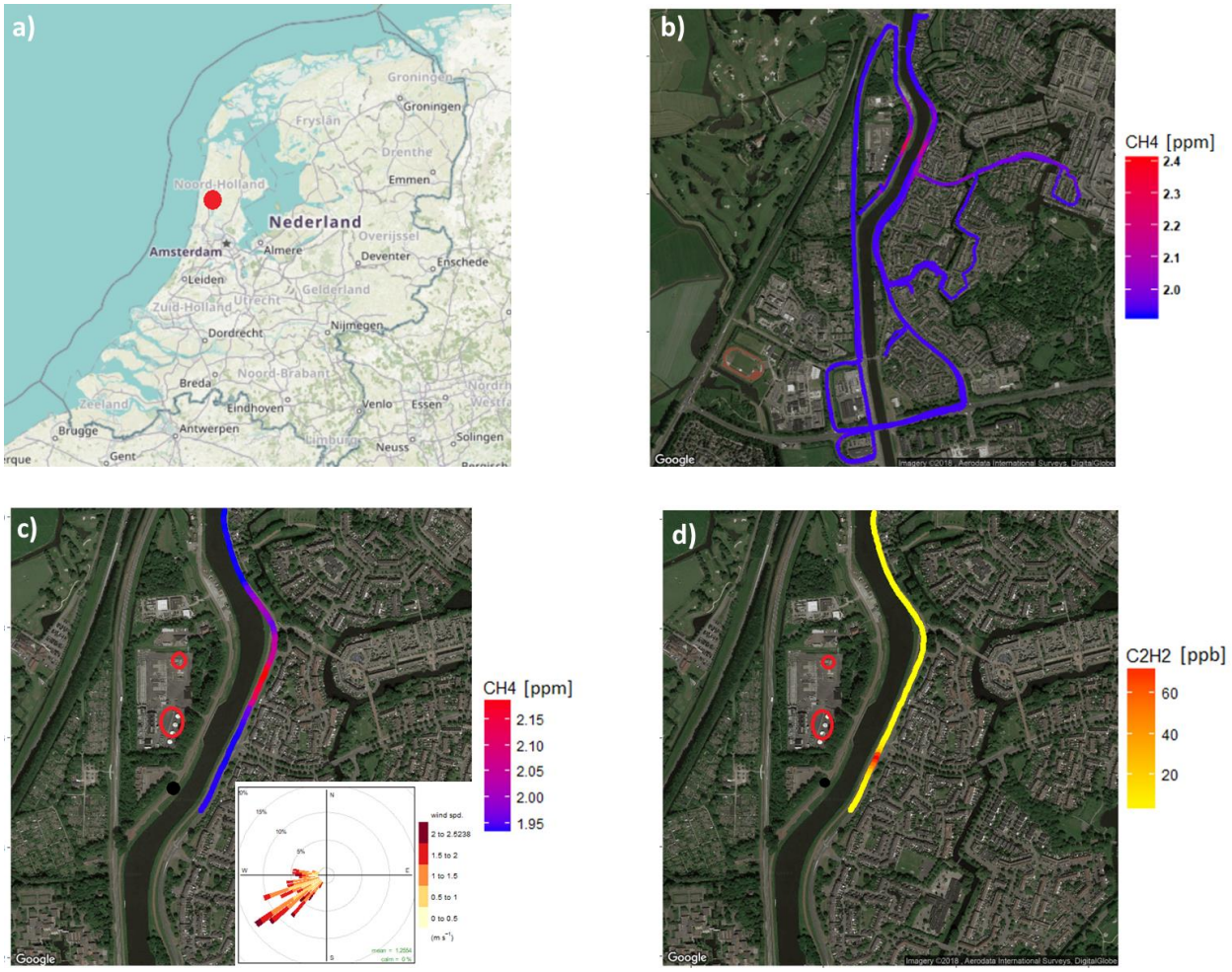

Figure 5.6 Koedijk gas compressor station. a) localization b) CH_4 mixing ratio observed during survey on 12.02.2018 c) CH_4 mixing ratio during one individual transect d) C_2H_2 mixing ratio during one individual transect. Figure c) and d): red circles – probable CH_4 sources, black dot – C_2H_2 cylinder position. The background is not subtracted.

Fourteen transects were made during the survey. C_2H_2 peak was not observed during every transect. Consequently, ten transects were used for further analysis, where both CH_4 and C_2H_2 plumes were observed (Figure 5.7). Table 5.5 presents the calculated CH_4 emission rate for individual transects using the tracer release method. Based on these ten transects, the averaged emission rate is equal to 2.87 ± 0.65 kg CH_4 h^{-1}. The uncertainty is calculated as one standard deviation divided by a square root of the transect number.

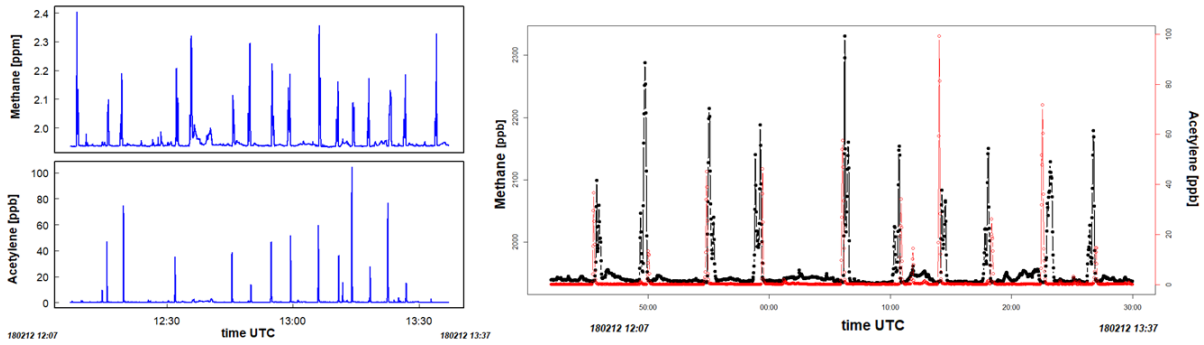

Figure 5.7 CH_4 and C_2H_2 mixing ratio measured on the Koedijk gas compressor station, 12.02.2018. Left: observed mixing ratio. Right: 10 transects chosen for further analysis, CH_4 (black) and C_2H_6 (red)

Table 5.5 Estimated emission for each transect during measurement on Koedijk gas station

N° Peak	1	2	3	4	5	6	7	8	9	10
Emission rate [kg CH_4 h^{-1}]	1.63	8.0	2.25	3.21	2.08	2.5	0.83	2.38	1.38	4.46

Afterward, emission rates were calculated using two different models: GRAL version 18.1 (Graz Lagrangian Model) and Polyphemus version 18.1 (Gaussian Model). As a Lagrangian model, GRAL is based on tracking many fictitious particles moving on trajectories within a three-dimension wind. The Gaussian model was used in the same way as in the controlled release experiment (section 5.2.3.2). The Graz Lagrangian model was used thanks to collaboration inside the MEMO^2 project. This computation was a part of the secondment of R. Morales, another Ph.D. candidate, who works with this model in the Swiss Federal Laboratories for Materials Science and Technology (EMPA). As part of his secondment at LSCE, he trained me to use the GRAL model. As the final step of the training, the GRAL model was applied to estimate emission rate of Koedijk gas compressor station. The GRAL model was used to estimate emission for acetylene (as control test) and the two methane sources. Figure 5.8 presents the modeled spatial dispersion of acetylene (5.8a) and methane (5.8b) for the first meteorological conditions (transect 1).

The GRAL model was run separately for each transect. Figure 5.9 shows the comparison of modeled and measured mixing ratio for one individual transect. For every transect, the meteorological conditions were set separately. Overall, difference in maximum value and peak shape, both for acetylene and methane, were observed. In most cases, the measured concentration was higher than the modeled one and also possibly shifted in time. In all cases plumes shapes were different. Modelled plumes were wider and more noise. It shows the bigger variability of modelled CH_4 plumes in short period than of observed CH_4 plumes.

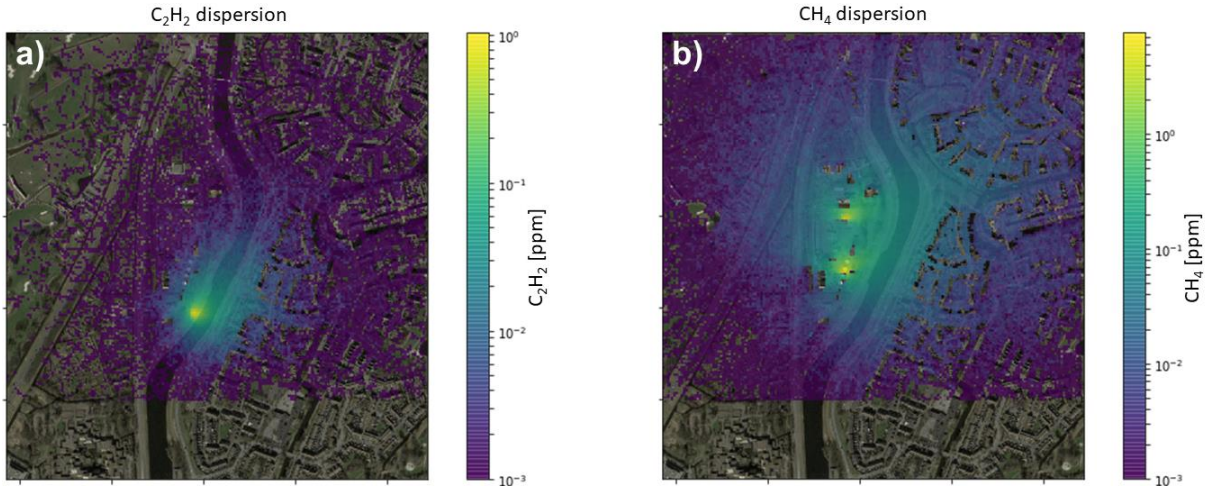

Figure 5.8 Modeled dispersion for first meteorological condition (1st transect) using GRAL model, Koedijk gas compressor, 12.02.2018. The presented grid map is larger than the simulation area, and there are no simulated particles in the bottom part of the map. Left: simulated dispersion for C_2H_2. Right: simulated dispersion for CH_4

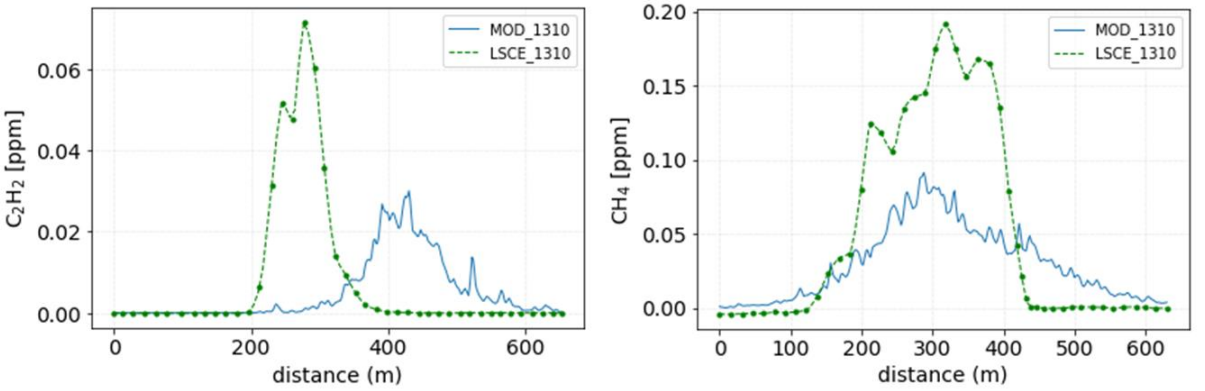

Figure 5.9 Koedijk gas compressor, 12.02.2018 Comparison of model and measurement of 9th peak. Left: C_2H_2. Right: CH_4

Eventually, each plume concentration was integrated along the cross plume path, both for modeled and observed plumes. Using linear regression between modeled and observed integrated CH_4 concentration plume, the fit slope was determined. Afterward, the flux Q is calculated as:

$$Q = \frac{Q_{input}}{slope} \quad (5.6).$$

Emission estimation were made both for acetylene, which was used as tracer gas and for methane emitted from gas compressor station. For acetylene, released emission rate (0.313 kg C_2H_2 h^{-1}) of C_2H_2 was used in model as input emission rate (Q_{input}). The slope from linear fitting between modeled and observed area is equal to 0.834. Using equation 5.6, the estimated emission of C_2H_2 from the GRAL model is equal to 0.375 kg C_2H_2 h^{-1}, about 20% higher than released C_2H_2 emission rate.

For methane, two sources were observed during mobile measurements, so in the model, two CH_4 sources were simulated. One observed plume had bigger CH_4 mixing ratio than other. Thus, input emission rate of the source ascribed to bigger CH_4 plume was set up for 2 kg CH_4 h^{-1}, while for the

smaller plume, it was equal to 1 kg CH_4 h^{-1}. Total CH_4 input emission from the two sources was equal to 3 kg CH_4 h^{-1} and the slope from linear fitting between modeled and observed plume areas is equal to 0.936. Using the equation above, the estimated total emission of CH_4 from GRAL model is equal to 3.205 kg CH_4 h^{-1}.

Finally, the Polyphemus model was also used to calculate emission rate. In this case, acetylene was used to adjust the input meteorological conditions of the model. Two sources were set in the model: one emitted 0.7 g CH_4 s^{-1} (2.52 kg CH_4 h^{-1}) and the second 0.3 g CH_4 s^{-1} (1.08 kg CH_4 h^{-1}). The stability class B was used, and the boundary layer was equal to 1000 m. As an example, results for the 9th transect are presented in Figure 5.10.

To calculate the emission rate, the same protocol as for the controlled release experiment was applied (Section 5.2.3.2). First of all, the ratio between observed and modeled integrated CH_4 concentration plume was calculated, and initial emission rate were multiplied by the averaged ratio. Using this method, the emission rate for acetylene is equal to 0.292 ± 0.0216 kg CH_4 h^{-1}. For methane, the calculated emission rate is equal to 5.155 ± 1.318 kg CH_4 h^{-1}.

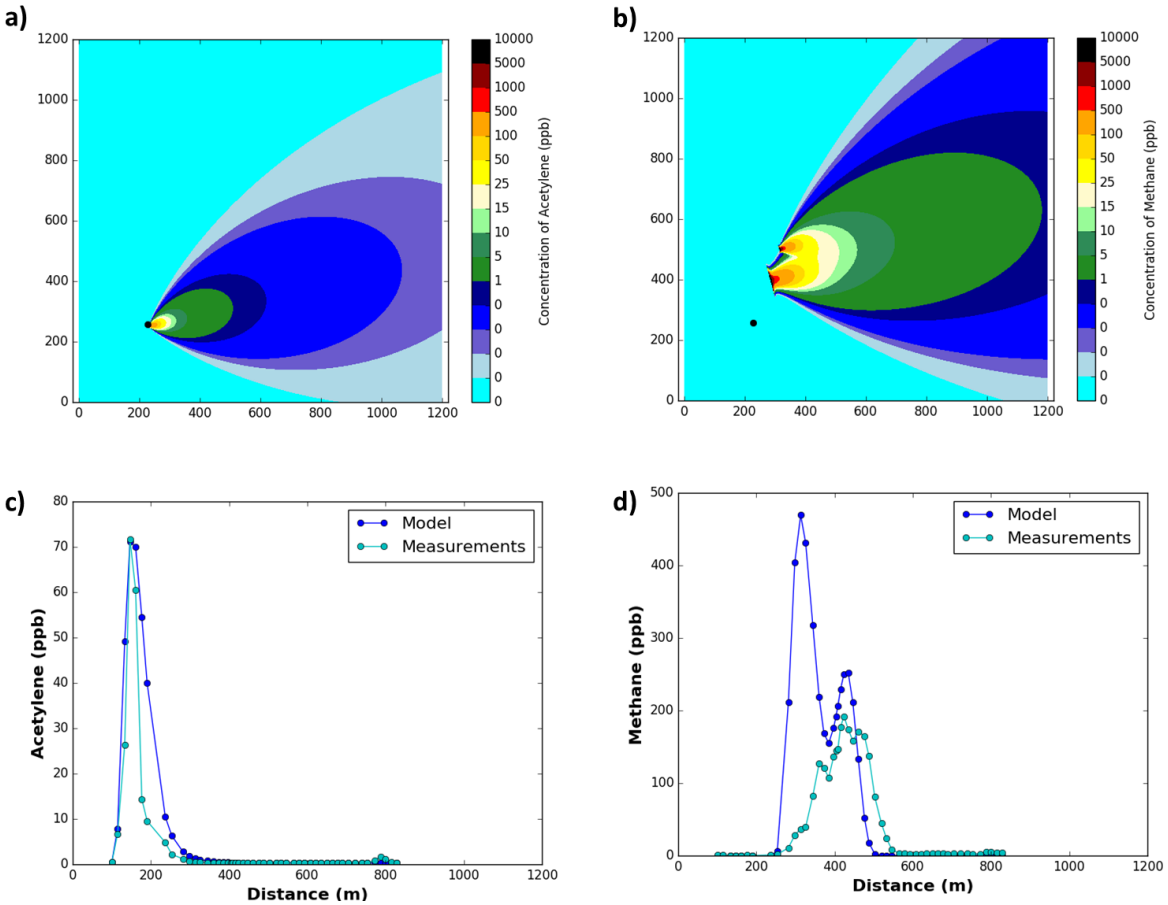

Figure 5.10 Gaussian model results for transect 9th, Koedijk gas compressor, 12.02.2018, Top: Modeled dispersion for 9st meteo condition. Bottom: Comparison of Model and observation. a) and c) C_2H_2 results b and d) CH_4 results

Overall, the calculated emission rates differ significantly between the tracer dispersion method and the two models. The smallest CH_4 emission rate was obtained using the tracer dispersion method (2.87 ± 0.65 kg CH_4 h^{-1}). The value obtained from the Lagrangian model is about 12% higher than determined with the tracer release method. The result from the Gaussian model is 79% higher than

for the tracer method. The C_2H_2 emission rate is overestimated using the Lagrangian model, about 20% and underestimated by the Gaussian model, about 7% (Table 5.6).

Table 5.6 CH_4 and C_2H_2 emission rate calculated for Koedijk gas compressor, 12.02.2018

Method	**CH_4 [kg CH_4 h^{-1}]**	**C_2H_2 [kg C_2H_2 h^{-1}]**
Tracer release	2.87 ± 0.65	0.313 (released)
Lagrangian model	3.205	0.375
Gaussian model	5.15 ± 1.31	0.292 ± 0.022

Different factors could cause difference between calculated emission rates. First of all, the tracer gas was misallocated more than 150 m sidewise compared to wind direction from the methane sources. Second, the distance between CH_4 source and transect path was about 120 m from the source what is less than the distance between tracer gas and methane sources. Also, the infrastructure around tracer gas and methane sources were different and CH_4 and C_2H_2 could experience different local turbulence. The gas compressor station was hidden behind the trees, while the tracer gas did not have any obstacles. These factors suggest that the flow from the tracer gas release in not a good reflection of the methane emitted from the gas compressor station, and the determined emission rate is burdened with an additional error. The infrastructure could also affect results of Gaussian model, as the canal was located between the source and transect path, and the survey was conducted in the urban area. In these more complicated conditions, especially combined with the trees situated in front of the gas compressor, the simple Gaussian plume model can yield a biased emission rate. Moreover, the stability class could be wrongly chosen. The GRAL model should cop better with complicated infrastructure as it uses the map as input data. In this study, the information from OpenStreetMap was used. Some misallocation from the building coordinates between OpenStreetMap and Google Maps were observed. It can also cause bias in the calculated emission rate. Considering the complicated topographic situation, placement of the tracer and multiple sources, using these different methods together give us a realistic range of the emission rate of this site.

Based on controlled release experiment (Section 5.2.3.2) and study on Koedijk gas compressor stations (Section 5.2.3.4), Gaussian model in Polyphemus platform overestimates emission rate. Moreover, the bias of estimated emission rate increase if the source is situated on the ground level (Figure 5.4), as Gaussian model do not include obstacle treatment or complex processes in the first meter above the ground. Also, here, standard deviations σ_y and σ_z are calculated with the Briggs parametrization, not from 3-dimension wind direction, what can have a crucial impact on the calculated emission rate. Finally, miscategorization of stability class can lead to the additional bias of estimated emission rate. One stability class discrepancy can cause up to 40% change of the modeled emission rate (Caulton et al. 2018).

Possibly, using tracer dispersion method instead of Gaussian model, estimated emission rate could be closer to the reality. Due to the time and organizational limitations, during my PhD study I did not make a controlled release experiment with acetylene release and the tracer dispersion method was used only on Koedijk gas compressor station as a testing case. However, previous study showed a good agreement between released and estimated CH_4 emission rate using tracer dispersion method with acetylene as an additional tracer (Borjesson et al. 2009; Mønster et al. 2014). However, using tracer dispersion method requires the access to the site, what can be the biggest limitation of this method. Also, the infrastructure

should allow to situate the acetylene cylinder close to the source and the measurements should be made from the distance where acetylene is a good representation of methane emission. The misallocation between acetylene and methane sources lead to under- or overestimations, depending on the configuration (Mønster et al. 2014, Roscioli et al. 2015, Ars et al. 2017).

Taking into account limitations of these two methods, the Gaussian model was used more often during my PhD study. It was caused by lack of access to measurement sites (i. g. gas compressor stations and one of landfills). Theoretically, it could be still possible to situate the acetylene cylinder out of the site and use the tracer dispersion method. However, as during my study the CH_4 plumes were visible only close to the source, the misallocation would cause too big bias and the method could not give reliable estimations. During surveys in IDF region, the tracer dispersion method was used only once on a landfill. In this case, the acetylene cylinder could be installed inside the site and the road was about 300 m from the landfill, so the acetylene was a good representation of methane. In the remaining cases, the emission rate was estimated using Gaussian model in Polyphemus platform.

5.3. Application of direct measurements methods in Île-de-France

In this step of my Ph.D., mobile measurements were conducted in IDF region, outside of the Paris city, at the site scale. Surveys were focused on three natural gas compressor stations (A, B and C) (Figure 5.11). During the first surveys, focused on the recognition of infrastructure and road access, CRDS G2203 was used. During subsequent measurements, G2201-i was used and details of mobile set-up are presented in Chapter 5.2. Surveys were also focused on landfill D and E. 6 surveys were conducted (landfill D – 4, landfill E - 2), using CRDS G2201-i. As in the Paris measurements, results are corrected and calibrated following the results from the laboratory tests (Chapter 2). To obtain wind data, the Gill Windmaster, 3D-axis sonic anemometer with U, V, W vector and sonic temperature outputs, was used. Data are saved with 20 Hz rata in the range 0-50 m/s and 0-359°. Meteorological data are used as model input to calculate the emission rates of observed sites.

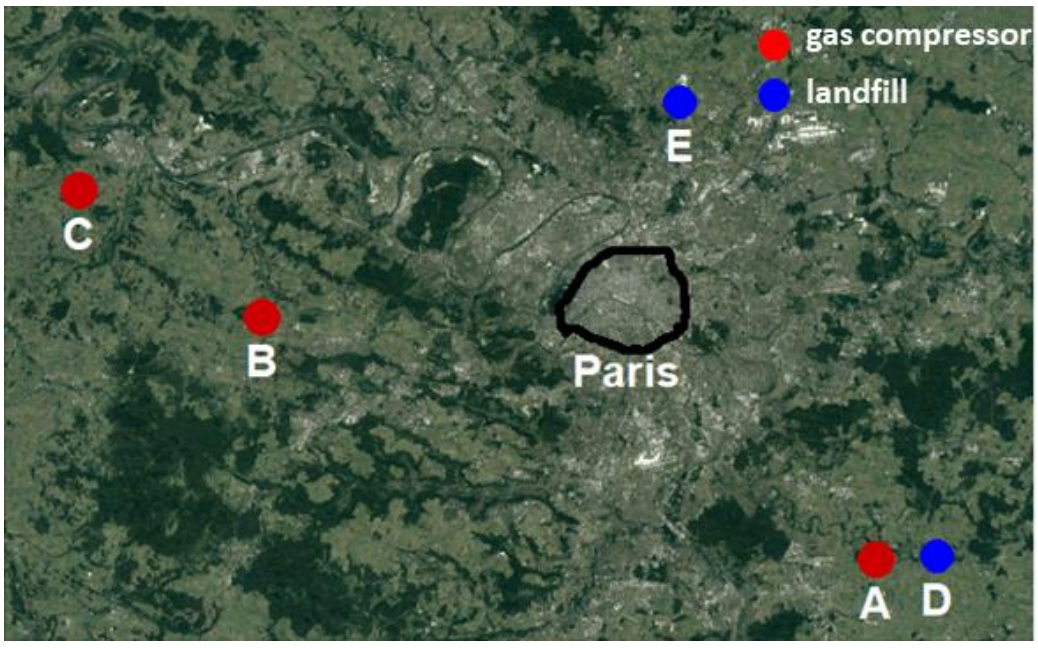

Figure 5.11 The location of landfills and gas compressors surveyed during the Ph.D. study

5.3.1. Gas compressors stations

Gas compressor stations are grouped under the energy CH_4 emission sector. Based on the study of Subramanian et al. (2015), conducted on 45 compressor stations in the U.S., vents, leaky isolation valves and equipment leaks are the major sources of CH_4 emissions inside a gas compressor station. CH_4 is emitted both during operating and standby mode. Typically, emission are 2-4 times smaller in standby mode than in operating mode. Also, gas compressor stations can become super emitters and cause skewed CH_4 distribution (Subramanian et al. 2015; Zavala-Araiza et al. 2015; Alvarez et al. 2018).

32 gas compressor stations are located in France. 6 of them is located in south-west France and they are operated by Terega. 26 gas compressor stations are operated by GRTgaz and 3 of them are in IDF. GRTgaz is a French natural gas transmission energy operator, which plans to reduce by three its methane emissions in 2020, based on the emissions in 2016. On all gas compressor stations in IDF, 2 gas compressors are located. Gas compressor stations A and B use the same technology. On facility B, not only gas compressors are located but also gas storage tanks. Gas compressor C operates more hours over a year than the other two stations.

5.3.1.1 Gas compressor station A

The gas compressor station A is situated about 35 km southeast of Paris, in a rural area with small villages and small industrial sites. On the station, two compressors and two venting zones are located. CH_4 plume emitted from the gas compressors is visible only from the street situated on the south side of the site. This road is at a small distance to the station, which potentially can cause bias during the calculation of emissions rate. The road is about 130 m from the compressors and ~50 m from one venting zone. On gas compressor station A, the surveys were conducted three times. Each time, the isotopic signature was measured using CRDS with AirCore tool.

During two days (10.01.2019 and 15.07.2019), only one plume was observed, and it probably came from one venting zone (Figure 5.12a-b). During a survey conducted on 16.05.2019, two CH_4 plumes were observed. Likely, one came from the venting zone, as in surveys when one plume was observed. However, as meteorological data are not available for that day, it is hard to identify the potential source of the second observed plume.

$\delta^{13}CH_4$ isotopic signature ranged between -44.0 ± 4.1 ‰ and -43.0 ± 2.9‰ using CRDS with AirCore tool (Table 5.7) for the plume coming from the venting zone. Also, the isotopic signature of the second plume did not differ statistically from the first one. Considering all surveys, during taking AirCore samples, measured CH_4 enhancement above background varied between 360 ppb and 2290 ppb. In total 22 AirCore samples were taken on gas compressor station A and 15 of them were used for further analysis. 7 samples were rejected cause their r^2 coefficient correlation was smaller than 0.85 and uncertainty was bigger than 10 ‰.

Additionally, during two surveys (10.01.2019 and 16.05.2019), bag samples were taken and analyzed afterward on IRMS at Utrecht University (UU). $\delta^{13}CH_4$ isotopic signature reached -45.8 ± 0.5 ‰ during first day and -44.3 ± 1.0 ‰ during second day. Isotopic signature obtained by CRDS with the AirCore tool are in good agreement within uncertainty with the results obtained from IRMS. The uncertainty of results from IRMS is smaller than for CRDS with AirCore tool. It is connected with better instrument precision (0.07 ‰ for IRMS and 3.7 ‰ for CRDS in low CH_4 mixing ratio).

Table 5.7 $\delta^{13}CH_4$ observed for gas compressor station A. CRDS results in this study are determined using the AirCore tool. For IRMS measurements, bag samples were taken and sent to UU.

Date	CRDS [‰]	Number of CRDS samples	IRMS [‰]	source
10.01.2019	-44.0 ± 4.1	2	-45.8 ± 0.5	Plume 1
16.05.2019	-44.2 ± 4.3	3	-44.3 ± 1.0	Plume 1
16.05.2019	-43.9 ± 1.6	6	-	Plume 2
15.07.2019	-43.0 ± 2.9	4	-	Plume 1

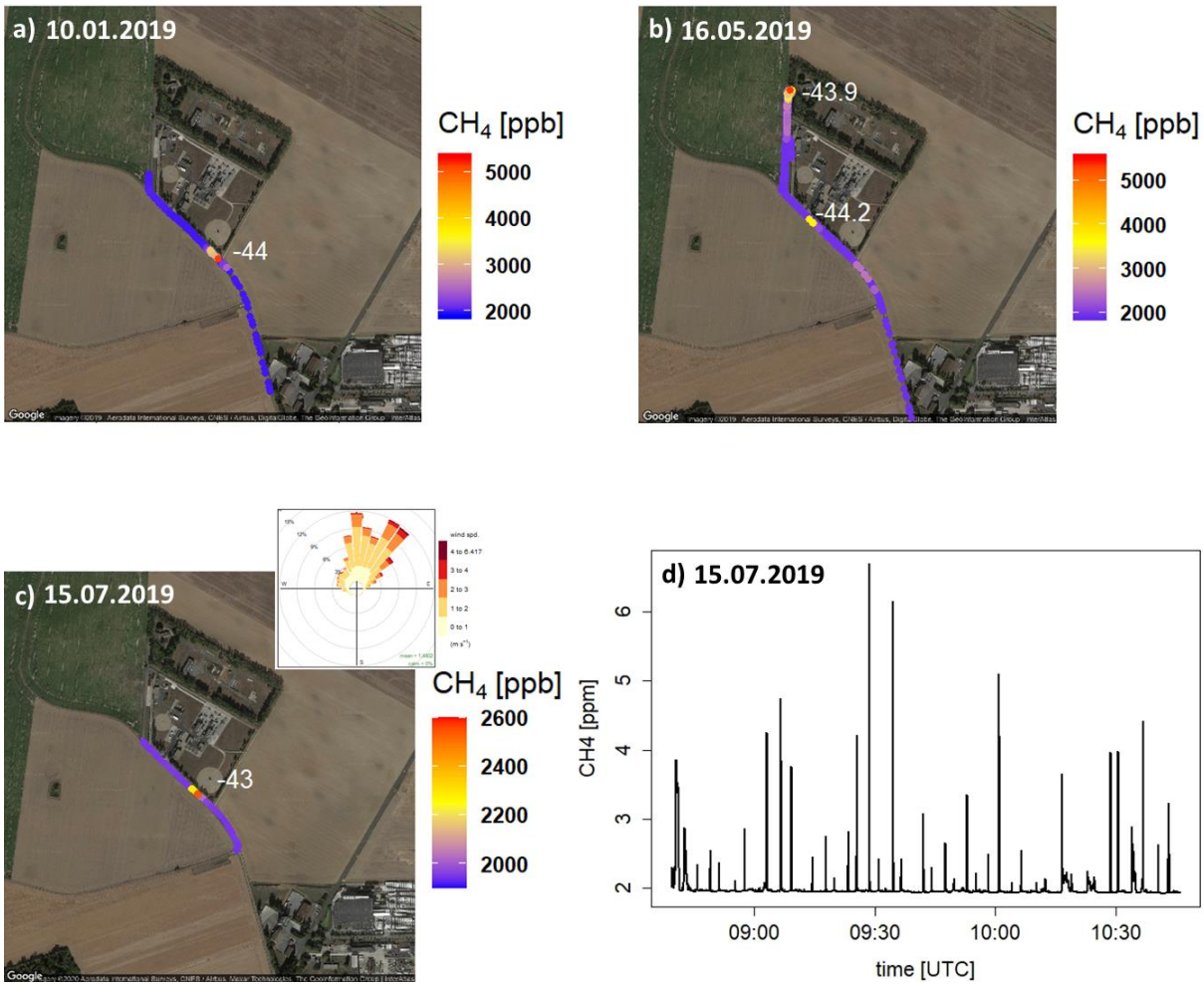

Figure 5.12 Gas compressor A. Observed CH_4 mixing ratio. The white number indicate $\delta^{13}CH_4$ [‰]. Background is not subtracted. c) and d) present CH_4 mixing ratio on 15.07.2010 when the emission rate was estimated. d) multiple crossing of the CH_4 plume.

During the last survey (15.07.2019), when one plume was observed, the emission rate was calculated using the Gaussian model (section 5.2.3.1). The plume was crossed 30 times. The wind station was situated outside of the site, about 70 m from the venting zone, assumed to be a source of observed CH_4 plume. During 2 hours, when the plume was crossed, the wind speed varied between 0.8 and 2.5 m/s, with a moderate insolation. Due to the challenge to identify a single stability class, the emission rate was calculated using two stability classes: A and B. For both stability classes, in the model 0.2 g CH_4 s^{-1} (0.73 kg CH_4 h^{-1}) was used as an input emission rate. Figure 5.13 presents model

output for a transect. Before comparing the observed and modeled CH_4 mixing ratio, the background was subtracted. The background was calculated separately for each plume as the 1st percentile of the observed CH_4 mixing ratio. The ratio of measured to modeled summed concentration was calculated and input CH_4 emission was multiplied by the averaged ratio to calculate the emission rate (Eq. 5.3). That day, for the gas compressor A, the CH_4 emission rate is equal to 2.45 ± 0.50 kg CH_4 h^{-1} for stability class A and 1.68 ± 0.34 kg CH_4 h^{-1} using stability class B.

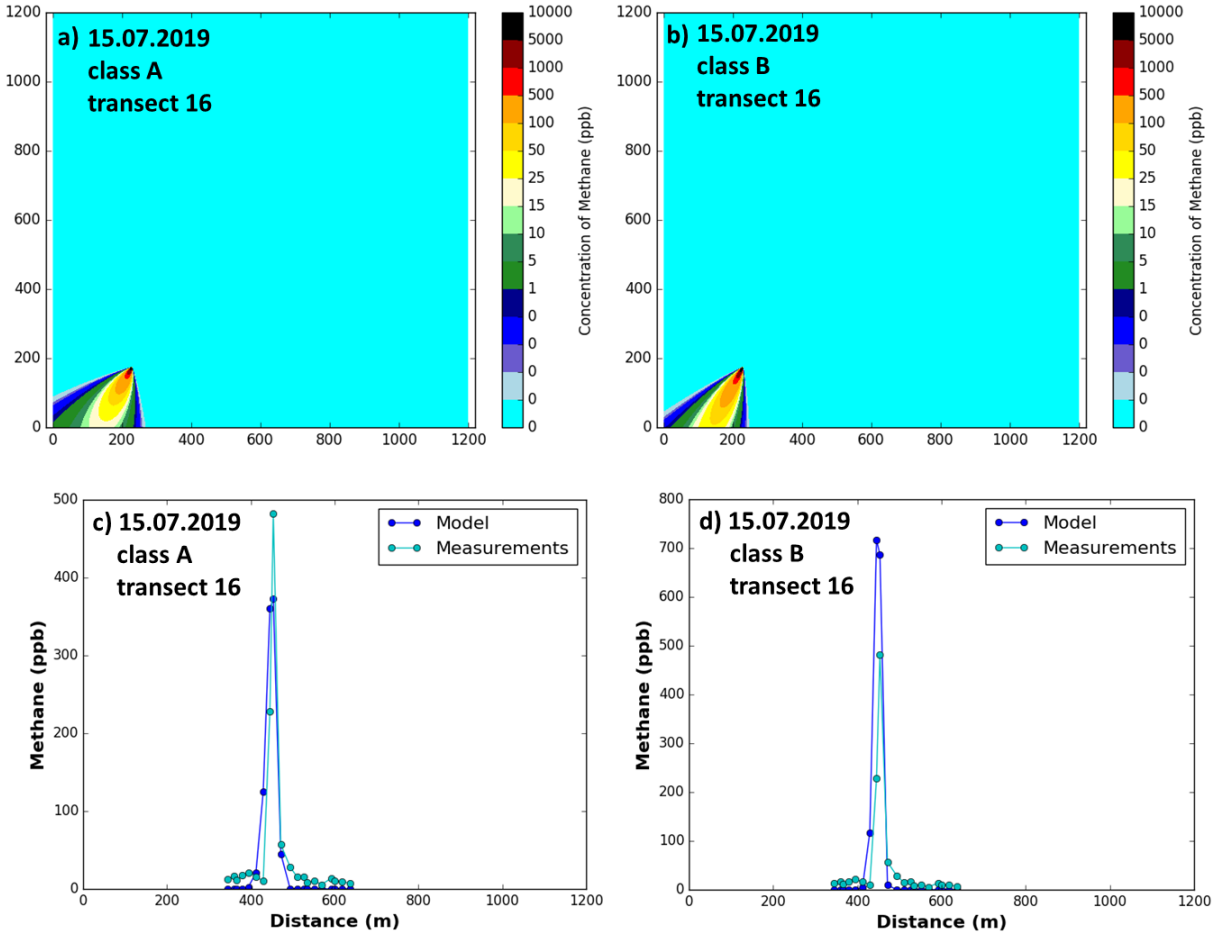

Figure 5.13 Gaussian model results for transect 16th, gas compressor A, 15.07.2019, Top: Spatial dispersion of CH_4 concentration, bottom: Comparison of model and observation. a) and c) stability class A b and d) stability class B

5.3.1.2 Gas compressor station B

The gas compressor B is situated about 40 km east of Paris. This is the biggest gas facility studied here and it includes not only gas compressors, but also gas storage tanks. Additionally, access around this site is much more limited compared to gas compressor stations A and C. This site is surrounded by forest on the north, west and south. The only available small road is on the east. Additionally, gas compressor station B is much larger than stations A and C. Likely, on gas compressor B, venting zone, gas storage tubes and above ground pipelines are possible sources of methane released to the atmosphere.

During two surveys, the isotopic composition was determined using CRDS with the AirCore tool. During the first survey (27.05.2019), $\delta^{13}CH_4$ was equal to -44.1 ± 1.9 ‰ using CRDS instrument and

-43.9 ± 0.4 ‰ using IRMS. (Table 5.8) These values are statistically in good agreement. The uncertainty of the value obtained from CRDS during AirCore sampling is lower than in the gas compressor A. It is caused by a higher observed CH_4 mixing ratio on site B than A. This value was obtained for the biggest plume observed that day. The maximum CH_4 enhancement of the plume varied between 750 ppb and 10 510 ppb during AirCore sampling. Moreover, this value is also in good agreement with the value obtained in December 2015, when the isotopic signature was measured for gas storage in this area. For that previous measurements, $\delta^{13}CH_4$ was equal to -43.4 ± 0.5 ‰, with bag samples collected and analyzed on IRMS at RHUL (Xueref-Remy et al. 2019).

During the second survey, $\delta^{13}CH_4$ was determined only using CRDS. The isotopic signature was more enriched and reached -40.1 ± 3.9 ‰. In this case, the $\delta^{13}CH_4$ uncertainty is higher, as the maximum CH_4 enhancement above background did not exceed 1000 ppb during AirCore sampling. In total, six AirCore samples were taken, but two samples were rejected from further analysis as their maximum enhancements were too low (<500 ppb). More enriched value suggests that natural gas of a different origin, but still thermogenic (i.e. extracted in different region) was processed that day on the gas compressor station B.

During measurements on 27.05.2019, 4 CH_4 plumes were detected, where one was bigger than the others (Figure 5.14). Measurement made on 12.07.2019 let suspect that this bigger plume is a combination of the two sources, localized close to each other. That day only one peak was observed and the measured CH_4 mixing ratio was smaller than previously.

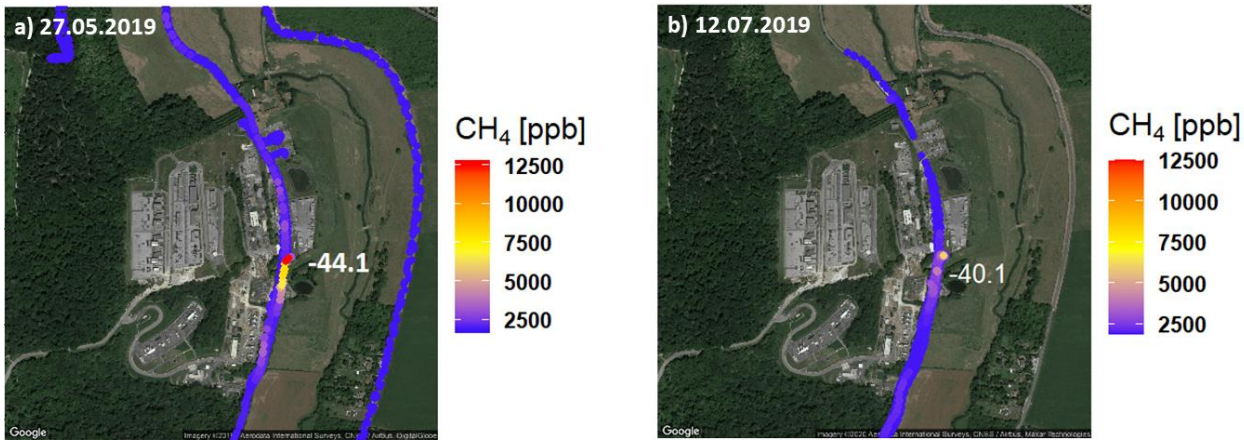

Figure 5.14 Gas compressor station B observed CH_4 mixing ratio. The white number indicates $\delta^{13}CH_4$ [‰]. Background is not subtracted.

Table 5.8 $\delta^{13}CH_4$ observed for gas compressor B. CRDS results in this study are determined using the AirCore tool. For IRMS measurements, bag samples were taken and sent * to RHUL or ** to UU.

Date	CRDS [‰]	Number of CRDS samples	IRMS [‰]	source
7.12.2015	-		-43.4 ± 0.5*	Gas storage (Xueref-Remy et al. 2019)
27.05.2019	-44.1 ± 4.1	5	-43.9 ± 0.5**	Plume 1
12.07.2019	-40.1 ±3.9	3	-	Plume 1

Additionally, on 12.07.2019 multiple transects were made to estimate emission rate of compressor station B. However, that day the meteorological station did not work properly and as consequence, Gaussian model could not be used to estimate emission rate. Additionally, amount and exact location of possible CH_4 sources inside site is unknown what would cause a strong bias to the emission rate. Previous study (Caulton et al. 2018) showed that for a single source, a wrong height caused 15% changes of estimated emission rate and a wrong source location caused 20% changes. Potentially, in the case of site B, this negative impact could increase as the number of sources is unknown and one day, four CH_4 plumes were observed and another day only one plume was observed. Because of these issues our analysis of compressor B remained limited.

5.3.1.3 Gas compressor station C

The gas compressor station C is the last studied gas facility in IDF. It is situated 60 km north-west of Paris. Similar to gas compressor A, it is located in a rural area. Around the site, there is a farmland and on the south-west side, a small forest. This site hosts two compressors and one venting zone. Four surveys were conducted on this site, three to determine the isotopic composition and one to determine the emission rate. Usually, only one CH_4 plume was observed on the gas compressor station C. Its position suggests that the plume comes from the venting zone. During first survey (28.02.2019) two CH_4 plumes were observed. Location of second plumes suggested gas compressors as possible source of the second plume.

During the first survey, the isotopic composition of the two plumes was measured. Likely, one plume came from venting zone and the second from area where two compressors are located. Two AirCore samples were taken for each plume. Averaged isotopic signature was equal to -40.8 ± 5.7 ‰ for the first plume and -45.2 ± 6.2 ‰ for the second plume. That day, bag samples were also collected and sent to RHUL and UU to measure with IRMS. The $\delta^{13}CH_4$ was equal -41.0 ± 3.5 ‰ and -43.5 ± 1.2 ‰, at RHUL and UU, respectively (Table 5.9). Results obtained by the two IRMS instruments differ and have much bigger uncertainty (calculated as the uncertainty of the fitting regression in the Keeling method) than during studies on gas compressor stations A and B and landfills D and E. Even though, the results still agree statistically within 1 sigma uncertainty.

There are two possible explanations of the observed bigger uncertainties. First of all, the observed CH_4 enhancement was small (< 600 ppb above background) for isotopic samples. During AirCore sampling, the maximum observed CH_4 enhancement above background reached 450 ppb. This relatively small enhancement is below CRDS limit to measure isotopic signature and cause larger uncertainty of detected value, as for isotopic sampling CH_4 enhancement should reach at least 500 ppb (e.g., Lopez et al. 2017; Hoheisel et al. 2019; Defratyka et al. 2020). Also, during bag samples collecting, CH_4 concentration varied between 1950 ppb and 2140 ppb, which is bellow required 500 ppb enhancement above background (chapter 5.2). Second, that day the wind was quite strong and changing over time, which caused the mixing of these two plumes in different proportions and during part of transects, only one plume was observed. Figure 5.15b presents changes in the shapes of

observed CH_4 plumes and their overlapping during part of transects. Unfortunately, during that day, the wind station did not work, so it is impossible to provide any detailed information.

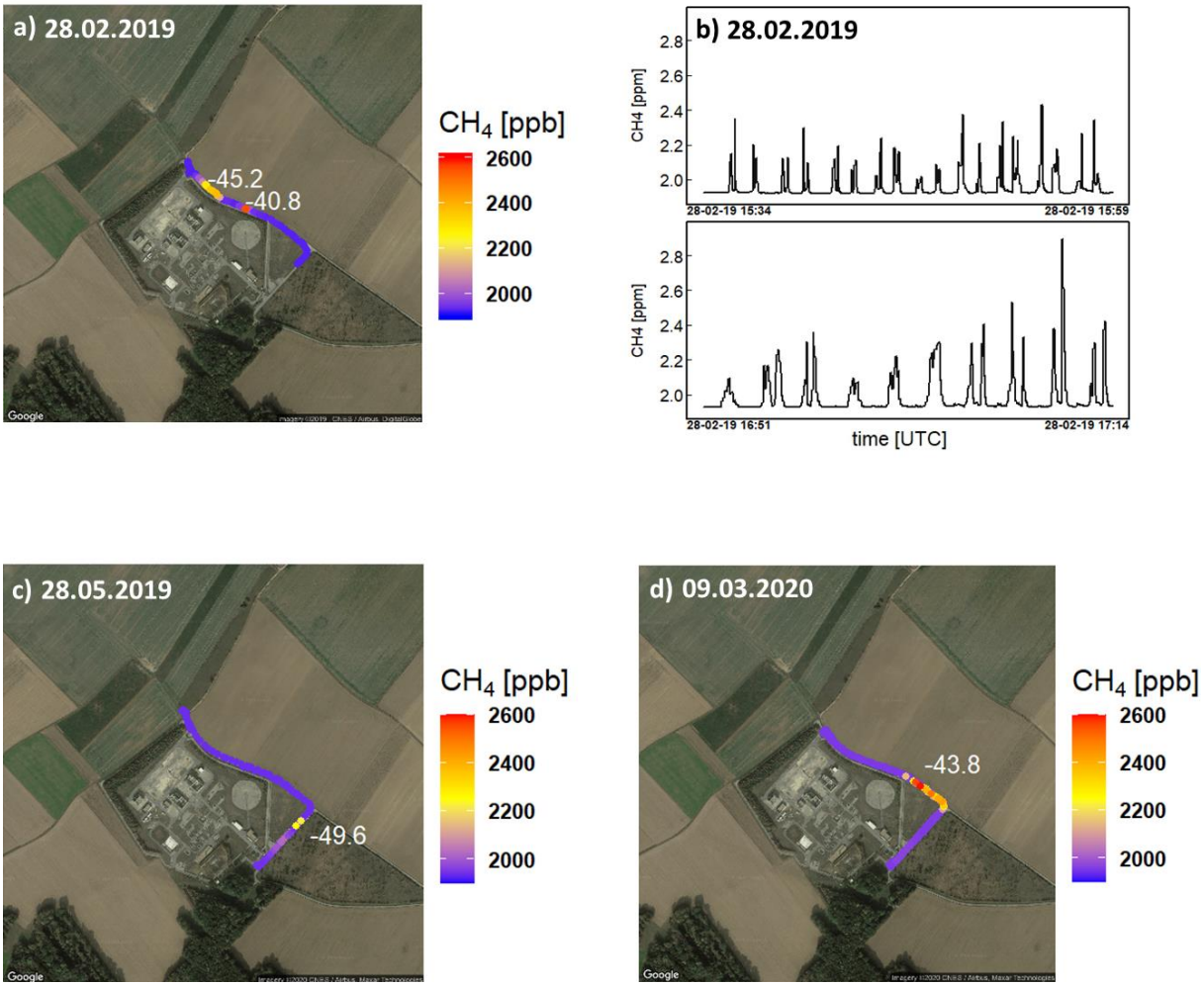

Figure 5.15 Gas compressor station C. Observed CH_4 mixing ratio above background. The white numbers indicate $\delta^{13}CH_4$. Background is not subtracted. b) multiple crossing of the CH_4 plume.

Three months later (28.05.2019), four AirCore samples were measured on the gas compressor station C. However, due to low CH_4 enhancement, three were rejected from further analysis as it caused large uncertainty and low r^2 coefficient correlation. Rejected isotopic signature ranged from -48.36 ± 9.8 ‰ (r^2 = 0.86) to -33.2 ± 36.2 ‰ (r^2 = 0.41). $\delta^{13}CH_4$ isotopic signature determined from remaining sample was equal to -49.6 ± 5.4‰ (r^2 = 0.95). For non-rejected sample CH_4 enhancement was equal to 1345 ppb, what is above instrument limitation threshold and it is higher than CH_4 enhancement observed in February.

On 28.05.2019 bag samples were also taken to analyze later at IRMS. Isotopic signature from IRMS reached -43.9 ± 0.4 ‰ and it is more enriched than isotopic signature from CRDS instrument (-49.6 ± 5.4‰). The isotopic signature from IRMS is similar to the other values, observed during summer 2019 in gas compressors A (-43.0 ± 2.9 ‰) and B (-40.1 ± 3.9 ‰). Moreover, an isotopic signature of -49.6 ± 5.4‰ obtained from CRDS analyzer is more depleted than other isotopic signatures determined for gas facilities in IDF, both in this study and in the study made by Xueref-

Remy et al. (2019). It suggests that, the value from CRDS should be rejected and could be caused by some instrumentation problems (e.g., leaking tubing in the mobile set-up).

Finally, the last survey to measure the isotopic composition was conducted on 12.03.2020. That day, the CRDS G2201-i was not available, and only bag samples were collected to measure on IRMS at UU. That day, determined $\delta^{13}CH_4$ was in good agreement with results from the second survey and reached -43.8 ± 0.2 ‰.

Table 5.9 $\delta^{13}CH_4$ observed for gas compressor C. CRDS results in this study are determined using the AirCore tool. For IRMS measurements, bag samples were taken and sent * to RHUL or ** to UU.

Date	CRDS [‰]	Number of CRDS samples	IRMS [‰]
28.02.2019	-40.8 ± 5.7 (plume 1; venting zone) -45.2 ± 6.2 (plume 2; compressors)	2 2	-41.0 ± 3.5* -43.5 ± 1.2**
28.05.2019	-49.6 ± 5.4	1	-43.9 ± 0.4 **
12.03.2020	-		-43.8 ± 0.2**

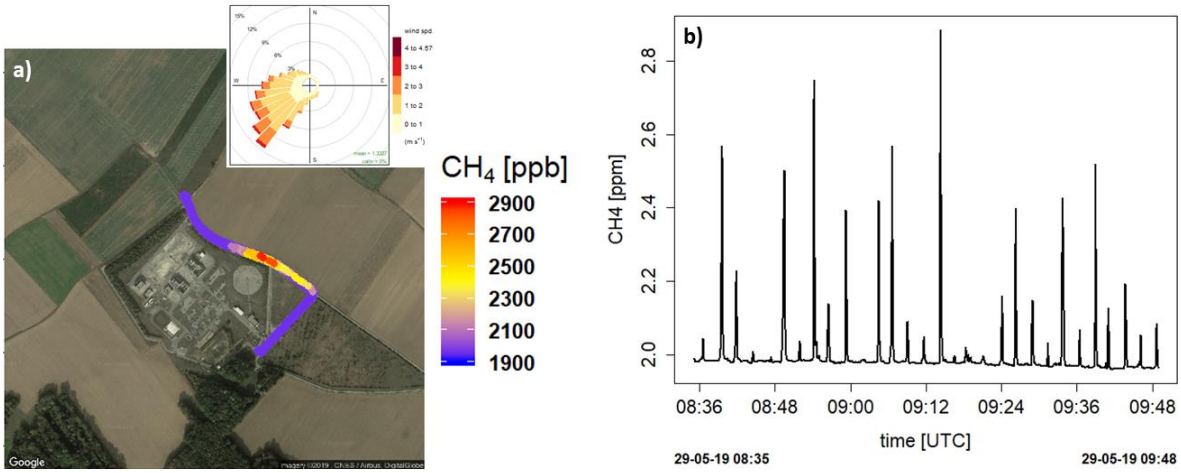

Figure 5.16 Gas compressors C, 29.05.2019. a) Observed CH_4 mixing ratio with rose wind b) multiple crossing of the CH_4 plume. Background is not subtracted

In addition to measurements of the isotopic composition, one day (29.05.2019) was dedicated to estimating CH_4 emission rate of the gas compressor station C. That day only one CH_4 plume was observed, and 30 transects were made (Figure 5.16). The meteorological conditions were similar to the conditions on gas compressor station A during the survey dedicated to making multiple transects. The wind speed varied between 0.01 m/s and 3 m/s with mean wind speed of 1.3 m/s, and the insolation was moderate. Similar to gas compressor station A, due to the challenge to identify a single stability class, the emission rate was calculated using two stability classes: A and B. The emission rates were calculated in the same way as for gas compressor station A. Figure 5.17 presents one transect for the two stability classes.

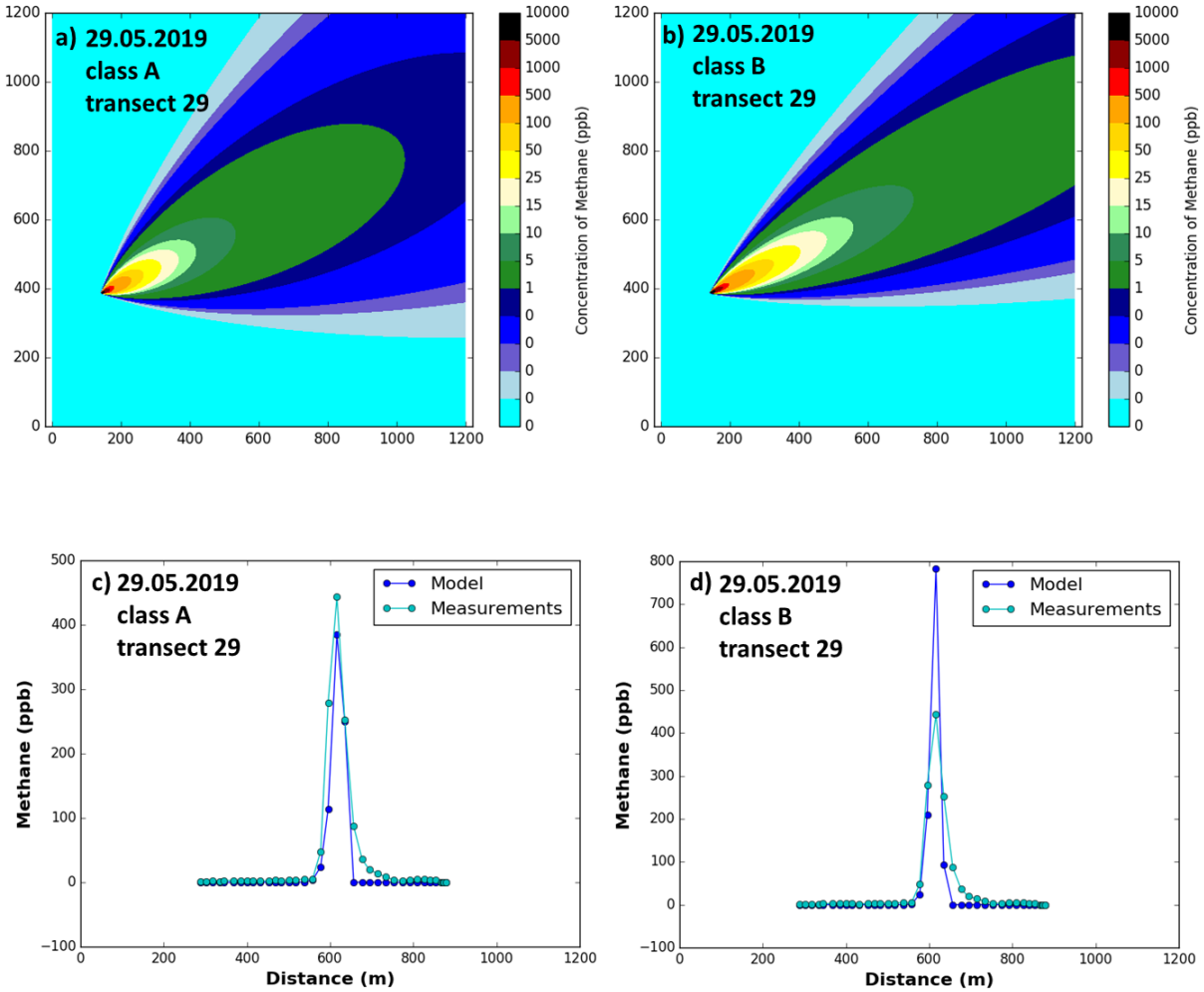

Figure 5.17 Gaussian model results for transect 29th, gas compressor station C, 29.05.2019, Top: Spatial dispersion of CH_4 concentration, bottom: Comparison of model and observation. a) and c) stability class A b and d) stability class B**.**

For that day, the calculated emission rate reached 0.81 ± 0.13 kg CH_4 h^{-1} using stability class A and 0.55 ± 0.09 kg CH_4 h^{-1}, using stability class B. As plumes from stability class A match better to plumes from observations, possibly estimations using stability class A are closer to the reality.

Compare to gas compressor station A, the emission rate for gas compressor station C is about three times smaller. Both gas compressors stations used two compressors. On site A are two venting zones and on site C there is only one venting zone. Gas compressors A and C use the same technology. The size of both sites is comparable. However, gas compressor C has bigger amount of working hours. Unfortunately, we do not know what type of works was conducted during measurement days on site A and C. Thus, it is not possible to explain observed differences by type of conducted works. However, as site C operates more hours than site A, possibly it is better monitored by owner company and hence, less fugitive emissions occur on site C than site A.

Overall, $\delta^{13}CH_4$ signature was determined for three gas compressor stations during different surveys made in 2019, both using CRDS with AirCore tool and bag samples measured on IRMS. Regarding all results, $\delta^{13}CH_4$ was stable over measurement period and similar on all three gas compressor stations. The $\delta^{13}CH_4$ signature is in the range from -45.2 ± 6.2‰ to -40.1 ± 3.9‰ using

CRDS with AirCore. Also, obtained from CRRDS values are in good agreement with IRMS results, where $\delta^{13}CH_4$ is in the range from -45.8 ± 0.5‰ to -41.0 ± 0.5‰. As expected after laboratory tests (chapter 2), the precision of determined $\delta^{13}CH_4$ is worse using CRDS than IRMS. Overall, observed $\delta^{13}CH_4$ do not change significantly between gas compressor stations and over a time.

Regarding estimation of emission rate, Gaussian model on Polyphemus platform was used to determine emission rate for gas compressor station A and C as they could be treated as point sources. In both cases, based on the meteorological conditions, stability class A and B where used during estimations. Estimated emission rate is about three times bigger for gas compressor station A than C, both using stability class A and B. Using the stability class A, the emission rate is estimated at 2.5 ± 0.5 kg CH_4 h^{-1} for site A and 0.8 ± 0.1 kg CH_4 h^{-1} for site C. As for the gas compressor station B, the amount and exact location of possible CH_4 sources inside site is unknown, the emission rate was not estimated for the site B. Because of this lack of the information, analysis of compressor B remained limited and using Gaussian model could be burdened with significant over- or underestimation.

5.3.2. Landfills

Considering IDF, waste management sector is the biggest CH_4 emitter in the region and contributing to 42% of total regional CH_4 emissions in 2015. Based on the study of Xueref-Remy (2019), according to AIRPARIF inventories for 2010, 10 landfills represent 98% of emissions from waste management sector. In 2010, landfill E was the second biggest CH_4 emitter from waste management sector and reached 5 kt CH_4 y^{-1} (30% of sectoral emission). Landfill D is smaller source of methane than landfill E and reached 1 kt CH_4 y^{-1} (6% of sectoral emission) (Xueref-Remy et al. 2019).

Intense microbial activity occurs on landfills and causes production of acetate, CO_2, H_2 and organic acids. On landfills, methane is produced by acetate fermentation and CO_2 reduction. Methane from CO_2 reduction is more ^{13}C depleted than from acetate fermentation (Whiticar 1999). With time, the productivity of organic matter decreases and methane become mainly produced from CO_2.

Also, bacterial oxidation can take place on landfills and leads to production of ^{13}C enriched methane (Whiticar 1999). Oxidation depends on pH, temperature and moisture and presents seasonal variability. Bacterial oxidation reaches its maximum in summer and can lead to $\delta^{13}CH_4$ about -40‰ (Chanton and Liptay 2000). More depleted $\delta^{13}CH_4$ isotopic signature would suggest that methane is emitted from leaking boreholes than from topsoil where oxidation occurs.

Looking for landfills emissions, gradient of atmospheric pressure highly affects methane emissions from the landfill surface (Xu et al. 2014). When the atmospheric pressure decreases, landfill gas is transported by the air turbulence and CH_4 emissions increase. The opposite process occurs when the increase of ambient air is observed. Then, the ambient air is injected into landfill what impedes CH_4 emissions from the landfill surface to the atmosphere. This phenomenon is known as barometric bumping and it was observed on landfills without active gas collection system. In the case of landfills with active collection system, CH_4 emissions strongly depends on the negative pressure from the gas collecting system. As a consequence, landfill surface emissions are lower and more resistant to changes in atmospheric pressure (Xu et al. 2014).

5.3.2.1 Landfill D

Landfill D is situated about 35 km south-west of Paris, in a rural area with small villages and small industrial sites. The only possible access is on the road on the south side of the landfill (Figure 5.18). Typically, from the road, one CH_4 plume from the active part of the landfill is observed. Depending on the meteorological conditions, it is also possible to observe a second, smaller plume from a close-by already closed landfill. During my Ph.D. study, four surveys were conducted on this site. Three days were dedicated for measurements of isotopic signature and one to estimate the emission rate.

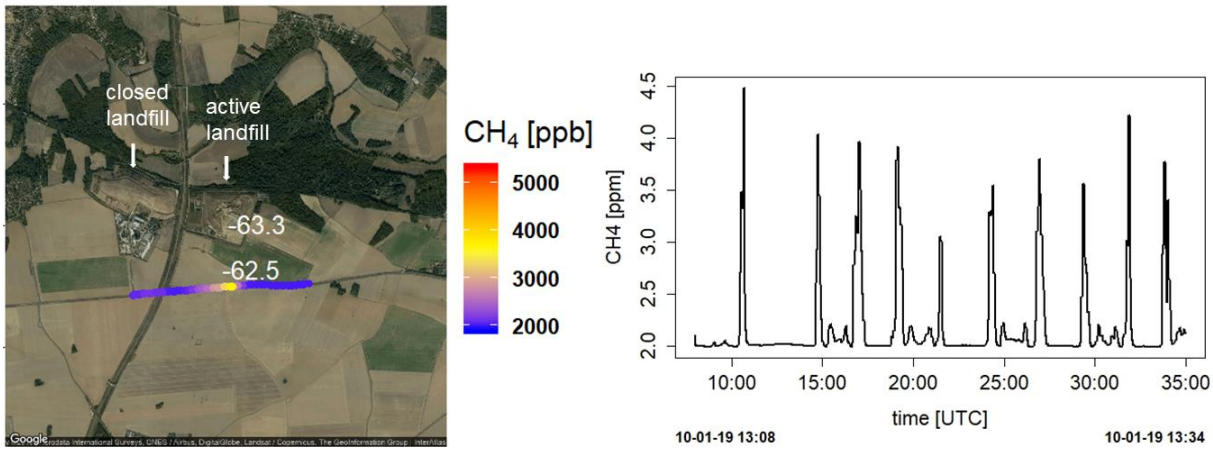

Figure 5.18 Landfill D, 10.01.2019. a) Observed CH_4 mixing ratio above background. The white numbers indicate $\delta^{13}CH_4$ measured inside landfill (27.11.2018) and outside landfill (10.01.2019). b) multiple crossing of the CH_4 plume. Background is not subtracted

On 27.11.2018 and 10.01.2019, the isotopic composition was determined using a CRDS analyzer with an AirCore tool on the mobile platform and taking bag samples. Bag samples were analyzed afterward on IRMS at UU (Table 5.10). During the first day, measurements were made inside the landfill, while during the second day they were made outside the landfill. Using these two methods, obtained isotopic signatures are in good agreement and reached -63.3 ± 1.5 ‰ during the first survey and -62.5 ± 1.1 ‰ during the second survey, using CRDS analyzer. $\delta^{13}CH_4$ from CRDS are in good agreement with $\delta^{13}CH_4$ observed by IRMS instrument. They are also in good agreement with the value obtained in 2015 by Xueref-Remy et al. (2019). $\delta^{13}CH_4$ from my study and study made by Xueref-Remy et al. (2019) are more depleted than the isotopic signature determined in 2016 by Assan (2017), equaled to -60.0 ±1.3 ‰. During study of Assan (2017), the $\delta^{13}CH_4$ was calculated from data obtained during crossing a CH_4 plume eight times, so when the car was in motion. As the car motion increases the fluctuation of measured $^{13}CH_4$, it could affect the measured $\delta^{13}CH_4$.

Finally, the last measurement of $\delta^{13}CH_4$ was made on 16.05.2019. During this survey, only bag samples were taken and isotopic signature was determined from IRMS measurements. The observed value was equal to -64.4 ± 1.0 ‰. It was the only survey conducted in summer instead of winter. The value from summer survey is a bit more depleted than from surveys made during winter. However, they are still in good agreement within uncertainties.

Table 5.10 $\delta^{13}CH_4$ observed for landfill D. CRDS results in this study are determined using the AirCore tool, *** measured during crossing plume. For IRMS measurements, bag samples were taken and sent * to RHUL or ** to UU.

Date	CRDS [‰]	Number of CRDS samples	IRMS [‰]	References
08.12.2015	-		-63.2 ± 0.1*	Xueref-Remy et al. 2019
02.12.2016	-60.0 ± 1.3***	8	-	Assan 2017
27.11.2018	-63.3 ± 1.5	3	-63.0 ± 0.9**	this study
10.01.2019	-62.5 ± 1.1	3	-62.9 ± 0.5**	this study
16.05.2019	-		-64.4 ± 1.0**	this study

To calculate the emission rate of landfill D, the survey was made on 06.10.2017. The tracer dispersion method was used to determine the emission rate. (Figure 5.19). 50 L cylinder with C_2H_2 (purity higher than 99.6%) was installed inside the landfill. The flowmeter (Sho-rate, Brooks) was used to control the flow rate of the target gas with 3% of C_2H_2 flux. Based on 20 transects, the calculated emission rate was equal to -62 ± 13 kg CH_4 h^{-1}. The emission rate is smaller than the ones observed during previous campaigns (Table 5.11). Compare to the first survey, made in 2016, the estimated emission rate has been divided by four. Observed reduction is likely an effect of implemented mitigation actions on landfills like extension of the collection network (made between September and November 2016) and covering closed parts with geomembrane (made between November and December 2016).

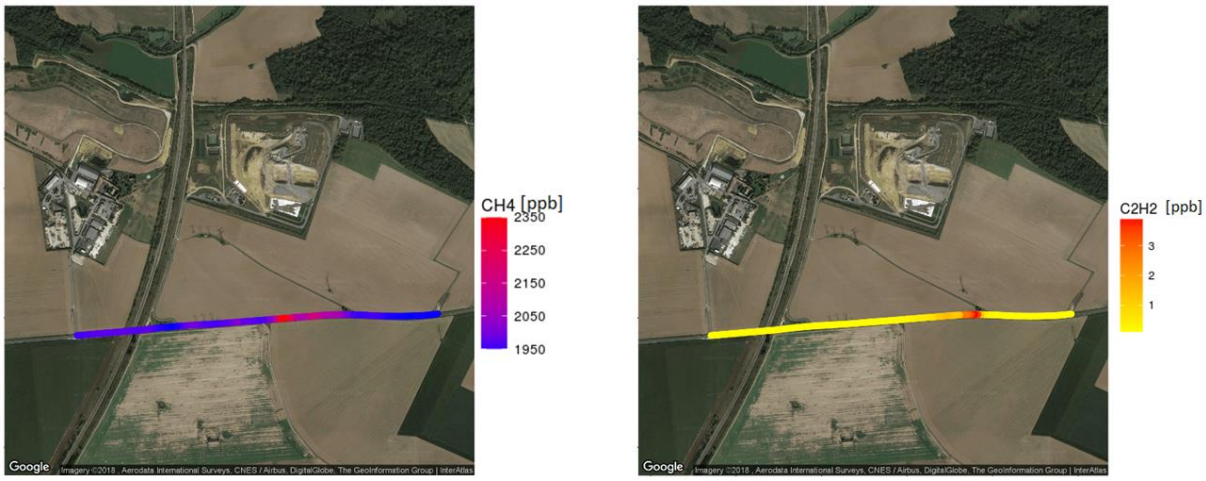

Figure 5.19 Landfill D, 06.10.2017, observed mixing ratio. Example of individual transect. Left: CH_4 mixing ratio. Right: C_2H_2 mixing ratio. Background is not subtracted.

Table 5.11 CH_4 emission calculated on landfill D over time using the tracer release method.

date	CH_4 emission rate [kg CH_4 h^{-1}]	Min CH_4 emission rate [kg CH_4 h^{-1}]	Max CH_4 emission rate [kg CH_4 h^{-1}]	Number of transects	Reference
19.09.2016	242 ± 16	138	326	12	Ars 2017
14.11.2016	152 ± 22	55	204	6	Ars 2017
05.12.2016	84 ± 9	46	105	6	Ars 2017
06.10.2017	62 ± 13	10	58	20	this study

5.3.2.2 Landfill E

Landfill E is situated 20 km north of Paris. This landfill is bigger than landfill D. According to inventories, in 2010, it accounted for 30% of CH_4 emission from the solid waste management sector in IDF region. The CH_4 plumes can be observed from different roads around the landfill, which suggest multiple sources of methane inside the landfill and complex dispersion patterns (Figure 5.20). The landfill is situated in a rural area with small villages. On the west side, woods are situated between road and landfill, and on the north, there is a highway. Thus, measurements can be done from the roads situated on the east and south of landfill E.

Two surveys were made on this landfill: on 25.01.2019 and on 01.03.2019 (Table 5.12). During both surveys, the isotopic composition was determined using CRDS with the AirCore tool. In January 2019, $\delta^{13}CH_4$ was equal to -57.4 ± 4.1 ‰, and in March 2019, it was equal to -58.0 ± 3.2 ‰. Moreover, in March, bag samples were also taken and measured afterward on IRMS at RHUL and UU. The obtained results are not statistically different within 1 standard deviation as from CRDS and reached -58.1 ± 0.3 ‰ at RHUL and -57.5 ± 0.4 ‰ at UU. The isotopic signature is in good agreement with the one determined in December 2015. Then, it equaled to -58.2 ± 0.3 ‰ (Xueref-Remy et al. 2019). The isotopic signature of the landfill E is more enriched than for landfill D. It can be explained by the different waste composition or different proportion of processes responsible for methane production (i.e. acetate fermentation and CO_2 reduction) (Liptay et al. 1998; Zazzeri et al. 2015). Additionally, CH_4 oxidation by methanotrophic bacteria occurs when methane produced in deep layers of landfill travels to topsoil. As ^{12}C is more preferably oxidized, emitted remaining methane is more ^{13}C enriched (Chanton and Liptay 2000).

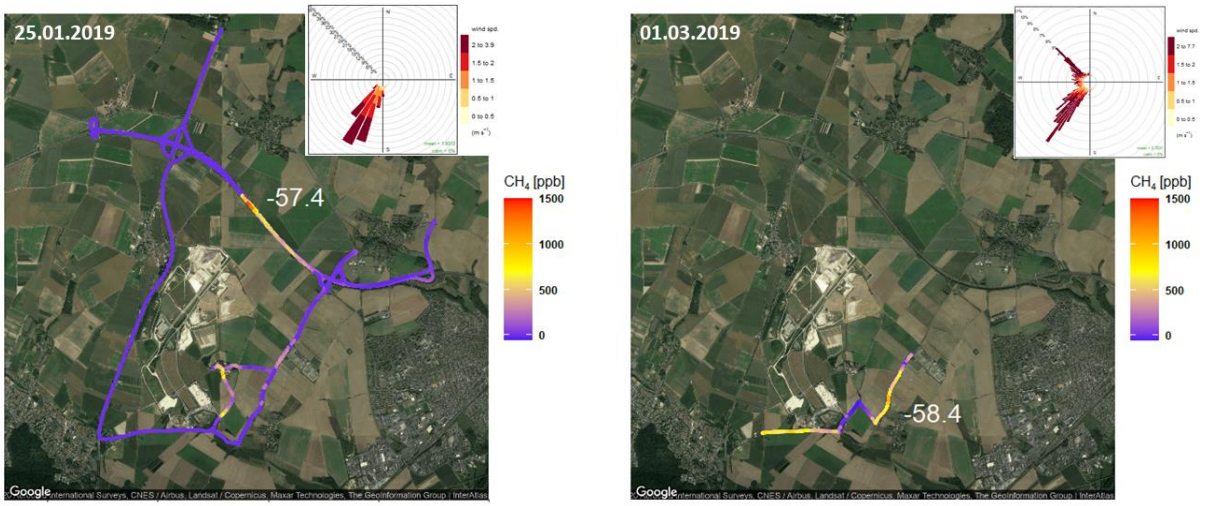

Figure 5.20 Landfill E, observed CH_4 mixing ratio above background. The white numbers indicate $\delta^{13}CH_4$ [‰]. Inert plots - rose wind.

Table 5.12 $\delta^{13}CH_4$ observed for landfill D. CRDS results in this study are determined using the AirCore tool. For IRMS measurements, bag samples were taken and sent * to RHUL or ** to UU.

Date	CRDS [‰]	Number of CRDS samples	IRMS [‰]	References
10.12.2015	-		-58.2 ± 0.3*	Xueref-Remy et al. 2019
25.01.2019	-57.4 ± 4.1	1	-	this study
01.03.2019	-58.0 ± 3.2	2	-58.1 ± 0.3* -57.5± 0.4**	this study

Landfill E is more complicated than landfill D to analyze (i. g., bigger with multiple sources). Moreover, at this moment, information about the possible location of the sources inside the landfill is not available for administrative reasons, and it is impossible to install a release gas so the tracer dispersion method could not be used. Also, a simple Gaussian model could not give reliable values. Size, height, location and amount of CH_4 sources inside landfill E are unknown. Based on study made by Caulton et al. (2018), in the case of single, point emitter, source misallocation causes 20% change of estimated emission rate, comparing to released emission rate. Moreover, wrong source height leads to additional 15% change. As numerous CH_4 plumes were observed around landfill, multiple sources should be simulated in the model or landfill should be treated as an area source rather than point source. Thus, the emission rate was not calculated for landfill E. However, after obtaining information about possible sources inside landfill, a combination of the Gaussian model with the statistical inversion (Ars et al. 2017) could be applied to make a first attempt to calculate the emission rate from the landfill E. This method was not implemented yet but clearly it is a foreseen perspective.

Regarding $\delta^{13}CH_4$ observed on landfill D and E, its value fluctuates around –63‰ for landfill D and around -58‰ for landfill E. Similar to measurements made on gas compressor stations, the results from IRMS and CRDS are in good agreement and observed values do not fluctuate significantly over a measurement time. During my study, the emission rate was estimated only for landfill D. Here, the tracer dispersion method was used and the emission rate was estimated at 62 ± 13 kg CH_4 h^{-1}. As landfill E is more complicated case, with bigger area and multiple CH_4 plumes observed, the simple Gaussian model and tracer dispersion method could not be sufficient to obtained reliable estimation of emission rate.

5.3.3. Other proxies for partitioning CH_4 sources – ethane to methane ratio and δDCH_4

In addition to $\delta^{13}CH_4$, other proxies can be used to distinguish between methane sources. For sites A, B, C, D and E, the ethane to methane ratio and δDCH_4 were determined. C_2H_6:CH_4 ratio can be used to separate thermogenic and biogenic methane sources (e.g., Aydin et al. 2011; Simpson et al. 2012; Schwietzke et al. 2014; Helmig et al. 2016; Hausmann et al. 2016; Sherwood et al. 2017). As the detailed discussion about C_2H_6:CH_4 ratio is presented in an article published in discussion (Defratyka et al. 2020) and described in Chapter 3, here the results are only briefly reminded. The C_2H_6:CH_4 [ppb/ppb] ratio was determined for all three gas compressors and landfill D. It was calculated as the slope of the linear regression of measured C_2H_6 versus measured CH_4 (Table 5.13). The air must be dried before the measurement. Also, the maximum of the CH_4 plume above background must be higher than 1 ppm to use the CRDS G2201-i to determine C_2H_6:CH_4. Observed CH_4 plumes were smaller

than 1 ppm during surveys on gas compressors C. Thus, it was not possible to determine its C_2H_6:CH_4 ratio with sufficient accuracy. Also, on 29.05.2019 the attempt to measure C_2H_6:CH_4 ratio was made on landfill E. That day, the maximum CH_4 enhancement was equal to 350 ppb and it was too small to determine C_2H_6:CH_4 ratio.

Table 5.13. From Defratyka et al. (2020): Ratio measured at different gas compressor stations (A, B) and a landfill (D); Numbers after identification letters refer to different surveys. ΔCH_4 and ΔC_2H_6 are defined as the difference between background value (1st percentile) and the observed value inside the peak

id	max ΔCH_4 [ppm]	max ΔC_2H_6 [ppm]	C_2H_6:CH_4 ratio 1 s	n (data point)	Date
A2	1.737	0.269	0.060 ± 0.005	533	16.05.2019
A3	5.85	0.414	0.045 ± 0.002	495	15.07.2019
B3	1.454	0.260	0.052 ± 0.007	613	12.07.2019
B4	1.677	0.236	0.046 ± 0.008	336	12.07.2019
D1	1.516	0.266	0.000 ± 0.006	712	16.05.2019

Based on my study (Defratyka et al. 2020), it is possible to separate CH_4 sources between biogenic (C_2H_6:CH_4 ratio about 0.0), natural gas leaks and compressors (C_2H_6:CH_4 ratio about 0.06, varies between 0.02 and 0.17) and processed natural gas liquids (C_2H_6:CH_4 ratio about 0.3). C_2H_6:CH_4 ratio observed in IDF is similar to ratios obtained in other places over the world, like Canada (Lopez et al. 2017), the U.S. (Yacovitch et al. 2015) and the U.K. (Lowry et al. 2020). Observed differences in C_2H_6:CH_4 ratio are caused by daily variation of natural gas processed on gas compressor stations A-C. Typically, landfills do not co-emit ethane. Indeed, during measurements on landfill D, detected C_2H_6 mixing ratio was within the instrument noise (50 ppb) and C_2H_6:CH_4 ratio was equal to 0.000 as supposed.

Also, δDCH_4 can be used as an additional proxy to determine CH_4 source during mobile measurements. Currently, it can be done by collecting bag/flask samples and analyzed in the laboratory afterward. Here, for part of measurements sites, when bag samples were measured and sent to UU, δDCH_4 was also calculated (Table 5.14). δDCH_4 is reported in the international standard of Vienna Standard Mean Ocean Water (VSMOW). The bag samples are measured with the precision of 5 ‰ on IRMS (Röckmann et al. 2016). To determine δDCH_4, three bags were collected inside CH_4 plume and one bag outside, as a background sample. The same bag samples were analyzed to determine δDCH_4 and $\delta^{13}CH_4$ and Keeling approach (Pataki et al. 2003) was used for both isotopic signature.

Based on previous study (Sherwood et al. 2017), for fossil fuels, global averaged δDCH_4 reached -197 ‰, with range from -415‰ to -62 ‰. In the case of gas compressor station A-C, δDCH_4 ranged from -185 ± 11‰ to -143 ±17 ‰, which is a bit less depleted than global average for thermogenic sources. In fact, the two extreme values come from gas compressor station C. Moreover, for site C, δDCH_4 uncertainties are typically one order of magnitude larger than for other sites (A, B, D, E). Likely, larger fluctuation and uncertainties are caused by relatively low CH_4 enhancement above background observed on site C. The maximum of CH_4 plume fluctuated around 500 ppb and it is just the minimum required CH_4 enhancement to determine isotopic signature. On the contrary, at gas compressor

station A, CH_4 enhancement reached more than 1000 ppb and only a small difference was observed between δDCH_4 from the two surveys (-175.9 ± 3.7 ‰ versus -183.0 ± 3.6 ‰).

Considering biogenic sources, on a global scale, δDCH_4 varies between -442 ‰ and -281 ‰ with average equals to -317 ‰ (Sherwood et al. 2017). For Landfill D, δDCH_4 was analyzed three times and varied between -316.5 ± 4.1 ‰ and -307.1 ± 1.2 ‰. The most enriched value was observed during first measurements on 27.11.2018. For the two remaining surveys, made 10.01.2019 and 16.05.2019, δDCH_4 did not change significantly. Overall, δDCH_4 of landfill D is similar to global average δDCH_4 for biogenic sources.

Table 5.14 δDCH_4 observed in IDF. Bag samples were taken and sent to UU.

Type	site	date	δDCH_4 [‰]
Gas compressor	A	10.01.2019	-175.9 ± 3.7
	A	16.05.2019	-183.0 ± 3.6
Gas compressor	B	27.05.2019	-157.40 ± 0.66
Gas compressor	C	28.02.2019	-185.3 ± 11.0
	C	28.05.2019	-143.0 ± 17.0
	C	12.03.2020	-176.5 ± 8.3
Landfill	D	27.11.2018	-307.1 ± 1.2
	D	10.01.2019	-314.4 ± 1.7
	D	16.05.2019	-316.5 ± 4.1
Landfill	E	01.03.2019	-214.2 ± 2.7

A different situation was observed for landfill E. Here, δDCH_4 reached -214.2 ± 2.7 ‰, which is out of range from biogenic samples collected so far over the world. There exist two possible reasons (and their combination) of enriched δDCH_4 observed on landfill E. First of all, methanogens can produce methane by acetate fermentation or by CO_2 reduction. During CO_2 reduction δDCH_4 is more enriched than during acetate fermentation (Whiticar 1999). However, $\delta^{13}CH_4$ is more depleted during CO_2 reduction than during acetate fermentation. Emission of methane with more enriched $\delta^{13}CH_4$ and δDCH_4 can be caused by methane oxidation. The process occurs when methane is produced in deep layers of landfill and travels to the topsoil (Chanton and Liptay 2000). Access to information about waste composition and age accumulated on landfill E would empower better data interpretation.

5.4. Synthesis and discussion

Outside of Paris city, measurements were made on three gas compressor stations and two landfills. Previously, on part of these sites, some initial studies were done as well (Ars 2017; Assan 2017; Xueref-Remy et al. 2019). Table 5.15 presents all results from the surveys in IDF region made during my Ph.D., outside of Paris city. $\delta^{13}CH_4$ and δDCH_4 are averaged for individual sites. In most of the cases determined here, $\delta^{13}CH_4$ isotopic composition was in good agreement with previous studies. However, to observe possible seasonal variation, more surveys in different months should be conducted.

Additionally, the discrepancy between CRDS and IRMS values is smaller than CRDS uncertainty. Moreover, it is similar to the difference between two IRMS instruments. Only on gas compressor C, some larger difference was observed. It is caused by the limited CH_4 enhancement observed on this site. As a conclusion it can be assumed that for gas compressors in IDF, $\delta^{13}CH_4$ varies around -44 ‰. For landfills, two different values were observed: about -63 ‰ for landfill D and more enriched -58 ‰ for landfill E.

Compared to previous studies in this region, mobile measurements were extended to measure δDCH_4 and C_2H_6:CH_4. For gas compressors, ethane to methane ratio varies between 0.045 and 0.060, similar to the previously observed ratio in other countries (e.g., Yacovitch et al. 2015; Assan et al. 2017; Lopez et al. 2017; Lowry et al. 2020). Observed difference in C_2H_6:CH_4 ratio are caused by daily variation of natural gas processed on gas compressor stations A-C. In the landfill D, no ethane enhancement was observed.

Table 5.15 Characteristics of three gas compressors (A, B, C) and two landfills (D, E) in the IDF region. $\delta^{13}CH_4$, δDCH_4 and C_2H_6:CH_4 are presented as averaged values from all surveys for individual sites

site	$\delta^{13}CH_4$ [‰] CRDS	$\delta^{13}CH_4$ [‰] IRMS	δDCH_4 [‰]	C_2H_6:CH_4 [ppm/ppm]	emission rate [kg CH_4 h^{-1}]
Gas compressor station A	-43.8 ± 6.8	-45.1 ± 1.1	-179.4 ± 5.2	0.053 ± 0.005	2.45 ± 0.50 (class A) 1.68 ± 0.34 (class B)
Gas compressor station B	-42.1 ± 5.7	-43.9 ± 0.5	-157.40 ± 0.66	0.049 ± 0.009	-
Gas compressor station C	-43.0 ± 8.4	-43.1 ± 3.7	-168 ± 21	-	0.81 ± 0.13 (class A) 0.55 ± 0.09 (class B)
Landfill D	-62.9 ± 1.9	-63.4 ± 1.4	-312.7 ± 4.6	0.000 ± 0.006	62 ± 13
Landfill E	-57.7 ± 5.2	-57.8 ± 0.5	-214.2 ± 2.7	-	-

For δDCH_4, in the case of gas compressor stations A-C, δDCH_4 ranged from -185 ± 11‰ to -143 ±17 ‰, which is a bit less depleted than the global average for fossil fuels (-197 ‰). Similar to $\delta^{13}CH_4$, the biggest uncertainty was observed for site C. δDCH_4 of landfill D is similar to global average δDCH_4 for biogenic sources (-317 ‰). For landfill E, δDCH_4 is more enriched and reached -214.2 ± 2.7 ‰. ^{13}C enrichment can be caused or by CO_2 reduction or methane oxidation.

For two gas compressors and one landfill, the CH_4 emission rate was also calculated. In the case of gas compressors, the emission rate was calculated using the Gaussian model. In both cases, calculations were made based on 30 transects and meteorological data from the 3D sonic station situated close to the site. The emission rate was calculated using stability classes A and B and was about one third bigger using class A than class B, for both gas compressor stations. The emission rate from gas compressor A is almost three times bigger than from the site C.

Limitation of Gaussian model increase uncertainty of estimated emission rate for gas compressor station A and C. First of all, the distance of the transect path from the source is small (less than 100 m), which can cause bias in the calculated emission rate as in small distance from source the role of turbulence increases (e.g., Gifford 1968). Second, the possibly wrong choice of stability class could underestimate the emission rate. Calculation of the Gaussian plume standard deviations, σ_y and σ_z directly from U, V, W wind directions instead of using stability classes would decrease misestimating.

Also, the tracer release method was used to determine the emission rate from the landfill D on 06.10.2017. This emission rate (62 ±13 kg CH_4 h^{-1}) is lower than calculated during previous studies on this site. Compare to first survey, made one year before, the emission rate decreased four times. Observed reduction is likely an effect of implemented mitigation actions on the landfill like the extension of the collection network between September and November 2016 and the covering of the closed part by geomembrane between November and December.

Based on mobile measurement, CH_4 emission rate is estimated for short-term (i.e. few hours). For gas compressor stations, estimated emission rate varies depending on maintenance work inside facilities (e.g., USEPA 2012; Zavala-Araiza et al. 2015; Saunois et al. 2020). Based on study made by Subramanian et al. (2015), in operating mode gas facilities emit more methane than during standby mode. About 50% of methane emitted from 45 gas compressor stations in the U.S. come from compressor venting. Also, more CH_4 reaches atmosphere during abnormal conditions (e.g., malfunctioning equipment and irregular events like uncontrolled flashing and venting), which can change over a year (Subramanian et al. 2015; Zavala-Araiza et al. 2015; Alvarez et al. 2018).

On landfills, temporal variation of CH_4 emissions can be caused by variable methane oxidation, which strongly depends on moisture and temperature (Liptay et al. 1998; Chanton and Liptay 2000). Previous study (Chanton and Liptay 2000) showed correlation between lower CH_4 emissions in summer and larger methane oxidations on landfill surface. Thus, during summer methane oxidation consumed about 40% of CH_4 from landfill. During winter, when CH_4 emissions are higher, methane oxidation consumed from 3% to 5% of CH_4 emitted in landfill. Moreover, CH_4 emission rate can also depend on gradient of atmospheric pressure and more methane is emitted during decrease of ambient pressure (Xu et al. 2014). This dependence is smaller for landfills with active gas collecting system, as lower CH_4 emissions are observed from landfill surface.

Regarding temporal variation, the emission rate calculated during one mobile measurement cannot be extrapolated to annual emission by simply multiplying the calculated rate by time, both for landfills and gas facilities. More regular surveys should be done to estimate the emission rate of sites over a year.

Chapter 6 Conclusions and Outlooks

6.1. Conclusions

The present Ph.D. study aimed at characterizing specific anthropogenic methane sources at the city and industrial site scales in the Île-de-France (IDF) region using direct and mobile measurements methods. Emissions from the waste management and energy sectors are key methane sources at the regional scale in IDF. CH_4 mixing ratio and isotopic signature were observed using a mobile measurement platform, with a Cavity Ring-Down Spectroscopy (CRDS) analyzer embedded in a car. Additionally, the AirCore tool was part of the mobile set-up, allowing to remeasure the stored air for chosen situations, and making possible in-situ measurements of $\delta^{13}CH_4$. The CRDS G2201-i instrument was the base of the mobile set-up, and it was thoroughly tested, both in laboratory and in field conditions.

Instrument set-up and tests The tests I performed showed the applicability of the CRDS G2201-i instrument to realize mobile measurements close to sources. The continuous measurement repeatability (CMR) (also known as "precision") and Allan deviations at 10 s, 60 s and 60 min are under 1 ppb. It is much smaller than the excess CH_4 mixing ratio inside a CH_4 plume in the vicinity of most point sources. Also, the instrument's stability was estimated during short- and long-term repeatability tests at less than 1 ppb. This good stability was further tested during measurements of a tank with known mixing ratios before and after surveys. For $\delta^{13}CH_4$, the CMR of CRDS G2201-i is about 3.5 ‰ for the ambient CH_4 mixing ratio. It improves to 0.7 ‰ with the increase of CH_4 mixing ratio to about 10 ppm. Therefore, using CRDS with AirCore tool, it has the ability to disentangle typical signatures of biogenic versus thermogenic methane origins with a precision of 5 ‰ on the $\delta^{13}CH_4$ for CH_4 enhancements about 500 ppb above background. The precision of $\delta^{13}CH_4$ source increases to 1 ‰ for plumes of 8 ppm CH_4 enhancement above background.

In the field, CRDS G2201-i with AirCore tool was used to determine isotopic signatures. Collected data were grouped in 50 ppb bins and analyzed using the Miller-Tans approach (Miller and Tans 2003). Then samples, where r^2 correlation coefficient were smaller than 0.85 and the uncertainty was bigger than 10 ‰ were rejected from further analysis, in order to balance precise results and quantity of kept values. These criteria were applied for the sources in Paris city and at industrial sites (landfills and gas compressor stations). However, during surveys on industrial sites, observed CH_4 enhancement above background was usually higher than for surveys inside the city. As a consequence, $\delta^{13}CH_4$ precision was better, and for most of samples selected for further analysis did not reached more than 6 ‰.

I also assessed the opportunity to use CRDS G2201-i in the field to determine the C_2H_6:CH_4 ratio. This work was made in three steps. During laboratory tests, for ethane, the CMR was equal to 50 ppb, and Allan deviation was equal to 25 ppb for raw data. Typical background values of C_2H_6 vary between 0.6 ppb and 3 ppb, hence the signal to noise ratio would be insufficient to characterize ambient air variability. However, the controlled release experiment and field work showed a good agreement between observed and released ethane to methane ratio. Based on these tests, the CRDS G2201-i can determine the C_2H_6:CH_4 ratio with sufficient precision (smaller than 0.01) if the car is stopped during measurements. It can be done either by standing some period inside the CH_4 plume or by AirCore sampling. The air should be dried before measurements, and CH_4 enhancement above background should be higher than 1 ppm. The observed C_2H_6 mixing ratio must be corrected for the interference

from other species and calibrated as the instrument is not dedicated to C_2H_6 measurements. In fine, CRDS G2201-i can be used for C_2H_6:CH_4 under these specific conditions.

Paris emissions Using this mobile set-up, between September 2018 and March 2019, 17 surveys were made in Paris, and 500 km of road length were visited. Additionally, 28 AirCores from 17 locations were taken during these measurement sessions. Based on the above criteria, 12 AirCore samples from 11 locations were used to characterize CH_4 origin in Paris. $\delta^{13}CH_4$ in seven locations was more depleted (< -50 ‰) and ascribed to biogenic emissions, while in four locations, $\delta^{13}CH_4$ was more enriched (> -50 ‰) and attributed to thermogenic sources. Additionally, walking measurements with Los Gatos Research (LGR) analyzer model MGGA were made during four days in Paris. They allowed measuring CH_4 plumes from covers of sewage and natural gas network. Additionally, CH_4 emissions were observed from buildings' venting grids of boiler room. In this case, emissions probably come from leaking furnaces systems. In total, 90 leak indications were observed in Paris. Twenty-seven of them were attributed to three sources: gas leaks, sewage and furnaces, based on the isotopic signature and walking measurements. The furnaces category was not previously reported in studies focused on the city's CH_4 emissions (e.g., Townsend-Small et al. 2012; Jackson et al. 2014; McKain et al. 2015; von Fischer et al. 2017; Zazzeri et al. 2017) and this category was discovered during walking measurements. In the case of leak indications visible from the road, gas leaks constitute 66% of them and sewage - 34%. This proportion is simply extended for the remaining 63 leak indications with unknown origin. Overall, based on this assumption, 56 leak indications are determined as gas leaks, 30 as sewage and 4 as furnaces.

In Paris, two emission clusters were found with a bigger amount of detected leak indications. 22% of leak indications are from cluster area A, and 56% from cluster area B. These areas represent only 10% (area A) and 20% (area B) of the unique km of the surveyed area.

Based on the equation proposed by von Fischer et al. (2017) and Weller et al. (2019), the emission rate of determined leak indications is calculated and reached 140 L CH_4 min^{-1} over 90 leaks indications from 500 driven kilometers. This emission rate was simply extended to whole road length (1800 km) of Paris city and was found equal to 500 L CH_4 min^{-1} (190 t CH_4 yr^{-1}). Based on our attribution assumption, 56% of emission observed in Paris are ascribed to leaks in the natural gas distribution network (106 t CH_4 yr^{-1}), which is fifteen times less than in the AIRPARIF inventory. The gas leak indication rate (number of gas leak indication/ km of driven streets) was found equal to 0.11 km^{-1}.

Overall, results for the leak rate in Paris are two to four times smaller than the rates calculated for the cities with old pipeline system in the U.S. and two to forty times higher than cities with modern pipeline system in the U.S. (von Fischer et al. 2017). Regarding previous studies (McKain et al. 2015; Jackson et al. 2014; Lamb et al. 2016; von Fischer et al. 2017), number of gas leaks in U.S. cities, with older corrosion-prone pipeline network (Boston, New York, Staten Island and Syracuse), is higher than for cities with a higher proportion of plastic or protected steel low-pressure distribution systems (Burlington and Indianapolis). In the case of the study made by von Fischer et al. (2017), leak rates vary from 0.004 leaks km^{-1} (Indianapolis) to 0.63 leaks km^{-1} (Staten Island).

Based on our findings, efficiently limiting CH_4 emissions in the Paris area could be obtained by reducing the sewage-related sources and by treating the few hotspots detected. Currently, CH_4 emissions from sewage sector are omitted in the AIRPARIF inventory. Moreover, furnaces emissions were not observed in previous studies in cities (e.g., Townsend-Small et al. 2012; Lamb et al. 2016; von Fischer et al. 2017; Zazzeri et al. 2017). Thus, this category should be further investigated. In the

case of natural gas distribution network, 40 km of pipelines are renovated every year, which decreases CH_4 emissions from natural gas distribution network (GRDF on Twitter 2019; La Tribune 2019).

Measurements in Paris city were repeated during summer 2019. Over five days, 200 km of streets were driven. Thirty-six leak indications were observed. 9 AirCore samples were taken, and 6 of them were used for further analysis. Three of them were determined as coming from sewage and two as gas leaks. The last one was more enriched and observed once and thus was attributed to traffic. Contrary to the previous campaigns, no CH_4 plumes were observed in cluster A. Over 36 leak indications, the emission rate is equal to 41 L CH_4 min^{-1}. Then, after extrapolating to all streets in Paris, the total emission rate is equal to 370 L CH_4 min^{-1} (140 t CH_4 yr^{-1}). Although having the same order of magnitude, it is about 50 t CH_4 less than emission rate observed during the first campaign. It can be caused by the emissions from furnaces that do not occur during summer or by the natural gas network's renovations. Observed discrepancy can by also caused by sampling biases as during summer only 5 surveys were made and some CH_4 sources could have been omitted.

Industrial sites Measurements were also made outside of Paris on three gas compressor stations and two landfills. Based on mobile measurements, $\delta^{13}CH_4$ and δDCH_4 isotopic signatures, CH_4 emission rates and ethane to methane ratios were observed. The $\delta^{13}CH_4$ measured on the three gas compressor stations were similar and varied around -43 ‰, (from -45.2 ± 6.2 ‰ to -40.1 ± 3.9 ‰). δDCH_4 varied from -179.4 ± 5.2 ‰ to -157.40 ± 0.66‰, which is a bit less depleted than the global average for fossil fuels (-197 ‰) (Sherwood et al. 2017). Observed $\delta^{13}CH_4$ and δDCH_4 indicate a thermogenic origin of natural gas used in IDF region, which was confirmed with the natural gas operator company. Both for $\delta^{13}CH_4$ and δDCH_4, the biggest uncertainty was observed for gas compressor station C. Likely, it is caused by the limited CH_4 enhancement observed on this site. The sampling done for isotopic analysis revealed that the maximum of CH_4 plume varied about 500 ppb above background, what is just the minimum required CH_4 enhancement to robustly determine isotopic signature for CRDS with AirCore tool (Hoheisel et al. 2019).

Different isotopic signatures were observed in two different landfills. For the landfill D, the smaller one, the $\delta^{13}CH_4$ varies around -62.9 ± 1.9 ‰, while for the landfill E, it is about -57.7 ± 5.2 ‰. For both landfills, $\delta^{13}CH_4$ is in good agreement with isotopic signatures observed previously in these landfills by Xueref-Remy et al. (2019). The δDCH_4 differs more, and it reaches -312.7 ± 4.6 ‰ for the first landfill and -214.2 ± 2.7 ‰ for the second. The δDCH_4 observed on landfill E is more enriched than global average (-317 ‰) (Sherwood et al. 2017). Observed differences between isotopic signature of landfills D and E can be caused by different age and composition of stored waste, as both can affect methane production. More depleted methane is created during acetate fermentation while more enriched methane can be caused by methane oxidation. Thus, more enriched isotopic signatures suggest that CH_4 emissions on landfill E come from topsoil covers, while more depleted signatures of landfill D indicate emissions from leaking boreholes (Whiticar 1999; Chanton and Liptay 2000).

Good agreement was observed between the values obtained using in-situ CRDS with AirCore tool and bag samples measured on IRMS. This agreement increases with higher observed CH_4 plume enhancement, again stressing the importance to have a good signal to noise ratio. It also shows that AirCore methods can be successfully used to determine $\delta^{13}CH_4$, but smaller precision is reached with CRDS than IRMS instrument. Overall, CRDS with AirCore tool gives reliable $\delta^{13}CH_4$ isotopic signatures. It can be useful, especially when it is impossible to stop the car to collect bag samples, for example, in places with large traffic or when unstable wind direction impedes stopping inside CH_4 plume.

Here, ethane to methane ratio was also determined for three gas compressor stations and one landfill. For gas compressor stations, C_2H_6:CH_4 ratio varied between 0.045 ± 0.008 and 0.060 ± 0.005. Observed differences in C_2H_6:CH_4 ratio are caused by daily variation of natural gas processed on gas compressor stations. Also, observed differences can be caused by the used instrument, as CRDS G2201-i is not dedicated to ethane measurements and precision reached 0.01. Regarding landfill CH_4 emissions, landfills do not co-emit ethane. Indeed, during measurements on landfill D, detected C_2H_6 mixing ratio was within the instrument noise (50 ppb) and C_2H_6:CH_4 ratio was equal to 0.000.

Finally, the emission rates were estimated for one day of measure in two gas compressor stations and one landfill. In the case of gas compressor stations, the Gaussian model in the Polyphemus platform was used. For the two stations, the emission rates were calculated using stability classes A and B. The emission rate from gas compressor station A is about three times bigger than from gas compressor station C. Using stability class A, estimated emission rate reached 2.5 ± 0.5 kg CH_4 h^{-1} for site A and 0.8 ± 0.1 kg CH_4 h^{-1} for site C. Using stability class B, estimated emission rates reached 1.7 ± 0.3 kg CH_4 h^{-1} and 0.55 ± 0.09 kg CH_4 h^{-1}, for sites A and C, respectively. Both gas compressor stations have two compressors and use the same technology. Site C operates more hours than site A and possibly it is better monitored by owner company and hence, less fugitive emissions occur on site C than site A. Also, different internal works could have been conducted on both sites during surveys, which could affect the estimated CH_4 emission rates.

Emission estimations could also be affected by the modelling choice. Distance from source was smaller than 100 m. As the role of turbulence increases inversely to distance, estimated emission rate could be more biased (Gifford 1968). Also, the possibly wrong choice of stability class could lead to underestimate emission rates (Caulton et al. 2018). Finally, Gaussian modelling does not include topography, which is another source of bias.

The emission rate was estimated in landfill D as well. In this case, the tracer release method could be used leading to an estimation of 62 ± 13 kg CH_4 h^{-1}. Compared to previous results (Ars 2017), the emission rate is smaller. It seems to be in agreement with the operating company's policy, which tries to reduce CH_4 emissions from the landfill. Compared to the first survey, made in 2016, the estimated emission rate has been divided by four. Observed reduction is likely an effect of implemented mitigation actions on landfills like extension of the collection network (made between September and November 2016) and covering closed parts with geomembranes (made between November and December 2016). More campaigns are necessary to confirm this statement.

Based on mobile measurement, CH_4 emission rate is estimated for short-term (i. g. few hours) durations. For gas compressor stations, estimated emission rate varies depending on maintenance work inside facilities (e.g., USEPA 2012; Zavala-Araiza et al. 2015; Saunois et al. 2020). Based on the study made by Subramanian et al. (2015) gas facilities emit methane both during standby and operating modes. Additionally, more CH_4 reaches the atmosphere during abnormal conditions (e.g., malfunctioning equipment and irregular events like uncontrolled flashing and venting), which can change over a year and usually is not included in inventories (Subramanian et al. 2015; Zavala-Araiza et al. 2015; Alvarez et al. 2018). Looking for landfills emissions, gradient of atmospheric pressure highly affects methane emissions. When atmospheric pressure decreases, landfill gas is transported by the air turbulence and CH_4 emissions increase (Xu et al. 2014). Also maintaining work affects CH_4 emissions from landfills (Ars 2017). Thus, the emission rate calculated during one mobile measurement cannot be easily extrapolated to annual emission by simply multiplying the calculated rate by time, both for

gas facilities and landfills. More regular surveys should be done to estimate the emission rate of sites over a year.

Overall, instrument tests allowed determining possibilities and limitations to using CRDS G2201-i in the field measurements, especially in the context of C_2H_6:CH_4 ratio. Here, relatively low CH_4 enhancement above background was the biggest limitation to properly apply the methodology and determine isotopic signatures and ethane to methane ratios. Using CRDS G2201-i, we determined that CH_4 enhancement should be at least 500 ppb above background for isotopic signature and 1000 ppb for ethane to methane ratio. Larger observed enhancement decrease uncertainty both of $\delta^{13}CH_4$ and C_2H_6:CH_4 ratios. The CH_4 enhancement detected here is high enough to estimate emission rate using a Gaussian model or the tracer dispersion method. However, access to observed sites were limited and tracer dispersion method could be used only once. The infrastructure and unfavorable wind direction were other limitation. Frequently, wind speed was too small (less than 1 m s^{-1}) and CH_4 plumes were not observed. Finally, more surveys were planned on gas compressor stations during Summer 2019. However, at that time, a heat wave occurred and planned surveys had to be cancelled as car and instrument are not adapted to high temperature, around 40 °C. Thus, limited number of conducted measurements on industrial sites prevents upscaling of estimated emissions rate to yearly emissions and comparison with regional inventories.

Despite the limitations of methods deployed on the field, this Ph.D. brings additional observations and analyses to the current knowledge about CH_4 on city and industrial site scales. The field work extended the knowledge about city-level emissions and localized possible CH_4 sources inside the city. Additionally, studies conducted on gas compressor stations initiated collaboration with GRTgaz company, which is a French national gas transmission operator. Information provided by the operator company were used in the article about the possibility of use CRDS G2201-i to measure C_2H_6:CH_4 ratio (Defratyka et al. 2020). Some collaborative measurements were also made and are described in a (confidential) Master thesis (Lozano 2020). Also, this Ph.D. extended the isotopic methane database, including measurements of δDCH_4, which are still rarely observed. Some future actions can be considered following my Ph.D. study and improve the methods and analyses presented here.

6.2. Outlooks

This Ph.D. work leads to perspectives of future developments and observations to improve our knowledge of atmospheric methane in the city environment and for industrial sites.

Increasing city scale observation in time When the expected variability of methane emissions is significant, it appeared that the punctual campaigns in time made in this PhD were not sufficient to derive annual estimates of emission rates. In this case, more campaigns are necessary. At the city scale, more surveys could be made, both during winter and summer seasons to get more robust Paris emission estimations and better characterize their possible seasonal variations. Repeating measurements in different seasons would allow verifying if differences in my Ph.D. campaigns come from renovation and decreased leak in natural gas distribution network or sewage network or if it is caused by seasonal variation resulted, for example by furnaces utilization or meteorological conditions. Between September 2018 and March 2019, Paris cluster A was determined as an area with a bigger number of leak indications (13 leak indications over 50 km of streets). During measurements made in summer 2019, no leak indications were observed in this area. Thus, measurements should be

repeated in this area to verify if observed primary leak indications came from furnaces emissions and are observed only during winter seasons. The emission could also come from punctual gas leaks, which were limited during possible pipeline renovations. In Paris, 40 km of pipelines out of 2000 km are repaired every year, while the exact location of repair work is unknown.

Increasing city scale observations in space Also, spatial extrapolations can be an issue. In Paris city, I could only monitor 500 km of 1 800 km total road length. Different districts were chosen to represent CH_4 emissions from different city infrastructures. Both, major roads and part of the smaller roads were covered, while some streets were driven multiple times. The streets with bigger leak indications (> 500 ppb above threshold) and smaller traffic jams had a priority for revisit. As some streets were omitted, possible larger leak indications could be omitted and estimated emission rate is underestimated. Based on U.S. studies (von Fischer et al. 2017), the small gas leak indications contribute to 83%-100% of total detected gas leak indications. However, gas leak indications categorized as medium (0-17%) and large (0-2%) are responsible for the majority of the emissions, and repairs of 8% of the largest leak indications could reduce about 30% of city CH_4 emissions. Also, observed CH_4 leak indications have stochastic nature, so driving through street minimum twice increases possibility of observing leak indication, especially for small CH_4 enhancements (von Fischer et al. 2017). As a consequence, ideally, every street in Paris should be driven twice with repetition during different seasons. Seasonal repetition allows determining seasonal variations of Paris CH_4 emissions and after upscaling to annual CH_4 emissions it would be a better representation of actual emissions.

Adding proxies to the mobile setup for source apportionment Between September 2018 and March 2019, 27 out of 90 leak indications were attributed to source categories based on isotopic signature or walking measurements in Paris. In the future, this source attribution could be improved by embedding additional instruments as a part of a mobile set-up. Continuous measurement of C_2H_6:CH_4 ratio during mobile measurements would help separate the biogenic and thermogenic origin of CH_4 enhancements, as ethane is co-emitted from thermogenic sources (Turner et al. 2019; Schwietzke et al. 2014; Sherwood et al. 2017). In Paris $\delta^{13}CH_4$ was used to distinguish thermogenic and biogenic CH_4 sources. However, due to method limitation (CRDS with AirCore tool), only for CH_4 plumes higher than 500 ppb, $\delta^{13}CH_4$ could be determined. Therefore, co-measurements of C_2H_6:CH_4 ratio would enable separating of smaller CH_4 plumes.

Moreover, CO is co-emitted from combustion sources (Saunois et al. 2016; Turner et al. 2019). Thus, measuring CO would help to extend knowledge about emissions observed from venting grids, which are ascribed to leaking furnaces installations. These venting grids are situated on the height about ~20 cm above ground and can be visible during ground surveys. However, potentially, main venting systems of buildings can be additional CH_4 source in city. Their exhausts (e.g., stacks and chimneys) are situated on roofs of buildings so it is not possible to observe their emissions from ground measurements. Additional surveys with drones or aircraft could be done to determine total city emissions. However, these methods are more expensive and require more advanced techniques and trained operators. Moreover, due to the safety reason flying above city can be limited or even forbidden.

Finally, the contribution of the traffic to the CH_4 emission from Paris city should be determined. In this case CH_4 is emitted from car exhaust. As the emission is connected with combustion, also CO is co-emitted with methane. According to AIRPARIF inventory only 3% of emissions comes from traffic.

However, increasing buses powered by natural gas and biogas is planned, which potentially can cause additional CH_4 emissions from this sector.

Refining and enhancing emissions estimates at site scale At industrial sites, emission rates were calculated for two gas compressor stations and one landfill. In the future, other sources should also be taken into account and more surveys should be conducted on already surveyed sites, especially to refine emission calculations. First, possible drivers of CH_4 emissions inside the sites should be determined and quantified. Also, their variations depending on external (e.g. meteorological conditions) and internal (e.g. maintaining work) conditions should be verified. Then, more often, systematically repeated measurements could broaden the knowledge about the emission from the individual sites in IDF region and be compared with values reported in inventories. Also, repetitive measurements would give information about possible seasonal variation, both in terms of the emission rate and isotopic signature and therefore provide a more realistic picture of these site emission rates. As 42% of regional CH_4 emissions come from the solid waste management sector, more surveys should be focused on this source. Multiple surveys in different landfills could improve our knowledge about the major source of methane in the IDF. Here, only two landfills were surveyed and studies should be expanded to other landfills in region.

Extending the study to wastewater sector Surveys could also be extended to wastewater treatment plants (WWTP), as this source is not reported officially in the regional inventories (AIRPARIF 2018). Based on personal communication with AIRPARIF, for 2010, CH_4 emissions for this WWTP was equal to 66 t CH_4 y^{-1} (7.5 kg CH_4 h^{-1}), contributing to 0.2% of total regional CH_4 emission (Xueref-Remy et al. 2019). It raises some doubts about the underestimation of WWTP emissions in inventories, as the biggest WWT plant in Europe is localized in IDF region, in Achères. A first attempt to observe CH_4 emissions from two WWTPs in the region was made (Ars 2017). The tracer release method, combined with statistical inversion (Ars 2017), was used during two campaigns made in WWTP in Achères, one in November 2014 and second in April 2015. Based on that study, the estimated emission rate was equal to 123 ± 2 kg CH_4 h^{-1} for the part of the site treating the wastewater sludge. The emission rate obtained during these campaigns is about sixteen times higher than the values from inventories for the year 2010. Thus, mobile measurements clearly showed that the CH_4 emissions from WWTP should be included in the regional inventories and more measurements on different WWTPs in IDF region should be done to recognize and estimate their contribution to regional CH_4 emissions.

Enhancing collaboration with industrials Measurements could be more effective if they are conducted in collaboration with industrial companies running the facilities. Thanks to such active collaboration, the effect on estimated CH_4 emissions of different maintenance works or of changing the industrial processes could be better documented. For instance, the impact of landfill characteristics (e.g. age, type of waste, size) on CH_4 emissions could be verified. Moreover, thanks to cooperation with operator companies, emissions estimated from atmospheric measurements could be compared with currently used emission factors (comparison of top-down and bottom-up studies). For example, in IDF region, the TRACE programme (TRAcking Carbon Emissions) aims to estimating CH_4 emissions in collaboration with SUEZ company, which is a global operator in the waste sector. This collaborative effort targets identifying, characterizing and verifying CH_4 emissions, what can help the site operator to control CH_4 emissions. This Ph.D. within CACC Methane Studies, initiated cooperation with GRTgaz company. Further, joined campaigns are planned. Again, the collaborative actions will aim comparing bottom up and top down emission estimations. Systematical measurements on different gas compressor stations would extend knowledge about daily variation in CH_4 emissions and

in final step would aim to compare atmospheric measurements with inventories. Moreover, it gives opportunity to compare results from energy sector in IDF with the numerous studies conducted in U.S (e.g. Zavala-Araiza et al. 2015; Subramanian et al. 2015; Yacovitch et al. 2015). Moreover, as CH_4 enhancement was previously observed on gas storages (Xueref-Remy et al. 2019), these gas facilities could be included in future surveys.

Refining the modelling tool Based on near-source mobile measurements, more advanced methods could be used to calculate the emission rate. Here, I used the Gaussian model in the Polyphemus platform, which uses stability classes to determine standard deviations in the horizontal and vertical directions. Potentially, one stability class discrepancy can cause bias about 40% of released CH_4 emission rate (Caulton et al. 2018). Using U, V and W wind direction to calculate these standard deviations should decrease the bias. Additionally, as it is a simple Gaussian model, it cannot be used to more complex cases, with multiple sources as in gas compressor station B or landfill E. Moreover, Gaussian models do not include topography, which also lead to biased estimations, especially when the CH_4 source is on the ground level. It could be improved by coupling the tracer release technique and local scale modeling with statistical atmospheric inversion, as done in Ars et al. (2017). Using different, more adapted models should also improve computation and allow calculations for different, more complex cases than gas compressors. Again, with the collaboration of the site owners, knowing the possible location of the source's position inside the site and access them to install the tracer gas in the same position as the CH_4 sources would improve emission rates' calculation with any modelling tool.

Deploying more measurement approaches To characterize CH_4 emissions in IDF region, other measurement techniques could be applied. Regarding mobile, near sources measurements, drone and aircraft could be used (Chen et al. 2010; Klausner et al. 2020; Shah et al. 2020). Additionally, satellites allow measuring for larger, regional scale thus giving the possibility for direct comparison of regional measurements and inventories. Potentially, small satellites, like Bluefield and GHGSat, could also verify effectiveness of implemented mitigation actions by quantifying CH_4 emissions from local intense point sources like industrial sites or from more spread CH_4 emissions like in cities, the latter not being yet demonstrated.

Significant costs of CH_4 instrumentation limits the possibility of broad measurements of CH_4 mixing ratios and estimations of emission rates. Also, some instrumentals require trained operator and cannot be conducted without frequent maintenance works (e.g., calibration, time drift correction). Currently, intensive works are underway worldwide to develop low-cost CH_4 sensors (e.g., van den Bossche et al. 2017; Riddick et al. 2020, TRACE programme). These low-cost and low-power methane sensors are tested for use in measurement networks. Their accuracy is lower than the accuracy of advanced, more expensive instrument, however it can be improved by frequent calibration. A network of low- cost CH_4 sensors can be used on industrial sites to monitor CH_4 mixing ratio, estimate emissions and then verify efficiency of mitigation actions. It can also be deployed in cities, compensating the quality of individual measurement by their quantity.

List of abbreviations

ADEME - Agence de l'environemnt et de la maîtrise de l'energie
AGAGE - Advanced Global Atmospheric Gases Experiment
AIRPARIF - Air quality monitoring network in Île-de-France region
C_2H_2 - Acetylene
C_2H_6 - Ethane
CCAC - Climate and Clean Air Coalition
CCMI – Chemistry Climate Model Initiative
CH_4 - Methane
CITEPA - Centre Interprofessionel Technique d'Etudes de la Pollution Atmospherique
CSIRO - Commonwealth Scientific and Industrial Research Organization
CO - Carbon Monoxide
CO_2 - Carbon Dioxide
CMR - Continuous Measurement Repeatability
CRDS - Cavity Ring-Downs Spectroscopy
EDGAR - Emission Database for Global Atmospheric Research
EMPA - Swiss Federal Laboratories for Material Science and Technology
G_{ATM} - Annual Growth Rate [ppb y^{-1}]
GIE - Gas Infrastructure Europe
GWP - Global Warming Potential
IDF - Île-de-France
IPCC - Intergovernmental Panel on Climate Change
IRMS - Isotope ratio mass spectrometry
NOAA - National Oceanic Atmospheric Administration
$MEMO^2$ - MEthane goes Mobile- MEasuremnts and MOdeling
MFC - Mass Flow Controller
$MG(ClO_4)_2$ - Magnesium Perchlorate
N_2O - Nitrous Oxide
NPL- National Physical Laboratory
OLS - Ordinary Least Squares
RCP - Representative Concentration Pathway
RHUL - Royal Holloway University of London
SCCM - Standard Cubic Centimeters Per Minute
SF_6 - Sulfur Hexafluoride
TRACE programme - TRAcking Carbon Emissions programme
U.C.I - University of California, Irvine
UU - Utrecht University
VOC - Volatile Organic Compounds
VSMOW - Vienna Standard Mean Ocean Water
WWTP - Wastewater Treatment Plant
$\delta^{13}CH_4$ - methane isotopic signature $\delta(^{13}C, CH_4)$ in VPDB scale
δDCH_4 - methane isotopic signature $\delta(D, CH_4)$ in VSMOW scale
^{14}C - Radiocarbon

References

1) “CCAC.” 2020. 2020. https://www.ccacoalition.org/en.

2) “CITEPA, April 2019, Format SECTEN.” n.d. Accessed June 5, 2019. http://www.citepa.org/fr/activites/inventaires-des-emissions/secten.

3) AIRPARIF. 2013. “Emission Bilans of Pollutants Ang Greenhouse Gases in Ile-de-France Region in 2010 and History 2000/2005.”

4) AIRPARIF. 2018. “Ile-de-France Inventoires for a Year 2015.”

5) AIRPARIF. Analyss of Inventory and Emissions’ Cadastres of Principal Greenhouse Gasses in Ile-de-France Region; 2005.

6) AIRPARIF. Emission Bilans of Pollutants Ang Greenhouse Gases in Ile-de-France Region in 2010 and History 2000/2005; 2013; p 109.

7) AIRPARIF. Ile-de-France Inventoires for a Year 2015. 2018.

8) Allan, D.W. 1966. “Statistics of Atomic Frequency Standards.” Proceedings of the IEEE 54 (2): 221–30. https://doi.org/10.1109/PROC.1966.4634.

9) Allen, David T., Vincent M. Torres, James Thomas, David W. Sullivan, Matthew Harrison, Al Hendler, Scott C. Herndon, et al. 2013. “Measurements of Methane Emissions at Natural Gas Production Sites in the United States.” Proceedings of the National Academy of Sciences 110 (44): 17768–73. https://doi.org/10.1073/pnas.1304880110.

10) Alvarez, Ramón A., Daniel Zavala-Araiza, David R. Lyon, David T. Allen, Zachary R. Barkley, Adam R. Brandt, Kenneth J. Davis, et al. 2018. “Assessment of Methane Emissions from the U.S. Oil and Gas Supply Chain.” Science, June, eaar7204. https://doi.org/10.1126/science.aar7204.

11) Ars, Sébastien, Grégoire Broquet, Camille Yver Kwok, Yelva Roustan, Lin Wu, Emmanuel Arzoumanian, and Philippe Bousquet. 2017. “Statistical Atmospheric Inversion of Local Gas Emissions by Coupling the Tracer Release Technique and Local-Scale Transport Modelling: A Test Case with Controlled Methane Emissions.” Atmospheric Measurement Techniques 10 (12): 5017–37. https://doi.org/10.5194/amt-10-5017-2017.

12) Ars, Sebastien. 2017. “Characterization of local scale methane emissions using a statistical inversion method based on a Gaussian model parameterized with tracer gas observations.” PhD thesis, LSCE: UVSQ.

13) Assan, Sabina, Alexia Baudic, Ali Guemri, Philippe Ciais, Valerie Gros, and Felix R. Vogel. 2017. “Characterization of Interferences to in Situ Observations of Delta13CH4 and C2H6 When Using a Cavity Ring-down Spectrometer at Industrial Sites.” Atmospheric Measurement Techniques 10 (6): 2077–91. https://doi.org/10.5194/amt-10-2077-2017.

14) Assan, Sabina. 2017. “Towards Improved Source Apportionment of Anthropogenic Methane Sources.” PhD thesis, LSCE: UVSQ.

15) Aydin, Murat, Kristal R. Verhulst, Eric S. Saltzman, Mark O. Battle, Stephen A. Montzka, Donald R. Blake, Qi Tang, and Michael J. Prather. 2011. “Recent Decreases in Fossil-Fuel Emissions of Ethane and Methane Derived from Firn Air.” Nature 476 (7359): 198–201. https://doi.org/10.1038/nature10352.

16) Baertschi, P. 1976. “ABSOLUTE 180 CONTENT OF STANDARD MEAN OCEAN WATER.” Earth and Planetary Science Letters 31: 341–44.

17) Baker, Angela K., Andreas J. Beyersdorf, Lambert A. Doezema, Aaron Katzenstein, Simone Meinardi, Isobel J. Simpson, Donald R. Blake, and F. Sherwood Rowland. 2008. “Measurements of Nonmethane Hydrocarbons

in 28 United States Cities." Atmospheric Environment 42 (1): 170–82. https://doi.org/10.1016/j.atmosenv.2007.09.007.

18) Bergamaschi, Peter, Ute Karstens, Alistair J. Manning, Marielle Saunois, Aki Tsuruta, Antoine Berchet, Alexander T. Vermeulen, et al. 2018. "Inverse Modelling of European CH4 Emissions during 2006–2012 Using Different Inverse Models and Reassessed Atmospheric Observations." Atmospheric Chemistry and Physics 18 (2): 901–20. https://doi.org/10.5194/acp-18-901-2018.

19) Blake, Donald R., Van H. Woo, Stanley C. Tyler, and F. Sherwood Rowland. 1984. "Methane Concentrations and Source Strengths in Urban Locations." Geophysical Research Letters 11 (12): 1211–14. https://doi.org/10.1029/GL011i012p01211.

20) Bogner, J., and K. Spokas. 1993. "Landfill CH4: Rates, Fates, and Role in Global Carbon Cycle." Chemosphere 26 (1–4): 369–86. https://doi.org/10.1016/0045-6535(93)90432-5.

21) Bonsang, B. and Kanakidou, M.: Non-methane hydrocarbon variability during the FIELDVOC'94 campaign in Portugal, Chemosphere - Global Change Science, 3(3), 259–273, doi:10.1016/S1465-9972(01)00009-5, 2001.

22) Borjesson, Gunnar, Jerker Samuelsson, Jeffrey Chanton, Rolf Adolfsson, Bo Galle, and Bo H. Svensson. 2009. "A National Landfill Methane Budget for Sweden Based on Field Measurements, and an Evaluation of IPCC Models." Tellus B: Chemical and Physical Meteorology 61 (2): 424–35. https://doi.org/10.1111/j.1600-0889.2008.00409.x.

23) Bossche, Michael van den, Nathan Tyler Rose, and Stephan Franz Joseph De Wekker. 2017. "Potential of a Low-Cost Gas Sensor for Atmospheric Methane Monitoring." Sensors and Actuators B: Chemical 238 (January): 501–9. https://doi.org/10.1016/j.snb.2016.07.092.

24) Bourtsoukidis, E., Ernle, L., Crowley, J. N., Lelieveld, J., Paris, J.-D., Pozzer, A., Walter, D. and Williams, J.: Non Methane Hydrocarbon sources and sinks around the Arabian Peninsula, Atmospheric Chemistry and Physics Discussions, 1–45, doi:https://doi.org/10.5194/acp-2019-92, 2019.

25) Briggs, Gary A. 1973. "Diffusion Estimaion for Small Emissions." Air REsources Atmopsheric Turbulence and Diffusion Laboratory, NOAA.

26) Bruhwiler, L. M., S. Basu, P. Bergamaschi, P. Bousquet, E. Dlugokencky, S. Houweling, M. Ishizawa, et al. 2017. "U.S. CH4 Emissions from Oil and Gas Production: Have Recent Large Increases Been Detected?: U.S. Emissions From Oil and Gas Production." Journal of Geophysical Research: Atmospheres 122 (7): 4070–83. https://doi.org/10.1002/2016JD026157.

27) Caulton, Dana R., Qi Li, Elie Bou-Zeid, Jeffrey P. Fitts, Levi M. Golston, Da Pan, Jessica Lu, et al. 2018. "Quantifying Uncertainties from Mobile-Laboratory-Derived Emissions of Well Pads Using Inverse Gaussian Methods." Atmospheric Chemistry and Physics 18 (20): 15145–68. https://doi.org/10.5194/acp-18-15145-2018.

28) Caulton, Dana R., Qi Li, Elie Bou-Zeid, Jessica Lu, Haley M. Lane, Jeffrey P. Fitts, Bernhard Buchholz, et al. 2017. "Improving Mobile Platform Gaussian-Derived Emission Estimates Using Hierarchical Sampling and Large Eddy Simulation." Atmospheric Chemistry and Physics Discussions, November, 1–39. https://doi.org/10.5194/acp-2017-961.

29) Cegibat, G. Aménagement d'une chaufferie en sous-sol https://cegibat.grdf.fr/reglementation-gaz/amenagement-chaufferie-sous-sol (accessed Oct 29, 2019).

30) Chanton, Jeffrey P., Christine M. Rutkowski, Candace C. Schwartz, Darold E. Ward, and Lindsay Boring. 2000. "Factors Influencing the Stable Carbon Isotopic Signature of Methane from Combustion and Biomass Burning." Journal of Geophysical Research: Atmospheres 105 (D2): 1867–77. https://doi.org/10.1029/1999JD900909.

31) Chanton, Jeffrey, and Karen Liptay. 2000. “Seasonal Variation in Methane Oxidation in a Landfill Cover Soil as Determined by an in Situ Stable Isotope Technique.” Global Biogeochemical Cycles 14 (1): 51–60. https://doi.org/10.1029/1999GB900087.

32) Chen, H., A. Karion, C. W. Rella, J. Winderlich, C. Gerbig, A. Filges, T. Newberger, C. Sweeney, and P. P. Tans. 2013. “Accurate Measurements of Carbon Monoxide in Humid Air Using the Cavity Ring-down Spectroscopy (CRDS) Technique.” Atmospheric Measurement Techniques 6 (4): 1031–40. https://doi.org/10.5194/amt-6-1031-2013.

33) Chen, H., J. Winderlich, C. Gerbig, A. Hoefer, C. W. Rella, E. R. Crosson, A. D. Van Pelt, et al. 2010. “High-Accuracy Continuous Airborne Measurements of Greenhouse Gases (CO2 and CH4) Using the Cavity Ring-down Spectroscopy (CRDS) Technique.” Atmospheric Measurement Techniques 3 (2): 375–86. https://doi.org/10.5194/amt-3-375-2010.

34) Clark, N. N.; Johnson, D. R.; McKain, D. L.; Wayne, W. S.; Li, H.; Rudek, J.; Mongold, R. A.; Sandoval, C.; Covington, A. N.; Hailer, J. T. Future Methane Emissions from the Heavy-Duty Natural Gas Transportation Sector for Stasis, High, Medium, and Low Scenarios in 2035. Journal of the Air & Waste Management Association 2017, 67 (12), 1328–1341. https://doi.org/10.1080/10962247.2017.1368737.

35) CPER. 2017. “Contrat de Plan Etat-Region 2015-2020 Ile-de-France.”

36) Craig, Harmon. 1957. “Isotopic Standards for Carbon and Oxygen and Correction Factors for Mass-Spectrometric Analysis of Carbon Dioxide.” Geochemica et Cosmochemica Acta 12: 133–49.

37) Crippa, M., Oreggioni, G., Guizzardi, D., Muntean, M., Schaaf, E., Lo Vullo E., Solazzo, E., Monforti-Ferrario, F., Olivier, J.G.J., and Vignati, E. 2019. “Fossil CO2 and GHG Emissions of All World Countries - 2019 Report, EUR 29849 EN.” Publications Office of the European Union, Luxembourg,.

38) Crosson, E.R. 2008. “A Cavity Ring-down Analyzer for Measuring Atmospheric Levels of Methane, Carbon Dioxide, and Water Vapor.” Applied Physics B 92 (3): 403–8. https://doi.org/10.1007/s00340-008-3135-y.

39) Daelman, Matthijs R J, Ellen M. van Voorthuizen, Udo G.J.M. van Dongen, Eveline I.P. Volcke, and Mark C.M. van Loosdrecht. 2012. “Methane Emission during Municipal Wastewater Treatment.” Water Research 46: 3657–70. https://doi.org/doi:10.1016/j.watres.2012.04.024.

40) Defratyka, Sara M, Jean-Daniel Paris, Camille Yver-Kwok, Daniel Loeb, James France, Nigel Yarrow, Valérie Gros, and Philippe Bousquet. 2020. “Ethane Measurement by Picarro CRDS G2201-i in Laboratory and Field Conditions: Potential and Limitations,” Atmospheric Measurements Techniques. https://doi.org/10.5194/amt-2020-410. Article currently in open discussion

41) Defratyka, Sara, Jean-Daniel Paris, Camille Yver-Kwok, Julianne M. Fernandez, Piotr Korben, and Philippe Bousquet. 2020. “Mapping Urban Methane Sources in Paris, France.” Manuscript Submitted for Publication.

42) Dlugokencky, E. 2020. “NOAA/ESRL.” (www.esrl.noaa.gov/gmd/ccgg/trends_ch4/).

43) Duren, Riley M., and Charles E. Miller. 2012. “Measuring the Carbon Emissions of Megacities.” Nature Climate Change 2 (8): 560–62. https://doi.org/10.1038/nclimate1629.

44) Duren, Riley M., Andrew K. Thorpe, Kelsey T. Foster, Talha Rafiq, Francesca M. Hopkins, Vineet Yadav, Brian D. Bue, et al. 2019. “California’s Methane Super-Emitters.” Nature 575 (7781): 180–84. https://doi.org/10.1038/s41586-019-1720-3.

45) Espic, C, M Liechti, M Battaglia, D Paul, T Röckmann, and S Szidat. 2019. “Compound-Specific Radiocarbon Analysis of Atmospheric Methane: A New Preconcentration and Purification Setup.” Radiocarbon 61 (5): 1461–76. https://doi.org/10.1017/RDC.2019.76.

46) Fischer, Joseph C. von, Daniel Cooley, Sam Chamberlain, Adam Gaylord, Claire J. Griebenow, Steven P. Hamburg, Jessica Salo, Russ Schumacher, David Theobald, and Jay Ham. 2017. “Rapid, Vehicle-Based

Identification of Location and Magnitude of Urban Natural Gas Pipeline Leaks." Environmental Science & Technology 51 (7): 4091–99. https://doi.org/10.1021/acs.est.6b06095.

47) Fisher, Rebecca, David Lowry, Owen Wilkin, Srimathy Sriskantharajah, and Euan G. Nisbet. 2006. "High-Precision, Automated Stable Isotope Analysis of Atmospheric Methane and Carbon Dioxide Using Continuous-Flow Isotope-Ratio Mass Spectrometry." Rapid Communications in Mass Spectrometry 20 (2): 200–208. https://doi.org/10.1002/rcm.2300.

48) Gardiner, T., Helmore, J., Innocenti, F. and Robinson, R. 2007. "Field Validation of Remote Sensing Methane Emission Measurements, Remote Sensing", 9(9), 956, doi:10.3390/rs9090956.

49) GIE, and MARCOGAZ. 2019. "Potential Ways the Gas Industry Can Contribute to the Reduction of Methane Emissions Report for the Madrid Forum." https://www.gie.eu/index.php/gie-publications/methane-emission-report-2019.

50) Gifford, F.A. Jr. 1968. "AN OUTLINE OF THEORIES OF DIFFUSION IN THE LOWER LAYERS OF THE ATMOSPHERE." TID--24190, 4501607. https://doi.org/10.2172/4501607.

51) Gioli, B.; Toscano, P.; Lugato, E.; Matese, A.; Miglietta, F.; Zaldei, A.; Vaccari, F. P. Methane and Carbon Dioxide Fluxes and Source Partitioning in Urban Areas: The Case Study of Florence, Italy. Environmental Pollution 2012, 164, 125–131. https://doi.org/10.1016/j.envpol.2012.01.019.

52) Global Carbon Project (GCP) https://www.globalcarbonproject.org/methanebudget/index.htm (accessed Dec 5, 2019).

53) GRDF on Twitter. 2019. "GRDF sur Twitter : "[Communiqué de Presse] « Réaction de #GRDF suite aux propos de Monsieur @A_Vesperini sur la sécurité du réseau #gaz à #Paris » #Trévise #Explosion #Paris9." Twitter. January 13, 2019. https://twitter.com/grdf/status/1084437895841280000/photo/1.

54) Gros, V., Gaimoz, C., Herrmann, F., Custer, T., Williams, J., Bonsang, B., Sauvage, S., Locoge, N., d'Argouges, O., Sarda-Estève, R. and Sciare, J.: Volatile organic compounds sources in Paris in spring 2007. Part I: qualitative analysis, Environ. Chem., 8(1), 74, doi:10.1071/EN10068, 2011.

55) GRTgaz. 2019. "Plan decennal de developpement du reseau de transport de GRTgaz 2018-2027." http://www.grtgaz.com/grands-projets/plan-decennal.html.

56) Haghnegahdar, Mojhgan A, Edwin A Schauble, and Edward D Young. 2017. "A Model for 12CH2D2 and 13CH3D as Complementary Tracers for the Budget of Atmospheric CH4." Global Biogeochemical Cycles 31: 1387–1407. https://doi.org/10.1002/2017GB005655.

57) Hausmann, Petra, Ralf Sussmann, and Dan Smale. 2016. "Contribution of Oil and Natural Gas Production to Renewed Increase in Atmospheric Methane (2007–2014): Top–down Estimate from Ethane and Methane Column Observations." Atmospheric Chemistry and Physics 16 (5): 3227–44. https://doi.org/10.5194/acp-16-3227-2016.

58) Helmig, Detlev, Samuel Rossabi, Jacques Hueber, Pieter Tans, Stephen A. Montzka, Ken Masarie, Kirk Thoning, et al. 2016. "Reversal of Global Atmospheric Ethane and Propane Trends Largely Due to US Oil and Natural Gas Production." Nature Geoscience 9 (7): 490–95. https://doi.org/10.1038/ngeo2721.

59) Hesterberg, T. W.; Lapin, C. A.; Bunn, W. B. A Comparison of Emissions from Vehicles Fueled with Diesel or Compressed Natural Gas. Environ. Sci. Technol. 2008, 42 (17), 6437–6445. https://doi.org/10.1021/es071718i.

60) Hilst, Glenn R. 1957. "The Dispersion of Stack Gases In Stable Atmospheres." Journal of the Air Pollution Control Association 7 (3): 205–10. https://doi.org/10.1080/00966665.1957.10467804.

61) Hoheisel, A.: Characterisation of delta13CH4 source signatures from methane sources in Germany using mobile measurements, University of Heidelberg, Institute of Environmental Physics, 1 October., 2018.

62) Hoheisel, Antje, Christiane Yeman, Florian Dinger, Henrik Eckhardt, and Martina Schmidt. 2019. “An Improved Method for Mobile Characterisation of δ13CH4 Source Signatures and Its Application in Germany.” Atmospheric Measurement Techniques 12 (2): 1123–39. https://doi.org/10.5194/amt-12-1123-2019.

63) Hopkins, Francesca M., James R. Ehleringer, Susan E. Bush, Riley M. Duren, Charles E. Miller, Chun-Ta Lai, Ying-Kuang Hsu, Valerie Carranza, and James T. Randerson. 2016. “Mitigation of Methane Emissions in Cities: How New Measurements and Partnerships Can Contribute to Emissions Reduction Strategies: URBAN METHANE MITIGATION.” Earth’s Future 4 (9): 408–25. https://doi.org/10.1002/2016EF000381.

64) I.A.U. 2019. “Les enjeux de la filière méthanisation en Île-de-France.” Institut d’aménagement et d’urbanisme de la région île de France. January 2019. https://www.iau-idf.fr/nos-travaux/publications/les-enjeux-de-la-filiere-methanisation-en-ile-de-france.html.

65) INSEE. 2019. “INSEE.” (https://www.insee.fr/fr/statistiques/1893198).

66) IPCC. 2006. “2006 IPCC Guidelines for National Greenhouse Gas Inventories: Industrial Processes and Product Use,.” Kanagawa, JP: Institute for Global Environmental Strategies.

67) IPCC. 2018. “Climate Change 2013: The Physical Science Basis. Contribution of Working Group I to the Fifth Assessment Report of the Intergovernmental Panel on Climate Change.” Cambridge, United Kingdom and New York, NY, USA: Cambridge University Press.

68) Isotopic Measurements | Aerodyne Research, Inc. http://www.aerodyne.com/application/isotopic-measurements (accessed Dec 6, 2019).

69) Jackson, R B, M Saunois, P Bousquet, J G Canadell, B Poulter, A R Stavert, P Bergamaschi, Y Niwa, A Segers, and A Tsuruta. 2020. “Increasing Anthropogenic Methane Emissions Arise Equally from Agricultural and Fossil Fuel Sources.” Environmental Research Letters 15 (7): 071002. https://doi.org/10.1088/1748-9326/ab9ed2.

70) Jackson, Robert B., Adrian Down, Nathan G. Phillips, Robert C. Ackley, Charles W. Cook, Desiree L. Plata, and Kaiguang Zhao. 2014. “Natural Gas Pipeline Leaks Across Washington, DC.” Environmental Science & Technology 48 (3): 2051–58. https://doi.org/10.1021/es404474x.

71) Karion, Anna, Colm Sweeney, Pieter Tans, and Timothy Newberger. 2010. “AirCore: An Innovative Atmospheric Sampling System.” Journal of Atmospheric and Oceanic Technology 27 (11): 1839–53. https://doi.org/10.1175/2010JTECHA1448.1.

72) Keeling, Charles D. 1958. “The Concentration and Isotopic Abundances of Atmospheric Carbon Dioxide in Rural Areas.” *Geochimica et Cosmochimica Acta* 13 (4): 322–34. https://doi.org/10.1016/0016-7037(58)90033-4.

73) Kim-Hak, David, Derek Fleck, John Yiu, Zhiwei Lin, and Gregor Lucic. 2017. “FUGITIVE METHANE EMISSION IDENTIFICATION AND SOURCE ATTRIBUTION: ETHANE-TO- METHANE ANALYSIS USING A PORTABLE CAVITY RING-DOWN SPECTROSCOPY ANALYZER.” In, 1. https://www.picarro.com/support/literature/fugitive_methane_emission_identification_and_source_attribution_ethane_to.

74) Klausner, T, Mertens, M, Huntrieser, H, Galkowski, M, Kuhlmann, G, Baumann, R, Fiehn, A, Jockel, P, Puhl, M, and Roiger, A. 2020. “Urban Greenhouse Gas Emissions from the Berlin Area: A Case Study Using Airborne CO2 and CH4 in Situ Observations in Summer 2018.” Elementa: Science of the Anthropocene 8 (15): 24. https://doi.org/10.1525/elementa.411.

75) Kollamthodi, S. The Role of Natural Gas and Biomethane in the Transport Sector; 2016; p 85.

76) Korsakissok, Irène, and Vivien Mallet. 2009. “Comparative Study of Gaussian Dispersion Formulas within the Polyphemus Platform: Evaluation with Prairie Grass and Kincaid Experiments.” Journal of Applied Meteorology and Climatology 48 (12): 2459–73. https://doi.org/10.1175/2009JAMC2160.1.

77) Kort, E. A., M. L. Smith, L. T. Murray, A. Gvakharia, A. R. Brandt, J. Peischl, T. B. Ryerson, C. Sweeney, and K. Travis. 2016. “Fugitive Emissions from the Bakken Shale Illustrate Role of Shale Production in Global Ethane Shift: Ethane Emissions From the Bakken Shale.” Geophysical Research Letters 43 (9): 4617–23. https://doi.org/10.1002/2016GL068703.

78) La Tribune. 2019. “Polémique sur l’état du réseau de gaz parisien.” La Tribune. January 13, 2019. https://www.latribune.fr/entreprises-finance/industrie/energie-environnement/polemique-sur-l-etat-du-reseau-de-gaz-parisien-803664.html.

79) Lamb, Brian K., H. Westberg, and G. Allwine. 1986. “Isoprene Emission Fluxes Determined by an Atmospheric Tracer TechniquE.” Atmospheric Environment (1967) 20 (1): 1–8. https://doi.org/10.1016/0004-6981(86)90201-5.

80) Lamb, Brian K., J. B. McManus, Joanne H. Shorter, Charles E. Kolb, Byard. Mosher, Robert C. Harriss, Eugene. Allwine, et al. 1995. “Development of Atmospheric Tracer Methods To Measure Methane Emissions from Natural Gas Facilities and Urban Areas.” Environmental Science & Technology 29 (6): 1468–79. https://doi.org/10.1021/es00006a007.

81) Lamb, Brian K., Maria O. L. Cambaliza, Kenneth J. Davis, Steven L. Edburg, Thomas W. Ferrara, Cody Floerchinger, Alexie M. F. Heimburger, et al. 2016. “Direct and Indirect Measurements and Modeling of Methane Emissions in Indianapolis, Indiana.” Environmental Science & Technology 50 (16): 8910–17. https://doi.org/10.1021/acs.est.6b01198.

82) Lan, Xin, Pieter Tans, Colm Sweeney, Arlyn Andrews, Edward Dlugokencky, Stefan Schwietzke, Jonathan Kofler, et al. 2019. “Long-Term Measurements Show Little Evidence for Large Increases in Total U.S. Methane Emissions Over the Past Decade.” Geophysical Research Letters 46 (9): 4991–99. https://doi.org/10.1029/2018GL081731.

83) Le Figaro, AFP. 2019. “Paris resigne avec GRDF pour distribuer du gaz, mais plus propre.” Le Figaro.fr. November 15, 2019. https://www.lefigaro.fr/flash-eco/paris-resigne-avec-grdf-pour-distribuer-du-gaz-mais-plus-propre-20191115.

84) Liptay, K., J. Chanton, P. Czepiel, and B. Mosher. 1998. “Use of Stable Isotopes to Determine Methane Oxidation in Landfill Cover Soils.” Journal of Geophysical Research: Atmospheres 103 (D7): 8243–50. https://doi.org/10.1029/97JD02630.

85) Lopez, M., O.A. Sherwood, E.J. Dlugokencky, R. Kessler, L. Giroux, and D.E.J. Worthy. 2017. “Isotopic Signatures of Anthropogenic CH4 Sources in Alberta, Canada.” Atmospheric Environment 164 (September): 280–88. https://doi.org/10.1016/j.atmosenv.2017.06.021.

86) Lowe, David C., Carl A. M. Brenninkmeijer, Stanley C. Tyler, and Edward J. Dlugkencky. 1991. “Determination of the Isotopic Composition of Atmospheric Methane and Its Application in the Antarctic.” Journal of Geophysical Research 96 (D8): 15455. https://doi.org/10.1029/91JD01119.

87) Lowry, David, Craig W. Holmes, Nigel D. Rata, Phillip O’Brien, and Euan G. Nisbet. 2001. “London Methane Emissions: Use of Diurnal Changes in Concentration and $\delta^{13}C$ to Identify Urban Sources and Verify Inventories.” Journal of Geophysical Research: Atmospheres 106 (D7): 7427–48. https://doi.org/10.1029/2000JD900601.

88) Lowry, David, Rebecca E. Fisher, James L. France, Max Coleman, Mathias Lanoisellé, Giulia Zazzeri, Euan G. Nisbet, et al. 2020. “Environmental Baseline Monitoring for Shale Gas Development in the UK: Identification and Geochemical Characterisation of Local Source Emissions of Methane to Atmosphere.” Science of The Total Environment 708 (March): 134600. https://doi.org/10.1016/j.scitotenv.2019.134600.

89) Lozano, Mathis. 2020. “Estimation des émissions de méthane liées au transport du gaz naturel : comparaison d’approches top-down et bottom-up à l’échelle du site de compression.”

90) Mallet, V, D Quelo, B Sportisse, M Ahmed de Biasi, E Debry, I Korsakissok, L Wu, et al. 2007. “Technical Note: The Air Quality Modeling System Polyphemus.” Atmos. Chem. Phys., 9.

91) Marcotullio, Peter John, Andrea Sarzynski, Jochen Albrecht, Niels Schulz, and Jake Garcia. 2013. “The Geography of Global Urban Greenhouse Gas Emissions: An Exploratory Analysis.” Climatic Change 121 (4): 621–34. https://doi.org/10.1007/s10584-013-0977-z.

92) McKain, Kathryn, Adrian Down, Steve M. Raciti, John Budney, Lucy R. Hutyra, Cody Floerchinger, Scott C. Herndon, et al. 2015. “Methane Emissions from Natural Gas Infrastructure and Use in the Urban Region of Boston, Massachusetts.” Proceedings of the National Academy of Sciences 112 (7): 1941–46. https://doi.org/10.1073/pnas.1416261112.

93) Milkov, Alexei V., and Giuseppe Etiope. 2018. “Revised Genetic Diagrams for Natural Gases Based on a Global Dataset of >20,000 Samples.” Organic Geochemistry 125 (November): 109–20. https://doi.org/10.1016/j.orggeochem.2018.09.002.

94) Miller, John B., and Pieter P. Tans. 2003. “Calculating Isotopic Fractionation from Atmospheric Measurements at Various Scales.” Tellus B: Chemical and Physical Meteorology 55 (2): 207–14. https://doi.org/10.3402/tellusb.v55i2.16697.

95) Mønster, Jacob G., Jerker Samuelsson, Peter Kjeldsen, Chris W. Rella, and Charlotte Scheutz. 2014. “Quantifying Methane Emission from Fugitive Sources by Combining Tracer Release and Downwind Measurements – A Sensitivity Analysis Based on Multiple Field Surveys.” Waste Management 34 (8): 1416–28. https://doi.org/10.1016/j.wasman.2014.03.025.

96) Morgenstern, Olaf, Michaela I. Hegglin, Eugene Rozanov, Fiona M. O’Connor, N. Luke Abraham, Hideharu Akiyoshi, Alexander T. Archibald, et al. 2017. “Review of the Global Models Used within Phase 1 of the Chemistry–Climate Model Initiative (CCMI).” Geoscientific Model Development 10 (2): 639–71. https://doi.org/10.5194/gmd-10-639-2017.

97) Moriizumi, J.; Nagamine, K.; Iida, T.; Ikebe, Y. CARBON ISOTOPIC ANALYSIS OF ATMOSPHERIC METHANE IN URBAN AND SUBURBAN AREAS: FOSSIL AND NON-FOSSIL METHANE FROM LOCAL SOURCES. 1998, 9.

98) Nakagawa, F.; Tsunogai, U.; Komatsu, D. D.; Yamada, K.; Yoshida, N.; Moriizumi, J.; Nagamine, K.; Iida, T.; Ikebe, Y. Automobile Exhaust as a Source of ^{13}C- and D-Enriched Atmospheric Methane in Urban Areas. Organic Geochemistry 2005, 36 (5), 727–738. https://doi.org/10.1016/j.orggeochem.2005.01.003.

99) Nicewonger, Melinda R., Kristal R. Verhulst, Murat Aydin, and Eric S. Saltzman. 2016. “Preindustrial Atmospheric Ethane Levels Inferred from Polar Ice Cores: A Constraint on the Geologic Sources of Atmospheric Ethane and Methane.” Geophysical Research Letters 43 (1): 214–21. https://doi.org/10.1002/2015GL066854.

100) Nisbet, E. G., E. J. Dlugokencky, M. R. Manning, D. Lowry, R. E. Fisher, J. L. France, S. E. Michel, et al. 2016. “Rising Atmospheric Methane: 2007-2014 Growth and Isotopic Shift: RISING METHANE 2007-2014.” Global Biogeochemical Cycles 30 (9): 1356–70. https://doi.org/10.1002/2016GB005406.

101) Nisbet, E. G., M. R. Manning, E. J. Dlugokencky, R. E. Fisher, D. Lowry, S. E. Michel, C. Lund Myhre, et al. 2019. “Very Strong Atmospheric Methane Growth in the 4 Years 2014–2017: Implications for the Paris Agreement.” Global Biogeochemical Cycles 33 (3): 318–42. https://doi.org/10.1029/2018GB006009.

102) Ortech Report No. 26392. 2017. “Compustion Property Calculations for a Typical Union Gas Composition.”

103) Panopoulou, A., Liakakou, E., Gros, V., Sauvage, S., Locoge, N., Bonsang, B., Psiloglou, B. E., Gerasopoulos, E. and Mihalopoulos, N.: Non-methane hydrocarbon variability in Athens during wintertime: the role of traffic and heating, Atmos. Chem. Phys., 18(21), 16139–16154, doi:10.5194/acp-18-16139-2018, 2018.

104) Pasquill, F. 1961. “Estimation of the Dispersion of Windborne Material” 90 (Meteorol. Mag.): 33–49.

105) Pataki, D. E., J. R. Ehleringer, L. B. Flanagan, D. Yakir, D. R. Bowling, C. J. Still, N. Buchmann, J. O. Kaplan, and J. A. Berry. 2003. “The Application and Interpretation of Keeling Plots in Terrestrial Carbon Cycle Research: APPLICATION OF KEELING PLOTS.” Global Biogeochemical Cycles 17 (1). https://doi.org/10.1029/2001GB001850.

106) Patra, P. K., S. Houweling, M. Krol, P. Bousquet, D. Belikov, D. Bergmann, H. Bian, et al. 2011. “TransCom Model Simulations of CH_4 and Related Species: Linking Transport, Surface Flux and Chemical Loss with CH_4; Variability in the Troposphere and Lower Stratosphere.” *Atmospheric Chemistry and Physics* 11 (24): 12813–37. https://doi.org/10.5194/acp-11-12813-2011.

107) PCAE. 2018. “Le Plan Climat Air Energie.”

108) Reay, Dave, Pete Smith, and Andre Van Amstel, eds. 2010. Methane and Climate Change.

109) Rella, C. W., H. Chen, A. E. Andrews, A. Filges, C. Gerbig, J. Hatakka, A. Karion, et al. 2013. “High Accuracy Measurements of Dry Mole Fractions of Carbon Dioxide and Methane in Humid Air.” Atmospheric Measurement Techniques 6 (3): 837–60. https://doi.org/10.5194/amt-6-837-2013.

110) Rella, C. W., J. Hoffnagle, Y. He, and S. Tajima. 2015. “Local- and Regional-Scale Measurements of CH_4, $\delta^{13}CH_4$, and C_2H_6 in the Uintah Basin Using a Mobile Stable Isotope Analyzer.” Atmospheric Measurement Techniques 8 (10): 4539–59. https://doi.org/10.5194/amt-8-4539-2015.

111) Rella, Chris W., Tracy R. Tsai, Connor G. Botkin, Eric R. Crosson, and David Steele. 2015. “Measuring Emissions from Oil and Natural Gas Well Pads Using the Mobile Flux Plane Technique.” Environmental Science & Technology 49 (7): 4742–48. https://doi.org/10.1021/acs.est.5b00099.

112) Riddick, Stuart N., Denise L. Mauzerall, Michael Celia, Grant Allen, Joseph Pitt, Mary Kang, and John C. Riddick. 2020. “The Calibration and Deployment of a Low-Cost Methane Sensor.” Atmospheric Environment 230 (June): 117440. https://doi.org/10.1016/j.atmosenv.2020.117440.

113) Röckmann, Thomas, Simon Eyer, Carina van der Veen, Maria E. Popa, Béla Tuzson, Guillaume Monteil, Sander Houweling, et al. 2016. “In Situ Observations of the Isotopic Composition of Methane at the Cabauwtall Tower Site.” Atmospheric Chemistry and Physics 16 (16): 10469–87. https://doi.org/10.5194/acp-16-10469-2016.

114) Roscioli, J. R., T. I. Yacovitch, C. Floerchinger, A. L. Mitchell, D. S. Tkacik, R. Subramanian, D. M. Martinez, et al. 2015. “Measurements of Methane Emissions from Natural Gas Gathering Facilities and Processing Plants: Measurement Methods.” Atmospheric Measurement Techniques 8 (5): 2017–35. https://doi.org/10.5194/amt-8-2017-2015.

115) Satterthwaite, David. 2008. “Cities’ Contribution to Global Warming: Notes on the Allocation of Greenhouse Gas Emissions.” Environment and Urbanization 20 (2): 539–49. https://doi.org/10.1177/0956247808096127.

116) Saunois, M, R B Jackson, P Bousquet, B Poulter, and J G Canadell. 2016. “The Growing Role of Methane in Anthropogenic Climate Change.” Environmental Research Letters 11 (12): 120207. https://doi.org/10.1088/1748-9326/11/12/120207.

117) Saunois, M., Bousquet, P., Poulter, B., Peregon, A., Ciais, P., Canadell, J. G., Dlugokencky, E. J., Etiope, G., Bastviken, D., Houweling, S., Janssens-Maenhout, G., Tubiello, F. N., Castaldi, S., Jackson, R. B., Alexe, M., Arora, V. K., Beerling, D. J., Bergamaschi, P., Blake, D. R., Brailsford, G., Brovkin, V., Bruhwiler, L., Crevoisier, C., Crill, P., Covey, K., Curry, C., Frankenberg, C., Gedney, N., Höglund-Isaksson, L., Ishizawa, M., Ito, A., Joos, F., Kim, H.-S., Kleinen, T., Krummel, P., Lamarque, J.-F., Langenfelds, R., Locatelli, R., Machida, T., Maksyutov, S., McDonald, K. C., Marshall, J., Melton, J. R., Morino, I., Naik, V., O'Doherty, S., Parmentier, F.-J. W., Patra, P. K., Peng, C., Peng, S., Peters, G. P., Pison, I., Prigent, C., Prinn, R., Ramonet, M., Riley, W. J., Saito, M., Santini, M., Schroeder, R., Simpson, I. J., Spahni, R., Steele, P., Takizawa, A., Thornton, B. F., Tian, H., Tohjima, Y., Viovy, N., Voulgarakis, A., van Weele, M., van der Werf, G. R., Weiss, R., Wiedinmyer, C., Wilton, D. J.,

Wiltshire, A., Worthy, D., Wunch, D., Xu, X., Yoshida, Y., Zhang, B., Zhang, Z. and Zhu, Q.: The global methane budget 2000–2012, Earth System Science Data, 8(2), 697–751, doi:10.5194/essd-8-697-2016, 2016.

118) Saunois, M., Stavert, A. R., Poulter, B., Bousquet, P., Canadell, J. G., Jackson, R. B., Raymond, P. A., Dlugokencky, E. J., Houweling, S., Patra, P. K., Ciais, P., Arora, V. K., Bastviken, D., Bergamaschi, P., Blake, D. R., Brailsford, G., Bruhwiler, L., Carlson, K. M., Carrol, M., Castaldi, S., Chandra, N., Crevoisier, C., Crill, P. M., Covey, K., Curry, C. L., Etiope, G., Frankenberg, C., Gedney, N., Hegglin, M. I., Höglund-Isaksson, L., Hugelius, G., Ishizawa, M., Ito, A., Janssens-Maenhout, G., Jensen, K. M., Joos, F., Kleinen, T., Krummel, P. B., Langenfelds, R. L., Laruelle, G. G., Liu, L., Machida, T., Maksyutov, S., McDonald, K. C., McNorton, J., Miller, P. A., Melton, J. R., Morino, I., Müller, J., Murgia-Flores, F., Naik, V., Niwa, Y., Noce, S., O'Doherty, S., Parker, R. J., Peng, C., Peng, S., Peters, G. P., Prigent, C., Prinn, R., Ramonet, M., Regnier, P., Riley, W. J., Rosentreter, J. A., Segers, A., Simpson, I. J., Shi, H., Smith, S. J., Steele, L. P., Thornton, B. F., Tian, H., Tohjima, Y., Tubiello, F. N., Tsuruta, A., Viovy, N., Voulgarakis, A., Weber, T. S., van Weele, M., van der Werf, G. R., Weiss, R. F., Worthy, D., Wunch, D., Yin, Y., Yoshida, Y., Zhang, W., Zhang, Z., Zhao, Y., Zheng, B., Zhu, Q., Zhu, Q. and Zhuang, Q.: The Global Methane Budget 2000–2017, preprint, Atmosphere – Atmospheric Chemistry and Physics., 2020.

119) Scarpelli, Tia R.; Daniel J. Jacob; Joannes D. Maasakkers; Melissa P. Sulprizio; Jian-Xiong Sheng; Kelly Rose; Lucy Romeo; John R. Worden; Greet Janssens-Maenhout. A Global Gridded (0.1× 0.1) Inventory of Methane Emissions from Oil, Gas, and Coal Exploitation Based on National Reports to the United Nations Framework Convention on Climate Change. Earth System Science Data 2020, 12.1.

120) Schwietzke, Stefan, Owen A. Sherwood, Lori M. P. Bruhwiler, John B. Miller, Giuseppe Etiope, Edward J. Dlugokencky, Sylvia Englund Michel, et al. 2016. "Upward Revision of Global Fossil Fuel Methane Emissions Based on Isotope Database." Nature 538 (7623): 88–91. https://doi.org/10.1038/nature19797.

121) Schwietzke, Stefan, W. Michael Griffin, H. Scott Matthews, and Lori M. P. Bruhwiler. 2014. "Natural Gas Fugitive Emissions Rates Constrained by Global Atmospheric Methane and Ethane." Environmental Science & Technology 48 (14): 7714–22. https://doi.org/10.1021/es501204c.

122) Shah, Adil, Joseph R. Pitt, Hugo Ricketts, J. Brian Leen, Paul I. Williams, Khristopher Kabbabe, Martin W. Gallagher, and Grant Allen. 2020. "Testing the Near-Field Gaussian Plume Inversion Flux Quantification Technique Using Unmanned Aerial Vehicle Sampling." Atmospheric Measurement Techniques 13 (3): 1467–84. https://doi.org/10.5194/amt-13-1467-2020.

123) Sherwood, Owen A., Stefan Schwietzke, Victoria A. Arling, and Giuseppe Etiope. 2017. "Global Inventory of Gas Geochemistry Data from Fossil Fuel, Microbial and Burning Sources, Version 2017." Earth System Science Data 9 (2): 639–56. https://doi.org/10.5194/essd-9-639-2017.

124) Simpson, Isobel J., Mads P. Sulbaek Andersen, Simone Meinardi, Lori Bruhwiler, Nicola J. Blake, Detlev Helmig, F. Sherwood Rowland, and Donald R. Blake. 2012. "Long-Term Decline of Global Atmospheric Ethane Concentrations and Implications for Methane." Nature 488 (7412): 490–94. https://doi.org/10.1038/nature11342.

125) Smith, Mackenzie L., Eric A. Kort, Anna Karion, Colm Sweeney, Scott C. Herndon, and Tara I. Yacovitch. 2015. "Airborne Ethane Observations in the Barnett Shale: Quantification of Ethane Flux and Attribution of Methane Emissions." Environmental Science & Technology 49 (13): 8158–66. https://doi.org/10.1021/acs.est.5b00219.

126) Sokal, R. R., and F. J. Rohlf. 1995. Biometry: The Principles and Practice of Statistics in Biological Research. 3rd ed. W.H. Freeman and Company.

127) SRCAE. 2012. "Schéma Régional Du Climat, de l'Air et de l'Energie de l'Île-de-France."

128) Stolper, D A, M Lawson, C L Davis, A A Ferreira, E V Santos Neto, G S Ellis, M D Lewan, et al. 2014. "Formation Temperatures of Thermogenic and Biogenic Methane." Science 344 (6191): 1500–1503. https://doi.org/10.1126/science.1254509.

129) Subramanian, R., Laurie L. Williams, Timothy L. Vaughn, Daniel Zimmerle, Joseph R. Roscioli, Scott C. Herndon, Tara I. Yacovitch, et al. 2015. “Methane Emissions from Natural Gas Compressor Stations in the Transmission and Storage Sector: Measurements and Comparisons with the EPA Greenhouse Gas Reporting Program Protocol.” Environmental Science & Technology 49 (5): 3252–61. https://doi.org/10.1021/es5060258.

130) Taylor, J. R.: An introduction to error analysis. The study of uncertainties in physical measurements, second., University Science Books., 1997.

131) Thompson, Chelsea R., Jacques Hueber, and Detlev Helmig. 2014. “Influence of Oil and Gas Emissions on Ambient Atmospheric Non-Methane Hydrocarbons in Residential Areas of Northeastern Colorado.” Elementa: Science of the Anthropocene 2 (November): 000035. https://doi.org/10.12952/journal.elementa.000035.

132) Townsend-Small, Amy, Stanley C. Tyler, Diane E. Pataki, Xiaomei Xu, and Lance E. Christensen. 2012. “Isotopic Measurements of Atmospheric Methane in Los Angeles, California, USA: Influence of ‘Fugitive’ Fossil Fuel Emissions: LOS ANGELES METHANE EMISSIONS.” Journal of Geophysical Research: Atmospheres 117 (D7): n/a-n/a. https://doi.org/10.1029/2011JD016826.

133) Turner, Alexander J., C. Frankenberg, and Eric A. Kort. 2019. “Interpreting Contemporary Trends in Atmospheric Methane.” Proceedings of the National Academy of Sciences 116 (8): 2805–13. https://doi.org/10.1073/pnas.1814297116.

134) United Nations. 2018. “Department of Economic and Social Affairs, Population Division (2018).” World Urban Prospects: The 2018 Revision, Online Edition.

135) USEPA. 2012. “Global Anthropogenic Non-CO2 Greenhouse Gas Emissions: 1990 - 2030, EPA 430-R-12-006.” US Environmental Protection Agency, Washington DC.

136) Voulgarakis, A., V. Naik, J.-F. Lamarque, D. T. Shindell, P. J. Young, M. J. Prather, O. Wild, et al. 2013. “Analysis of Present Day and Future OH and Methane Lifetime in the ACCMIP Simulations.” Atmospheric Chemistry and Physics 13 (5): 2563–87. https://doi.org/10.5194/acp-13-2563-2013.

137) Warneke, C., F. Geiger, P. M. Edwards, W. Dube, G. Pétron, J. Kofler, A. Zahn, et al. 2014. “Volatile Organic Compound Emissions from the Oil and Natural Gas Industry in the Uintah Basin, Utah: Oil and Gas Well Pad Emissions Compared to Ambient Air Composition.” Atmospheric Chemistry and Physics 14 (20): 10977–88. https://doi.org/10.5194/acp-14-10977-2014.

138) Weil, J. C., and R. P. Brower. 1984. “An Updated Gaussian Plume Model for Tall Stacks.” Journal of the Air Pollution Control Association 34 (8): 818–27. https://doi.org/10.1080/00022470.1984.10465816.

139) Weller, Z. D.; Roscioli, J. R.; Daube, W. C.; Lamb, B. K.; Ferrara, T. W.; Brewer, P. E.; von Fischer, J. C. Vehicle-Based Methane Surveys for Finding Natural Gas Leaks and Estimating Their Size: Validation and Uncertainty. Environ. Sci. Technol. 2018, acs.est.8b03135. https://doi.org/10.1021/acs.est.8b03135.

140) Weller, Zachary D., Duck Keun Yang, and Joseph C. von Fischer. 2019. “An Open Source Algorithm to Detect Natural Gas Leaks from Mobile Methane Survey Data.” Edited by Matthias Mauder. PLOS ONE 14 (2): e0212287. https://doi.org/10.1371/journal.pone.0212287.

141) Whiticar, Michael J. 1999. “Carbon and Hydrogen Isotope Systematics of Bacterial Formation and Oxidation of Methane.” Chemical Geology 161 (1–3): 291–314. https://doi.org/10.1016/S0009-2541(99)00092-3.

142) Worden, John R., A. Anthony Bloom, Sudhanshu Pandey, Zhe Jiang, Helen M. Worden, Thomas W. Walker, Sander Houweling, and Thomas Röckmann. 2017. “Reduced Biomass Burning Emissions Reconcile Conflicting Estimates of the Post-2006 Atmospheric Methane Budget.” Nature Communications 8 (1): 2227. https://doi.org/10.1038/s41467-017-02246-0.

143) Wunch, D.; Toon, G. C.; Hedelius, J. K.; Vizenor, N.; Roehl, C. M.; Saad, K. M.; Blavier, J.-F. L.; Blake, D. R.; Wennberg, P. O. Quantifying the Loss of Processed Natural Gas within California’s South Coast Air Basin Using

Long-Term Measurements of Ethane and Methane. Atmos. Chem. Phys. 2016, 16 (22), 14091–14105. https://doi.org/10.5194/acp-16-14091-2016.

144) Xu, Liukang, Xiaomao Lin, Jim Amen, Karla Welding, and Dayle McDermitt. 2014. “Impact of Changes in Barometric Pressure on Landfill Methane Emission.” Global Biogeochemical Cycles 28 (7): 679–95. https://doi.org/10.1002/2013GB004571.

145) Xueref-Remy, I., G. Zazzeri, F.M. Bréon, F. Vogel, P. Ciais, D. Lowry, and E.G. Nisbet. 2019. “Anthropogenic Methane Plume Detection from Point Sources in the Paris Megacity Area and Characterization of Their $\delta^{13}C$ Signature.” Atmospheric Environment, October, 117055. https://doi.org/10.1016/j.atmosenv.2019.117055.

146) Yacovitch, Tara I., Conner Daube, and Scott C. Herndon. 2020. “Methane Emissions from Offshore Oil and Gas Platforms in the Gulf of Mexico.” Environmental Science & Technology 54 (6): 3530–38. https://doi.org/10.1021/acs.est.9b07148.

147) Yacovitch, Tara I., Scott C. Herndon, Gabrielle Pétron, Jonathan Kofler, David Lyon, Mark S. Zahniser, and Charles E. Kolb. 2015. “Mobile Laboratory Observations of Methane Emissions in the Barnett Shale Region.” Environmental Science & Technology 49 (13): 7889–95. https://doi.org/10.1021/es506352j.

148) Yacovitch, Tara I., Scott C. Herndon, Joseph R. Roscioli, Cody Floerchinger, Ryan M. McGovern, Michael Agnese, Gabrielle Pétron, et al. 2014. “Demonstration of an Ethane Spectrometer for Methane Source Identification.” Environmental Science & Technology 48 (14): 8028–34. https://doi.org/10.1021/es501475q.

149) Yang, K., Ting, C., Wang, J., Wingenter, O. and Chan, C. 2015. “Diurnal and seasonal cycles of ozone precursors observed from continuous measurement at an urban site in Taiwan”. Atmospheric Environment, 39(18), 3221–3230, doi:10.1016/j.atmosenv.2005.02.003.

150) Yver Kwok, C. E., D. Müller, C. Caldow, B. Lebègue, J. G. Mønster, C. W. Rella, C. Scheutz, et al. 2015. “Methane Emission Estimates Using Chamber and Tracer Release Experiments for a Municipal Waste Water Treatment Plant.” Atmospheric Measurement Techniques 8 (7): 2853–67. https://doi.org/10.5194/amt-8-2853-2015.

151) Yver Kwok, C., O. Laurent, A. Guemri, C. Philippon, B. Wastine, C. W. Rella, C. Vuillemin, et al. 2015. “Comprehensive Laboratory and Field Testing of Cavity Ring-down Spectroscopy Analyzers Measuring H_2O, CO_2, CH_4 and CO.” Atmospheric Measurement Techniques 8 (9): 3867–92. https://doi.org/10.5194/amt-8-3867-2015.

152) Zavala-Araiza, Daniel, David Lyon, Ramón A. Alvarez, Virginia Palacios, Robert Harriss, Xin Lan, Robert Talbot, and Steven P. Hamburg. 2015. “Toward a Functional Definition of Methane Super-Emitters: Application to Natural Gas Production Sites.” Environmental Science & Technology 49 (13): 8167–74. https://doi.org/10.1021/acs.est.5b00133.

153) Zazzeri, G., D. Lowry, R. E. Fisher, J. L. France, M. Lanoisellé, C. S. B. Grimmond, and E. G. Nisbet. 2017. “Evaluating Methane Inventories by Isotopic Analysis in the London Region.” Scientific Reports 7 (1). https://doi.org/10.1038/s41598-017-04802-6.

154) Zazzeri, G., D. Lowry, R.E. Fisher, J.L. France, M. Lanoisellé, and E.G. Nisbet. 2015. “Plume Mapping and Isotopic Characterisation of Anthropogenic Methane Sources.” Atmospheric Environment 110 (June): 151–62. https://doi.org/10.1016/j.atmosenv.2015.03.029.

Appendix A

Mapping urban methane sources in Paris, France

Sara M. Defratyka[1], Jean-Daniel Paris[1], Camille Yver-Kwok[1], Julianne M. Fernandez[2], Piotr Korben[3], Philippe Bousquet[1]

1 Laboratoire des Sciences du Climat et de l'Environnement (LSCE-IPSL) CEA-CNRS-UVSQ Université Paris Saclay, Gif-sur-Yvette, France

2 Royal Holloway University of London, Egham, United Kingdom

3 Heidelberg University, Institute of Environmental Physics, Germany

This PDF file is a 18-page document that includes:

Supplementary Text

Supplementary Tables S1 to S4

Supplementary Figures S1 to S12

Table of content

Supporting Section S1: Analyzers used during vehicle-mounted surveys

During surveys, depending on the availability, different analyzers were installed as part of the mobile set-up. The CRDS G2201-i was used during all the surveys. It gives one measurement point per 3.7 s. Its cell volume is less than 10 standard cm^3 and its effective measurements path length reaches up to 20 km. Additionally, if another analyzer was available (G2401 or G2203), it was also used. All the analyzers have an uncertainty below 1 ppb for CH_4. G2401 and G2203 have a higher sampling frequency (0.5 Hz) then G2201-i. The specification of analyzers is presented in Table S1. For all days, the emission rate was calculated using data from all instruments. Results were found comparable, and in the article, the results from the instrument with the higher sampling frequency are presented. There are two exceptions: On 07.09.18 results from G2201-i instead of G2401 are presented as technical problems with G2401 occurred during the survey. In the case of days 31.01.19 and 01.02.19, the inlet for the instrument G2203 was situated ~50 cm above the ground to verify the inlet position influence for observed leak indication. For these two days, data from G2201-i was used, as for this instrument, the inlet was installed on the roof of the care like for the other surveys. Table S2 presents the daily use of analyzers.

Table S1. Characteristics of the instruments used during the surveys

Analyzer	species	Rise/fall time	Measurements interval [s]	CH_4 operational range [ppm]	Time delay [s]
CRDS G2201-i	CO_2, $\delta^{13}CO_2$, CH_4, $\delta^{13}CH_4$, H_2O	~30 s	3.7	1.8 – 12	28 – 30
CRDS G2203	CH_4, C_2H_2, H_2O	< 3 s	2	0 – 20	20
CRDS G2401	CO_2, CO, CH_4, H_2O	< 5 s	2	0 – 20	25
LGR MGGA	CO_2, CH_4, H_2O	1 s	1	0 – 100	8

Table S2. Daily use of the instruments

Day	CRDS			LGR MGGA	Target measurement Before/After survey	Analyzer used for analysis
	G2201-i	G2203	G2401			
07.09.18	X		X			G2201-i
25.09.18	X		X		After	G2401
26.09.18	X		X			G2401
28.11.18	X	X			Before	G2201-i
12.12.18	X	X			After	G2203
13.12.18	X	X				G2203
14.12.18	X	X			Before & After	G2203
25.01.19	X	X				G2201-i
31.01.19	X	X			After	G2201-i
01.02.19	X	X			After	G2201-i
12.02.19	X				Before & After	G2201-i
13.02.19	X					G2201-i
26.02.19	X	X			Before & After	G2203
27.02.19	X	X		X	Before & After	G2203
05.03.19	X			X	Before & After	G2201-i
06.03.19			X	X		G2401
07.03.19	X			X	Before & After	G2201-i

Supporting Section S2: Inlet position

In our study, as during previous mobile measurements [1–3], the inlet was located on the top of the car roof. We investigated the influence of the inlet's position on the measured mixing ratios. During three days, two instruments with different inlet locations were used: one on the top of the car (~170 cm above ground) and the other on the lower skirt of the car (~50 cm above ground). During two days, CRDS analyzers G2201-i and G2203 were used for the upper and lower inlet, respectively. A third day, two CRDS of the same type (G2401) were used.

During part of the third day of the test, the car was parked measuring at the same location over 2 hours. The car was parked in a place where mostly no CH_4 enhancement above background was observed. Over this period, with the same type of instrument, all three leak indications, which were observed from the lower inlet, were not observed from the upper inlet. These leak indications could come from the exhaust of passing buses (some buses in Paris are using biogas and natural gas). Looking at measurements when the car was moving, all six other leak indications are detected in synchronicity by both of the inlets. Overall the regression slope between the upper and lower inlets, when the car was moving, is 0.871 ± 0.026 ppb/ppb, which points to an underestimation by the lower inlet of 13% compared to the upper inlet.

In the case of the two previous days, with two different instrument types, regression slope between upper and lower inlet is equal to 1.084 ± 0.004 ppb/ppb and 1.156 ± 0.015 ppb/ppb, respectively. Results from these two days suggest that using lower inlet allow measuring higher CH_4 mixing ratio. However, this discrepancy can come from different measurement time interval of two instruments used during these days (lower – 2 s, upper – 3.7 s). Moreover, the lower inlet is more sensitive to local pollution (like dust, water from puddles or melting snow) while the upper inlet is less affected by local pollution and less sensitive to the nearby bus and our car exhaust. Results from the 3 tests days are presented in Figure S1.

In conclusion, the inlet situated on the car roof was chosen for the mobile measurements. This decision was made regarding the results of the test when the same type of instrument was used. In this case, CH_4 mixing ratio measured by lower inlet is slightly underestimated compared to the upper inlet. Additionally, this location gives better protection of the instrument against water and pollution.

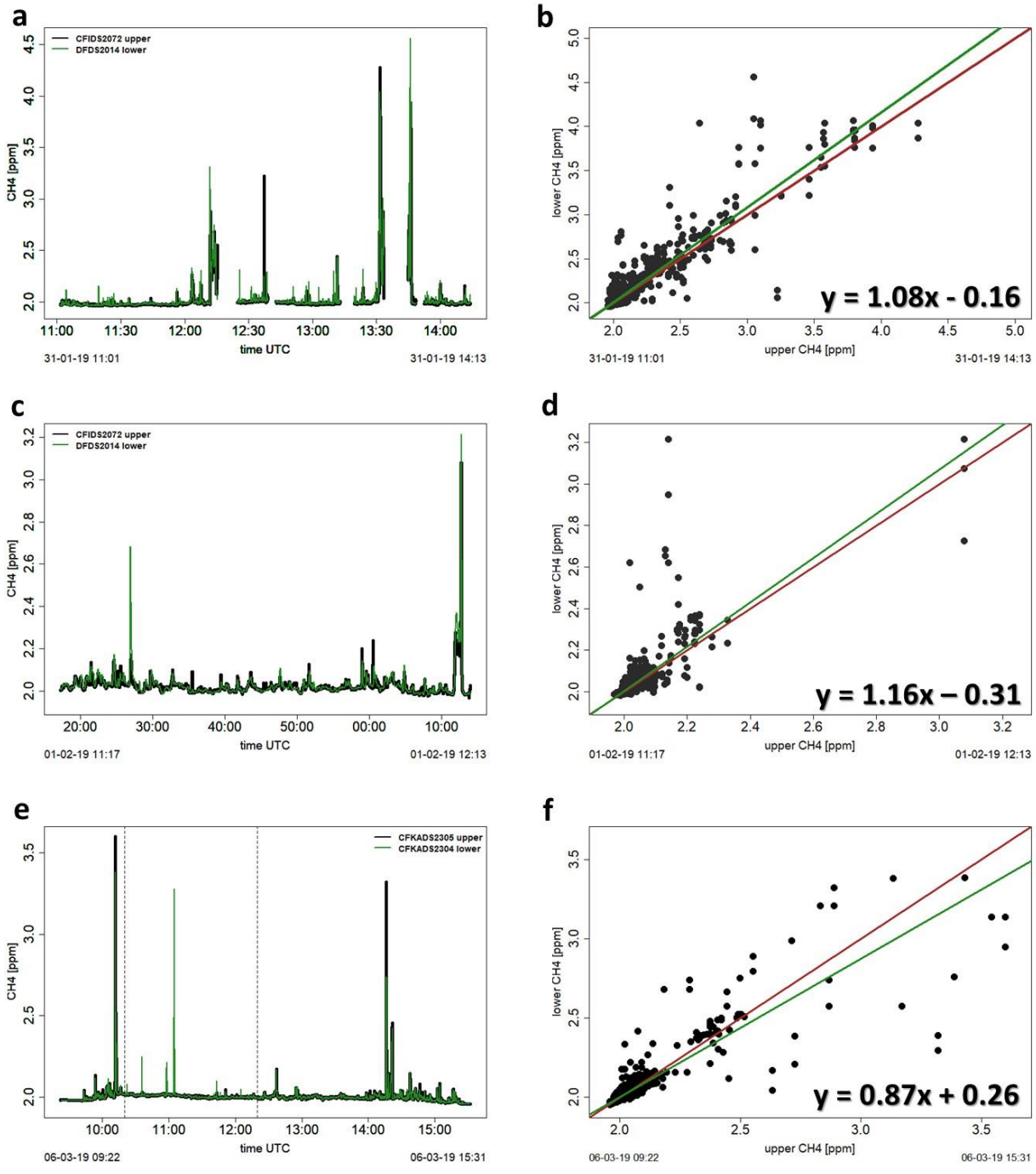

Figure S1. Observed mixing ratio at the lower and upper inlets; **left panel:** CH_4 mixing ratio over the time, **right panel:** correlation lower - upper inlet during comparison inlet position. The red line corresponds to y=x. The green line shows the linear fitting, **plot a and b** present results from 31.01.2019, **c and d** present results from 01.02.2019, **e and f** present results from 06.03.2019, wherein plot e dotted lines represent a time when the car was parked. f presents the linear fitting without the time when the car was parked. In the case of the days 31.01.2019 and 01.02.2019, two different types of instrument were used (G2201-i and G2203). During 06.03.2019, the same type of instrument was used (G2204).

Supporting Section 3: Calibration procedure

During the measurement period, a 3-point concentration and isotopic composition calibration was done (30.11.2019), when three calibration tanks were measured alternatively for 20 minutes, and the measurement cycle was repeated twice. The CH_4 and $\delta^{13}CH_4$ values were 2557.2 ppb and -25.86‰, 2176.2 ppb and -34.73‰, 2388.4 ppb and -56.02‰ for the 1st, 2nd and 3rd calibration tanks, respectively. The CH_4 mixing ratio is calibrated to the WMO X2004A scale and $\delta^{13}CH_4$ is reported according to the VPDB scale. The three calibration gases were made by different dilutions of pure CH_4 and CO_2 with ambient air. Then they were measured multiple times on IRMS at Royal Holloway University of London. The isotopic signature is determined with 0.05 ‰ precision [4]. The calibration equations are presented in Table S1. Additionally, during 11 campaigns, to check the analyzer stability and lack of influence of switching on/off analyzer for CH_4 and $\delta^{13}CH_4$ values, before and after campaigns, an additional gas tank was measured for 20 minutes. For the tank measured in autumn 2018, the values were 1942.83 ± 0.40 ppb and -49.6 ± 3.6 ‰, for CH_4 and $\delta^{13}CH_4$, respectively. In December 2018, the gas tank had to be refilled and for the new gas, values were 2026.89 ± 0.54 ppb and -50.1 ± 3.5 ‰, for CH_4 and $\delta^{13}CH_4$, respectively (Figure S2). In both cases, the analyzer was stable and no detectable influence of switching on/off the instrument was observed.

Table S3. Used calibration factor

Compound	slope	intercept
CH_4 [ppb]	0.9873	46.413
$\delta^{13}CH_4$ [‰]	0.9153	2.2578

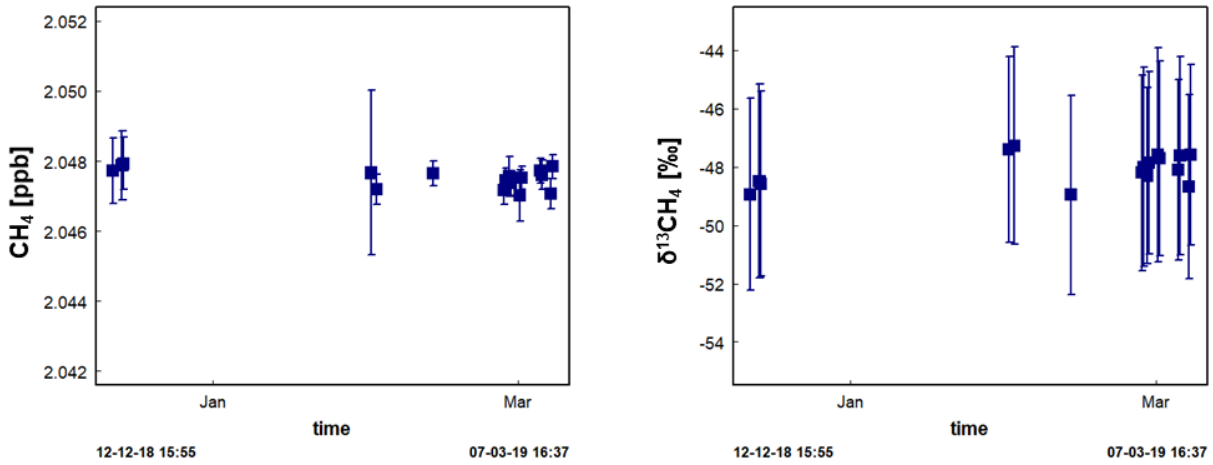

Figure S2. Values obtained during tank measurement before/after mobile measurements between December 2018 and March 2019. All uncertainties are applied (1 standard deviation), **left:** CH_4 over the time; **right:** $\delta^{13}CH_4$ over the time.

Supporting Section 4: Isotopes measurements

During this study, the isotopic composition of specific leak indications was measured in situ by CRDS G2201-i using the storage tube so-called AirCore [5]. This sampler tube allows to obtain a better time resolution and accuracy for $^{13}CH_4$ and therefore allows to estimate more precisely in situ the isotopic signature associated with a detected leak indication of CH_4 [6]. In

this study, the AirCore is built from 50 m of coiled Synflex tube with 3/8" inner diameter (Figure S3). Air is dried at the outlet of the AirCore using a 50 cm^3 cylinder filled with magnesium perchlorate. The AirCore is continuously flushed with air from the inlet. Using this tool, two measurements modes can be used alternatively: monitoring and replay mode. In the monitoring mode, the air is analyzed directly from the inlet in the CRDS analyzer. When a significant methane leak indication (at least 500 ppb above background) is detected, after crossing the leak indication, the system is manually switched to the replay mode. Then, the air stored in the AirCore is measured at a lower flow rate than during the monitoring mode (Figure S4).

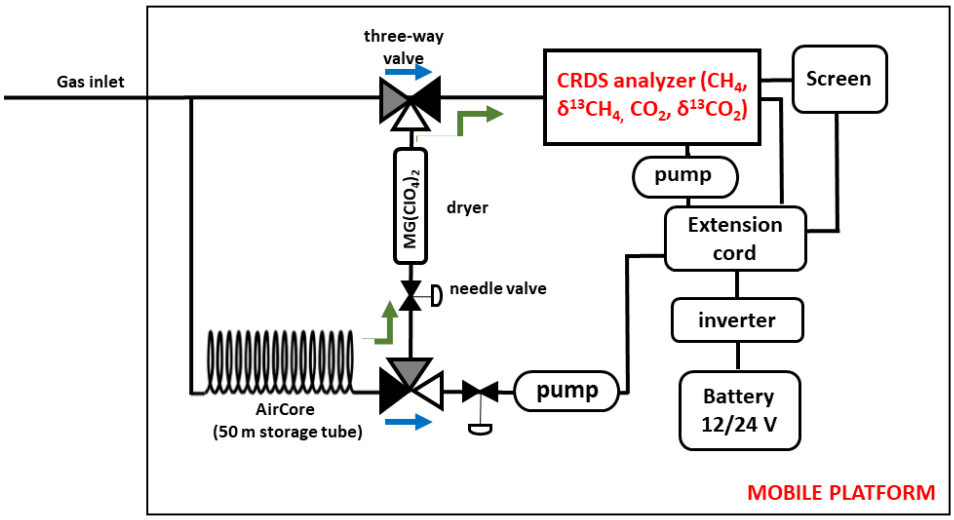

Figure S3. Scheme of AirCore tool used in the mobile platform. The blue arrows show the airflow in monitoring mode. The green arrows show the airflow in the replay mode.

The $\delta^{13}CH_4$ signatures are calculated using the Miller-Tans plot. It requires to subtract a background value, both for CH_4 and $\delta^{13}CH_4$. As the background around particular leak indications can be challenging to estimate in the urban environment, background values were calculated here as the mean value from the background immediately before and after the leak indication (called "local background") (Figure S4). We define a CH_4 enhancement above background as significant if its maximum mole fraction is higher than 500 ppb above local background. In total, 28 leak indications from 17 different sites met this criterion. We report here isotopic $\delta^{13}CH_4$ signature when the Miler-Tans approach yields a 1-sigma uncertainty less than 10‰ and a correlation coefficient r^2>0.85 in order to balance precise results and quantity of kept values. Only 12 from 28 AirCores samples fulfil these criteria. It allowed determining the isotopic signature of 11 leak indications, as for one leak indication 2 AirCore samples fulfilled the selection criteria.

Fitting of the observations was calculated as a linear regression type II (uncertainty of x- and y-axis influence fitting) with the ordinary least squares (OLS) method. Instead of calculating an average value from data obtained in replay mode, like in previous papers [2,7] (Hoheisel et al. – 15 s averaging time; Lopez et al. 2017 – 10 s averaging time), data were grouped in 50 ppb bins.

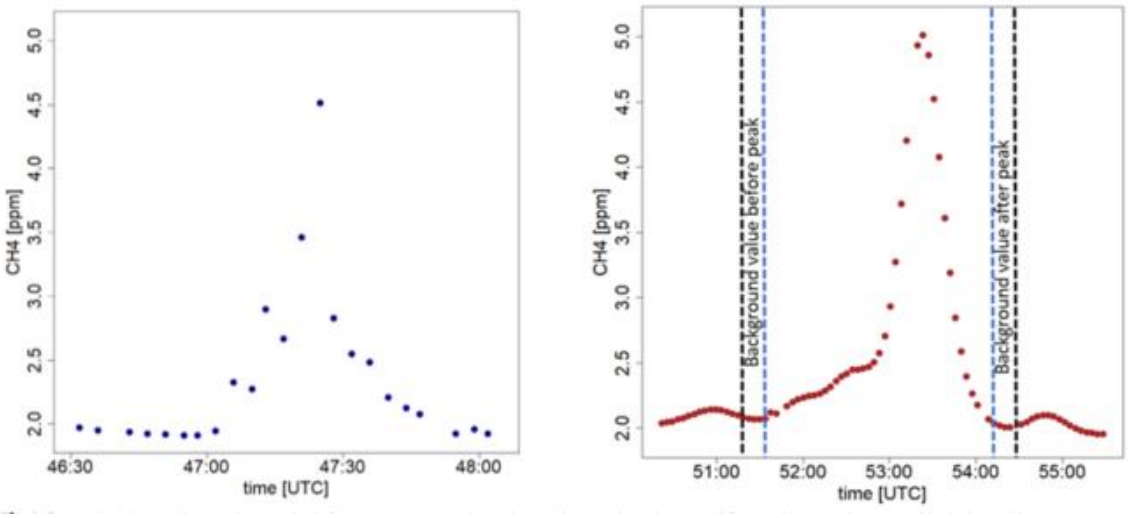

Figure S4. Example of measurements obtained in monitoring mode (**left**) and replay mode (**right**); data in replay mode used for analysis are between the black dotted line. Data between black and blue dotted lines are used to calculate background

References S2 and S4

(1) Ars, S.; Broquet, G.; Yver Kwok, C.; Roustan, Y.; Wu, L.; Arzoumanian, E.; Bousquet, P. Statistical Atmospheric Inversion of Local Gas Emissions by Coupling the Tracer Release Technique and Local-Scale Transport Modelling: A Test Case with Controlled Methane Emissions. Atmospheric Measurement Techniques 2017, 10 (12), 5017–5037. https://doi.org/10.5194/amt-10-5017-2017.

(2) Lopez, M.; Sherwood, O. A.; Dlugokencky, E. J.; Kessler, R.; Giroux, L.; Worthy, D. E. J. Isotopic Signatures of Anthropogenic CH4 Sources in Alberta, Canada. Atmospheric Environment 2017, 164, 280–288. https://doi.org/10.1016/j.atmosenv.2017.06.021.

(3) Zazzeri, G.; Lowry, D.; Fisher, R. E.; France, J. L.; Lanoisellé, M.; Grimmond, C. S. B.; Nisbet, E. G. Evaluating Methane Inventories by Isotopic Analysis in the London Region. Scientific Reports 2017, 7 (1). https://doi.org/10.1038/s41598-017-04802-6.

(4) Fisher, R.; Lowry, D.; Wilkin, O.; Sriskantharajah, S.; Nisbet, E. G. High-Precision, Automated Stable Isotope Analysis of Atmospheric Methane and Carbon Dioxide Using Continuous-Flow Isotope-Ratio Mass Spectrometry. Rapid Communications in Mass Spectrometry 2006, 20 (2), 200–208. https://doi.org/10.1002/rcm.2300.

(5) Karion, A.; Sweeney, C.; Tans, P.; Newberger, T. AirCore: An Innovative Atmospheric Sampling System. J. Atmos. Oceanic Technol. 2010, 27 (11), 1839–1853. https://doi.org/10.1175/2010JTECHA1448.1.

(6) Rella, C. W.; Hoffnagle, J.; He, Y.; Tajima, S. Local- and Regional-Scale Measurements of CH4, Δ13CH4, and C2H6 in the Uintah Basin Using a Mobile Stable Isotope Analyzer. Atmospheric Measurement Techniques 2015, 8 (10), 4539–4559. https://doi.org/10.5194/amt-8-4539-2015.

(7) Hoheisel, A.; Yeman, C.; Dinger, F.; Eckhardt, H.; Schmidt, M. An Improved Method for Mobile Characterisation of Δ13CH4 Source Signatures and Its Application in Germany. Atmospheric Measurement Techniques 2019, 12 (2), 1123–1139. https://doi.org/10.5194/amt-12-1123-2019.

Supporting Section 5: Walking measurements with LGR MGGA

Over the measurement period, LGR MGGA was available for four days. This instrument was used to find the exact source and location of leak indications observed from the car. The instrument was used two days in cluster area A, one day in cluster area B and one day in the north-east part of Paris. In the case of the measurements in cluster area A, the car was parked twice about two hours and then walking measurements were made (limitation of the instrument battery capacity). With this approach, the daily distance of walking measurements was equal

to 7 km. In total, in cluster area A, 14 km by walking was made. The same streets were driven and walked on the same day. During the rest of the measurements, which were made in cluster area B and north-east part of Paris, after crossing the leak indication, if it was possible, the car was stopped and we went walking with LGR MGGA to find exact location and source of the leak indication observed from the car.

Supporting Section S6: Maps of observed enhancement above background

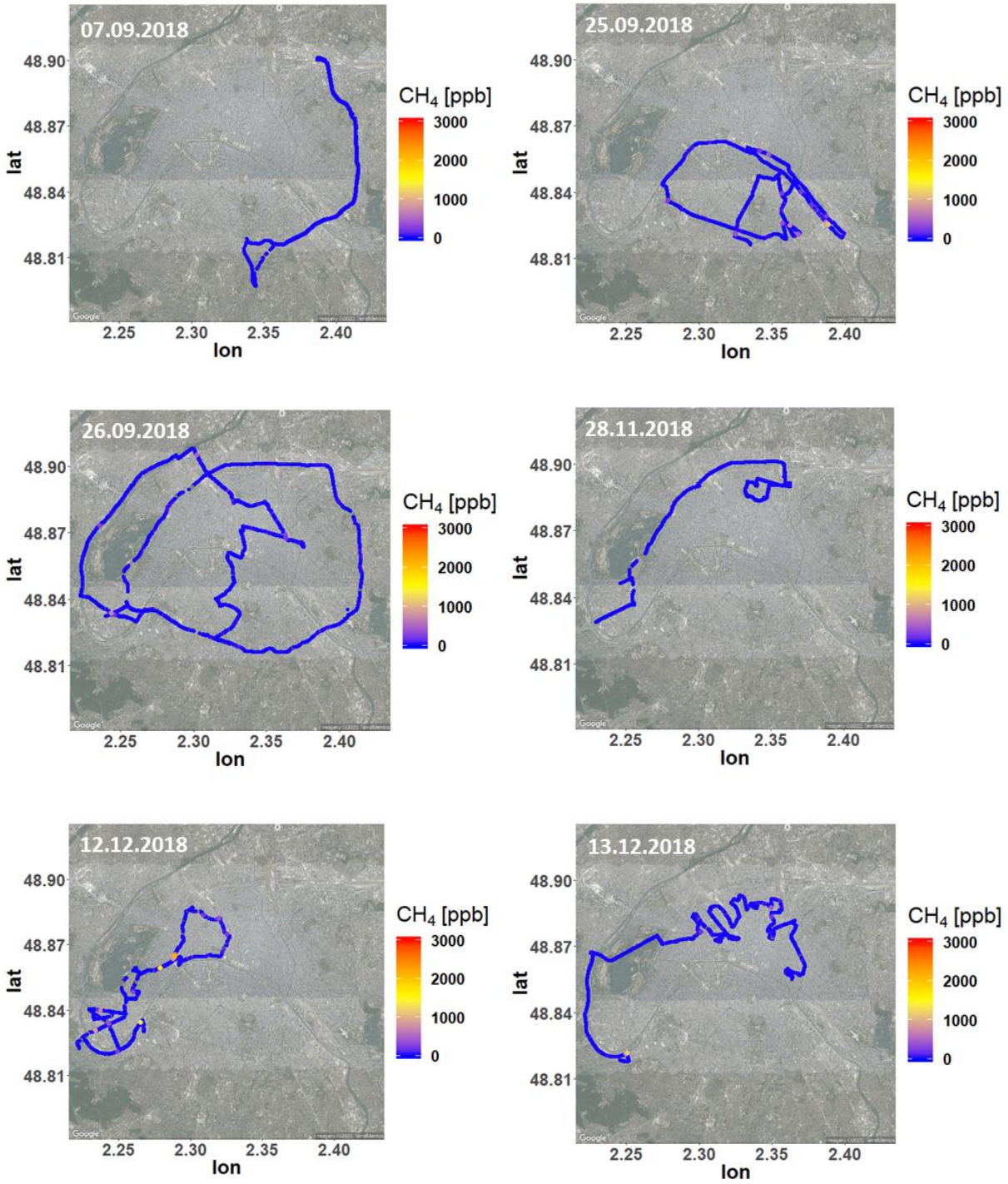

Figure S5. Daily maps of car measurements. Enhancement above background is in the range 0 – 3000 ppb. Mobile measurements were performed with CRDS G2201-i. Days 1-6 are presented.

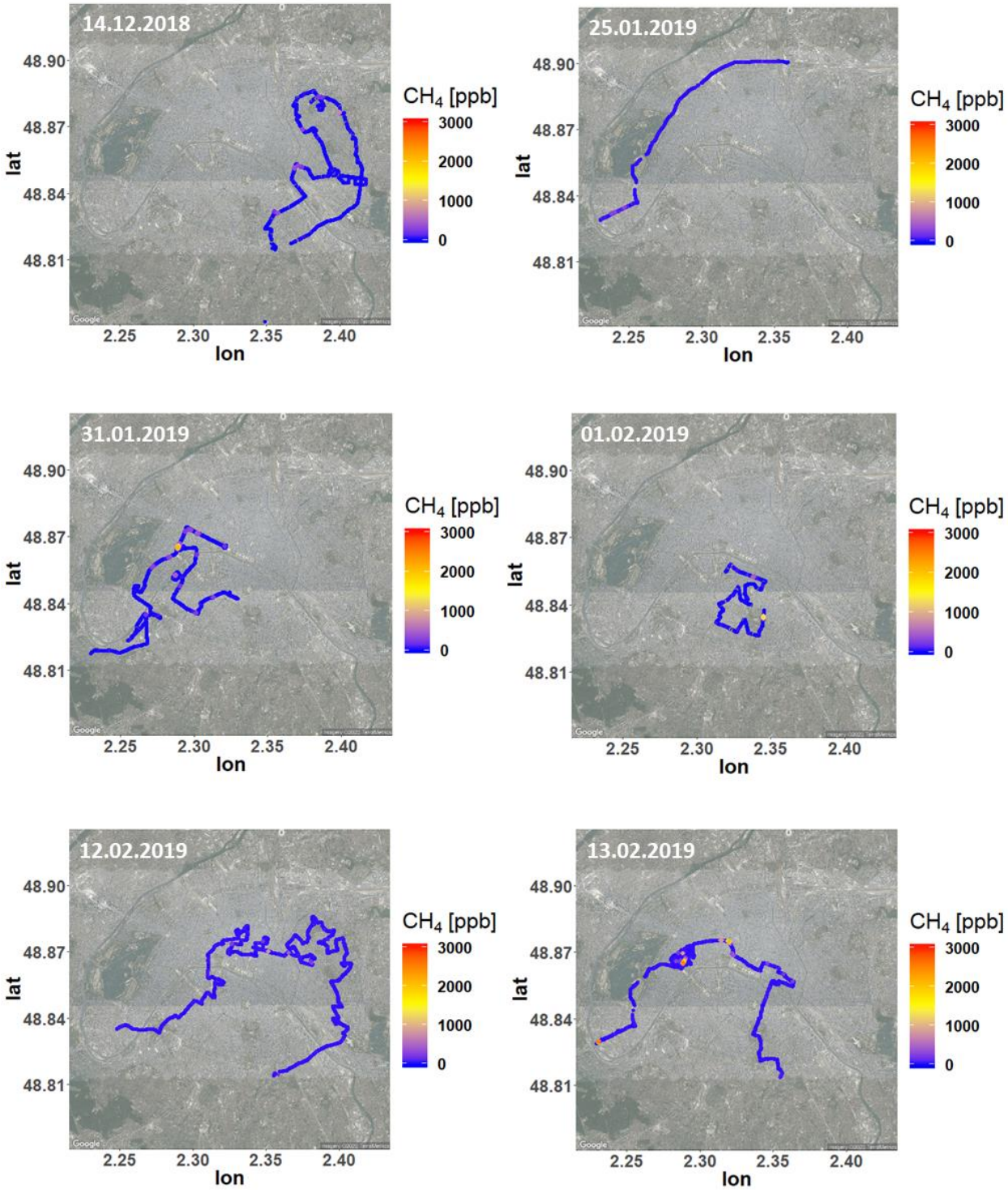

Figure S6. Daily maps of car measurements. Enhancement above background is in the range 0 – 3000 ppb. Mobile measurements were performed with CRDS G2201-i. Days 7-12 are presented.

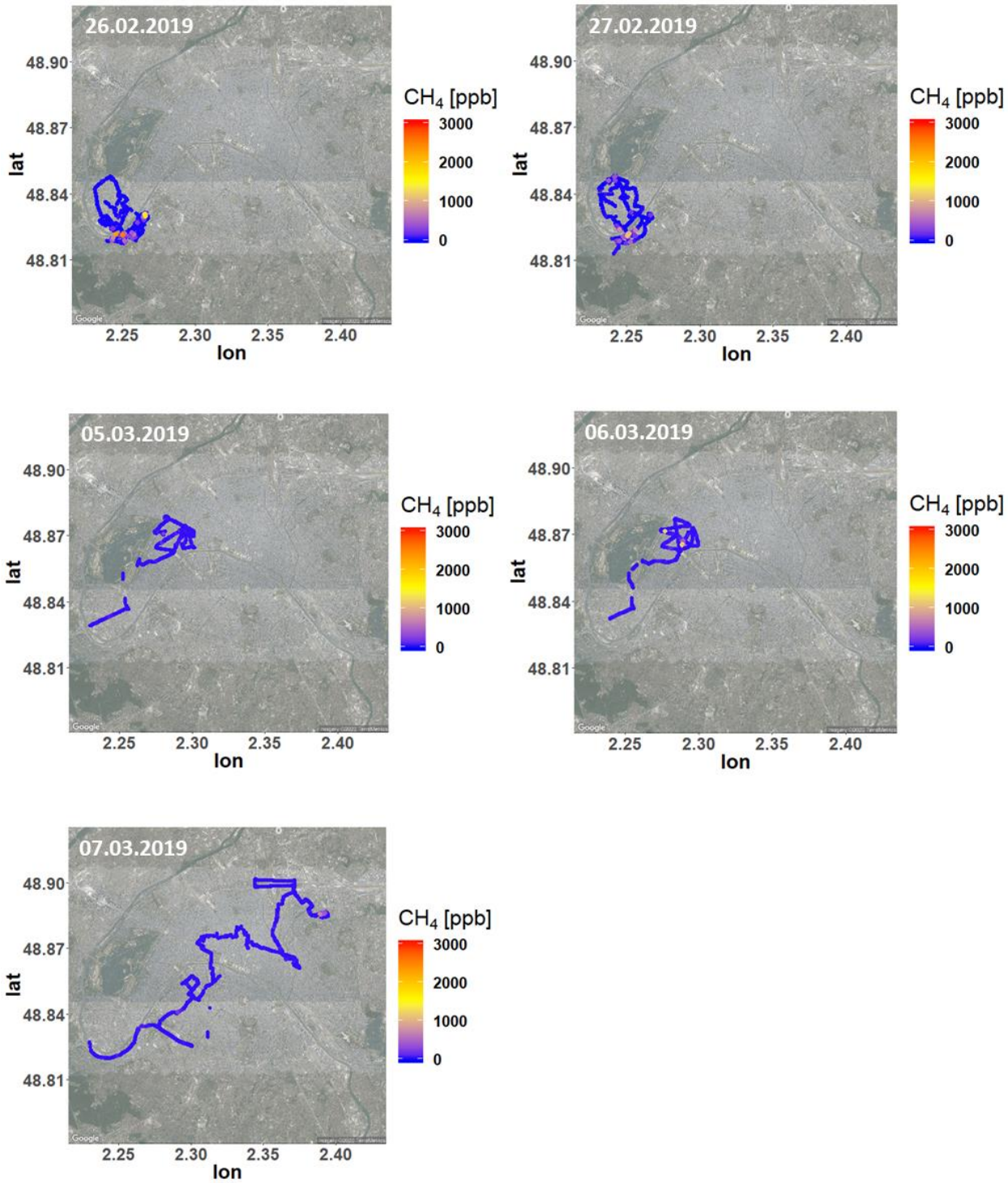

188 **Figure S7.** Daily maps of car measurements. Enhancement above background is in the range
189 0 – 3000 ppb. Mobile measurements were performed with CRDS G2201-i. Days 13-17 are
190 presented.

Supporting Section S7: Source type determined by mobile car measurements and walking measurements

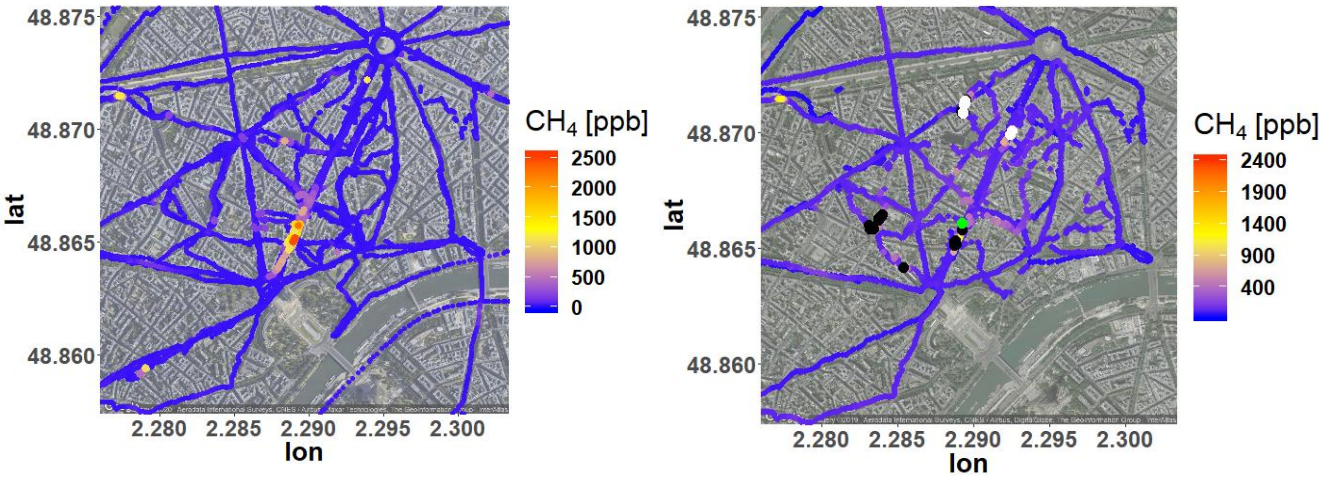

Figure S8. Cluster area A, enhancement above background is in the range 0 – 2500 ppb. **Left:** car mobile measurements with CRDS G2201-i, performed between 07.09.2018 and 07.03.2019. **Right:** combined car mobile measurements with CRDS G2201-i and walking measurements with LGR MGGA, made in March 2019. Direct sampling from the source during walking measurements is represented by black points (1000 ppb -2000 ppb above daily background), green points (2000 ppb -2730 ppb above daily background) and white points (>2730 ppb above daily background)

Figure S9. Emission from the sewage sector in cluster area B, 27.02.2019

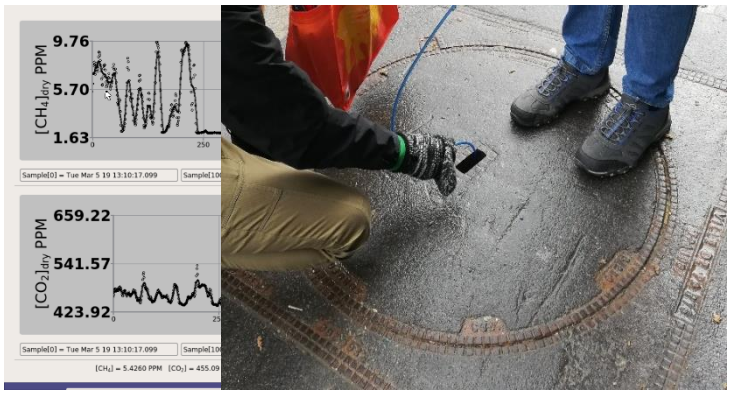

Figure S10. Emission from the natural gas distribution network in cluster area A, 05.03.2019

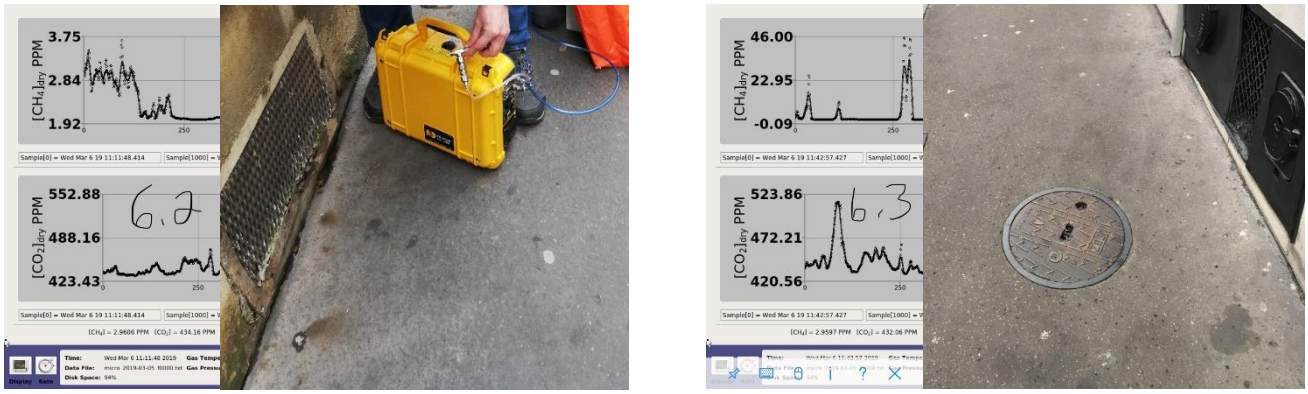

Figure S11. Emission from the buildings' boiler room ventilation (furnaces) in cluster area A, 05.03.2019

Table S4. Determined isotopic signature using AirCore

Date	CH_4 [ppb]	$\delta^{13}CH_4$]‰[	r2	latitude	longitude	n	source
31-01-2019	4170	-42.7 ± 1.8	0.95	48.86571	2.28928	1	furnaces
12-02-2019	2316	-52.2 ± 8.1	0.95	48.86996	2.35164	1	sewage
13-02-2019	2794	-49.2 ± 8.9	0.86	48.86573	2.28594	1	gas leak
13-02-2019	4000	-36.4 ± 2.6	0.95	48.86503	2.28892	2	furnaces
13-02-2019	2707	-50.8 ± 6.0	0.92	48.86949	2.28842	1	sewage
26-02-2019	3098	-55.5 ± 3.4	0.97	48.8202	2.24547	1	sewage
26-02-2019	2727	-57.5 ± 6.8	0.92	48.83062	2.26566	1	sewage
26-02-2019	3982	-52.4 ± 3.1	0.96	48.82142	2.25007	1	sewage
27-02-2019	2953	-59.5 ± 8.1	0.92	48.82453	2.24583	1	sewage
27-02-2019	3222	-53.4 ± 2.2	0.97	48.82251	2.25216	1	sewage
07-03-2019	2805	-39.5 ± 5.0	0.86	48.88578	2.38904	1	furnaces

Supporting Section S8: Daily measurements over time

Here (Figure S12) examples of two measurements days are presented: 12.12.2018 and 26.02.2019. The background is calculated as 2 minute's running average. Enhancement bigger than 10% of the background is treated as a leak indication detection threshold.

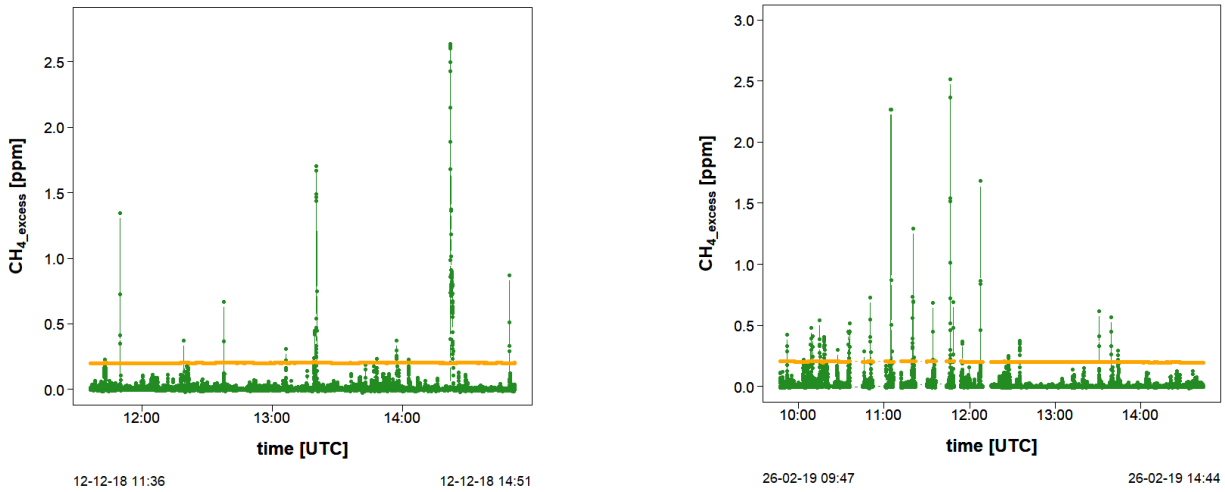

Figure S12. Example of the daily CH_4 enhancement above daily background over time. The orange line is the detection threshold, calculated as 10% of the background. **Left:** 12.12.2018 (5th measurement day), **Right:** 26.02.2019 (10th measurement day). In the case of the measurements made 26.02.2019, the AirCore measurements are removed from the plot.

Supporting Section S9: Excluding road transport

We exclude here mobile sources from road transport. Ideally, exhaust CO_2 could be used to distinguish this type of methane emission from the others. However, in Paris city, due to a large number of cars and different type of fuel used, CO_2 mixing ratio vary a lot and cannot be used as reliable information in this urban environment. We developed a method based on non-stationarity. When a road was passed twice in a short interval, and if an enhancement is identified only on one pass, then we consider this enhancement as related to a non-stationary source such as transport. The interval is short enough to neglect possible change in wind direction. Overall, using this selection method, only one leak indication was rejected from the analysis.

Appendix B

Résumé substantiel en français

Sujet de l'étude À l'échelle mondiale, les émissions de CH_4 sont relativement bien estimées. Cependant, la caractérisation des sources de CH_4 à l'échelle locale n'est pas encore suffisante et elle nécessite une analyse plus approfondie (Dlugokencky et al. 2011). Selon le rapport du GIEC, les émissions anthropiques de CH_4 sont en partie associées aux zones urbaines (GIEC, 2006). Les zones urbaines et suburbaines contribuent à hauteur de 30 à 40 % aux émissions anthropiques de gaz à effet de serre et concentrent plus de 50 % de la population mondiale. Cependant, ces zones couvrent seulement 2 % de la surface de la Terre.

Il est prévu que la population urbaine doublera d'ici 2050 (Satterthwaite, 2008 ; Duren et Miller, 2012). En outre, un écosystème urbain est un cas complexe, où de nombreuses sources différentes coexistent : réseaux de pétrole et de gaz naturel, système de chauffage/refroidissement, décharges et traitement des déchets, eaux usées et transport routier (Gioli et al. 2012 ; Townsend-Small et al. 2012 ; Zazzeri et al. 2017). Aux États-Unis, dans les mégalopoles comme Los Angeles, Boston et Washington, les principales sources de CH_4 sont les fuites de combustibles fossiles (Townsend-Small et al. 2012 ; Jackson et al. 2014 ; McKain et al. 2015) et une situation similaire a été observée à Florence, en Italie (Gioli et al. 2012). Cependant, dans le cas de Londres, ce sont les décharges et le secteur du traitement des déchets qui sont les principales sources de CH_4 (Lowry et al. 2001 ; Fisher et al. 2006).

En France, la région Île-de-France (l'IDF) est l'une des sources urbaines les plus importantes de CH_4 (nombre d'habitants : 12,14 millions, Paris contribuant à 18% de la population de l'IDF). En 2015, selon les inventaires, les émissions totales de CH_4 dans la région Ile de France étaient égales à 30 kt CH_4 an^{-1}. Les émissions des secteurs de traitement des déchets et de l'énergie sont les principales sources de méthane à l'échelle régionale en IDF et représentent respectivement 42 % et 31 % de ces émissions. Les émissions de méthane dans l'IDF nécessitent cependant des estimations indépendantes, source par source, utilisant des mesures atmosphériques.

L'objectif principal de ma thèse est une caractérisation des variations spatio-temporelles de la fraction molaire et de la signature isotopique du CH_4 en Île-de-France et d'en déduire les émissions de méthane à l'échelle des sites et des villes. Pour atteindre cet objectif, j'étais responsable de la conception, la réalisation et l'analyse de campagnes de terrain. Les concentrations en CH_4 et la signature isotopique de CH_4 ont été mesurés à l'aide d'une plate-forme de mesure mobile, constituée d'un analyseur CRDS (Cavity Ring-Down Spectroscopy - Spectroscopie en Cavité Résonante) embarqué dans une voiture (Figure B1) et de l'outil AirCore qui permet de remesurer l'air stocké pour des situations choisies avec une meilleure définition, rendant ainsi possible les mesures in-situ de $\delta^{13}CH_4$.

La stratégie choisie conduit à la caractérisation du méthane atmosphérique, suivie par des estimations des émissions à l'aide de la méthode de dispersion des traceurs et d'outils de modélisation. L'étude est menée à l'échelle de la ville et du site, car les mesures à petite échelle jouent un rôle clé pour expliquer les incertitudes sectorielles et peuvent contribuer à améliorer le bilan régional du méthane. Cet objectif est une étape nécessaire et importante pour améliorer les estimations des sources de méthane dans la région de l'IDF. En conséquence, ces objectifs visent à contribuer à l'amélioration des inventaires d'émissions, à réduire l'écart entre les études top-down et bottom-up et à donner des indications pour concevoir des mesures de réduction des GES plus

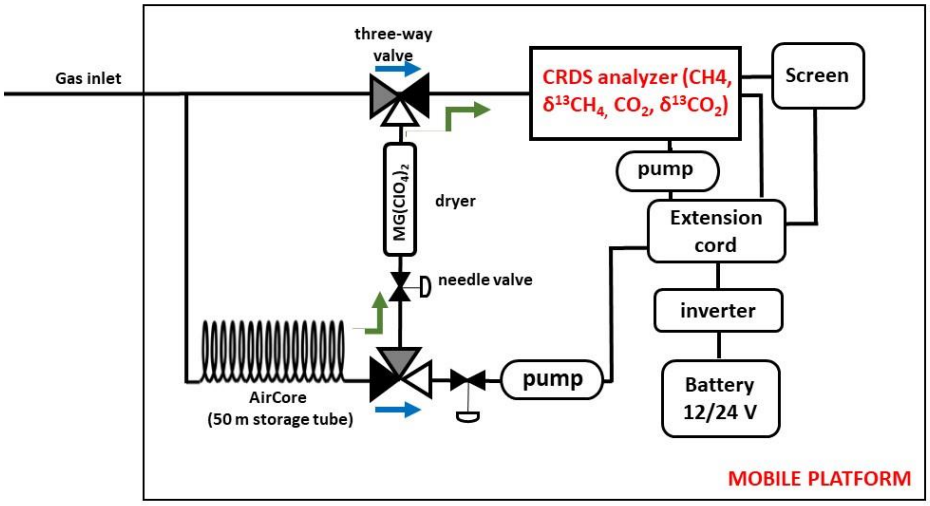

efficaces.

Figure B1 Schéma de la configuration de mesure mobile. Les flèches bleues indiquent le débit d'air en mode surveillance. Les flèches vertes indiquent le débit d'air en mode relecture.

Instruments et méthodes. La configuration et les tests de l'instrument que j'ai effectués ont montré la capacité de l'instrument CRDS G2201-i à réaliser des mesures mobiles à proximité des sources de méthane (Chapitre 2). La répétabilité des mesures en continu (CMR) (également appelée "précision") et les déviations d'Allan à 10 s, 60 s et 60 min sont inférieures à 1 ppb. Les CMRs et les déviations d'Allan sont beaucoup plus faible que l'excès de concentration en méthane à l'intérieur d'un panache de CH_4 à proximité de la plupart des sources ponctuelles. De plus, la stabilité de l'instrument a été estimée à moins de 1 ppb lors de tests de répétabilité à court et à long terme. Pour $\delta^{13}CH_4$, le CMR du CRDS G2201-i est d'environ 3,5 ‰ pour la concentration ambiante de CH_4. Elle s'améliore à 0,7 ‰ avec l'augmentation de la concentration de CH_4 à environ 10 ppm (Figure B2). Par conséquent, en utilisant le CRDS avec l'outil AirCore, il est possible de séparer les signatures typiques d'origine biogénique ou thermogénique du méthane avec une précision de 5 ‰ sur site pour des panaches de CH_4 500 ppb au-dessus des concentrations de fond. La précision de $\delta^{13}CH_4$ s'améliore à 1 ‰ pour des panaches à 8 ppm d'excès de CH_4 au-dessus des concentrations de fond.

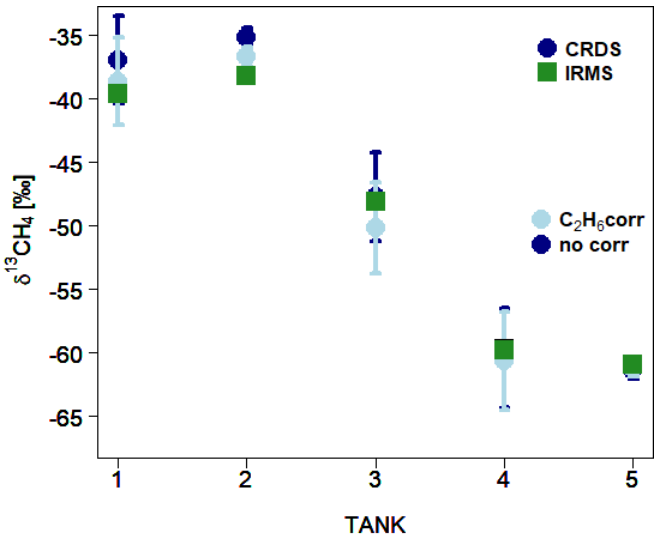

Figure B2 Comparaison $\delta^{13}CH_4$ valeur IRMS et CRDS, avec calibration de CRDS 2072 et correction C_2H_6, les barres d'erreur représentent 1 écart-type

Pendant les mesures mobiles, le CRDS G2201-i avec l'outil AirCore a été utilisé pour déterminer les signatures isotopiques. Les données recueillies ont été regroupées par intervalles de 50 ppb et analysées selon l'approche Miller-Tans (Miller and Tans 2003). Ensuite, les échantillons dont le coefficient de corrélation r^2 était inférieur à 0,85 et dont l'incertitude était supérieure à 10 ‰ ont été rejetés de l'analyse ultérieure, afin d'optimiser les résultats précis et la quantité de valeurs conservées. Ces critères ont été appliqués pour les sources à Paris et sur des sites industriels (décharges et stations de compression de gaz). Lors des études sur les sites industriels, l'excès de CH_4 au-dessus des concentrations de fond était généralement plus élevée que pour les études à l'intérieur de la ville. En conséquence, la précision de $\delta^{13}CH_4$ était meilleure, et pour la plupart des échantillons sélectionnés pour une analyse ultérieure, elle n'a pas dépassé 6 ‰.

J'ai également évalué la possibilité d'utiliser le CRDS G2201-i sur le terrain pour déterminer le ratio éthane:méthane (C_2H_6:CH_4, Chapitre 3). L'étude est présentée dans un article publié en discussion ouverte dans une revue à comité de lecture (doi.org/10.5194/amt-2020-410). Le travail a été réalisé en trois étapes. Lors des tests en laboratoire, pour l'éthane, la CMR était égale à 50 ppb, et la déviation d'Allan était égal à 25 ppb pour les données brutes. Les valeurs de fond typiques du C_2H_6 varient entre 0,6 ppb et 3 ppb, le ratio signal/bruit est donc insuffisant pour caractériser la variabilité de l'air ambiant. Cependant, l'expérience de diffusion contrôlée et le travail sur le terrain ont montré une concordance entre le ratio éthane:méthane observé et diffusé. Au cours des tests effectués, le ratio C_2H_6:CH_4 diffusé a varié entre 0,0355 et 0,0758. Dans tous les cas, l'incertitude des valeurs observées par le CRDS G2201-i était inférieure à 0,01. Dans le cas de la diffusion contrôlé de gaz, le ratio observé a été sous-estimé par rapport à la valeur diffusée. Cette différence a varié entre -0,018 et -0,002 (figure B3). Les différences entre les valeurs mesurées et les valeurs diffusées étaient plus faibles pour la mesure effectuée dans les stations de compression de gaz et plus symétriquement réparties sur la valeur diffusée. Dans ce cas, les résidus entre la valeur diffusée et la valeur observée étaient compris entre -0,006 et 0,009. Sur la base de ces tests, le CRDS G2201-i peut déterminer le ratio C_2H_6:CH_4 avec une précision suffisante (inférieure à 0,01) si la voiture est arrêtée pendant les mesures. Cela peut être fait soit en restant un certain temps à l'intérieur du panache de CH_4, soit par l'outil AirCore. L'air doit être séché avant les mesures, et l'excès de CH_4 doit être supérieur à 1 ppm au-dessus des

concentrations de fond. La concentration en C_2H_6 observée doit être corrigé pour tenir compte de l'interférence d'autres espèces et calibrée car l'instrument n'est pas dédié aux mesures de C_2H_6. Ainsi, le CRDS G2201-i peut être utilisé pour le C_2H_6:CH_4 dans ces conditions spécifiques.

Figure B3. C_2H_6:CH_4 observé en utilisant G2201-i dans le cadre d'une installation mobile. A gauche : mesuré debout à l'intérieur des panaches. A droite : mesuré à l'aide d'AirCore. Points rouges : C_2H_6:CH4 diffusé connu. Les barres d'erreur représentent 1σ d'écart-type. Les incertitudes des valeurs

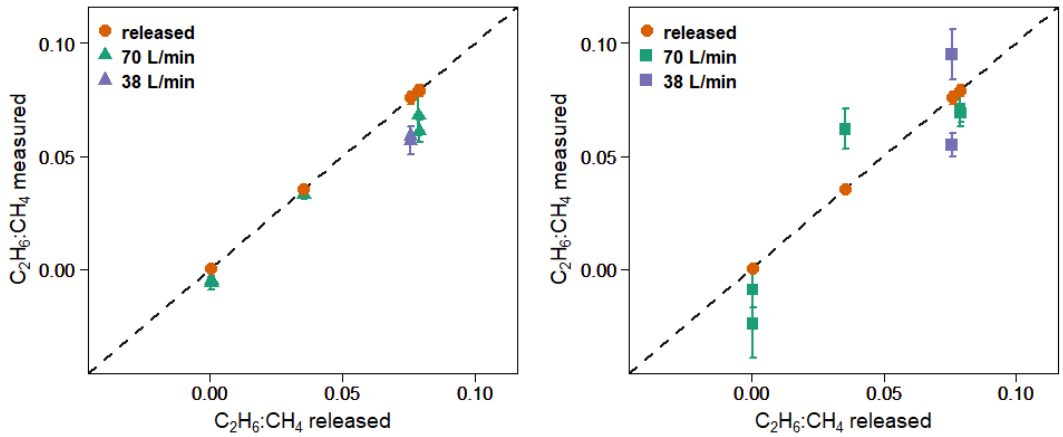

diffusées sont invisibles sur le graphique.

Émissions de Paris Les études de CH_4 à Paris sont présentées dans un article en phase de révision dans une revue à comité de lecture (Chapitre 4). Grâce à la plate-forme mobile, entre septembre 2018 et mars 2019, 17 études ont été réalisées à Paris, et 500 km de routes ont été visités (Figure B4). De plus, 28 AirCores provenant de 17 endroits ont été échantillonnés pendant ces séances de mesure. Sur la base des critères définis plus tôt, 12 échantillons AirCore provenant de 11 sites ont été utilisés pour caractériser l'origine du CH_4 à Paris. Le $\delta^{13}CH_4$ dans sept endroits était plus appauvri (< -50 ‰) et attribué aux émissions biogéniques, tandis que dans quatre endroits, le $\delta^{13}CH_4$ était plus enrichi (> -50 ‰) et attribué à des sources thermogéniques. De plus, des mesures à pied avec le modèle d'analyseur MGGA de Los Gatos Research (LGR) ont été effectuées pendant quatre jours à Paris. Elles ont permis de mesurer les panaches de CH_4 des couvertures des réseaux d'égouts et de gaz naturel. En complément, des émissions de CH_4 ont été observées sortant des grilles de ventilation des chaufferies des bâtiments. Dans ce cas, les émissions proviennent probablement de chaudières qui fuient. Au total, 90 indications de fuites ont été observées à Paris. Vingt-sept d'entre elles ont été attribuées à trois sources : fuites de gaz, eaux usées et chaudières, sur la base de la signature isotopique et des mesures de marche. La catégorie des chaudières n'avait pas été rapportée auparavant dans les études portant sur les émissions de CH_4 de la ville (par exemple, Townsend-Small et al. 2012 ; Jackson et al. 2014 ; McKain et al. 2015 ; von Fischer et al. 2017 ; Zazzeri et al. 2017) et cette catégorie a été découverte lors des mesures à pied. Dans le cas des indications de fuites visibles depuis la route, les fuites de gaz constituent 66 % d'entre elles et les eaux usées - 34 %. Cette proportion est extrapolée pour les 63 autres indications de fuites d'origine inconnue. Au total, sur la base de cette hypothèse, 56 indications de fuites sont déterminées comme étant des fuites de gaz, 30 comme venant des eaux usées et 4 comme venant des chaudières.

À Paris, deux clusters d'émissions ont été trouvés avec une plus grande quantité d'indications de fuites détectées. 22 % des indications de fuites proviennent de la zone A et 56 % de la zone B. Ces zones ne représentent que 10 % (zone A) et 20 % (zone B) du km unique de la zone étudiée.

Sur la base de l'équation proposée par von Fischer et al. (2017) et Weller et al. (2019), le taux d'émission des indications de fuites déterminées est calculé et atteint 140 L CH_4 min^{-1} sur 90 indications de fuites. Ce taux d'émission a été extrapolé à toute la longueur du réseau routier (1800 km) de la ville de Paris et a été trouvé égal à 500 L CH_4 min^{-1} (190 t CH_4 an^{-1}). Sur la base de notre hypothèse d'attribution, 56% des émissions observées à Paris sont attribuées à des fuites dans le réseau de distribution de gaz naturel (106 t CH_4 an^{-1}), ce qui est quinze fois moins que dans l'inventaire AIRPARIF. Le taux d'indication des fuites de gaz (nombre d'indication de fuites de gaz/km de rues empruntées) a été trouvé égal à 0,11 km^{-1}.

Dans l'ensemble, les résultats concernant le taux de fuite à Paris sont deux à quatre fois plus faibles que les taux calculés pour les villes disposant d'un ancien système de canalisation aux États-Unis et deux à quarante fois plus élevés que ceux des villes disposant d'un système de canalisation moderne aux États-Unis (von Fischer et al. 2017). Concernant les études précédentes (McKain et al. 2015 ; Jackson et al. 2014 ; Lamb et al. 2016 ; von Fischer et al. 2017), le nombre de fuites de gaz dans les villes américaines disposant d'un ancien réseau de gazoducs sujets à la corrosion (Boston, New York, Staten Island et Syracuse) est plus élevé que dans les villes ayant une plus grande proportion de systèmes de distribution basse pression en plastique ou en acier protégé (Burlington et Indianapolis). Dans le cas de l'étude réalisée par von Fischer et al. (2017), les taux de fuite varient de 0,004 fuite km^{-1} (Indianapolis) à 0,63 fuite km^{-1} (Staten Island).

Sur la base de nos conclusions, une limitation efficace des émissions de CH_4 en région parisienne pourrait être obtenue en réduisant les sources liées aux eaux usées et en traitant les points chauds détectés. Actuellement, les émissions de CH_4 provenant du secteur des eaux usées sont omises dans l'inventaire AIRPARIF. En outre, les émissions des chaudières n'ont pas été observées dans les études précédentes dans les villes (par exemple, Townsend-Small et al. 2012 ; Lamb et al. 2016 ; von Fischer et al. 2017 ; Zazzeri et al. 2017). Cette catégorie devrait donc faire l'objet d'une étude plus approfondie. Dans le cas du réseau de distribution de gaz naturel, 40 km de gazoducs sont rénovés chaque année, ce qui diminue les émissions de CH_4 du réseau de distribution de gaz naturel (GRDF sur Twitter 2019 ; La Tribune 2019).

Les mesures dans la ville de Paris ont été répétées durant l'été 2019 (figure B4). En cinq jours, 200 km de rues ont été traversés. Au total, trente-six indications de fuite ont été observées. 9 échantillons AirCore ont été prélevés, et 6 d'entre eux ont été utilisés pour des analyses ultérieures. Trois d'entre eux ont été déterminés comme provenant d'eaux usées et deux comme des fuites de gaz. Le dernier était enrichi et observé seulement une fois et a donc été attribué au trafic. Contrairement aux campagnes précédentes, aucun panache de CH_4 n'a été observé dans le cluster A. Sur 36 indications de fuites, le taux d'émission est égal à 41 L CH_4 min^{-1}. Ensuite, après extrapolation à l'ensemble des rues de Paris, le taux d'émission total est égal à 370 L CH_4 min^{-1} (140 t CH_4 min^{-1}) (Tableau B1). Bien qu'ayant le même ordre de grandeur, il est inférieur d'environ 50 t CH4 au taux d'émission observé lors de la première campagne. Il peut être dû aux émissions des chaudières qui sont moins utilisées pendant l'été ou aux rénovations du réseau de gaz naturel. L'écart observé peut également être dû à des biais d'échantillonnage, car durant l'été, seules 5 études ont été réalisées et certaines sources de CH_4 ont pu être omises.

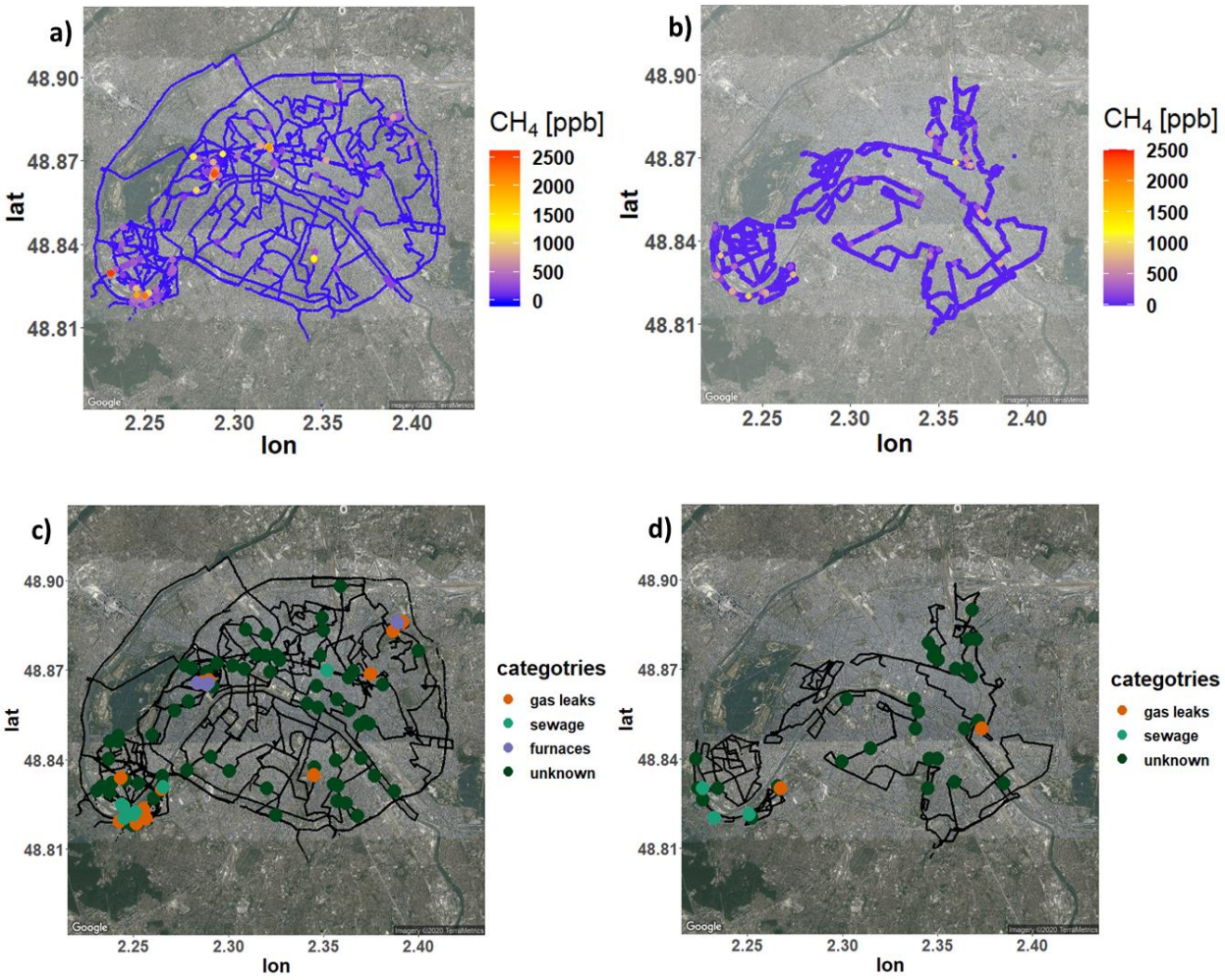

Figure B4 Comparaison entre la concentration de CH_4 observée entre septembre 2018 et mars 2019 (parcelles a) et c)) et de l'été 2019 (parcelles b) et d)). En haut : la concentration de CH_4 observée au-dessus des concentrations de fond. En bas : indications de fuite déterminées

Table B1 Comparaison du CH_4 observé à Paris entre septembre 2018 et mars 2019 avec l'été 2019

Caractéristique	septembre 2018 et mars 2019	l'été 2019
Nombre d'études	17	5
Km de rues traversés	500	200
Détection de panaches de CH4 (cluster A, cluster B))	90 (13, 32)	36 (0, 12)
Taux d'émission extrapolé à la totalité du réseau routier parisien	190 t/yr	140 t/yr
Taux d'émission moyen des fuites [L/min]	1.56 (0.47 – 10.50)	1.17 (0.46 – 4.49)
Taux d'émission médian [L/min]	0.86	0.81
Catégories de sources : petites(< 6 L/min,), moyennes (6-40 L/min)	88,2	36,0

Sites industriels Des mesures ont également été effectuées en dehors de Paris sur trois stations de compression de gaz et deux décharges (figure B5). Sur la base des mesures mobiles, les signatures isotopiques $\delta^{13}CH_4$ et δDCH_4, les taux d'émission de CH_4 et les ratios éthane/méthane ont été observés. Les $\delta^{13}CH_4$ mesurés sur les trois stations de compression de gaz étaient similaires et variaient autour de -43 ‰, (de -45,2 ± 6,2 ‰ à -40,1 ± 3,9 ‰). δDCH_4 variait de -179,4 ± 5,2 ‰ à -157,40 ± 0,66 ‰, et il est un peu inférieur que la moyenne mondiale pour les combustibles fossiles (-197 ‰) (Sherwood et al. 2017). Les observations de $\delta^{13}CH_4$ et δDCH_4 indiquent une origine thermogénique du gaz naturel utilisé dans la région de l'IDF, ce qui a été confirmé avec la société de l'opérateur de gaz naturel. Tant pour $\delta^{13}CH_4$ que pour δDCH_4, la plus grande incertitude a été observée pour la station de compression de gaz C. L'incertitude est probablement due à aux faibles concentrations observées sur ce site. L'échantillonnage effectué pour l'analyse isotopique a révélé que le maximum du panache de CH_4 variait d'environ 500 ppb au-dessus des concentrations de fond, ce qui correspond au minimum requis pour déterminer de manière robuste la signature isotopique du CRDS avec l'outil AirCore (Hoheisel et al. 2019).

Des signatures isotopiques différentes ont été observées dans deux décharges différentes. Pour la décharge D, la plus petite, le $\delta^{13}CH_4$ varie autour de -62,9 ± 1,9 ‰, tandis que pour la décharge E, il est d'environ -57,7 ± 5,2 ‰. Pour les deux décharges, $\delta^{13}CH_4$ est en bon accord avec les signatures isotopiques observées précédemment dans ces décharges par Xueref-Remy et al. (2019). Le δDCH_4 diffère plus, et il atteint -312,7 ± 4,6 ‰ pour la première décharge et -214,2 ± 2,7 ‰ pour la seconde. Le δDCH_4 observé sur la décharge E est plus enrichi que la moyenne mondiale (-317 ‰) (Sherwood et al. 2017). Les différences observées entre la signature isotopique des décharges D et E peuvent être dues à l'âge et à la composition des déchets stockés, car les deux peuvent affecter la production de méthane. La fermentation de l'acétate produit plus de méthane appauvri, tandis que l'oxydation du méthane peut produire plus de méthane enrichi. Ainsi, des signatures isotopiques plus enrichies suggèrent que les émissions de CH_4 sur la décharge E proviennent des couches supérieures, tandis que des signatures plus appauvries de la décharge D indiquent des émissions provenant de trous de forage qui fuient (Whiticar 1999 ; Chanton et Liptay 2000).

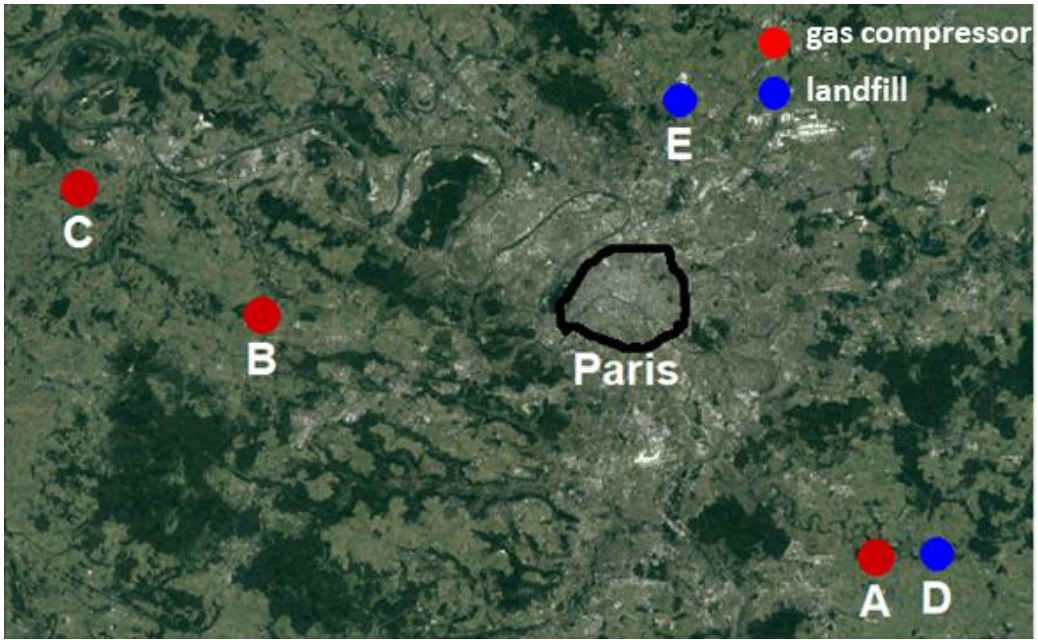

Figure B5 La localisation des décharges et des compresseurs de gaz étudiés pendant ma thèse

Un bon accord a été observé entre les valeurs obtenues à l'aide du CRDS in-situ avec l'outil AirCore et les échantillons prélevés dans des poches mesurées par IRMS. Cet accord augmente avec l'augmentation du panache de CH_4 observée, ce qui souligne à nouveau l'importance d'avoir un bon rapport signal/bruit. Il montre également que les méthodes AirCore peuvent être utilisées avec succès pour déterminer $\delta^{13}CH_4$, mais que la précision obtenue avec le CRDS est plus faible que celle obtenue avec l'instrument IRMS. Dans l'ensemble, le CRDS avec l'outil AirCore donne des signatures isotopiques fiables pour $\delta^{13}CH_4$. Il peut être utile, en particulier lorsqu'il est impossible d'arrêter la voiture pour prélever des échantillons, par exemple dans des endroits à forte circulation ou lorsque la direction instable du vent empêche de s'arrêter à l'intérieur du panache de CH_4.

Le ratio éthane/méthane a également été déterminé pour trois stations de compression de gaz et une décharge. Pour les stations de compression de gaz, le rapport C_2H_6:CH_4 varie entre 0,045 ± 0,008 et 0,060 ± 0,005. Les différences observées dans le ratio C_2H_6:CH_4 sont dues à la variation quotidienne du gaz naturel traité dans les stations de compression de gaz. Les différences observées peuvent également être causées par l'instrument utilisé, car le CRDS G2201-i n'est pas dédié aux mesures de l'éthane et la précision est de 0,01. Concernant les émissions de CH_4 des décharges, les décharges ne co-émettent pas d'éthane. En effet, lors des mesures effectuées sur la décharge D, la concentration de C_2H_6 détecté était dans les limites du bruit de l'instrument (50 ppb) et le ratio C_2H_6:CH_4 était égal à 0,000.

Enfin, les taux d'émission ont été estimés pour une journée de mesure dans deux stations de compression de gaz et une décharge. Dans le cas des stations de compression de gaz, le modèle gaussien dans la plate-forme Polyphémus a été utilisé. Pour les deux stations, les taux d'émission ont été calculés en utilisant les classes de stabilité A et B. Le taux d'émission de la station de compression de gaz A est environ trois fois supérieur à celui de la station de compression de gaz C. En utilisant la classe de stabilité A, le taux d'émission estimé atteint 2,5 ± 0,5 kg CH_4 h^{-1} pour le site A et 0,8 ± 0,1 kg CH_4 h^{-1} pour le site C. En utilisant la classe de stabilité B, les taux d'émission estimés ont atteint 1,7 ± 0,3 kg CH_4 h^{-1} et 0,55 ± 0,09 kg CH_4 h^{-1}, pour les sites A et C, respectivement. Les deux stations de compression de gaz ont chacune deux compresseurs et utilisent la même technologie. Le site C

fonctionne plus d'heures que le site A et il est peut-être mieux surveillé par l'entreprise propriétaire, ce qui explique que les émissions fugitives soient moins importantes sur le site C que sur le site A. De plus, les deux sites fonctionnaient peut-être dans des modes différents (compression, stand-by, …) lors des études, ce qui pourrait affecter les taux d'émission de CH_4 estimés.

Les estimations des émissions pourraient également être affectées par le choix de la modélisation. La distance de la source était inférieure à 100 m. Comme le rôle des turbulences augmente inversement à la distance, le taux d'émission estimé pourrait être plus biaisé que dans le cas idéal (Gifford 1968). En outre, le choix éventuellement erroné de la classe de stabilité pourrait conduire à une sous-estimation des taux d'émission (Caulton et al. 2018). Enfin, la modélisation gaussienne n'inclut pas la topographie, ce qui constitue une autre source de biais.

Le taux d'émission a également été mesuré dans la décharge D. Dans ce cas, la méthode de diffusion d'un traceur a pu être utilisée, ce qui a permis d'obtenir une estimation de 62 ± 13 kg de CH_4 h^{-1}. Par rapport aux résultats précédents (Ars 2017), le taux d'émission est plus faible. Il semble être en accord avec la politique de la société d'exploitation, qui tente de réduire les émissions de CH_4 de la décharge. Par rapport à la première étude, réalisée en 2016, le taux d'émission estimé a été divisé par quatre. La réduction observée est probablement un effet des mesures d'atténuation mises en œuvre sur les décharges, comme l'extension du réseau de collecte (réalisée entre septembre et novembre 2016) et le recouvrement des parties fermées avec des géomembrane (réalisé entre novembre et décembre 2016). D'autres campagnes sont nécessaires pour confirmer cette affirmation.

Tableau B2 Caractéristiques de trois compresseurs de gaz (A, B, C) et de deux décharges (D, E) d'IDF. $\delta^{13}CH_4$, δDCH_4 et C_2H_6:CH_4 sont présentés comme les valeurs moyennes de toutes les études pour chaque site.

site	**$\delta^{13}CH_4$ [‰] CRDS**	**$\delta^{13}CH_4$ [‰] IRMS**	**δDCH_4 [‰]**	**C_2H_6:CH_4 [ppm/ppm]**	**taux d'émission [kg CH_4 h^{-1}]**
Compresseurs de gaz A	-43.8 ± 6.8	-45.1 ± 1.1	-179.4 ± 5.2	0.053 ± 0.005	2.45 ± 0.50 (class A) 1.68 ± 0.34 (class B)
Compresseurs de gaz B	-42.1 ± 5.7	-43.9 ± 0.5	-157.40 ± 0.66	0.049 ± 0.009	-
Compresseurs de gaz C	-43.0 ± 8.4	-43.1 ± 3.7	-168 ± 21	-	0.81 ± 0.13 (class A) 0.55 ± 0.09 (class B)
Décharge D	-62.9 ± 1.9	-63.4 ± 1.4	-312.7 ± 4.6	0.000 ± 0.006	62 ± 13
Décharge E	-57.7 ± 5.2	-57.8 ± 0.5	-214.2 ± 2.7	-	-

Avec des mesures mobiles, le taux d'émission de CH_4 est estimé pour des durées courtes (par exemple quelques heures). Pour les stations de compression de gaz, le taux d'émission estimé varie en fonction des travaux de maintenance effectués à l'intérieur des installations (USEPA 2012 ; Zavala-Araiza et al. 2015 ; Saunois et al. 2020). D'après l'étude réalisée par Subramanian et al. (2015), les installations de gaz émettent du méthane à la fois en mode veille et en fonctionnement. En outre, une plus grande quantité de CH_4 atteint l'atmosphère dans des conditions anormales (par exemple, équipement

défectueux et événements irréguliers comme le dégazage pour raison de sécurité), qui peuvent changer sur une année et ne sont généralement pas inclus dans les inventaires (Subramanian et al. 2015 ; Zavala-Araiza et al. 2015 ; Alvarez et al. 2018). Si l'on regarde les émissions des décharges, le gradient de pression atmosphérique affecte fortement les émissions de méthane. Lorsque la pression atmosphérique diminue, les gaz des décharge sont transportés par la turbulence de l'air et les émissions de CH_4 augmentent (Xu et al. 2014). Le travaux affectent également les émissions de CH_4 des décharges (Ars 2017). Ainsi, le taux d'émission calculé lors d'une mesure mobile ne peut pas être facilement extrapolé à l'émission annuelle en multipliant simplement le taux calculé par le temps, tant pour les installations de gaz que pour les décharges. Des enquêtes plus régulières devraient être effectuées pour estimer le taux d'émission des sites sur une année.

Dans l'ensemble, les tests instrumentaux ont permis de déterminer les possibilités et les limites de l'utilisation du CRDS G2201-i dans les mesures sur le terrain, en particulier dans le contexte de C_2H_6:CH_4. Pendant les études, l'élévation relativement faible du CH_4 au-dessus des concentrations de fond a été la principale limite à l'application correcte de la méthodologie et à la détermination des signatures isotopiques et des ratios éthane/méthane. En utilisant le CRDS G2201-i, nous avons déterminé que l'augmentation du CH_4 devait être d'au moins 500 ppb au-dessus des concentrations de fond pour la signature isotopique et de 1000 ppb pour le ratio éthane/méthane. Une augmentation plus forte observée diminue l'incertitude de $\delta^{13}CH_4$ et de ratio C_2H_6:CH_4. L'augmentation de CH_4 détectée ici est suffisamment élevée pour estimer le taux d'émission en utilisant un modèle gaussien ou la méthode de dispersion des traceurs. Cependant, l'accès aux sites observés était limité et la méthode de dispersion des traceurs n'a pu être utilisée qu'une seule fois. L'infrastructure et la direction défavorable du vent constituaient d'autres limitations. Souvent, la vitesse du vent était trop faible (moins de 1 m s^{-1}) et les panaches de CH_4 n'ont pas été observés. Le nombre limité de mesures effectuées sur les sites industriels empêche d'extrapoler le taux d'émission estimé aux émissions annuelles.

Malgré les limites des méthodes déployées sur le terrain, ce doctorat apporte des observations et des analyses supplémentaires aux connaissances actuelles sur le CH_4 à l'échelle des villes et des sites industriels. Le travail sur le terrain a permis d'élargir les connaissances sur les émissions à l'échelle de la ville et de localiser les sources possibles de CH_4 à l'intérieur de la ville. De plus, les études menées sur les stations de compression de gaz ont permis d'initier une collaboration avec la société GRTgaz, qui est un opérateur national français de transport de gaz. Les informations fournies par l'opérateur ont été utilisées dans l'article sur la possibilité d'utiliser le CRDS G2201-i pour mesurer le ratio C_2H_6:CH_4 (Defratyka et al. 2020). Certaines mesures collaboratives ont également été effectuées et sont décrites dans une thèse de master (confidentielle) (Lozano 2020). De plus, ce doctorat a élargi la base de données sur le méthane isotopique, y compris les mesures de δDCH_4, qui sont encore rarement observées.

ÉCOLE DOCTORALE
Sciences de l'Environnement d'Île-de-France (SEIF)

Titre : Caractérisation des émissions de CH_4 en milieu urbain (Paris)

Mots clés : méthane, éthane, gaz naturel, environnement urbain, isotopes, calcul des émissions

Résumé :
Le but de cette thèse est de mesurer les concentrations de méthane (CH_4), sa signature isotopique en carbone ($\delta^{13}CH_4$) et le ratio éthane/méthane (C_2H_6:CH_4) de diverses sources en Île-de-France avec des mesures mobiles proche des sources en utilisant un analyseur CRDS.

Les tests en laboratoire ont montré que le CRDS G2201-i présentaient de bonnes performances, notamment un bon accord avec les mesures de $\delta^{13}CH_4$ par IRMS. En effet, la précision du CRDS est moins élevée que celle de l'IRMS, mais elle s'améliore avec des concentrations plus élevées en méthane (Chapitre 2). Les performances et les limites de l'instrument ont été également testées pour la mesure du ratio C_2H_6:CH_4 au laboratoire et sur le terrain. Il est possible d'utiliser le G2201-i quand l'excès de CH_4 au-dessus des valeurs ambiantes est supérieure à 1 ppm et que l'air mesuré est séché. Cela permet d'utiliser un seul instrument pour mesurer deux proxies des sources de méthane ($\delta^{13}CH_4$ et C_2H_6:CH_4) (Chapitre 3).

Ensuite, la plateforme de mesures mobiles a été adaptées pour des campagnes de mesure dans Paris et sa petite couronne.

Là, trois sources de CH_4 ont été trouvées: des fuites du réseau de gaz naturel, des fuites du réseau d'assainissement et des fuites au niveau de grilles d'aération associées à des chaudières. Cette dernière catégorie a été découverte lors de mesures à pied et n'était pas décrite précédemment dans la littérature. Par rapport à d'autres villes, en majorité américaine, les émissions parisiennes de CH_4 sont relativement faibles et comparables à celles des villes ayant un réseau moderne de distribution de gaz. La comparaison avec les inventaires a montré que pour le secteur de l'énergie, les émissions estimées étaient quinze fois plus faibles que celles de d'AIRPARIF ajustées pour Paris (Chapitre 4). Enfin, à l'échelle du site industriel, $\delta^{13}CH_4$ et δDCH_4 ont été déterminés et contribuent à enrichir la base de données de signatures isotopiques européenne pour CH_4. Le ratio C_2H_6:CH_4 mesuré sur les stations de compression de gaz sont comparables à celles observées dans d'autres études dans d'autres pays. Pour certains sites, les émissions sont été également estimées, soit avec un modèle Gaussien soit avec le méthode traceur (Chapitre 5).

Les résultats de cette thèse peuvent être utilisés comme support pour de futures campagnes de mesures en Île-de-France.

Maison du doctorat de l'Université Paris-Saclay
2ème étage aile ouest, Ecole normale supérieure Paris-Saclay
4 avenue des Sciences,
91190 Gif sur Yvette, France

ÉCOLE DOCTORALE
Sciences de l'Environnement d'Île-de-France (SEIF)

Title : Characterization of CH_4 emissions in urban environments (Paris)

Keywords : methane, ethane, natural gas, urban environment, isotopes, emission calculation

Abstract : This Ph.D. aimed to measure methane (CH_4) mixing ratio, its carbon isotope ($\delta^{13}CH_4$) and ethane to methane ratio (C_2H_6:CH_4) of diverse Île-de-France sources using CRDS G2201-i during near-source mobile measurements.

Laboratory tests showed good performances of CRDS G2201-i, notably a good agreement between $\delta^{13}CH_4$ determined using CRDS G2201-i and IRMS. Indeed, precision of CRDS is less good than for IRMS, but it improves with larger CH_4 mixing ratio (chapter 2). Possibilities and limitation of using CRDS G2201-i instrument to determine C_2H_6:CH_4 ratio were also verified in laboratory and field conditions. Using CRDS G2201-i to measure C_2H_6:CH_4 ratio is possible when enhancement is higher than 1 ppm above background and dried air is measured, which allows to use only one instrument to measure two proxies of CH_4 sources ($\delta^{13}CH_4$ and C_2H_6:CH_4) (chapter 3).

Then, the mobile set-up was adapted for mobile surveys in Paris city.

There, three main CH_4 sources where found: natural gas leaks, sewage network leaks and venting grid leaks ascribed to leaking furnaces installations. The latest category was discovered during walking measurements and was not described in previous studies. Compared to other cities, mostly surveyed in the U.S., Paris CH_4 emissions are relatively small and comparable to cities with modern pipeline system. Comparison with inventories showed that for the energy sector, CH_4 emissions are about fifteen times smaller than downscaled AIRPARIF inventories (chapter 4). Finally, at the industrial site scale, $\delta^{13}CH_4$ and δDCH_4 were determined and contributed to extend the database of isotopic signatures of European CH_4 emissions. C_2H_6:CH_4 observed from gas compressor stations are comparable with those in previous studies in other countries. For part of the sites, emission rates were also estimated using a Gaussian model or the tracer dispersion method (chapter 5).

Results of this Ph.D. can serve as a basis for a future 'wall-to-wall' independent estimation of sectorial CH_4 emissions from the Paris area and other large urban areas.

Maison du doctorat de l'Université Paris-Saclay
2ème étage aile ouest, Ecole normale supérieure Paris-Saclay
4 avenue des Sciences,
91190 Gif sur Yvette, France